ESTABLISHING AND MAINTAINING CELL POLARITY

EDITED BY: Benjamin Lin, Yi Wu and Zhiyi Lv
PUBLISHED IN: Frontiers in Cell and Developmental Biology

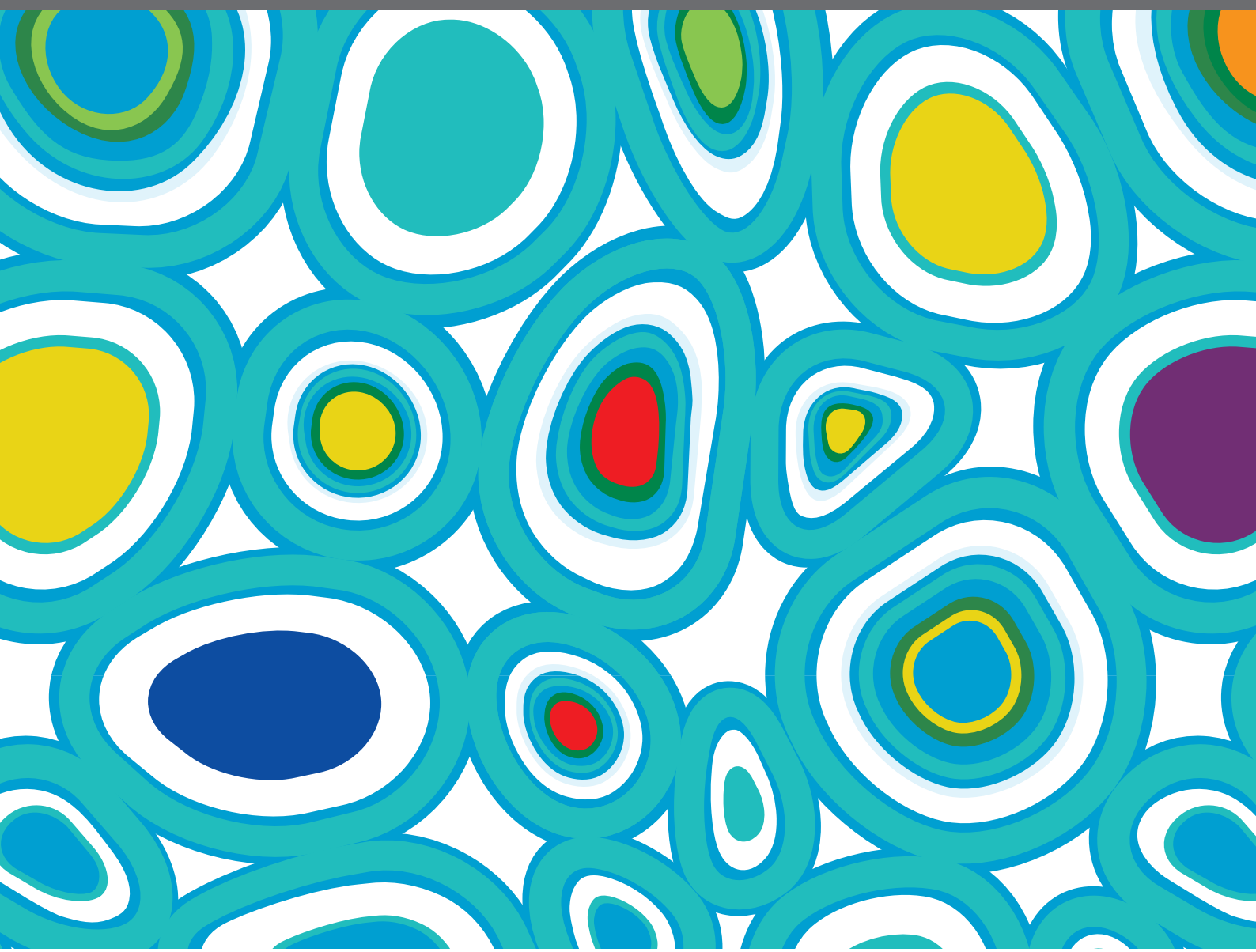

frontiers Research Topics

frontiers

ISSN 1664-8714
ISBN 978-2-88971-856-6
DOI 10.3389/978-2-88971-856-6

About Frontiers

Frontiers is more than just an open-access publisher of scholarly articles: it is a pioneering approach to the world of academia, radically improving the way scholarly research is managed. The grand vision of Frontiers is a world where all people have an equal opportunity to seek, share and generate knowledge. Frontiers provides immediate and permanent online open access to all its publications, but this alone is not enough to realize our grand goals.

Frontiers Journal Series

The Frontiers Journal Series is a multi-tier and interdisciplinary set of open-access, online journals, promising a paradigm shift from the current review, selection and dissemination processes in academic publishing. All Frontiers journals are driven by researchers for researchers; therefore, they constitute a service to the scholarly community. At the same time, the Frontiers Journal Series operates on a revolutionary invention, the tiered publishing system, initially addressing specific communities of scholars, and gradually climbing up to broader public understanding, thus serving the interests of the lay society, too.

Dedication to Quality

Each Frontiers article is a landmark of the highest quality, thanks to genuinely collaborative interactions between authors and review editors, who include some of the world's best academicians. Research must be certified by peers before entering a stream of knowledge that may eventually reach the public - and shape society; therefore, Frontiers only applies the most rigorous and unbiased reviews.
Frontiers revolutionizes research publishing by freely delivering the most outstanding research, evaluated with no bias from both the academic and social point of view. By applying the most advanced information technologies, Frontiers is catapulting scholarly publishing into a new generation.

What are Frontiers Research Topics?

Frontiers Research Topics are very popular trademarks of the Frontiers Journals Series: they are collections of at least ten articles, all centered on a particular subject. With their unique mix of varied contributions from Original Research to Review Articles, Frontiers Research Topics unify the most influential researchers, the latest key findings and historical advances in a hot research area! Find out more on how to host your own Frontiers Research Topic or contribute to one as an author by contacting the Frontiers Editorial Office: frontiersin.org/about/contact

ESTABLISHING AND MAINTAINING CELL POLARITY

Topic Editors:
Benjamin Lin, NYU Grossman School of Medicine, United States
Yi Wu, UCONN Health, United States
Zhiyi Lv, Ocean University of China, China

Citation: Lin, B., Wu, Y., Lv, Z., eds. (2021). Establishing and Maintaining Cell Polarity. Lausanne: Frontiers Media SA. doi: 10.3389/978-2-88971-856-6

Table of Contents

frontiers in Cell and Developmental Biology

EDITORIAL
published: 30 June 2021
doi: 10.3389/fcell.2021.722003

Editorial: Establishing and Maintaining Cell Polarity

Benjamin Lin[1]*, *Zhiyi Lv*[2] and *Yi Wu*[3]

[1] Department of Cell Biology, Kimmel Center for Biology and Medicine of the Skirball Institute, New York University School of Medicine, New York, NY, United States, [2] Sars-Fang Centre, Institute of Evolution and Marine Biodiversity, Ocean University of China, Qingdao, China, [3] Department of Cell Biology, R.D. Berlin Center for Cell Analysis and Modeling, UConn Health, Farmington, CT, United States

Keywords: mechanotransduction, polarity (cell), signaling/signaling pathways, development, multi-cue integration

Editorial on the Research Topic

Establishing and Maintaining Cell Polarity

Cell polarity arises from compartmentalizing molecular effectors within the membrane, cortex, and/or cytoplasm. These asymmetric molecular ensembles serve as templates for signaling cascades which drive essential cell functions, including cell division and migration, and are coordinated across the tissue scale during morphogenesis and barrier formation. Polarity is initiated through symmetry breaking via an internal or external cue and is typically maintained through antagonistic interactions amongst opposing effectors. At present, many of the molecular components involved in generating polarity have been identified, in large part through genetic screens in model organisms. Furthermore, an ever expanding palette of genetically encoded fluorescent proteins and biosensors coupled with continued advances in microscopy have made observing polarity extremely tractable. This has led to an expansion of quantitative imaging which in turn has fueled the development of mathematical models, which both describe and predict new properties of polarity systems. Despite this progress, the complex interplay between core polarity modules, the various external cues which influence them and the cytoskeleton are still being unraveled in pursuit of understanding how polarity is disrupted in disease.

In this Research Topic, one of our aims was to provide a venue for members of the polarity field to review its current state and propose future directions. Given the ubiquity of polarity in development, we have accordingly received contributions from the perspective of several model organisms, including *Drosophila*, *C. Elegans*, *Ciona*, and *S. cerevisiae*. We also highlighted specific areas of interest, including how cells might resolve multiple cues, how polarity can be reconstituted in apolar cells, and how mechanical and chemical cues are integrated. We were delighted to not only receive original research, reviews, and methods articles which explore these questions but other underrepresented areas as well. Below we provide a brief synopsis of the articles in this collection and encourage readers to delve further into each one.

Polarity is initiated through symmetry breaking via the amplification of a local asymmetry through positive feedback. Local asymmetries can arise spontaneously or can be induced by a cue. Gan and Motegi provide a comprehensive review of the interplay between mechanical forces and chemical signaling during symmetry breaking in the *C. Elegans* zygote. Along with membrane and cortical polarity, cytoplasmic polarity also contributes to important cell functions, including the specification of soma and germline. Kim and Griffin review the role of Polo-like kinase 1 (PLK-1) in the first asymmetric division of the *C. Elegans* embryo, noting how cytoplasmic gradients of PLK-1 play pleiotropic roles in establishing cortical domains and regulating the correct segregation of fate determinants to the germline.

Edited and reviewed by:
Ana Cuenda,
Consejo Superior de Investigaciones Científicas (CSIC), Spain

***Correspondence:**
Benjamin Lin
Benjamin.lin@nyulangone.org

Specialty section:
This article was submitted to Signaling, a section of the journal Frontiers in Cell and Developmental Biology

Received: *08 June 2021*
Accepted: *11 June 2021*
Published: *30 June 2021*

Citation:
Lin B, Lv Z and Wu Y (2021) Editorial: Establishing and Maintaining Cell Polarity. Front. Cell Dev. Biol. 9:722003. doi: 10.3389/fcell.2021.722003

The two contributions above exemplify the complexities arising when studying polarity. In particular, teasing apart how different polarity modules influence each other is not trivial when the networks are interconnected. Johnston describes a reductionist technique to reconstitute polarity in apolar cells which has been successfully utilized to assess the sufficiency of different proteins to orient cell division. Controlling the cell division axis is particularly crucial in blood vessel development, where divisions parallel to the vessel can elongate it while perpendicular divisions can expand the diameter of the existing vessel or support sprouting of new vessels. Wu et al. review how mitotic spindle polarity is oriented in blood vessel development, highlighting the roles of electric currents and vascular endothelial growth factor (VEGF) in this process.

Individual cell polarity can be coordinated across cell collectives during morphogenesis via mechanotransduction through trans-interacting junctional complexes connected to the cortex. Canonical examples include ratcheted apical constrictions driving tissue involution and folding during gastrulation and planar polarized forces producing tissue elongation through convergent extension. Kong and Großhans review E-cadherin mechanotransduction in two contexts- (1) planar polarity dependent convergent extension in *Drosophila* embryonic epidermal cells and (2) interactions between two epithelial populations during tissue closure. The importance of polarity coordination between multiple cell populations is also apparent in an original research contribution from Kunz et al. which reveals that apical constriction and dendritic towing act to correctly position sensory organs in a proteasome dependent manner. Mechanical forces from polarized extracellular matrix (ECM) and supracellular cytoskeletal structures can also influence tissue morphogenesis. Popkova et al. review how planar polarity movement aligned ECM and basal supracellular actin stress fiber contractions act to sequentially elongate *Drosophila* eggs along the anterior-posterior axis through constraining isotropic growth. Although planar cell polarity (PCP) and apical-basal (AB) polarity can act in isolation in some contexts, interactions between these two polarity systems can be critical for tissue morphogenesis. Peng et al. review the interplay between PCP and AB polarity during notochord formation in *Ciona* as notochord cells transition from a planar sheet to an ECM wrapped tube with a hollow lumen.

Polarity can be influenced by a variety of cues, including electric fields, shear stress, cell contact, and chemical ligands. How does the presence of one cue modify the response to another and is there a context dependent hierarchy between them? Tardy et al. utilize *Drosophila* embryonic hemocytes (macrophage equivalent in *Drosophila*) to provide some insight into these questions. They uncover how Spitz [a *Drosophila* epidermal growth factor (EGF) ligand] signaling from ectopic sources can compete and dampen hemocyote responses toward both developmental migratory cues, such as apoptotic cells, and acute migratory wound cues.

Lastly, an intriguing question is how existing polarities are remodeled. Epithelial cells can transiently redistribute both apical and basolateral polarity proteins during cell division and re-establish polarity afterwards. Similarly, bud growth in *Saccharomyces cerevisiae* transitions from apical to isotropic by removing polarized Cdc42 activity at the bud tip via redistribution of its activator. Quadri et al. propose a general role for Ras in resolving polarity and highlight its role downstream of a kinase, Haspin, in binding and changing the localization of a Cdc42 activator to prevent hyperpolarization during mitosis. In another contribution from this group (Galli et al.), Haspin is shown to be involved in enforcing the morphogenesis checkpoint, which halts the cell cycle until proper polarity is established.

We would like to thank the authors and reviewers for their efforts in compiling this impressive set of articles in this Research Topic which provide a bird's eye view of the polarity field through the lens of model organisms and addresses underrepresented aspects of polarity, such as multi-cue interpretation, resolution, and reconstitution. We hope this collection provides an impetus for further work to ultimately understand how polarity is dysregulated in disease.

AUTHOR CONTRIBUTIONS

BL wrote the manuscript and received input from ZL and YW. All authors contributed to the article and approved the submitted version.

FUNDING

BL was supported by a New York Stem Cell Foundation Druckenmiller fellowship. ZL was supported by the General Program of National Natural Science Foundation of China (NSFC: 32070786) and the Shandong Province Taishan program for young scientist, China (qnts201909055). YW was supported by NIH grant GM117061.

Conflict of Interest: The authors declare that the research was conducted in the absence of any commercial or financial relationships that could be construed as a potential conflict of interest.

frontiers in Cell and Developmental Biology

MINI REVIEW
published: 17 September 2020
doi: 10.3389/fcell.2020.583325

Orientation of the Mitotic Spindle in Blood Vessel Development

*Xuemei Wu[1], Jun Zhou[1,2] and Dengwen Li[1]**

[1] State Key Laboratory of Medicinal Chemical Biology, College of Life Sciences, Nankai University, Tianjin, China, [2] Shandong Provincial Key Laboratory of Animal Resistance Biology, Collaborative Innovation Center of Cell Biology in Universities of Shandong, College of Life Sciences, Institute of Biomedical Sciences, Shandong Normal University, Jinan, China

Angiogenesis requires coordinated endothelial cell specification, proliferation, and collective migration. The orientation of endothelial cell division is tightly regulated during the earliest stages of blood vessel formation in response to morphogenetic cues and the controlled orientation of the mitotic spindle. Consequently, oriented cell division is a vital mechanism in vessel morphogenesis, and defective spindle orientation can perturb the spatial arrangement of daughter cells and consequently contribute to several diseases related to vascular development. Many factors affect endothelial cell proliferation and orientation and therefore blood vessel formation, with the relationship between improper spindle orientation in endothelial cells and various diseases extensively studied. Here we review the molecular mechanisms driving the orientation of endothelial cell division, particularly with respect to the mitotic spindle, and how these processes affect vascular development, disease pathogenesis, and their potential as novel targets.

Keywords: spindle orientation, angiogenesis, mitotic spindle, cell proliferation, blood vessel development

OPEN ACCESS

Edited by:
Zhiyi Lv,
Ocean University of China, China

Reviewed by:
Marina Mapelli,
European Institute of Oncology (IEO), Italy
Jorge Torres,
UCLA Department of Chemistry and Biochemistry, United States

****Correspondence:***
Dengwen Li
dwli@nankai.edu.cn

Specialty section:
This article was submitted to Signaling, a section of the journal Frontiers in Cell and Developmental Biology

Received: *14 July 2020*
Accepted: *01 September 2020*
Published: *17 September 2020*

Citation:
Wu X, Zhou J and Li D (2020) Orientation of the Mitotic Spindle in Blood Vessel Development. Front. Cell Dev. Biol. 8:583325. doi: 10.3389/fcell.2020.583325

INTRODUCTION

Blood vessel development, which includes vasculogenesis and angiogenesis, is crucial for the formation of the cardiovascular system and blood vessel regeneration after injury. The vasculature is one of the first organ systems to develop during vertebrate embryogenesis (Wilkinson and van Eeden, 2014). Angiogenesis is important in a number of pathophysiological processes (Sajib et al., 2018), not only supporting the developing embryo and in wound healing but also in many diseases including cancer, infectious arthritis, and psoriasis (Carmeliet, 2000; Sajib et al., 2018). The formation of the vascular plexus requires exquisite regulation and integration of several cellular processes: endothelial cells sprout in response to morphogenetic cues and must actively divide to expand the endothelial cell pool. As a consequence, abnormal blood vessel development contributes to numerous diseases such as cancer and intraocular vascular disorders (Apte et al., 2019), with aberrant endothelial cell proliferation, migration, polarity, and the maintenance of intercellular junctions central processes (Hogan and Schulte-Merker, 2017).

Spindle orientation determines the fate and position of daughter cells during mitosis (Li J. et al., 2019) and plays an important role in development, including epithelium and vascular endothelium development. Epithelium development plays a critical role in organ development and tissue repair (Ting Song, 2020), which requires proper orientation of the mitotic spindle (Xie and Zhou, 2017; Xie et al., 2017). In proliferating epithelium, planar cell division occurs by orienting mitotic spindles into the epithelial plane to ensure organized tissue formation (Luo et al., 2016; Nakajima, 2018). Asymmetric positioning of the mitotic spindle during endothelial tip cell division generates

multicellular polarity, which drives coordinated and collective cell migration in angiogenesis (Costa et al., 2016). During asymmetric division, mitotic spindles must be placed on the polarization axis to ensure the correct orientation of daughter cells (Liro and Rose, 2016). In view of the direct and intimate connection between spindle orientation and endothelial cell division and polarization, spindle orientation during mitosis is essential to blood vessel development, so, when abnormal, the proteins and processes related to abnormal spindle orientation might be expected to participate in vascular development diseases (Zhong and Zhou, 2017; **Figure 1**). In this review, we summarize how spindle orientation regulates endothelial cell division to affect vascular development and discuss the relationship between misorientation and pathological state.

BLOOD VESSEL DEVELOPMENT

Oxygen and nutrient transport in developing embryos depends on the formation of vascular networks (Ma and Zhou, 2020), and many pathologies involve blood vessel development and remodeling (Potente et al., 2011). Each organ in the human body has its own capillary bed with both general and specific functions to respond to dynamic systemic and local changes (Augustin and Koh, 2017). Blood vessel development includes vasculogenesis and angiogenesis. Vasculogenesis,the formation of embryonic blood vessels, involves the differentiation, migration, and coalescence of angioblasts and the polarization of endothelial cells to form a vascular lumen and create a primordial vascular network. During angiogenesis, new blood vessels are formed from existing capillaries or venules by endothelial cell proliferation, differentiation, and migration (Carmeliet and Jain, 2011). When endothelial cells form sprouts, two distinct phenotypes are undertaken by the endothelial cells asymmetric division in the nascent blood vessel sprout, namely the tip cell phenotype and the stalk cell phenotype (Koon et al., 2018). Tip cells bring about motile behavior which migrate toward the angiogenic source upon stimulation by chemotactic factors. Stalk cells trail behind the tip cells to support the growth of the vessel by their proliferative capacity (Gerhardt et al., 2003; **Figure 1B**). In addition, stalk cells ensure stability and integrity of the young sprout by forming adherent and tight junctions (Blanco and Gerhardt, 2013). Therefore, its dysfunction can cause inflammatory, infectious and immune disorders (Carmeliet, 2003). Furthermore, polarized positioning of the mitotic spindle functions to generate intrinsically asymmetric daughters of tip cell division, which is essential for vessel sprout formation. Many aspects in tissue morphogenesis are attributed to a collective behavior of the participating cells (Lv et al., 2020). Daughters of tip cell rapidly self-organize into leading and trailing cells following division, which maintains uninterrupted collective migration during vessel proliferation (Costa et al., 2016). During vascular development, endothelial cell migration, proliferation, polarity, differentiation, and intercellular communication must be tightly coordinated for functional vascular morphogenesis (Herbert and Stainier, 2011). Blood vessel development plays an important role in vascular barrier formation (Tam and Watts, 2010), tumorigenesis (Yadav et al., 2015), and ischemic, inflammatory, infectious, and immune disorders (Carmeliet, 2003).

THE ROLE OF SPINDLE ORIENTATION IN BLOOD VESSEL DEVELOPMENT

The correct separation of chromosomes into daughter cells of different sizes or cell fates requires precise spindle orientation to control cell fate choices, tissue architecture, and tissue morphogenesis (Morin and Bellaïche, 2011; di Pietro et al., 2016; Chen et al., 2020). Blood vessel development depends on vascular lumen formation, which requires the precise mitotic spindle orientation of endothelial cells and the establishment of polarity to form opposed apical cell surfaces (Neufeld et al., 2014). Endothelial cleavage plane oriented perpendicular to the blood vessel long axis would effectively lengthen the blood vessel, whereas divisions oriented parallel to the blood vessel long axis would effectively increase the blood vessel diameter (**Figure 1A**). In particular, during angiogenesis, the asymmetric division of endothelial tip cells generates heterogeneous daughter cells that maintain hierarchical tip-stalk organization and synchronize collective movements (Costa et al., 2016). These processes are closely related to mitotic spindle orientation, which is precisely controlled by many cues, either intrinsic or extrinsic, such as natural direct current electric fields (DC-EFs) and many signaling pathways and proteins that play an important role in spindle orientation including VEGF signaling, the Rho family of GTPases Cdc42 are also indispensable to vascular development and regeneration. Highlighting its importance in blood vessel development, the aberrant regulation of spindle orientation has been linked to a variety of human diseases.

VEGF Signaling

Among the already identified pro-angiogenic molecules, vascular endothelial growth factor (VEGF) is established as the key angiogenic growth factor (Melincovici et al., 2018; Li S. et al., 2019), by regulating blood vessel growth and maintenance. Pioneering studies showed that VEGF signaling affects vascular morphogenesis by controlling the orientation of endothelial cell division perpendicular to the vessel long axis (Zeng et al., 2007). It is reported that this process is affected by a number of factors. First, oriented endothelial divisions appear to be associated with VEGF but is independent of blood flow during early development (Bautch, 2012). Blood vessels derived from embryonic stem cells do not undergo flow-directed endothelial cell division, whose plane of division is perpendicular to the long axis of the vessel, and retinal vessels near the vascular front that likely have low shear stress also orient endothelial divisions (Zeng et al., 2007). Within the vascularized retina, by binding to VEGFR2, VEGF alters the orientation of endothelial cell cleavage planes during anaphase in the major veins and arterioles to further increase vessel tortuosity and dilation independent of eNOS (Hartnett et al., 2008). Therefore, eNOS does not appear to be essential in VEGF-mediated orientation of endothelial cell division.

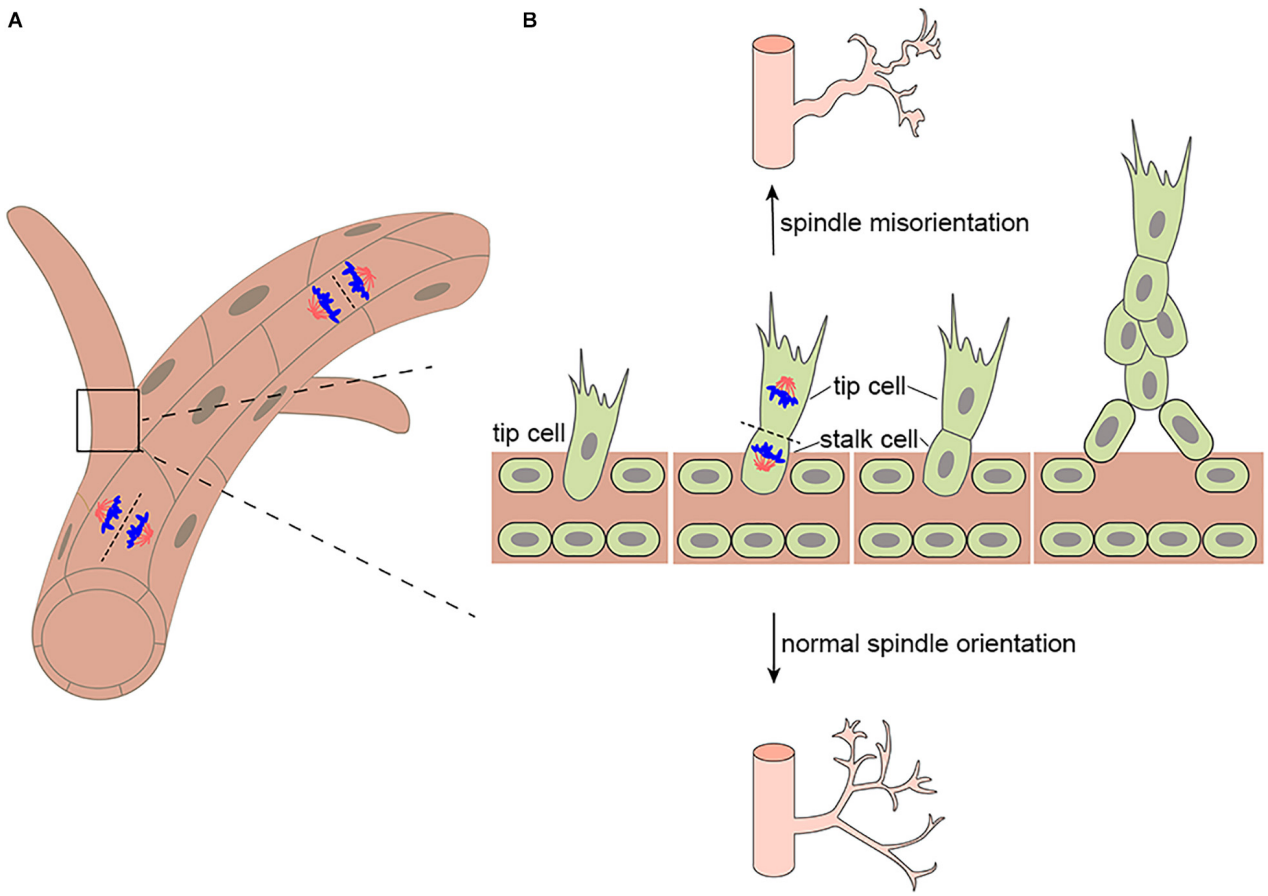

FIGURE 1 | Mitotic spindle orientation in endothelial cell affects vessel morphogenesis. **(A)** Endothelial divisions oriented perpendicular to the vessel long axis (on top) would effectively lengthen the vessel, whereas divisions oriented parallel to the vessel long axis (on bottom) would effectively increase the vessel diameter. **(B)** During branching morphogenesis, highly motile endothelial tip cells sprout from parental vessels and lead stalk cells. Upon tip cell division, the mitotic spindle is displaced to the proximal pole of the cell before anaphase. This introduces cell size asymmetry and generates daughter cells with distinct VEGF signaling levels. In addition, aberrant mitotic spindle orientation changes endothelial cell cleavage plane and further increasing vessel tortuosity and dilation.

In the process of forming new blood vessel branches through angiogenesis, endothelial tip cells, which lead nascent vessels (Herbert and Stainier, 2011), likely underpin asymmetric cell division by asymmetric positioning of the mitotic spindle to form asymmetries in cell size and VEGFR signaling components during anaphase (Costa et al., 2017). In this way, the formation of the leading tip and trailing stalk endothelial cells is precisely regulated. Importantly, asymmetries in VEGF signaling following division have been shown to be essential for normal vessel formation by instantly re-establishing the tip-stalk hierarchy and maintaining uninterrupted collective migration during proliferative growth (Costa et al., 2016). Costa et al., confirmed that the larger distal daughter of tip cell division inherited a greater proportion of the VEGF signaling machinery and displayed higher levels of VEGF signaling, establishing it as the leading tip cell. In the absence of differential VEGFR activity the tip-stalk arrangement of daughters was disrupted and cells display symmetric motilities (Costa et al., 2016). We can guess this may explain why abnormal vascular patterns develop in some pathological angiogenesis. Furthermore, in a model of human retinopathy of prematurity (ROP), endothelial NADPH oxidase 4 regulated VEGF receptor (VEGFR)2-mediated angiogenesis and intravitreal neovascularization through activated STAT3 (Wang et al., 2014). However, whether this process further influences angiogenesis by influencing spindle orientation is not clear.

Natural Direct Current Electric Fields (DC-EFs)

Endogenous electric fields, which have been measured directly in animals and in humans, are ubiquitous and may play a significant role in development (McCaig and Zhao, 1997). Electrical stimulation has emerged as a novel approach to induce angiogenesis *in vivo*, and this process is regulated through increased expression of VEGF in muscle cells (Cuevas and Asin-Cardiel, 2000). DC EFs of 200 mV/mm increased secretion of vascular endothelial growth factor (VEGF) and interleukin 8 (IL-8) in starved HUVEC cells (Zhao et al., 2004; Bai et al., 2011). It has been proved that electric fields of 150–400 mV/mm induced reorientation of the long axis of the

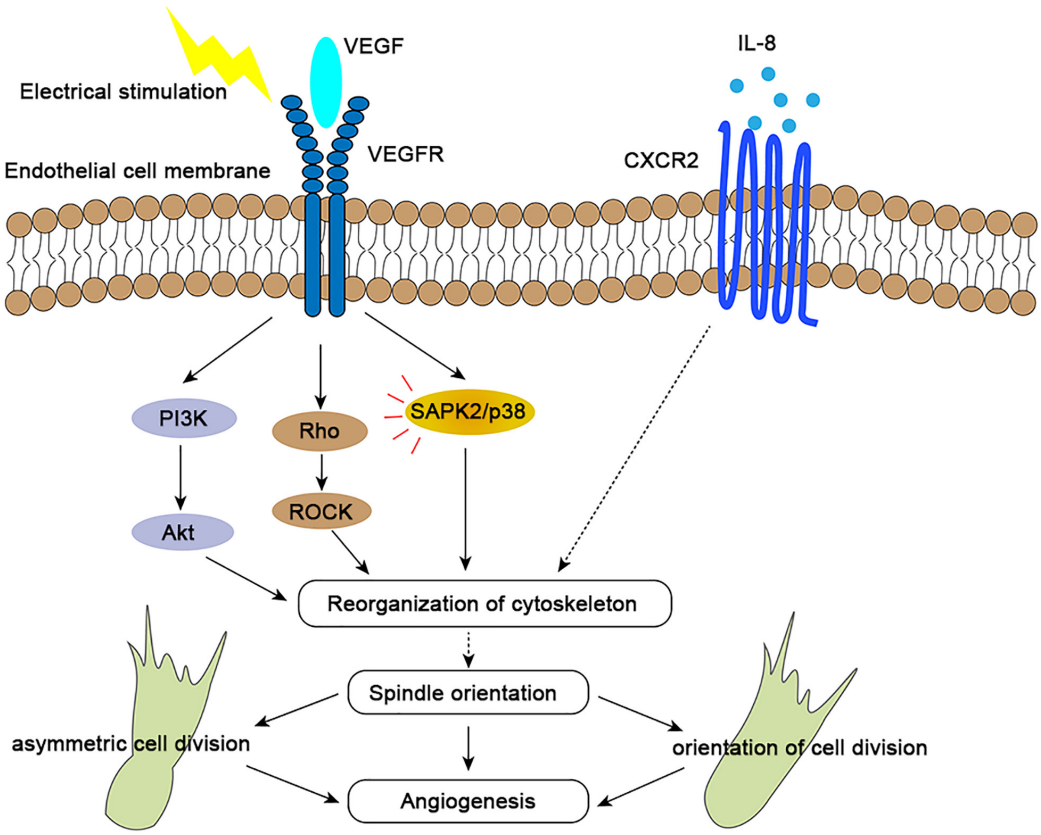

FIGURE 2 | Molecular mechanisms of spindle orientation effects in angiogenesis. By binding to VEGFR2, VEGF activates the PI3K/Akt, Rho/ROCK, and SAPK/p38 signaling pathways (red lines), which results in precise orientation of the mitotic spindle, endothelial cell asymmetry and orientation, and consequent directional angiogenesis. Interleukin-8 (IL-8) binds with high affinity to the chemokine receptor CXCR2, which may also regulate spindle orientation by influencing reorganization of cytoskeleton to further affect spindle orientation, further impacting angiogenesis. Both receptors and signaling pathways are upregulated upon electrical stimulation.

endothelial cells perpendicular to the EF vector (Zhao et al., 2004; Cunha et al., 2019). This process were mediated by VEGFR activation, with downstream Rho-ROCK and PI3K-Akt activation leading to cytoskeletal reorganization and the mitotic spindle orientation (Zhao et al., 2004; **Figure 2**). Electric fields also upregulate the expression of the chemokine receptors CXCR4 and CXCR2 (Cunha et al., 2019). Interleukin 8 (IL-8) with high-affinity binding to the CXCR2 chemokine receptors may stimulate endothelial cell proliferation (Holmes et al., 1991; Baggiolini et al., 1997; Leclair et al., 2014). However, how these chemokines affect orientation of endothelial cell division is still unclear (**Figure 2**). In general, electrical stimulation may play a spatial organization role in angiogenesis by regulating the endothelial mitotic spindle orientation (Bai et al., 2004).

G-Protein-Signaling Modulator 2 (GPSM-2 or LGN)

Proper mitotic spindle orientation requires that astral microtubules are connected to the cell cortex by the microtubule-binding protein NuMA. Its cortical recruitment is mediated via direct binding to the adaptor protein LGN which participates in MT-orienting complexes to further regulate mitotic spindle orientation (Yang et al., 2014; Takayanagi et al., 2019). In many cell types, mitotic spindle orientation relies on the canonical "LGN complex" composed of Pins/LGN, Mud/NuMA, and Gαi subunits, which is evolutionary conserved in Drosophila and vertebrates (Saadaoui et al., 2017; Kschonsak and Hoffmann, 2018). In vertebrates, the Gαi-LGN-NuMA complex anchors astral microtubules and orients spindles to regulate asymmetric divisions (Zhu et al., 2011). However, although LGN knockdown perturbs overall endothelial sprouting, spindle orientation in sprouting endothelial cells do not require LGNLGN instead influences interphase microtubule dynamics in endothelial cells to regulate migration, cell adhesion, and sprout extension (Wright et al., 2015). So the potential role of LGN in the blood vessel development may be focused on cell migration and adhesion. In addition, these data might also indicate that different mechanisms regulate spindle orientation in vascular endothelial cells and other cells, and this requires further study. At the same time, there may be novel pathway contributing to spindle orientation during blood vessel formation and therefore possible new therapeutic targets need to be discovered.

The Rho Family of GTPases: Cdc42

Cdc42, a small GTPase, controls spindle orientation during cell division to regulate epithelial morphogenesis and repair (Jaffe et al., 2008; Mitsushima et al., 2009; Xia et al., 2015). With regards to the development of blood vessels, Cdc42 is essential in embryonic development and a vital regulator of endothelial cell development, regulating actin-based morphogenesis and cell polarity. An absence of Cdc42 results in embryonic death through angiogenesis defects (Jin et al., 2013; Barry et al., 2015). Cdc42 also plays an important role in endothelial regeneration and vascular repair (Flentje et al., 2019). Endothelial cell regeneration is important in the resolution of inflammation and the restoration of vascular integrity after inflammatory vascular injury (Zhao et al., 2014). Cdc42 was shown to affect endothelial cell proliferation through the PAK1/Akt pathway to further regulate vascular recovery after inflammatory lung injury (Lv et al., 2018).

Cdc42 is also involved in sphingosine-1-phosphate (S1P) signal transduction to enhance the barrier function of endothelial monolayers, which can promote vascular stability (Reinhard et al., 2017). It has also been proposed that an absence of Cdc42 leads to defective endothelial axial polarization, sparing endothelial cell proliferation but preventing them from precisely re-distributing within the vascular network and resulting in severe vascular malformations as a consequence of defective cell migration (Laviña et al., 2018). Whether mitotic spindle orientation is of relevance for vascular malformations remains to be further elucidated.

SPINDLE MISORIENTATION IS ASSOCIATED WITH DISEASES

The orientation of the cell division axis determines the positions of daughter cells in a tissue and is therefore crucial to tissue morphogenesis and cell fate decisions (Théry and Bornens, 2006; di Pietro et al., 2016; Chen et al., 2019). Recent studies have shown that a number of factors can regulate the orientation of mitotic spindles and therefore cell division orientation (Li J. et al., 2019). As is stated above, intrinsic factor VEGF signaling and extrinsic factor electric fields (EFs) play an important role in affecting the mitotic spindle orientation to regulate the blood vessel development. An increasing number of vascular development disorders have been reported to result from spindle orientation defects.

Firstly, human retinopathy of prematurity (ROP) has been linked to altered spindle orientation. aberrant mitotic spindle orientation causes ROP by changing endothelial cell cleavage plane and further increasing vessel tortuosity and dilation (Hartnett et al., 2008; **Figure 1B**). Secondly, diabetic retinopathy (DR), the most common microvascular complication of diabetes maybe also be associated with spindle misorientation. VEGF is overexpressed in hyperglycemic environments and is up-regulated by tissue hypoxia, which increases vessel tortuosity and dilation by altering the orientation of endothelial cell cleavage planes during anaphase in the major veins and arterioles within the vascularized retina (**Figure 1B**; Hartnett et al., 2008; Capitão and Soares, 2016). Moreover, blood vessels provide nutrients and oxygen to tumors, and insufficient or abnormal angiogenesis contributes to tumor survival, invasion, and metastasis (Saman et al., 2020). In addition to providing nutrients and oxygen to the tumor and the removal of metabolic waste, new vessel formation also enables cancer cells to metastasize and proliferate to distant sites through entry into the newly formed blood and lymphatic system and subsequent extravasation (Nishida et al., 2006). Thus, spindle orientation in the tumor vasculature has become a new key anti-tumor therapeutic target. It is imperative that future studies determine in which of these diseases spindle misorientation contributes to pathogenesis. Beyond that, the mechanisms that prevent spindle misorientation need to be uncovered.

CONCLUSION AND PERSPECTIVES

Cell division orientation plays an essential role in tissue morphogenesis and cell fate decisions. This is achieved through the formation of the mitotic spindle (Lu and Johnston, 2013). The VEGF/VEGFR signaling pathways is key regulator of spindle orientation during angiogenesis (Hartnett et al., 2008), which controlling the orientation of endothelial cell division perpendicular to the vessel long axis to further affect vascular morphogenesis (Zeng et al., 2007). At the same time, IL-8/CXCR2 signaling pathway also was activated during electric fields exposure. Therefore, there has been a hypothetical mechanism that VEGF induces CXCR2 production by endothelial cells, creating a positive-feedback loop to influence spindle orientation (Cunha et al., 2019). Although many of the mechanisms by which planar spindle orientation are tightly regulated and the roles of mitotic spindle orientation in epithelial development and disease have been well studied (di Pietro et al., 2016), further research is needed to see the details of the underlying mechanisms of how spindle orientation affects vascular development by regulating endothelial cell orientation. The differences between the epithelium and endothelium are important to take into consideration. For example, some spindle orientation-related proteins playing important roles in epithelia, such as LGN, did not affect the oriented division of endothelial cell (Wright et al., 2015). Consequently, further studies of the basic molecular mechanisms of how spindle orientation in endothelial cells influences angiogenesis are required, not least to identify potential therapeutic targets. A key challenge will be to determine the precise *in vivo* mechanism of plane spindle orientation and its involvement in blood vessel development.

Aberrant spindle orientation is hypothesized to contribute to tissue disorganization (Qin et al., 2017; Xie et al., 2019). Targeted anti-VEGF therapies have been widely researched, but they cause various side-effects such as hypertension, and are susceptible to drug resistance (Bergers and Hanahan, 2008). Advances in electrical stimulation and an improved understanding of the biological effects of stimulation might lead to new therapies to enhance blood vessel repair and regeneration and to treat diseases or conditions in which angiogenesis is part of the pathogenesis (Cunha et al., 2019). ES has been widely used to induce

neurogenic and cardiomyogenic regeneration (Ragnarsson, 2008; Zhang et al., 2011) through regulating endothelial cell migration to wound site (Jeong et al., 2017) and affecting endothelial cell division orientation via VEGF signaling (Zhao et al., 2004). However, spindle orientation proteins have yet to be targeted directly in endothelial cell therapy, and further work is required to establish how mitotic spindles control the orientation and asymmetry of endothelial cells during angiogenesis to leverage the process for the treatment of vascular development-related diseases. Overall, investigation of the role of spindle misorientation in diseases is just beginning, and the most intriguing questions remain to be addressed.

AUTHOR CONTRIBUTIONS

XW wrote the manuscript and drew the figures. JZ revised the manuscript. DL conceived the study and edited the manuscript. All authors contributed to the article and approved the submitted version.

FUNDING

This work was supported by a grant from the National Natural Science Foundation of China (31771542 and 31871347).

REFERENCES

Apte, R. S., Chen, D. S., and Ferrara, N. (2019). VEGF in signaling and disease: beyond discovery and development. *Cell* 176, 1248–1264. doi: 10.1016/j.cell.2019.01.021

Augustin, H. G., and Koh, G. Y. (2017). Organotypic vasculature: from descriptive heterogeneity to functional pathophysiology. *Science* 357:6353.

Baggiolini, M., Dewald, B., and Moser, B. (1997). Human chemokines: an update. *Annu. Rev. Immunol.* 15, 675–705. doi: 10.1146/annurev.immunol.15.1.675

Bai, H., Forrester, J. V., and Zhao, M. (2011). DC electric stimulation upregulates angiogenic factors in endothelial cells through activation of VEGF receptors. *Cytokine* 55, 110–115. doi: 10.1016/j.cyto.2011.03.003

Bai, H., McCaig, C. D., Forrester, J. V., and Zhao, M. (2004). DC electric fields induce distinct preangiogenic responses in microvascular and macrovascular cells. *Arterioscler. Thromb. Vasc. Biol.* 24, 1234–1239. doi: 10.1161/01.atv.0000131265.76828.8a

Barry, D. M., Xu, K., Meadows, S. M., Zheng, Y., Norden, P. R., Davis, G. E., et al. (2015). Cdc42 is required for cytoskeletal support of endothelial cell adhesion during blood vessel formation in mice. *Development* 142, 3058–3070. doi: 10.1242/dev.125260

Bautch, V. L. (2012). VEGF-directed blood vessel patterning: from cells to organism. *Cold Spring Harb. Perspect. Med.* 2:a006452. doi: 10.1101/cshperspect.a006452

Bergers, G., and Hanahan, D. (2008). Modes of resistance to anti-angiogenic therapy. *Nat. Rev. Cancer* 8, 592–603. doi: 10.1038/nrc2442

Blanco, R., and Gerhardt, H. (2013). VEGF and Notch in tip and stalk cell selection. *Cold Spring Harb. Perspect. Med.* 3:a006569. doi: 10.1101/cshperspect.a006569

Capitão, M., and Soares, R. (2016). Angiogenesis and inflammation crosstalk in diabetic retinopathy. *J. Cell. Biochem.* 117, 2443–2453. doi: 10.1002/jcb.25575

Carmeliet, P. (2000). Mechanisms of angiogenesis and arteriogenesis. *Nat. Med.* 6, 389–395. doi: 10.1038/74651

Carmeliet, P. (2003). Angiogenesis in health and disease. *Nat. Med.* 9, 653–660.

Carmeliet, P., and Jain, R. K. (2011). Molecular mechanisms and clinical applications of angiogenesis. *Nature* 473, 298–307. doi: 10.1038/nature10144

Chen, M., Cao, Y., Dong, D., Zhang, Z., Zhang, Y., Chen, J., et al. (2019). Regulation of mitotic spindle orientation by phosphorylation of end binding protein 1. *Exp. Cell Res.* 384, 111618. doi: 10.1016/j.yexcr.2019.111618

Chen, M., Wang, J., Yang, Y., Zhong, T., Zhou, P., Ma, H., et al. (2020). Redox-dependent regulation of end-binding protein 1 activity by glutathionylation. *Sci. China Life Sci.*

Costa, G., Harrington, K. I, Lovegrove, H. E., Page, D. J., Chakravartula, S., Bentley, K., et al. (2016). Asymmetric division coordinates collective cell migration in angiogenesis. *Nat. Cell Biol.* 18, 1292–1301. doi: 10.1038/ncb3443

Costa, G., Lovegrove, H. E., and Herbert, S. P. (2017). Endothelial cells divide unequally to sprout fairly. *Cell Cycle* 16, 595–596. doi: 10.1080/15384101.2017.1294942

Cuevas, P., and Asin-Cardiel, E. (2000). Electromagnetic therapeutic angiogenesis: the next step. *Neurol. Res.* 22, 349–350. doi: 10.1080/01616412.2000.11740682

Cunha, F., Rajnicek, A. M., and McCaig, C. D. (2019). Electrical stimulation directs migration, enhances and orients cell division and upregulates the chemokine receptors CXCR4 and CXCR2 in endothelial cells. *J. Vasc. Res.* 56, 39–53. doi: 10.1159/000495311

di Pietro, F., Echard, A., and Morin, X. (2016). Regulation of mitotic spindle orientation: an integrated view. *EMBO Rep.* 17, 1106–1130. doi: 10.15252/embr.201642292

Flentje, A., Kalsi, R., and Monahan, T. S. (2019). Small GTPases and their role in vascular disease. *Int. J. Mol. Sci.* 20:917. doi: 10.3390/ijms20040917

Gerhardt, H., Golding, M., Fruttiger, M., Ruhrberg, C., Lundkvist, A., Abramsson, A., et al. (2003). VEGF guides angiogenic sprouting utilizing endothelial tip cell filopodia. *J. Cell Biol.* 161, 1163–1177. doi: 10.1083/jcb.200302047

Hartnett, M. E., Martiniuk, D., Byfield, G., Geisen, P., Zeng, G., and Bautch, V. L. (2008). Neutralizing VEGF decreases tortuosity and alters endothelial cell division orientation in arterioles and veins in a rat model of ROP: relevance to plus disease. *Invest. Ophthalmol. Vis. Sci.* 49, 3107–3114. doi: 10.1167/iovs.08-1780

Herbert, S. P., and Stainier, D. Y. (2011). Molecular control of endothelial cell behaviour during blood vessel morphogenesis. *Nat. Rev. Mol. Cell Biol.* 12, 551–564. doi: 10.1038/nrm3176

Hogan, B. M., and Schulte-Merker, S. (2017). How to plumb a pisces: understanding vascular development and disease using zebrafish embryos. *Dev. Cell* 42, 567–583. doi: 10.1016/j.devcel.2017.08.015

Holmes, W. E., Lee, J., Kuang, W. J., Rice, G. C., and Wood, W. I. (1991). Structure and functional expression of a human interleukin-8 receptor. *Science* 253, 1278–1280.

Jaffe, A. B., Kaji, N., Durgan, J., and Hall, A. (2008). Cdc42 controls spindle orientation to position the apical surface during epithelial morphogenesis. *J. Cell Biol.* 183, 625–633. doi: 10.1083/jcb.200807121

Jeong, G. J., Oh, J. Y., Kim, Y. J., Bhang, S. H., Jang, H. K., Han, J., et al. (2017). Therapeutic angiogenesis via solar cell-facilitated electrical stimulation. *ACS Appl. Mater. Interfaces* 9, 38344–38355. doi: 10.1021/acsami.7b13322

Jin, Y., Liu, Y., Lin, Q., Li, J., Druso, J. E., Antonyak, M. A., et al. (2013). Deletion of Cdc42 enhances ADAM17-mediated vascular endothelial growth factor receptor 2 shedding and impairs vascular endothelial cell survival and vasculogenesis. *Mol. Cell. Biol.* 33, 4181–4197. doi: 10.1128/mcb.00650-13

Koon, Y. L., Zhang, S., Rahmat, M. B., Koh, C. G., and Chiam, K. H. (2018). Enhanced delta-notch lateral inhibition model incorporating intracellular notch heterogeneity and tension-dependent rate of delta-notch binding that reproduces sprouting angiogenesis patterns. *Sci. Rep.* 8:9519.

Kschonsak, Y. T., and Hoffmann, I. (2018). Activated ezrin controls MISP levels to ensure correct NuMA polarization and spindle orientation. *J. Cell Sci.* 131:jcs214544. doi: 10.1242/jcs.214544

Laviña, B., Castro, M., Niaudet, C., Cruys, B., Álvarez-Aznar, A., Carmeliet, P., et al. (2018). Defective endothelial cell migration in the absence of Cdc42 leads to capillary-venous malformations. *Development* 145:dev161182. doi: 10.1242/dev.161182

Leclair, H. M., Dubois, S. M., Azzi, S., Dwyer, J., Bidère, N., and Gavard, J. (2014). Control of CXCR2 activity through its ubiquitination on K327 residue. *BMC Cell Biol.* 15:38. doi: 10.1186/s12860-014-0038-0

Li, J., Cheng, L., and Jiang, H. (2019). Cell shape and intercellular adhesion regulate mitotic spindle orientation. *Mol. Biol. Cell* 30, 2458–2468. doi: 10.1091/mbc.e19-04-0227

Li, S., Xu, H. X., Wu, C. T., Wang, W. Q., Jin, W., Gao, H. L., et al. (2019). Angiogenesis in pancreatic cancer: current research status and clinical implications. *Angiogenesis* 22, 15–36. doi: 10.1007/s10456-018-9645-2

Liro, M. J., and Rose, L. S. (2016). Mitotic spindle positioning in the EMS cell of *Caenorhabditis elegans* requires LET-99 and LIN-5/NuMA. *Genetics* 204, 1177–1189. doi: 10.1534/genetics.116.192831

Lu, M. S., and Johnston, C. A. (2013). Molecular pathways regulating mitotic spindle orientation in animal cells. *Development* 140, 1843–1856. doi: 10.1242/dev.087627

Luo, Y., Ran, J., Xie, S., Yang, Y., Chen, J., Li, S., et al. (2016). ASK1 controls spindle orientation and positioning by phosphorylating EB1 and stabilizing astral microtubules. *Cell Discov.* 2:16033.

Lv, J., Zeng, J., Guo, F., Li, Y., Xu, M., Cheng, Y., et al. (2018). Endothelial Cdc42 deficiency impairs endothelial regeneration and vascular repair after inflammatory vascular injury. *Respir. Res.* 19:27.

Lv, Z., Rosenbaum, J., Mohr, S., Zhang, X., Kong, D., Preiss, H., et al. (2020). The emergent yo-yo movement of nuclei driven by cytoskeletal remodeling in pseudo-synchronous mitotic cycles. *Curr. Biol.* 30, 2564.e5–2573.e5.

Ma, N., and Zhou, J. (2020). Functions of endothelial cilia in the regulation of vascular barriers. *Front. Cell Dev. Biol.* 8:626. doi: 10.3389/fcell.2020.00626

McCaig, C. D., and Zhao, M. (1997). Physiological electrical fields modify cell behaviour. *Bioessays* 19, 819–826. doi: 10.1002/bies.950190912

Melincovici, C. S., Boşca, A. B., Şuşman, S., Mărginean, M., Mihu, C., Istrate, M., et al. (2018). Vascular endothelial growth factor. (VEGF) - key factor in normal and pathological angiogenesis. *Rom. J. Morphol. Embryol.* 59, 455–467.

Mitsushima, M., Toyoshima, F., and Nishida, E. (2009). Dual role of Cdc42 in spindle orientation control of adherent cells. *Mol. Cell. Biol.* 29, 2816–2827. doi: 10.1128/mcb.01713-08

Morin, X., and Bellaïche, Y. (2011). Mitotic spindle orientation in asymmetric and symmetric cell divisions during animal development. *Dev. Cell* 21, 102–119. doi: 10.1016/j.devcel.2011.06.012

Nakajima, Y. I. (2018). Mitotic spindle orientation in epithelial homeostasis and plasticity. *J. Biochem.* 164, 277–284.

Neufeld, S., Planas-Paz, L., and Lammert, E. (2014). Blood and lymphatic vascular tube formation in mouse. *Semin. Cell Dev. Biol.* 31, 115–123. doi: 10.1016/j.semcdb.2014.02.013

Nishida, N., Yano, H., Nishida, T., Kamura, T., and Kojiro, M. (2006). Angiogenesis in cancer. *Vasc. Health Risk Manag.* 2, 213–219.

Potente, M., Gerhardt, H., and Carmeliet, P. (2011). Basic and therapeutic aspects of angiogenesis. *Cell* 146, 873–887. doi: 10.1016/j.cell.2011.08.039

Qin, J., Yang, Y., Gao, S., Liu, Y., Yu, F., Zhou, Y., et al. (2017). Deregulated ALG-2/HEBP2 axis alters microtubule dynamics and mitotic spindle behavior to stimulate cancer development. *J. Cell. Physiol.* 232, 3067–3076. doi: 10.1002/jcp.25754

Ragnarsson, K. T. (2008). Functional electrical stimulation after spinal cord injury: current use, therapeutic effects and future directions. *Spinal Cord* 46, 255–274. doi: 10.1038/sj.sc.3102091

Reinhard, N. R., Mastop, M., Yin, T., Wu, Y., Bosma, E. K., Gadella, T. W. J. Jr., et al. (2017). The balance between Gα(i)-Cdc42/Rac and Gα(1)(2)/(1)(3)-RhoA pathways determines endothelial barrier regulation by sphingosine-1-phosphate. *Mol. Biol. Cell* 28, 3371–3382. doi: 10.1091/mbc.e17-03-0136

Saadaoui, M., Konno, D., Loulier, K., Goiame, R., Jadhav, V., Mapelli, M., et al. (2017). Loss of the canonical spindle orientation function in the Pins/LGN homolog AGS3. *EMBO Rep.* 18, 1509–1520. doi: 10.15252/embr.201643048

Sajib, S., Zahra, F. T., Lionakis, M. S., German, N. A., and Mikelis, C. M. (2018). Mechanisms of angiogenesis in microbe-regulated inflammatory and neoplastic conditions. *Angiogenesis* 21, 1–14. doi: 10.1007/s10456-017-9583-4

Saman, H., Raza, S. S., Uddin, S., and Rasul, K. (2020). Inducing angiogenesis, a key step in cancer vascularization, and treatment approaches. *Cancers* 12:1172. doi: 10.3390/cancers12051172

Takayanagi, H., Hayase, J., Kamakura, S., Miyano, K., Chishiki, K., Yuzawa, S., et al. (2019). Intramolecular interaction in LGN, an adaptor protein that regulates mitotic spindle orientation. *J. Biol. Chem.* 294, 19655–19666. doi: 10.1074/jbc.ra119.011457

Tam, S. J., and Watts, R. J. (2010). Connecting vascular and nervous system development: angiogenesis and the blood-brain barrier. *Annu. Rev. Neurosci.* 33, 379–408. doi: 10.1146/annurev-neuro-060909-152829

Théry, M., and Bornens, M. (2006). Cell shape and cell division. *Curr. Opin. Cell Biol.* 18, 648–657. doi: 10.1016/j.ceb.2006.10.001

Ting Song, J. Z. (2020). Primary cilia in corneal development and disease. *Zool. Res.* 41, 495–502.

Wang, H., Yang, Z., Jiang, Y., and Hartnett, M. E. (2014). Endothelial NADPH oxidase 4 mediates vascular endothelial growth factor receptor 2-induced intravitreal neovascularization in a rat model of retinopathy of prematurity. *Mol. Vis.* 20, 231–241.

Wilkinson, R. N., and van Eeden, F. J. (2014). The zebrafish as a model of vascular development and disease. *Prog. Mol. Biol. Transl. Sci.* 124, 93–122. doi: 10.1016/b978-0-12-386930-2.00005-7

Wright, C. E., Kushner, E. J., Du, Q., and Bautch, V. L. (2015). LGN directs interphase endothelial cell behavior via the microtubule network. *PLoS One* 10:e0138763. doi: 10.1371/journal.pone.0138763

Xia, J., Swiercz, J. M., Bañón-Rodríguez, I., Matkoviæ, I., Federico, G., Sun, T., et al. (2015). Semaphorin-plexin signaling controls mitotic spindle orientation during epithelial morphogenesis and repair. *Dev. Cell.* 33, 299–313. doi: 10.1016/j.devcel.2015.02.001

Xie, S., Wu, Y., Hao, H., Li, J., Guo, S., Xie, W., et al. (2019). CYLD deficiency promotes pancreatic cancer development by causing mitotic defects. *J. Cell. Physiol.* 234, 9723–9732. doi: 10.1002/jcp.27658

Xie, W., Yang, Y., Gao, S., Song, T., Wu, Y., Li, D., et al. (2017). The tumor suppressor CYLD controls epithelial morphogenesis and homeostasis by regulating mitotic spindle behavior and adherens junction assembly. *J. Genet. Genomics* 44, 343–353. doi: 10.1016/j.jgg.2017.06.002

Xie, W., and Zhou, J. (2017). Regulation of mitotic spindle orientation during epidermal stratification. *J. Cell. Physiol.* 232, 1634–1639. doi: 10.1002/jcp.25750

Yadav, L., Puri, N., Rastogi, V., Satpute, P., and Sharma, V. (2015). Tumour angiogenesis and angiogenic inhibitors: a review. *J. Clin. Diagn. Res.* 9, Xe01–Xe05.

Yang, Y., Liu, M., Li, D., Ran, J., Gao, J., Suo, S., et al. (2014). CYLD regulates spindle orientation by stabilizing astral microtubules and promoting dishevelled-NuMA-dynein/dynactin complex formation. *Proc. Natl. Acad. Sci. U.S.A.* 111, 2158–2163. doi: 10.1073/pnas.1319341111

Zeng, G., Taylor, S. M., McColm, J. R., Kappas, N. C., Kearney, J. B., Williams, L. H., et al. (2007). Orientation of endothelial cell division is regulated by VEGF signaling during blood vessel formation. *Blood* 109, 1345–1352. doi: 10.1182/blood-2006-07-037952

Zhang, P., Liu, Z. T., He, G. X., Liu, J. P., and Feng, J. (2011). Low-voltage direct-current stimulation is safe and promotes angiogenesis in rabbits with myocardial infarction. *Cell Biochem. Biophys.* 59, 19–27. doi: 10.1007/s12013-010-9107-y

Zhao, M., Bai, H., Wang, E., Forrester, J. V., and McCaig, C. D. (2004). Electrical stimulation directly induces pre-angiogenic responses in vascular endothelial cells by signaling through VEGF receptors. *J. Cell Sci.* 117(Pt 3), 397–405. doi: 10.1242/jcs.00868

Zhao, Y. D., Huang, X., Yi, F., Dai, Z., Qian, Z., Tiruppathi, C., et al. (2014). Endothelial FoxM1 mediates bone marrow progenitor cell-induced vascular repair and resolution of inflammation following inflammatory lung injury. *Stem Cells* 32, 1855–1864. doi: 10.1002/stem.1690

Zhong, T., and Zhou, J. (2017). Orientation of the mitotic spindle in the development of tubular organs. *J. Cell. Biochem.* 118, 1630–1633. doi: 10.1002/jcb.25865

Zhu, J., Wen, W., Zheng, Z., Shang, Y., Wei, Z., Xiao, Z., et al. (2011). LGN/mInsc and LGN/NuMA complex structures suggest distinct functions in asymmetric cell division for the Par3/mInsc/LGN and Gαi/LGN/NuMA pathways. *Mol. Cell.* 43, 418–431. doi: 10.1016/j.molcel.2011.07.011

Conflict of Interest: The authors declare that the research was conducted in the absence of any commercial or financial relationships that could be construed as a potential conflict of interest.

frontiers in Cell and Developmental Biology

OPINION
published: 15 October 2020
doi: 10.3389/fcell.2020.589993

gRASping Depolarization: Contribution of RAS GTPases to Mitotic Polarity Clusters Resolution

Roberto Quadri, Sarah Sertic and Marco Muzi-Falconi**

Dipartimento di Bioscienze, Università degli Studi di Milano, Milan, Italy

Keywords: depolarization, Ras, mitosis, GTPase, phosphorylation, *Saccharomyces cerevisiae*

OPEN ACCESS

Edited by:
Benjamin Lin,
New York University, United States

Reviewed by:
Eurico Morais-de-Sá,
Universidade do Porto, Portugal

****Correspondence:***
Roberto Quadri
roberto.quadri@unimi.it
Marco Muzi-Falconi
marco.muzifalconi@unimi.it

Specialty section:
This article was submitted to Signaling, a section of the journal Frontiers in Cell and Developmental Biology

Received: *31 July 2020*
Accepted: *31 August 2020*
Published: *15 October 2020*

Citation:
Quadri R, Sertic S and Muzi-Falconi M (2020) gRASping Depolarization: Contribution of RAS GTPases to Mitotic Polarity Clusters Resolution. Front. Cell Dev. Biol. 8:589993. doi: 10.3389/fcell.2020.589993

INTRODUCTION

During their growth, all living cells undergo a process of polarization, defined as an asymmetric deposition and confinement of molecules and cellular functions. Much effort has been put into understanding how polarization is achieved and maintained and how it can be artificially induced, a field that has also been fueled by the fact that loss of polarity is a prerequisite for tumor development (Royer and Lu, 2011). This led to a vast comprehension of the mechanisms underlying polarity establishment and of the molecular components involved. On the other hand, we have limited knowledge on how polarity clusters are resolved when they are no longer necessary and what happens when this process fails. Here, we integrate our findings on polarity dispersion in budding yeast with literature evidence for a mitotic role of Ras proteins. We then propose a unifying view of how this GTPase might drive depolarization by direct recruitment of polarity factors.

DEALING WITH CELLULAR POLARIZATION

Polarization is a key event in cell life, as it allows the cell to compartmentalize the different features that are required for its growth, differentiation, and for the development of the whole organism. In all eukaryotes, polarity is controlled by the essential small GTPase Cdc42 (Etienne-Manneville, 2004), and cells direct polarized growth by spatial modulation of Cdc42 activity. A versatile tool to regulate the distribution of Cdc42-GTP in budding yeast is represented by the relocalization of its main GEF Cdc24 (Zheng et al., 1994; Caviston et al., 2002). In late G1, Cdc24 is found at the presumptive bud site, thus contributing to bud emergence; whereas in S and M phases, it accumulates at polarity clusters accounting for the growth of the daughter cell, before being sequestered in the nucleus in late mitosis (Nern and Arkowitz, 1999, 2000). Until now, most of the scientific efforts have focused on the way Cdc24 accumulation at the presumptive bud site drives bud emergence and growth. However, besides the relevance of polarity establishment, the polarization machinery must eventually be dispersed throughout mitosis to allow relocation of cellular factors and functions. We have reported a role for Haspin kinase in promoting depolarization in budding yeast. Exploiting haspin mutants, we have identified the consequences of failures in such process, which dooms the cells to death upon mitotic delays (Panigada et al., 2013). We recently built up on these data to identify the underlying pathway, unveiling the pivotal contribution played by Ras to the dispersion of polarity clusters (Quadri et al., 2020).

SHAPING THE CELL THROUGH GTP-Ras: EVIDENCE FROM Cdc24

Ras is a eukaryotic small GTPase with a prominent role in cell-cycle commitment. In particular, it integrates intracellular and extracellular signals (e.g., nutrient availability or growth factors) to trigger cellular proliferation (Stacey and Kazlauskas, 2002). Accordingly, hyperactivation of Ras pathway is frequently observed in tumors (Fernández-Medarde and Santos, 2011), where it drives the growth of the malignant mass and resistance to apoptosis (Cox and Der, 2003). As a consequence, this GTPase has long been studied with regard to its high relevance in cell proliferation and carcinogenesis (Murugan et al., 2019).

We have recently reported a novel contribution of Ras to mitotic depolarization in budding yeast cells (Quadri et al., 2020), where it acts as a part of a bipartite pathway differentially regulating localization of Cdc24 during the cell cycle. In early stages of the cell cycle, Cdc24 binds to Bem1 and Rsr1 at the presumptive bud site (Butty et al., 2002; Park et al., 2002), where it promotes clustered Cdc42 activity leading to bud emergence and growth (Woods et al., 2015). Highlighting the exclusive role played by Bem1 and Rsr1 in the budding process, *bem1*Δ*rsr1*Δ mutants are virtually unviable (Irazoqui et al., 2003) (with few exceptions that possibly reflect a minor contribution by other proteins; Smith et al., 2013; Woods et al., 2015). Later in mitosis, polarized Cdc24 has to be dispersed (Gulli et al., 2000; Quadri et al., 2020), causing the redistribution of Cdc42-GTP to the whole daughter PM. Failure of this process leads to a persistence of polarity clusters (Quadri et al., 2020), potential nuclear missegregation, and cell death (Panigada et al., 2013). Thus, a system that couples the formation and resolution of polarity clusters to cell-cycle progression must be present. A convenient mechanism would be a switch in binding partners of Cdc24 upon reversible cell-cycle–dependent posttranslational modifications. The idea of a dependence of Cdc24 localization on its PTMs was first proposed by Gulli et al. (2000). The article reports a strong preferential binding of Bem1 to hypophosphorylated Cdc24 and a Bem1-dependent bud tip hyperaccumulation of the GEF upon failures in its phosphorylation (Gulli et al., 2000). Consistently, Cdc24 phosphorylation peaks after bud emergence, and Cdc28-Cln and the PAK Cla4 were identified as the kinases responsible for such PTMs (Gulli et al., 2000; Bose et al., 2001; Wai et al., 2009; Rapali et al., 2017). However, until now, the change in localization of the GEF was seen as a mere dissociation from the bud tip in late stages of the cell cycle, and no roles for this process were described. We have recently shown that mitotic Cdc24 is actively redistributed from the bud tip to the whole daughter PM in a phosphorylation-dependent manner. Bem1 and Rsr1 are completely dispensable to this process, which rather relies on a direct physical interaction of Cdc24 with GTP-loaded Ras (Quadri et al., 2020), which is evenly distributed by vesicles to the PM in mitosis (Quadri et al., 2020). By relocalizing Cdc24, this pathway redistributes Cdc42 activity from the bud tip to the whole PM, ultimately promoting depolarization. When this mechanism is impaired, cells accumulate polarity factors at the bud tip that, in case of mitotic delays, leads to unbalanced nuclear segregation and cell death (Quadri et al., 2020). Following polarity clusters removal, at the time of cytokinesis, Cdc24 is dephosphorylated (Bose et al., 2001), likely disrupting Ras interaction and making it available for the next cell cycle.

Our findings integrate Gulli's hypothesis that mitotic phosphorylation of Cdc24 by Cla4 acts as a molecular switch to modulate its physical interactions. Accordingly, mitotic cells lacking Ras are characterized by a diffused, cytoplasmic Cdc24 with only a residual accumulation of the GEF at the bud tip (Quadri et al., 2020). This excludes a competition between Ras and Bem1/Rsr1 in favor of a change in the GEF interactors upon its phosphorylation. Noteworthy, Cdc24, Cdc42-GTP, Bem1, and Cla4 have been reported to constitute a positive feedback loop to build robust polarity clusters promoting symmetry breaking and bud emergence in G1 (Howell and Lew, 2012; Witte et al., 2017). However, our results (Quadri et al., 2020), along with previous findings (Gulli et al., 2000; Rapali et al., 2017), support a bipartite role of this complex, with a second, negative feedback loop promoting polarisome dispersal later in the cell cycle. The molecular switch that triggers Cla4 activity toward Cdc24 is still to be elucidated, but likely resides in a priming phosphorylation event on the GEF by a G2/M-specific kinase. An ideal candidate might be Clb-coupled Cdc28, as it promotes the switch from apical to isotropic growth (Lew and Reed, 1993), and mutants that fail to activate Cdc28-Clb kinase accumulate Bem1-bound Cdc24 at the bud tip (Gulli et al., 2000).

EXTENDING THE MODEL: A MITOTIC SIGNATURE FOR Ras-GTP BINDING AND CELLULAR DEPOLARIZATION IN YEAST

A similar system has been described to regulate the localization of Lte1, a putative GEF that takes a non-essential part in the mitotic exit network (Falk et al., 2011) and shows an impact on polarity in budding yeast (Geymonat et al., 2009, 2010). The pattern and mechanism regulating Lte1 distribution along the cell cycle exhibit remarkable analogies with those of Cdc24, possibly highlighting a common mean to drive mitotic relocalization of polarized proteins to the PM. Recruitment of Lte1 to the bud tip in early cell-cycle stages depends on a physical interaction with a polarisome component, Kel1 (Seshan et al., 2002; Gould et al., 2014). Similarly to Cdc24, Lte1 is phosphorylated by Cla4 and Clb-Cdc28 (Seshan and Amon, 2005; Geymonat et al., 2010), and overexpression of *CLA4* is sufficient to promote recruitment of Lte1 to the bud cortex in the absence of Kel1 (Seshan et al., 2002). This suggests that the phosphorylation of Lte1 acts as a molecular switch to promote binding to different cortex scaffolds. Accordingly, later works have shown that phosphorylation by Cdc28 and Cla4 primes Lte1 for direct physical interaction with GTP-Ras (Yoshida et al., 2003; Seshan and Amon, 2005; Geymonat et al., 2009, 2010), leading to its accumulation along the bud cortex. Similarly to Cdc24, at the end of mitosis dephosphorylation of Lte1 leads to its dispersion in the cytoplasm (Jensen et al., 2002; Seshan et al., 2002). Although the exact contribution of Lte1 to depolarization has not been unveiled, the observation that Lte1 mutants defective for Ras-binding experience hyperpolarized growth (Geymonat et al.,

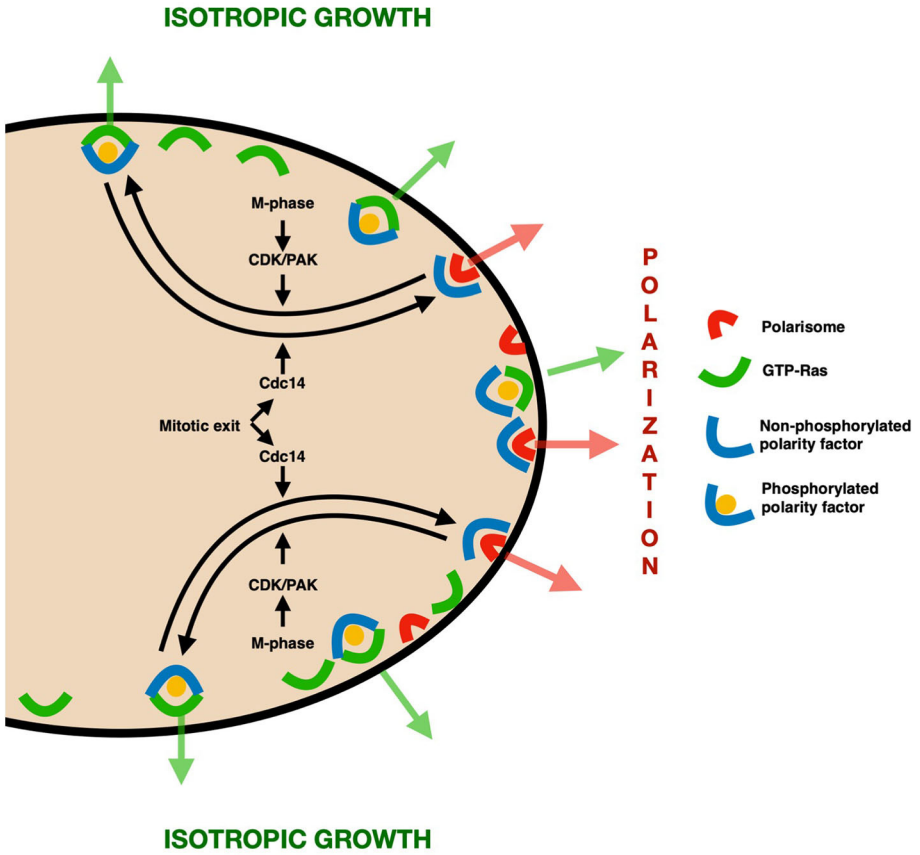

FIGURE 1 | Model—In the early stages of the cell cycle, bud emergence and growth are promoted through the accumulation of polarity factors (e.g., Cdc24 and Lte1) at the presumptive bud site and later on at the bud tip, thanks to physical interaction with polarisome components. At the time of G2/M phase, however, some of these proteins need to be redistributed to the whole daughter cortex to prevent the detrimental effects of hyperpolarization. This redistribution is regulated by Cdc-Clb/PAK–mediated phosphorylation of such polarity factors, which acts as a molecular switch to promote their binding to the evenly distributed GTP-Ras, thereby leading to isotropic growth. At the end of the cell cycle, the phosphatase Cdc14 removes the phosphate groups, replenishing the cellular pool of polarization-promoting proteins.

2010) highlights the role of the GTPase in promoting polarity cluster dissolution.

A common scheme thus emerges from these observations (**Figure 1**). Proteins (possibly bearing a GEF-like domain) that take part in polarization first accumulate at the presumptive bud site by physical interaction with components of the polarisome. By the time of mitosis, however, the polarity clusters have to be redistributed to promote an isotropic growth and prevent detrimental hyperpolarization. To this end, a convenient docking site is provided by GTP-loaded Ras, which is at this stage evenly distributed to the whole PM (Quadri et al., 2020). We propose that the molecular switch that regulates this change in interactions is represented by phosphorylation events performed by Clb-Cdc28 and the kinase Cla4, whose activity is coupled to late stages of the cell cycle, thus preventing unscheduled depolarization. At the end of the cell cycle, mitotic phosphorylation is removed by Cdc14, detaching polarisome components from GTP-Ras and making them available for a new cell cycle.

Ras CONTRIBUTION TO CELL SHAPE IN OTHER ORGANISMS

All the components of the pathway described in *Saccharomyces cerevisiae*, namely, Ras, Cdc42, and its GEFs and PAK, are conserved throughout the eukaryotic lineage. Several lines of evidence suggest that similar mechanisms might promote mitotic depolarization in other eukaryotes.

Links between Ras and polarity have been reported in *Schizosaccharomyces pombe* and *Cryptococcus neoformans* (Chang et al., 1994; Nichols et al., 2007), where a physical interaction between GTP-Ras and Cdc24 has been observed. However, although hyperpolarization has been observed in Ras mutants (Ballou et al., 2013), the GTPase seems to be mainly related to polarity establishment rather than to the resolution of polarity clusters.

A major difference between interphase and most mitotic animal cells is represented by the loss of cellular protrusions, substrate attachments, and cell–cell interactions observed during

mitotic roundup (Théry and Bornens, 2008). In this scenario, Cdc42 is required to regulate the actin cytoskeleton and determine mitotic spindle orientation, which in turn will define the polarity axis of the daughter cells (Jaffe et al., 2008). Although the underlying mechanisms are still to be elucidated, alterations in Ras pathway impact on spindle orientation (Tang et al., 2011). Moreover, multiple high-throughput screenings identified physical interactions between RAS and CDC42 regulators and effectors (Adhikari and Counter, 2018; Steklov et al., 2018; Kovalski et al., 2019), including several RHO GEFs with putative activity for CDC42, although none of these have been validated yet.

On the other hand, the idea that mitotic redistribution of Cdc42 activity drives cellular depolarization is backed by multiple observations. Indeed, several studies highlight a loss of cellular polarity upon increased Cdc42 activity in multiple systems (Florian et al., 2012; Gao et al., 2019). Although it is not clear whether the observed phenotype is induced by an active depolarization mechanism or a deficient polarization machinery, this clearly demonstrates that a diffuse Cdc42 activity might be a mean to counteract cellular polarization. Moreover, a previous work in *Drosophila melanogaster* reported a redistribution Cdc42 to achieve a homogenous PM localization in mitosis (Rosa et al., 2015). The authors also reported that overexpression of the Pbl Cdc42 GEF leads to a diffuse relocalization of a Cdc42-containing polarity complex in non-mitotic cells, suggestive of a GEF-based mechanism to induce cellular depolarization in this stage of the cell cycle.

Although such evidence does not directly infer the existence of a mechanism for depolarization based on Ras-dependent mitotic redistribution of Cdc42 activity, it suggests that a similar network might be present also in other eukaryotes.

Mitotic cellular depolarization results from the integration of multiple pathways that ensure proper cell division and that share some remarkable features with the proposed Ras-based mechanism. The planar cell polarity (PCP) is a network active in epithelial cells that detects environmental cues and transduces them in a tissue-homogeneous planar polarization (Butler and Wallingford, 2017). The establishment of this polarity axis is granted in interphase by a differential accumulation of PCP components at opposite domains with distinct functions. However, during mitosis, PCP clusters must be resolved to avoid disruption of tissue polarity (Devenport et al., 2011). This process is promoted by the mitotic kinase Plk1, which phosphorylates the PCP subunit Celsr1 (Shrestha et al., 2015), priming it for internalization by endocytosis (Devenport et al., 2011; Heck and Devenport, 2017). Thus, it appears that phosphorylation of polarity factors by mitotic kinases and vesicle-driven mechanisms might be a conserved way to couple cell-cycle progression with resolution of polarity clusters. Additional studies will be required to elucidate this possibility and to dissect the contribution of Ras to mitotic depolarization in higher eukaryotes, eventually lighting a path for further Ras targeting to tackle cancer progression.

AUTHOR CONTRIBUTIONS

RQ and MM-F interpreted the data and wrote the paper. SS contributed to data interpretation and discussions. All authors contributed to the article and approved the submitted version.

FUNDING

Research in MM-F lab was supported by AIRC (15631 and 21806), Telethon (GGP15227), MIUR. RQ was supported by an AIRC fellowship (17919).

ACKNOWLEDGMENTS

We thank Federico Lazzaro and all the members of the laboratory for critical discussions.

REFERENCES

Adhikari, H., and Counter, C. M. (2018). Interrogating the protein interactomes of RAS isoforms identifies PIP5K1A as a KRAS-specific vulnerability. *Nat. Commun.* 9:3646. doi: 10.1038/s41467-018-05692-6

Ballou, E. R., Kozubowski, L., Nichols, C. B., and Alspaugh, J. A. (2013). Ras1 Acts through duplicated Cdc42 and Rac proteins to regulate morphogenesis and pathogenesis in the human fungal pathogen *Cryptococcus neoformans*. *PLoS Genet.* 9:e1003687. doi: 10.1371/journal.pgen.1003687

Bose, I., Irazoqui, J. E., Moskow, J. J., Bardes, E. S. G., Zyla, T. R., and Lew, D. J. (2001). Assembly of scaffold-mediated complexes containing Cdc42p, the exchange factor Cdc24p, and the effector Cla4p required for cell cycle-regulated phosphorylation of Cdc24p. *J. Biol. Chem.* 276, 7176–7186. doi: 10.1074/jbc.M010546200

Butler, M. T., and Wallingford, J. B. (2017). Planar cell polarity in development and disease. *Nat. Rev. Mol. Cell Biol.* 18, 375–388. doi: 10.1038/nrm.2017.11

Butty, A. C., Perrinjaquet, N., Petit, A., Jaquenoud, M., Segall, J. E., Hofmann, K., et al. (2002). A positive feedback loop stabilizes the guanine-nucleotide exchange factor Cdc24 at sites of polarization. *EMBO J.* 21, 1565–1576. doi: 10.1093/emboj/21.7.1565

Caviston, J. P., Tcheperegine, S. E., and Bi, E. (2002). Singularity in budding: a role for the evolutionarily conserved small GTPase Cdc42p. *Proc. Natl. Acad. Sci. U.S.A.* 99, 12185–12190. doi: 10.1073/pnas.182370299

Chang, E. C., Barr, M., Wang, Y., Jung, V., Xu, H. P., and Wigler, M. H. (1994). Cooperative interaction of *S. pombe* proteins required for mating and morphogenesis. *Cell* 79, 131–141. doi: 10.1016/0092-8674(94)90406-5

Cox, A. D., and Der, C. J. (2003). The dark side of Ras: regulation of apoptosis. *Oncogene* 22, 8999–9006. doi: 10.1038/sj.onc.1207111

Devenport, D., Oristian, D., Heller, E., and Fuchs, E. (2011). Mitotic internalization of planar cell polarity proteins preserves tissue polarity. *Nat. Cell Biol.* 13, 893–902. doi: 10.1038/ncb2284

Etienne-Manneville, S. (2004). Cdc42–the centre of polarity. *J. Cell Sci.* 117, 1291–1300. doi: 10.1242/jcs.01115

Falk, J. E., Chan, L. Y., and Amon, A. (2011). Lte1 promotes mitotic exit by controlling the localization of the spindle position checkpoint kinase Kin4. *Proc. Natl. Acad. Sci. U.S.A.* 108, 12584–12590. doi: 10.1073/pnas.1107784108

Fernández-Medarde, A., and Santos, E. (2011). Ras in cancer and developmental diseases. *Genes Cancer* 2, 344–358. doi: 10.1177/1947601911411084

Florian, M. C., Dörr, K., Niebel, A., Daria, D., Schrezenmeier, H., Rojewski, M., et al. (2012). Cdc42 activity regulates hematopoietic stem cell aging and rejuvenation. *Cell Stem Cell* 10, 520–550. doi: 10.1016/j.stem.2012.04.007

Gao, J., Yu, H., Bai, X., Liu, C., Chen, L., Belguise, K., et al. (2019). Loss of cell polarity regulated by PTEN/Cdc42 enrolled in the process of Hepatopulmonary Syndrome. *J. Cell. Mol. Med.* 23, 5542–5552. doi: 10.1111/jcmm.14437

Geymonat, M., Spanos, A., De Bettignies, G., and Sedgwick, S. G. (2009). Lte1 contributes to Bfa1 localization rather than stimulating nucleotide exchange by Tem1. *J. Cell Biol.* 187, 497–511. doi: 10.1083/jcb.200905114

Geymonat, M., Spanos, A., Jensen, S., and Sedgwick, S. G. (2010). Phosphorylation of Lte1 by Cdk prevents polarized growth during mitotic arrest in *S. cerevisiae*. *J. Cell Biol.* 191, 1097–1112. doi: 10.1083/jcb.201005070

Gould, C. J., Chesarone-Cataldo, M., Alioto, S. L., Salin, B., Sagot, I., and Goode, B. L. (2014). *Saccharomyces cerevisiae* Kelch proteins and Bud14 protein form a stable 520-kDa formin regulatory complex that controls actin cable assembly and cell morphogenesis. *J. Biol. Chem.* 289, 18290–18301. doi: 10.1074/jbc.M114.548719

Gulli, M. P., Jaquenoud, M., Shimada, Y., Niederhäuser, G., Wiget, P., and Peter, M. (2000). Phosphorylation of the Cdc42 exchange factor Cdc24 by the PAK-like kinase Cla4 may regulate polarized growth in yeast. *Mol. Cell* 6, 1155–1167. doi: 10.1016/S1097-2765(00)00113-1

Heck, B. W., and Devenport, D. (2017). Trans-endocytosis of planar cell polarity complexes during cell division. *Curr. Biol.* 27, 3725–3733. doi: 10.1016/j.cub.2017.10.053

Howell, A. S., and Lew, D. J. (2012). Morphogenesis and the cell cycle. *Genetics* 190, 51–77. doi: 10.1534/genetics.111.128314

Irazoqui, J. E., Gladfelter, A. S., and Lew, D. J. (2003). Scaffold-mediated symmetry breaking by Cdc42p. *Nat. Cell Biol.* 5, 1062–1070. doi: 10.1038/ncb1068

Jaffe, A. B., Kaji, N., Durgan, J., and Hall, A. (2008). Cdc42 controls spindle orientation to position the apical surface during epithelial morphogenesis. *J. Cell Biol.* 183, 625–633. doi: 10.1083/jcb.200807121

Jensen, S., Geymonat, M., Johnson, A. L., Segal, M., and Johnston, L. H. (2002). Spatial regulation of the guanine nucleotide exchange factor Lte1 in *Saccharomyces cerevisiae*. *J. Cell Sci.* 115, 4977–4991. doi: 10.1242/jcs.00189

Kovalski, J. R., Bhaduri, A., Zehnder, A. M., Neela, P. H., Che, Y., Wozniak, G. G., et al. (2019). The functional proximal proteome of oncogenic Ras includes mTORC2. *Mol. Cell* 73, 830–844. doi: 10.1016/j.molcel.2018.12.001

Lew, D. J., and Reed, S. I. (1993). Morphogenesis in the yeast cell cycle: regulation by Cdc28 and cyclins. *J. Cell Biol.* 120, 1305–1320. doi: 10.1083/jcb.120.6.1305

Murugan, A. K., Grieco, M., and Tsuchida, N. (2019). RAS mutations in human cancers: roles in precision medicine. *Semin. Cancer Biol.* 59, 23–35. doi: 10.1016/j.semcancer.2019.06.007

Nern, A., and Arkowitz, R. A. (1999). A Cdc24p-Far1p-G beta gamma protein complex required for yeast orientation during mating. *J. Cell Biol.* 144, 1187–1202. doi: 10.1083/jcb.144.6.1187

Nern, A., and Arkowitz, R. A. (2000). Nucleocytoplasmic shuttling of the Cdc42p exchange\rFactor Cdc24p. *J. Cell Biol.* 148, 1115–1122. doi: 10.1083/jcb.148.6.1115

Nichols, C. B., Perfect, Z. H., and Alspaugh, J. A. (2007). A Ras1-Cdc24 signal transduction pathway mediates thermotolerance in the fungal pathogen Cryptococcus neoformans. *Mol. Microbiol.* 63, 1118–1130. doi: 10.1111/j.1365-2958.2006.05566.x

Panigada, D., Grianti, P., Nespoli, A., Rotondo, G., Gallo Castro, D., Quadri, R., et al. (2013). Yeast haspin kinase regulates polarity cues necessary for mitotic spindle positioning and is required to tolerate mitotic arrest. *Dev. Cell* 26, 1–13. doi: 10.1016/j.devcel.2013.07.013

Park, H., Kang, P. J., and Rachfal, A. W. (2002). Localization of the Rsr1/Bud1 GTPase involved in selection of a proper growth site in yeast. *J. Biol. Chem.* 277, 26721–26724. doi: 10.1074/jbc.C200245200

Quadri, R., Galli, M., Galati, E., Rotondo, G., Gallo, G. R., Panigada, D., et al. (2020). Haspin regulates Ras localization to promote Cdc24-driven mitotic depolarization. *Cell Discov.* 6:42. doi: 10.1038/s41421-020-0170-2

Rapali, P., Mitteau, R., Braun, C., Massoni-Laporte, A., Ünlü, C., Bataille, L., et al. (2017). Scaffold-mediated gating of cdc42 signalling flux. *Elife* 6:e25257. doi: 10.7554/eLife.25257

Rosa, A., Vlassaks, E., Pichaud, F., and Baum, B. (2015). Ect2/Pbl Acts via Rho and polarity proteins to direct the assembly of an isotropic actomyosin cortex upon mitotic entry. *Dev. Cell* 32, 604–616. doi: 10.1016/j.devcel.2015.01.012

Royer, C., and Lu, X. (2011). Epithelial cell polarity: a major gatekeeper against cancer? *Cell Death Differ.* 18, 1470–1477. doi: 10.1038/cdd.2011.60

Seshan, A., and Amon, A. (2005). Ras and the Rho effector Cla4 collaborate to target and anchor Lte1 at the bud cortex. *Cell Cycle* 4, 940–946. doi: 10.4161/cc.4.7.1785

Seshan, A., Bardin, A. J., and Amon, A. (2002). Control of Lte1 localization by cell polarity determinants and Cdc14. *Curr. Biol.* 12, 2098–2110. doi: 10.1016/S0960-9822(02)01388-X

Shrestha, R., Little, K. A., Tamayo, J. V., Li, W., Perlman, D. H., and Devenport, D. (2015). Mitotic control of planar cell polarity by polo-like kinase 1. *Dev. Cell* 33, 522–534. doi: 10.1016/j.devcel.2015.03.024

Smith, S. E., Rubinstein, B., Pinto, I. M., Slaughter, B. D., Unruh, J. R., and Li, R. (2013). Independence of symmetry breaking on Bem1-mediated autocatalytic activation of Cdc42. *J. Cell Biol.* 202, 1091–1106. doi: 10.1083/jcb.201304180

Stacey, D., and Kazlauskas, A. (2002). Regulation of Ras signaling by the cell cycle. *Curr. Opin. Genet. Dev.* 12, 44–46. doi: 10.1016/S0959-437X(01)00262-3

Steklov, M., Pandolfi, S., Baietti, M. F., Batiuk, A., Carai, P., Najm, P., et al. (2018). Mutations in LZTR1 drive human disease by dysregulating RAS ubiquitination. *Science* 362, 1177–1182. doi: 10.1126/science.aap7607

Tang, N., Marshall, W. F., McMahon, M., Metzger, R. J., and Martin, G. R. (2011). Control of mitotic spindle angle by the RAS-regulated ERK1/2 pathway determines lung tube shape. *Science* 333, 342–345. doi: 10.1126/science.1204831

Théry, M., and Bornens, M. (2008). Get round and stiff for mitosis. *HFSP J.* 2, 65–71. doi: 10.2976/1.2895661

Wai, S. C., Gerber, S. A., and Li, R. (2009). Multisite phosphorylation of the guanine nucleotide exchange factor Cdc24 during yeast cell polarization. *PLoS ONE* 4:e6563. doi: 10.1371/journal.pone.0006563

Witte, K., Strickland, D., and Glotzer, M. (2017). Cell cycle entry triggers a switch between two modes of Cdc42 activation during yeast polarization. *Elife* 6:e26722. doi: 10.7554/eLife.26722

Woods, B., Kuo, C. C., Wu, C. F., Zyla, T. R., and Lew, D. J. (2015). Polarity establishment requires localized activation of Cdc42. *J. Cell Biol.* 211, 19–26. doi: 10.1083/jcb.201506108

Yoshida, S., Ichihashi, R., and Tohe, A. (2003). Ras recruits mitotic exit regulator Lte1 to the bud cortex in budding yeast. *J. Cell Biol.* 161, 889–897. doi: 10.1083/jcb.200301128

Zheng, Y., Cerione, R., and Bender, A. (1994). Control of the yeast bud-site assembly GTPase Cdc42. Catalysis of guanine nucleotide exchange by Cdc24 and stimulation of GTPase activity by Bem3. *J. Biol. Chem.* 269, 2369–2372.

Conflict of Interest: The authors declare that the research was conducted in the absence of any commercial or financial relationships that could be construed as a potential conflict of interest.

frontiers in Cell and Developmental Biology

METHODS
published: 26 October 2020
doi: 10.3389/fcell.2020.598492

A Cell Adhesion-Based Reconstitution Method for Studying Cell Polarity

*Christopher A. Johnston**

Department of Biology, University of New Mexico, Albuquerque, NM, United States

Cell polarity is an evolutionarily conserved process of asymmetric spatial organization within cells and is essential to tissue structure, signal transduction, cell migration, and cell division. The establishment and maintenance of polarity typically involves extensive protein-protein interactions that can be made further intricate by cell cycle-dependent regulation. These aspects can make interpreting phenotypes within traditional *in vivo* genetic systems challenging due to pleiotropic effects in loss-of-function experiments. Minimal reconstitution methods offer investigators the advantage of stricter control of otherwise complex systems and allow for more direct assessment of the role of individual components to the process of interest. Here I provide a detailed protocol for a cell adhesion-based method of inducing cell polarity within non-polarized *Drosophila* S2 cells. This technique is simple, cost effective, moderate throughput, and amenable to RNAi-based loss-of-function studies. The ability to "plug-and-play" genes of interest allows investigators to easily assess the contribution of individual protein domains and post-translational modifications to their function. The system is ideally suited to test not only the requirement of individual components but also their sufficiency, and can provide important insight into the epistatic relationship among multiple components in a protein complex. Although designed for use within *Drosophila* cells, the general premise and protocol should be easily adapted to mammalian cell culture or other systems that may better suit the interests of potential users.

Keywords: cell polarity, spindle orientation, mitosis, reconstitution, neuroblast

OPEN ACCESS

Edited by:
Zhiyi Lv,
Ocean University of China, China

Reviewed by:
Shrivani Pirahas,
University of Calgary, Canada
Alexandra Schambony,
University of Erlangen Nuremberg, Germany
Luke McCaffrey,
McGill University, Canada

***Correspondence:**
Christopher A. Johnston
johnstca@unm.edu

Specialty section:
This article was submitted to Signaling, a section of the journal Frontiers in Cell and Developmental Biology

Received: *24 August 2020*
Accepted: *07 October 2020*
Published: *26 October 2020*

Citation:
Johnston CA (2020) A Cell Adhesion-Based Reconstitution Method for Studying Cell Polarity. Front. Cell Dev. Biol. 8:598492. doi: 10.3389/fcell.2020.598492

INTRODUCTION

Broadly defined, cell polarity can refer to any asymmetric assembly, organization, or segregation of cellular components. Polarity can involve different subcellular structures, including the cytoskeleton, organelles, and protein complexes at the cell membrane (referred to as "cortical polarity" herein). Cortical polarity involves segregation of protein complexes to discrete regions of the cell cortex, such as apical-basal polarity seen classically in epithelial cells as well as several other diverse cell types (Rodriguez-Boulan and Macara, 2014). One critical function of cortical polarity complexes, which will be the focus of my discussion herein, is directing the orientation of cell division by instructing the positioning of the mitotic spindle. Oriented cell divisions ensure that tissue architecture is properly maintained and also facilitates cell fate acquisition following

asymmetric stem cell divisions (Ragkousi and Gibson, 2014). In this paradigm, cortically polarized factors serve as positioning cues for the spindle, which is carried out by microtubule (MT)-associating factors within the polarity complexes. For example, in *Drosophila* neural stems cells (called neuroblasts, NBs) the spindle orientation complex is apically polarized and facilitates spindle positioning through interactions with the Dynein/Dynactin complex and the kinesin protein Khc-73, both direct MT-binding motor proteins (Lu and Johnston, 2013). Although the precise molecular details can differ, similar processes have been identified in epithelial cells of the developing wing disc and ovarium, as well as in the mammalian epidermis, gut epithelia, and developing neocortex (Dewey et al., 2015b; di Pietro et al., 2016). Thus, coupling of cortical polarity with spindle MTs is an evolutionarily conserved mechanism for orienting cell divisions during development.

Much of our knowledge regarding the components involved in this complex process has come from genetic mutants and knockdowns in model organism tissue. While these systems represent ideal models for examining the requirement of a particular gene, and the *in vivo* setting has imminent biological relevance, they are not without potential inherent disadvantages. For example, if the gene of interest is essential for viability of the organism it may not be possible to examine its effects at the desired developmental stage (although this can often be overcome through cell/tissue-specific knockdown strategies). Moreover, loss-of-function in one polarity component can often have deleterious consequences on the expression or localization of one or more other factors, leading to complications in phenotype interpretation. Such outcomes make it challenging to build accurate molecular models and to ascertain the sufficiency of one component or complex. Finally, genetic or functional redundancy in a system can mask otherwise important functions of a single mutated gene.

One way to overcome such drawbacks is through the use of minimal reconstitution systems. "Bottom-up" synthetic approaches offer users a simpler environment to observe complex processes while also providing them with greater experimental control over the construction and operation of the chosen system and its spatial-temporal dynamics (Thery, 2010; Kim et al., 2016; Carbone et al., 2017; Ganzinger and Schwille, 2019). This often results in unique molecular insights that synergize with knowledge obtained from traditional *in vivo* genetic experiments. Such approaches can range from cell-free *in vitro* reconstitutions to fabrication of a minimal network within simple cell culture model and can be used to study a diverse range of cellular processes. Cell polarity is an ideal process to study in a minimal system as it suffers from many of the caveats described above. In recent years, several methods have been developed that offer novel means of reconstituting polarity in non-polar environments (**Table 1**). Several approaches have also been developed for prokaryotic and simple eukaryotic yeast cells (Vendel et al., 2019). Here, I describe an "induced polarity" assay protocol used in cultured *Drosophila* S2 cells that utilizes the cell adhesion protein, Echinoid (Ed), to reconstitute cortical polarity in these otherwise non-polar cells (**Figure 1**; Johnston et al., 2009). The method is simple, time- and cost-effective, amenable to RNAi-based loss-of-function analysis, and can be easily adapted for use in other cell culture systems (di Pietro et al., 2017).

Ed is a key component of the adherens junction complex that, cooperating with DE-cadherin, controls cell-cell adhesion in *Drosophila* through homotypic, intercellular interactions (Wei et al., 2005). In addition to this structural role, Ed also functions in numerous intracellular signaling pathways that contribute to tissue development and dynamics (Shimono et al., 2012). The Ed domain architecture, shown in **Figure 1A**, is typified by a series of extracellular Immunoglobulin (Ig) and fibronectin (FN) adhesion domains, followed by a transmembrane insertion region and an intracellular C-terminal tail. This short intracellular tail is responsible for protein-protein interactions, most notably with the actin-associated factor Canoe (Afadin in mammals) (Wei et al., 2005; Sawyer et al., 2009). The method presented here capitalizes on this rather simple topology in two principal ways: (1) upon extracellular Ig domain-mediated adhesion, membrane-inserted Ed molecules redistribute specifically to cortical regions at the sites of cell-cell contact, and (2) a specific gene of interest is cloned in-frame with a truncated intracellular tail lacking interactions with other known polarity factors (**Figure 1B**). Together, these factors lead to the induction of Ed-mediated cortical polarity of ostensibly any protein of interest within non-polar S2 cells (**Figure 2**). Users can then design experiments that address specific research questions related to polarity or linked processes such as mitotic spindle orientation. This system is highly adaptable and should therefore be useful in reconstituting diverse polarity components that emulate diverse native systems, with *Drosophila* neuroblasts being an ideal example used for illustration and discussion herein (**Figure 2A**). Expression vectors are designed for simple, "plug-and-play" molecular cloning, and S2 cells are ideally suited for RNA interference (RNAi) loss-of-function screens (Rogers and Rogers, 2008). Overall, this system offers researchers a simple and rapid means of studying cell polarity that can complement studies in traditional genetic systems.

MATERIALS AND EQUIPMENT

Cell Culture

The protocol detailed below is specifically adapted for *Drosophila* Schneider 2 (S2) cells, a cell line originally isolated from late stage embryos thought to be derived from a macrophage-like origin (Schneider, 1972). S2 cells are grown and maintained in Schneider insect media (SIM; Invitrogen) supplemented with 10% fetal bovine serum at 25–29°C without the need for CO_2 humidification. Standard S2 cell stocks can be purchased from Invitrogen or the Drosophila Genomics Resource Center (DGRC;[1]), which also maintains additional lines stably expressing fluorescent markers for various cell structures (e.g., tubulin). Growth medium can be supplemented with penicillin-streptomycin, although this is not necessary in our experience and should be considered optional. As with other cell

[1]https://dgrc.bio.indiana.edu/Home

TABLE 1 | Comparison of various *in vitro* methods for reconstituting polarity.

Method	Utility	Notable examples of applications and key discoveries
Cell-free	Most minimal *in vitro* system using specific components selected by user in isolation. Specific concentrations of all components determined by user. Can assess direct interactions among components. Easily adapted to variety of microscopy approaches (e.g., TIRF).	Defining the role of spatial protein concentration gradients in cellular organization and cell division placement site ("Min System") (Zieske and Schwille, 2014). Determining the molecular organization and function of T-cell immunological synapse (Carbone et al., 2017) [*Also see* (James and Vale, 2012) *for a cell-based method*]. Delineating the role of actin-myosin dynamics in symmetry breaking during polarity initiation (Abu Shah and Keren, 2014).
Micropatterning	User-controlled cell shape dynamics. User-controlled extracellular environment, particularly related to mechano-sensitive signals and cell stiffness. Ability to alter and mimic diverse extracellular matrix patterns.	Determining the role of the extracellular matrix in oriented cell division (Thery et al., 2005). Defining how cell adhesion influences orientation of cell polarity axis (Thery et al., 2006). Identifying a role for cadherins in nuclear and centrosome positioning (Dupin et al., 2009). Defining how extracellular cues and cortical forces influence spindle orientation (Thery et al., 2007).
Optogenetic-based approaches	Highly configurable system to examine structure-function relationships. Ability to test both requirement and sufficiency of specific components. Ability to control both *spatial* and *temporal* aspects of polarization. Adaptable to live-cell imaging.	Identifying organization of cortical force generators and establishing their sufficiency in controlling spindle positioning in human cells (Okumura et al., 2018). Molecular dissection of spindle orientation in *C. elegans* (Fielmich et al., 2018). Probing cell cycle-dependent pathways sufficient to establish polarity in yeast (Witte et al., 2017).
Induced polarity	Similar to optogenetic systems but without specific need for light-sensitive protein fusions. Highly configurable, rapid, and cost-effective. Simple cell shaking protocol for inducing polarity. No requirements for advanced microscope or cell plating technologies.	Discovery of a phosphorylation-dependent Pins/Dlg spindle orientation pathway (Johnston et al., 2009), as well as additional novel regulatory mechanisms for Pins function (Wee et al., 2011; Mauser and Prehoda, 2012; Lu and Prehoda, 2013). Discovery of an actin-mediated spindle orientation pathway involved in Frizzled/Disheveled planar polarity (Johnston et al., 2013), as well as mapping interactions with Mud and Dlg effectors (Segalen et al., 2010; Garcia et al., 2014). Identification of actin regulators involved in spindle orientation in human cells (di Pietro et al., 2017).

culture systems, users should routinely monitor for *Mycoplasma* contamination using standard methods to avoid compromising validity of results (Roth et al., 2020).

RNAi Preparation

Another distinct advantage of S2 cells is their ability to take up dsRNA directly from media, which is subsequently processed into small interfering sequences avoiding the need to clone and transfect shRNA constructs (Rogers and Rogers, 2008). Rather, dsRNA can be directly transcribed *in vitro* using standard T7 RNA Polymerase with PCR-amplified dsDNA as a template. We typically use the MegaScript T7 synthesis kit (ThermoFisher), although many alternatives are available. Primer design is carried out using the SnapDragon dsRNA Design tool freely available at the Harvard DRSC/TRiP Functional Genomics Resource site[2]. Sequences are chosen based on predicted efficiency and specificity for the selected target, and can be designed in an isoform/spliceform-specific or -universal manner. All primers are then synthesized with 5′ T7 recognition sequences appended (5′-TAATACGACTCACTATAGGG-3′).

Immunostaining and Microscopy

Cells are plated on glass coverslips treated with poly-lysine to increase their adherence. S2 cells are relatively small (diameter of ∼10 μm) and can be further flattened by coating glass coverslips with the lectin molecule Concanavalin A (ConA). We typically use 12 mm diameter coverslips placed individually into 24-well culture dishes. Fixation conditions should be chosen based on individual experiment outcomes, but paraformaldehyde and ice-cold methanol are the most commonly used agents. Primary antibodies must be adapted to specific needs, and we typically use non-crossreactive secondary antibodies from Jackson ImmunoResearch or Invitrogen conjugated with desired fluorophores. Imaging is conducted using a standard fluorescence microscope, although the use of a confocal system may yield better imaging resolution overall. Representative S2 cell images presented below were acquired on an Olympus IX83 or Zeiss 780 m confocal.

Data Analysis

Data analysis is performed using the ImageJ software package[3]. For example, spindle positioning can be measured using the angle tool with vertices perpendicular to the midpoint of the Ed crescent and through the spindle midzone. Excel and GraphPad Prism are additional software programs ideally suited for further analysis and graphical output of the data.

[2]https://www.flyrnai.org/snapdragon

[3]https://imagej.nih.gov/ij/download.html

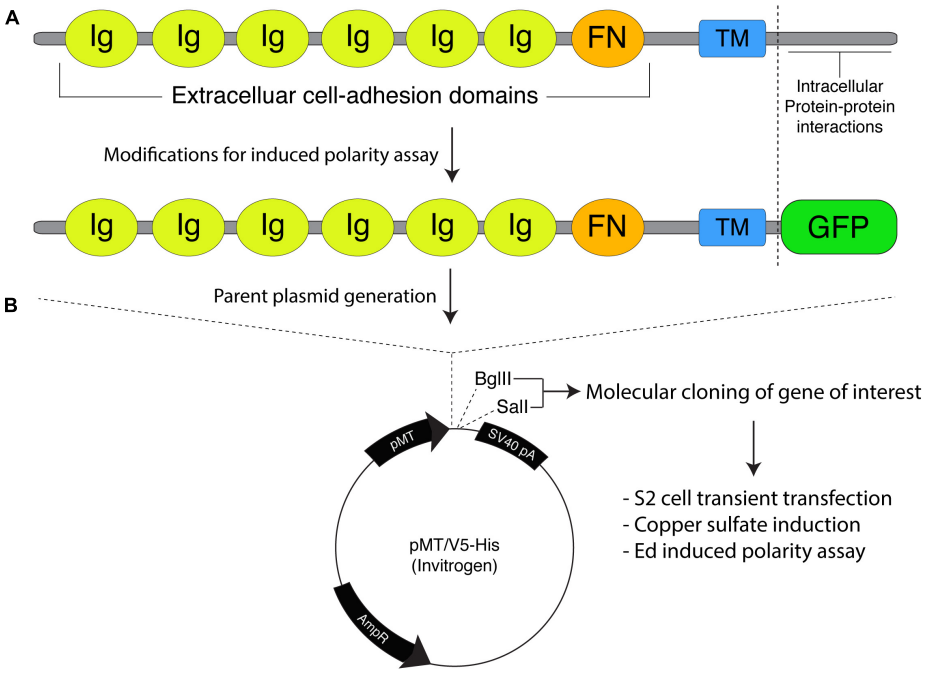

FIGURE 1 | Molecular framework for the Echinoid-based polarity reconstitution system. **(A) Top:** Domain architecture of the full-length Ed protein depicts an extracellular region containing several Immunoglobulin (Ig; yellow) and Fibronectin (FN; orange) cell adhesion domains that participate in formation of cell clusters. The transmembrane (TM; blue) region allows for insertion as an integral plasma membrane protein. The C-terminal tail (sequence following vertical dash line) resides intracellularly and is responsible for protein-protein interactions that participate in maintenance of adherens junction function and signaling. **Bottom:** Cloning of Ed for use in the induced polarity assay omits most of the intracellular tail to avoid interactions with known binding partners. This sequence is replaced with an in-frame green fluorescence protein (GFP; green) coding sequence. **(B)** The modified Ed:GFP sequence (with GFP replacing native C-terminal sequence) is cloned into the pMT/V5-His plasmid followed by 5′-*Bgl*II and 3′-*Sal*I cloning sites. Standard molecular cloning can easily generate Ed:GFP fusions to ostensibly any gene or sequence fragment the user wishes to examine. Cells are then transiently transfected with the cloned plasmid, and Ed:GFP fusion proteins are expressed using copper sulfate activation of the pMT promotor (see "Stepwise procedures").

STEPWISE PROCEDURES

Molecular Cloning of Ed Fusion Constructs

Expression of Ed fusion constructs in S2 cells is achieved using the copper inducible metallothionein promotor within the pMT expression vector (Thermo Fisher). Cloning and construction of pMT:Ed plasmids has been previously detailed (Johnston et al., 2009). We have generated plasmids that yield either GFP- or FLAG-tagged versions of the Ed fusion, with the general structure of Ed:GFP-X, where X represents the desired cloned gene of interest (**Figure 1**). Both plasmids are linearized using 5′-*Bgl*II and 3′-*Sal*I restriction digest, which can be ligated with identically digested inserts or those digested with isocaudameric enzymes such as 5′-*Bam*HI and 3′-*Xho*I. Cloning should be done using standard molecular techniques and verified using Sanger sequencing methods.

Transient Transfection of S2 Cells

One significant drawback to the use of S2 cells are their relatively low transfection efficiency compared with many other cell culture lines. However, liposome-based transfection reagents are still recommended as standard practice. We typically use Effectene (Qiagen), the protocol for which is described below, although many alternatives exist.

1. Seed S2 cells in 6-well dishes at a density of 1–2 × 10^6 cells in 2.5 mL of SIM.
2. Prepare Effectene-DNA mixtures according to manufacturer protocol. Cells are typically transfected with a total of 0.5–1 μg of total plasmid DNA.
3. Add transfection mixtures dropwise to respective wells and incubate for 24–48 h.

Note: For standard experiments proceed to step 4; for RNAi-based loss-of-function studies see next section for additional experimental steps.

4. Add 0.5 mM copper sulfate and incubate for an additional 24 h prior to proceeding to the Ed assay. Extending the induction time to 48 h may improve expression of larger Ed fusion constructs and should be optimized for individual genes being tested.

RNAi Preparation and Treatment (For Loss-of-Function Studies)

For studies examining the effects of specific gene knockdown, transfected cells are treated directly with dsRNA.

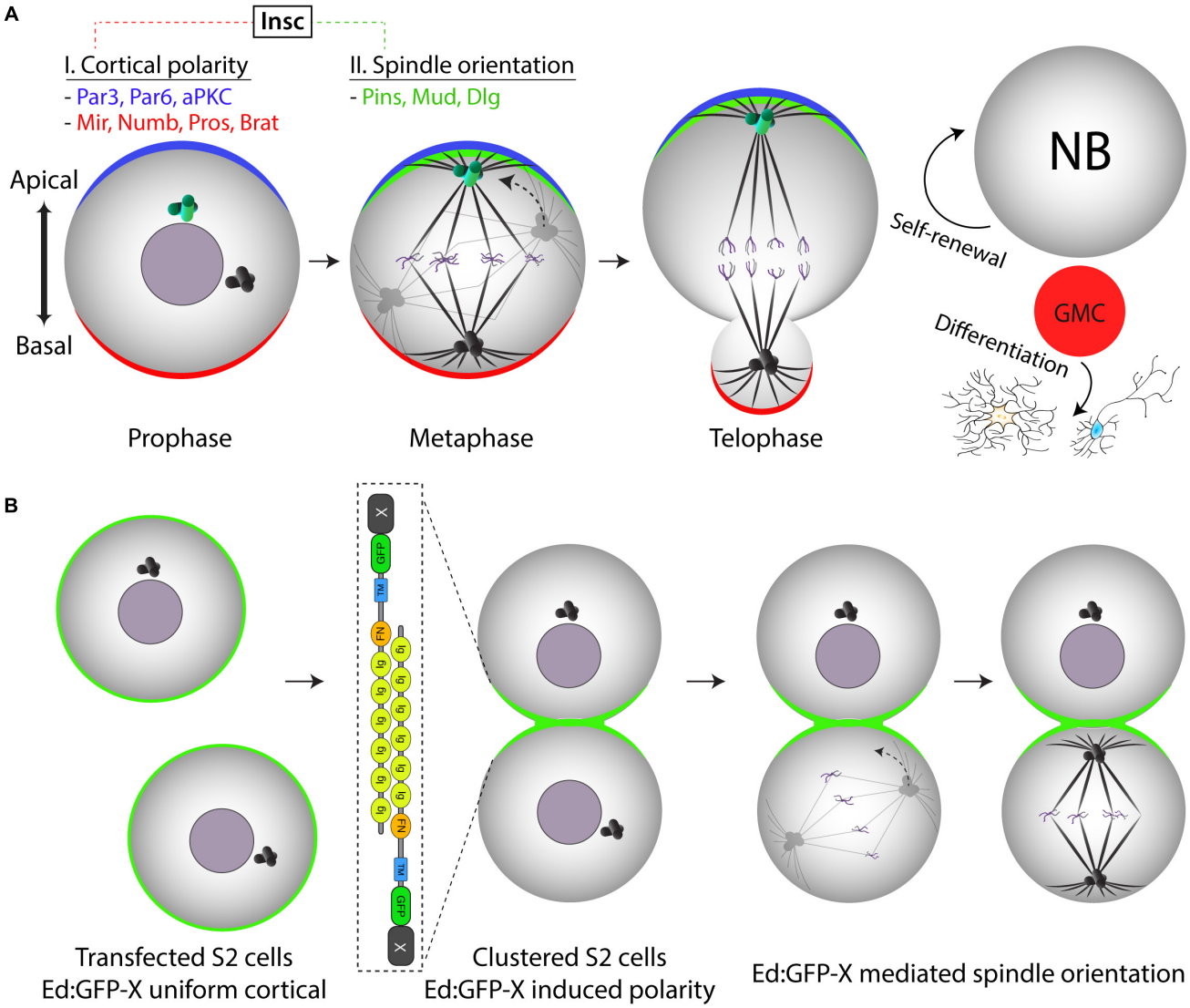

FIGURE 2 | Ed-induced polarity as a minimal reconstitution system to model *Drosophila* neural stem cell spindle orientation. **(A)** *Drosophila* neural stem cells (neuroblasts) establish apical-basal polarity in the early stages of mitosis. Both apical and basal polarity complexes (blue and red, respectively) consist of numerous components connected by a complex network of protein-protein interactions and regulatory relationships. At metaphase, the mitotic spindle aligns along this polarity axis through the activity of the apical Pins/Mud/Dlg spindle orientation complex (green). Mitosis proceeds through an asymmetric cell division that is essential for generating differentiated progeny (via the ganglion mother cell, GMC) while also maintaining the stem cell pool through self-renewal. **(B)** Illustration of how the Ed-induced polarity assay can model Pins-mediated spindle orientation in a minimal reconstituted system (i.e., "X" would represent Pins in this case). Isolated S2 cells initially express an Ed:GFP-X recombinant protein uniformly around the entire cell membrane. Shaking causes collisions that generate cell adhesions wherein cortical Ed:GFP-X proteins concentrate at sites of cell-cell contact within small clusters, the simplest of which is two adhered cells as shown. As cells enter and proceed through mitosis, spindle orientation can be measured relative to the Ed:GFP-X induced crescent similar to how one would with the native Pins crescent in the neuroblast. Note the simplification of this S2 cell system as compared with the complex environment established natively within NBs.

1. Centrifuge transfected cells (following step 3 above) for 3 min at 1,000 × *g*.
2. Resuspend cell pellets in serum free media (SFM) at 2×10^6 cells/mL.
3. Add 1 mL of resuspended cells to fresh wells of a 6-well dish.
4. Add desired dsRNA to respective wells. In our experience, 10 μg of dsRNA (dissolved in ∼100 μL of RNAase-free water) is sufficient for knockdown of most targets.
5. After 1 h incubation in SFM, add 2.5 mL of SIM and incubate for an additional 3–5 days.

Note: The amount of dsRNA and incubation times may need to be optimized for specific targets. Those listed above are a standard guideline.

6. Add 0.5 mM copper sulfate and incubate for an additional 24 h prior to proceeding to Ed polarity induction.

Inducing Ed-Based Cell Clusters

This protocol hinges upon the ability of transfected cells to form Ed-based adhesions that generate small (2–3 cells) clusters in which cortical Ed is redistributed and concentrated at sites of cell-cell contact (**Figures 2B**, **3A**). These cell clusters can easily be induced using the steps outlined below:

1. Prior to starting the Ed cell adhesion assay, place the desired number of glass coverslips in individual wells of a 24-well dish. Add 0.2 mL of poly-lysine solution and incubate at room temperature for 30–60 min. Aspirate and allow coverslips to dry for 1 h to overnight.

Note: To maximize collection of a suitable number of technical replicate measurements (typically ≥30) during imaging, it is recommended to prepare at least three coverslips for each condition.

2. When ready to begin, centrifuge transfected cells for 3 min at 1,000 × *g*.
3. Resuspend cell pellets in 3–4 mL of fresh serum-containing SIM supplemented with 0.5 mM copper sulfate.
4. Add cells to fresh wells of a 6-well dish. Agitate on a platform shaker at ∼250 rpm for 1–3 h at room temperature. Physical collisions among cells induces cell adhesions and cluster formation. While shaking times on the higher end of this scale may be needed for poorly transfected or expressing constructs, users should be cautious that longer shaking times may lead to formation of large clusters (>3 cells) that are typically not suitable for subsequent analysis (see description below).
5. Add 0.5 mL of fresh SIM to each coverslip-containing well of a 24-well dish. Add 0.25 mL of cells from step 4 to each well and allow to incubate at room temperature for 2 h. This incubation allows cells to firmly adhere to coverslips and begin to enter the cell cycle, increasing the percentage of cells in mitosis during subsequent fixation.

Fixation and Immunostaining

Fixation of S2 cells can be achieved by several methods. Formaldehyde and ice-cold methanol are fixatives typically used by most labs, and below are steps for the simpler formaldehyde-based approach.

1. Aspirate excess SIM from previous incubation step.
2. Gently add 0.5 mL of a 4% paraformaldehyde (PFA) solution in 1× PBS. Allow fixation to proceed for 15 min at room temperature.
3. Remove PFA and perform three quick washes with 0.5 mL of wash buffer (0.1% Triton-X100 in 1× PBS).
4. Following washes, permeabilize cells by incubating in wash buffer for 10 min.

Note: Permeabilization conditions may need to be optimized for specific antibodies. Triton X-100 concentrations of 0.1–0.5% and incubation times of 10–20 min should be adequate for most experiments.

5. Add block buffer (wash buffer supplemented with 1% BSA) and incubate for 1 h at room temperature.

Note: Users may find that alternative blocking agents, such as 5% goat serum, produce better results and are encourage to optimize blocking conditions for each specific experimental condition.

6. Dilute desired primary antibodies to appropriate concentrations in block buffer. For measuring spindle orientation, we typically use a rat anti-alpha-tubulin at 1:500 dilution (Abcam) to mark the spindle along with a rabbit anti-phosphohistone H3 (PH3) at 1:2000 dilution (ThermoFisher) to mark mitotic DNA. In our experience, natural GFP fluorescence is sufficient for visualizing Ed crescents, although users may consider addition of an anti-GFP antibody as well. Use of Ed:FLAG constructs requires the use of an anti-FLAG primary antibody (e.g., Sigma).
7. Add 0.2 mL primary antibody solution and incubate overnight at 4°C.
8. The next day, remove primary antibody solution and wash cells three times with block buffer.
9. Dilute desired secondary antibodies to appropriate concentrations in block buffer. Keep in mind that, if using Ed:GFP, polarity crescents will necessarily use the 488 nm (e.g., FITC) excitation filter channel. The use of Ed:FLAG allows for additional flexibility when choosing the conjugated fluorophore of the secondary antibody used against the anti-FLAG primary antibody.
10. Add 0.2 mL secondary antibody solution and incubate 1–2 h at room temperature.
11. Remove secondary antibody solution and wash cells three times with wash buffer.
12. Prepare microscope slides by adding a small drop of preferred mounting medium. We typically use VectaShield Hardset, but many alternatives are available. Use of DAPI-containing media should be considered as an alternative method of visualizing DNA, although this will not be specific for mitotic chromosomes.
13. Carefully remove coverslips from wells, dab dry, and mount with cells facing mounting solution.
14. Allow slides to dry for at least 1 h prior to imaging. If imaging on a later day, store slides at 4°C and protected from light.

Imaging: Rather than provide a detailed protocol suited for our specific microscopes, below are general steps and important considerations for imaging Ed-based cell clusters in experiments assessing mitotic spindle orientation.

1. After staging the slide on the microscope, begin searching for appropriate cell clusters suitable for imaging. In addition to their relatively low transfection efficiency, S2 cells also suffer from a lower mitotic index compared with many cell culture lines and, therefore, identifying clusters of transfected cells undergoing mitosis is most commonly

the bottleneck of the entire protocol. The following criteria are a guideline for selecting candidate cells:

- Clusters containing 2–3 cells are typically preferred. Clusters containing >3 cells often exhibit excessively wide Ed polarity crescents or multiple, non-continuous crescents per cell, both of which make accurate assessment of spindle positioning challenging or impossible. If cortical polarization of a potential cytoplasmic binding partner of the Ed-fused protein is the intended experimental outcome, rather than spindle orientation, such large clusters may still be suitable, however.
- The width of the Ed polarity should not exceed ∼30% of the cell circumference. This estimation reflects that of a typical *Drosophila* neuroblast, the native cell originally mimicked by this approach (**Figure 2A**; Johnston et al., 2009). However, this parameter should be considered *a priori* and adjusted accordingly based on the specific system that the user is attempting to reconstitute or emulate.

Note: S2 cells can naturally adhere to one another in an Ed-independent manner. In the case of one transfected cell adhering to a non-transfected cell, the Ed distribution in the transfected cell remains uniform cortical and not polarized. These can be easily distinguished from dual transfected, polarized cells and can be avoided in imaging experiments.

- For experiments measuring spindle orientation, cells with intact, bipolar spindles should be selected whenever possible to ensure accurate measurements. This criterion should also include cells in which the spindle is parallel to the slide surface and positioned at the approximate cell center. Cells with spindles significantly decentered should be avoided. Users should be especially cautious when selecting cells following RNAi treatment against genes that participate in spindle assembly, where bipolar spindles are not evident. In such cases, DAPI or PH3 staining of the congressed mitotic DNA may aid in analysis.
- For experiments assessing cell cycle-dependent endpoints, one should include markers of the desired stage for additional selection.

2. Focus the selected cell cluster such that both poles of the mitotic spindle are visible in the chosen focal plane.
3. Adjust other standard parameters (e.g., exposure time, laser intensity, pinhole opening, etc.), then capture and save image. Taking multiple images at evenly spaced z-stack depths may aid in resolving a slightly non-parallel spindle.
4. This process should be repeated for a number of technical replicates suitable for statistical power in data analysis. This is typically achieved with ∼30 replicate images. Biological replicates should then be obtained by repeating the experiment from the beginning of the protocol (e.g., cell transfection).

- *Note:* as mentioned above, image acquisition is most often the bottleneck of this protocol. To provide users a useful context in this regard, in our experience transfection efficiency of Ed fusions can approach ∼10%, with many of these cells ultimately forming productive clusters (a conservative estimation would be half, thus 5% of cells overall). The mitotic index of S2 cells is typically limited to 1–2%, leading to an overall fraction of cells that are transfected, forming useful polarity clusters, and undergoing mitosis at ∼0.1%. Treatment of cells with RNAi against Cdc27 can improve the mitotic index by accumulating metaphase cells (Goshima et al., 2007).
- Although not applied to this specific protocol, others have developed more advanced and high-throughput imaging and processing approaches. For example, RNAi-based screens have used automated imaging to assess genes required in spindle assembly (Goshima et al., 2007; Kwon et al., 2008). Khushi et al. (2017) recently developed an automated image analysis software for phenotypic descriptions of mitotic spindles. Finally, utilization of machine learning approaches may offer additional benefits to users with such expertise (Sommer and Gerlich, 2013).

Data Analysis

The specific method of data analysis should be tailored to the intended outcome metric. For brevity, a brief discussion of spindle orientation analysis is outlined below:

1. Open selected image with ImageJ software.
2. Measure the width of the Ed polarity crescent in mitotic cell and ensure it does not exceed ∼30% of the total cell circumference (or an alternative size determined by the user to best mimic the native system being reconstituted). Use this measurement to identify the center of the crescent.
3. Select the "Angle tool" from the tool selection window. This tool uses a 3-click input, with click-1 and -2 establishing the first vertex and click-3 defining the second of the angle.
4. Click on or directly above the midpoint of the Ed crescent and draw a line perpendicular and toward the cell center, which should be the approximate location of the spindle midzone. Click a second time here and then extend a line through the middle of the spindle toward the pole closer to either side of the Ed crescent. Click a third time to finish defining the desired angle and use the "Analyze > Measure" command. A separate window will appear with the measured angle listed.

Note: In this standard assay one cannot discriminate between the two centrosomes as with neuroblasts and other cell types (Roubinet and Cabernard, 2014). As such, the spindle pole proximal to the Ed crescent should be selected and the measured angle should never exceed 90°. In other words, a perfectly aligned spindle would measure 0°, and a perfectly misaligned spindle would measure 90°.

5. Repeat this process for all technical replicates.
6. Methods for plotting the data are at the user's discretion. Our style of choice is to plot the cumulative percentage of cells with spindle measuring ≤ a given angle (*y*-axis) as a function of spindle angle (*x*-axis). These calculations can be made in Excel using an ascending rank order of angles measured in steps 4–5.
7. Graphical representation is also a personal choice. Our program of choice is GraphPad Prism (**Figure 3D**).

ANTICIPATED RESULTS

We and others have used this procedure to both confirm *in vivo* results in a minimal system as well as a discovery tool for novel components of cell polarity and mitotic spindle orientation (Johnston et al., 2009, 2013; Dewey et al., 2015a; di Pietro et al., 2017). Presented here are representative results users can anticipate for a typical experiment examining known components of a conserved spindle positioning complex, that being the polarity protein Partner of Inscuteable (Pins; known as LGN in humans) and its direct binding partners Mushroom body defect (Mud; known as NuMA in humans) and Discs large (Dlg; also called SAP97 in humans). Cortically tethered Pins directs spindle orientation through these binding partners' association with the Dynein/Dynactin and KHC-73 kinesin microtubule motor complex complexes, respectively (Siegrist and Doe, 2005; Bowman et al., 2006; Siller et al., 2006; Johnston et al., 2009; Bergstralh et al., 2013). Loss-of-function in each of these components leads to spindle orientation defects in *Drosophila* neuroblasts as well as several other diverse cell types and organisms (**Figure 2A**). Untangling the underlying molecular mechanisms was facilitated greatly by the reconstitution system described herein (Johnston et al., 2009, 2013).

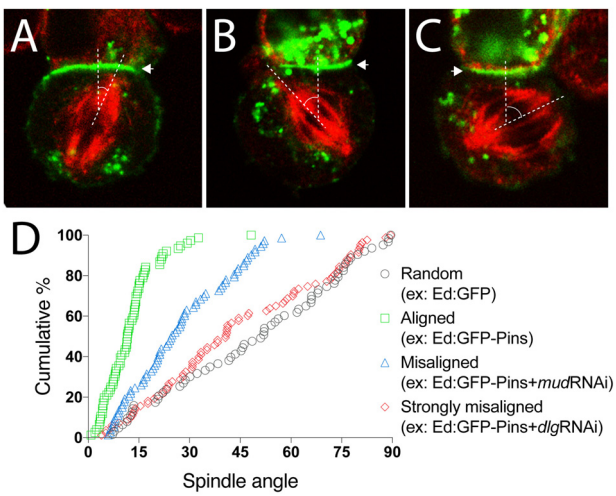

FIGURE 3 | Representative data for spindle orientation in the Ed-induced polarity system. **(A)** Representative image of a mitotic spindle (red) aligned under an Ed:GFP-X crescent (green; arrowhead). Dashed lines show vertices of spindle angle. Such result should be expected for Ed:GFP-Pins, for example. **(B)** Representative image of a misaligned spindle (red) relative to the Ed:GFP-X induced crescent. Dashed lines show vertices of spindle angle. **(C)** Representative image of a strongly misaligned spindle (red) relative to the Ed:GFP-X induced crescent. Dashed lines show vertices of spindle angle. **(D)** Plot of multiple technical and biological replicate spindle angle measurements for the indicated example conditions. Measurements are plotted as a function of the cumulative percentage of cells with an angle at or below a given angle. Random spindle angles measured in cells expressing Ed:GFP alone (gray circles) produces a line along the diagonal, whereas efficient spindle alignment in cells expressing Ed:GFP-Pins (green squares), for example, causes a steep, leftward deflection of this line. As an example of spindle misorientation, knockdown of Mud or Dlg (blue triangles and red diamonds, respectively), two effectors downstream of Pins, lead to different degrees of spindle misalignment.

Using Ed:GFP alone as a negative control, one should anticipate spindle orientation measurements evenly and randomly distributed between 0–90°. Plotting such results as cumulative percent of measurements as a function of spindle angle should produce a nearly linear line through the diagonal of the plot (**Figure 3D**). Additionally, calculating the mean of all measurements should yield ∼45° with a relatively large deviation due to the expected randomness of measurements.

When examining Ed:GFP-Pins, as a prototypical example, spindle orientation is biased toward the Ed-induced Pins polarity crescent center, similar to natively cortical Pins in neuroblasts (**Figure 2**), thus skewing measurements to small angles. Graphically, this leads to a steep and leftward shifted curve compared to the Ed:GFP alone as a greater percentage of cells accumulate within acute angles and few, if any, cells display grossly misoriented spindles with large angle measurements (**Figures 3A,D**). The resulting average spindle angle is ∼10° in a typical Ed:GFP-Pins experiment. In the event that a predicted spindle orientation factor does not produce these results, users should consider several possibilities. If the Ed-fused component being examined requires association with additional factors (e.g., Pins requires several downstream factors listed above) it is possible that S2 cells do not express these additionally required proteins. Several additional cultured *Drosophila* cells lines exist, are readily available for purchase[4], and transcriptomic analyses have shown differences in gene expression among them that might help identify an alternative system in this scenario (Cherbas et al., 2011). Similarly, if the component in question requires posttranslational modification, such as phosphorylation, it is possible that S2 cells do not express the necessary enzyme or signaling pathway. If the Ed-fused component requires specific structural features (e.g., oligomerization through sequences such as coiled-coil domains) it is possible that fusion to the Ed protein or its artificial tethering at the cell membrane does not allow such topology or assembly. Finally, it is possible that the component being tested is simply not sufficient to orient the spindle, even if cells express other binding factors.

Once a specific component has been found to orient mitotic spindles as an Ed fusion, users can design simple RNAi-mediated loss-of-function experiments to identify additional factors required for its function. For example, treatment with RNAi against Mud reduces the efficiency of spindle orientation to Ed:GFP-Pins crescents (**Figures 3B,D**),

[4]https://dgrc.bio.indiana.edu/cells/Catalog

a result similar to its established role in neuroblasts (Bowman et al., 2006; Siller et al., 2006). The observation that Ed:GFP-Pins retained partial activity following Mud knockdown, which was not initially anticipated, helped identify Dlg as a second direct component in Pins-mediated spindle orientation (Johnston et al., 2009). Knockdown of Dlg, in contrast, leads to a strongly misaligned spindle orientation phenotype in the Ed:GFP-Pins S2 cell system (**Figures 3C,D**). In addition to RNAi-mediated knockdown experiments, the relative ease with which users can generate point mutations, domain deletions, and chimeric constructs with standard molecular techniques allows for additional means toward rapid and precise dissection of the underlying molecular mechanisms and evolutionary conservation of a gene of interest. Collectively, these experiments can help identify novel spindle orientation pathways and their components as well as establish the epistatic relationship among previously known components, both of which can aid significantly in discerning molecular mechanisms of spindle positioning.

DISCUSSION

Cell polarity and processes such as mitotic spindle orientation linked closely with it are complex cellular events involving numerous components and regulatory inputs. Understanding how these components cooperate to control these processes and the underlying molecular mechanisms controlling their function can present challenges to traditional genetic approaches using *in vivo* model systems. Minimal reconstitution systems have proven powerful tools in addressing these drawbacks and provide alternative systems to dissect these molecular complexities. The protocol described here offers users a rapid and cost-effective method for inducing polarity within a simple, non-polar cell line that should help continue resolving unanswered questions in this conserved and essential cellular process. Although specifically designed for *Drosophila* cells, the protocol can be adapted for use in mammalian systems. For example, a recent study used a similar approach in HeLa cells, a mainstay in mitosis research in human cells (di Pietro et al., 2017). Such adaptations will help further define mechanisms of spindle positioning as well as in comparisons among evolutionarily related genes.

It should be discussed that this approach, like most, is not without limitations. First, as mentioned above, perhaps most substantive is the potential bottleneck one may encounter during imaging. Compounding issues of S2 cell transfection efficiency and mitotic index can sometimes limit the throughput of data collection. However, this has not been a terminal issue, as we and others have used this protocol in numerous studies that required extensive conditions to be tested using it as the primary method. Users are, nevertheless, cautioned to anticipate such limits when planning experiments. Second, studies using this protocol to investigate cortical polarity have mostly focused on how Ed-fused proteins affect localization of cytoplasmic proteins. As such, its application to studying effects on other integral membrane proteins has not yet been well-established. Finally, the system obviously requires first identifying an Ed fusion that is sufficient to evoke a measureable effect (e.g., Ed:Pins orienting the spindle). While this allows subsequent dissection of the molecular aspects of its function, the ability to specifically examine Ed fusions of its downstream effectors may not be possible if their function is required but not sufficient. For example, Pins functions through two effectors, Mud and Dlg, and whereas Dlg is sufficient to induce a partial orientation of spindles in this system, Mud is not. Thus, the Ed system was ideal to probe the mechanism of Dlg function further, but was limited in the information it could provide for Mud activity (Johnston et al., 2009).

DATA AVAILABILITY STATEMENT

The original contributions presented in the study are included in the article/supplementary material, further inquiries can be directed to the corresponding author/s.

AUTHOR CONTRIBUTIONS

CJ conceptualized and wrote the manuscript, generated the results, and prepared the figures and table.

FUNDING

This work was generously supported by a grant from the National Institutes of Health (R01 GM108756).

ACKNOWLEDGMENTS

I would like to thank Chris Q. Doe, Kenneth E. Prehoda, Keiko Hirono, and other former members of the Doe and Prehoda labs (University of Oregon) for their support and contributions to establishing the system and protocol described here.

REFERENCES

Abu Shah, E., and Keren, K. (2014). Symmetry breaking in reconstituted actin cortices. *eLife* 3:e01433. doi: 10.7554/eLife.01433

Bergstralh, D. T., Lovegrove, H. E., and St Johnston, D. (2013). Discs large links spindle orientation to apical-basal polarity in *Drosophila epithelia*. *Curr. Biol.* 23, 1707–1712. doi: 10.1016/j.cub.2013.07.017

Bowman, S. K., Neumuller, R. A., Novatchkova, M., Du, Q., and Knoblich, J. A. (2006). The *Drosophila* NuMA Homolog Mud regulates spindle orientation in asymmetric cell division. *Dev. Cell.* 10, 731–742. doi: 10.1016/j.devcel.2006.05.005

Carbone, C. B., Kern, N., Fernandes, R. A., Hui, E., Su, X., Garcia, K. C., et al. (2017). In vitro reconstitution of T cell receptor-mediated segregation of the CD45 phosphatase. *Proc. Natl. Acad. Sci. U.S.A.* 114, E9338–E9345. doi: 10.1073/pnas.1710358114

Cherbas, L., Willingham, A., Zhang, D., Yang, L., Zou, Y., Eads, B. D., et al. (2011). The transcriptional diversity of 25 *Drosophila* cell lines. *Genome Res.* 21, 301–314. doi: 10.1101/gr.112961.110

Dewey, E. B., Sanchez, D., and Johnston, C. A. (2015a). Warts phosphorylates mud to promote pins-mediated mitotic spindle orientation in *Drosophila*, independent of yorkie. *Curr. Biol.* 25, 2751–2762. doi: 10.1016/j.cub.2015.09.025

Dewey, E. B., Taylor, D. T., and Johnston, C. A. (2015b). Cell fate decision making through oriented cell division. *J. Dev. Biol.* 3, 129–157. doi: 10.3390/jdb3040129

di Pietro, F., Echard, A., and Morin, X. (2016). Regulation of mitotic spindle orientation: an integrated view. *EMBO Rep.* 17, 1106–1130. doi: 10.15252/embr.201642292

di Pietro, F., Valon, L., Li, Y., Goiame, R., Genovesio, A., and Morin, X. (2017). An RNAi screen in a novel model of oriented divisions identifies the actin-capping protein Z beta as an essential regulator of spindle orientation. *Curr. Biol.* 27, 2452.e8–2464.e8. doi: 10.1016/j.cub.2017.06.055

Dupin, I., Camand, E., and Etienne-Manneville, S. (2009). Classical cadherins control nucleus and centrosome position and cell polarity. *J. Cell Biol.* 185, 779–786. doi: 10.1083/jcb.200812034

Fielmich, L. E., Schmidt, R., Dickinson, D. J., Goldstein, B., Akhmanova, A., and van den Heuvel, S. (2018). Optogenetic dissection of mitotic spindle positioning in vivo. *eLife* 7:e38198. doi: 10.7554/eLife.38198

Ganzinger, K. A., and Schwille, P. (2019). More from less - bottom-up reconstitution of cell biology. *J. Cell Sci.* 132:jcs227488. doi: 10.1242/jcs.227488

Garcia, J. D., Dewey, E. B., and Johnston, C. A. (2014). Dishevelled binds the Discs large 'Hook' domain to activate GukHolder-dependent spindle positioning in *Drosophila*. *PLoS One* 9:e114235. doi: 10.1371/journal.pone.0114235

Goshima, G., Wollman, R., Goodwin, S. S., Zhang, N., Scholey, J. M., Vale, R. D., et al. (2007). Genes required for mitotic spindle assembly in *Drosophila* S2 cells. *Science* 316, 417–421. doi: 10.1126/science.1141314

James, J. R., and Vale, R. D. (2012). Biophysical mechanism of T-cell receptor triggering in a reconstituted system. *Nature* 487, 64–69. doi: 10.1038/nature11220

Johnston, C. A., Hirono, K., Prehoda, K. E., and Doe, C. Q. (2009). Identification of an Aurora-A/PinsLINKER/Dlg spindle orientation pathway using induced cell polarity in S2 cells. *Cell* 138, 1150–1163. doi: 10.1016/j.cell.2009.07.041

Johnston, C. A., Manning, L., Lu, M. S., Golub, O., Doe, C. Q., and Prehoda, K. E. (2013). Formin-mediated actin polymerization cooperates with Mushroom body defect (Mud)-Dynein during Frizzled-Dishevelled spindle orientation. *J. Cell Sci.* 126(Pt 19), 4436–4444. doi: 10.1242/jcs.129544

Khushi, M., Dean, I. M., Teber, E. T., Chircop, M., Arthur, J. W., and Flores-Rodriguez, N. (2017). Automated classification and characterization of the mitotic spindle following knockdown of a mitosis-related protein. *BMC Bioinformatics* 18(Suppl. 16):566. doi: 10.1186/s12859-017-1966-4

Kim, A. K., DeRose, R., Ueno, T., Lin, B., Komatsu, T., Nakamura, H., et al. (2016). Toward total synthesis of cell function: reconstituting cell dynamics with synthetic biology. *Sci. Signal.* 9:re1. doi: 10.1126/scisignal.aac4779

Kwon, M., Godinho, S. A., Chandhok, N. S., Ganem, N. J., Azioune, A., Thery, M., et al. (2008). Mechanisms to suppress multipolar divisions in cancer cells with extra centrosomes. *Genes Dev.* 22, 2189–2203. doi: 10.1101/gad.1700908

Lu, M. S., and Johnston, C. A. (2013). Molecular pathways regulating mitotic spindle orientation in animal cells. *Development* 140, 1843–1856. doi: 10.1242/dev.087627

Lu, M. S., and Prehoda, K. E. A. (2013). NudE/14-3-3 pathway coordinates dynein and the kinesin Khc73 to position the mitotic spindle. *Dev. Cell* 26, 369–380. doi: 10.1016/j.devcel.2013.07.021

Mauser, J. F., and Prehoda, K. E. (2012). Inscuteable regulates the Pins-Mud spindle orientation pathway. *PLoS One* 7:e29611. doi: 10.1371/journal.pone.0029611

Okumura, M., Natsume, T., Kanemaki, M. T., and Kiyomitsu, T. (2018). Dynein-Dynactin-NuMA clusters generate cortical spindle-pulling forces as a multi-arm ensemble. *eLife* 7:e36559. doi: 10.7554/eLife.36559

Ragkousi, K., and Gibson, M. C. (2014). Cell division and the maintenance of epithelial order. *J. Cell Biol.* 207, 181–188. doi: 10.1083/jcb.201408044

Rodriguez-Boulan, E., and Macara, I. G. (2014). Organization and execution of the epithelial polarity programme. *Nat. Rev. Mol. Cell Biol.* 15, 225–242. doi: 10.1038/nrm3775

Rogers, S. L., and Rogers, G. C. (2008). Culture of *Drosophila* S2 cells and their use for RNAi-mediated loss-of-function studies and immunofluorescence microscopy. *Nat. Protoc.* 3, 606–611. doi: 10.1038/nprot.2008.18

Roth, J. S., Lee, T. D., Cheff, D. M., Gosztyla, M. L., Asawa, R. R., Danchik, C., et al. (2020). Keeping it clean: the cell culture quality control experience at the national center for advancing translational sciences. *SLAS Discov.* 25, 491–497. doi: 10.1177/2472555220911451

Roubinet, C., and Cabernard, C. (2014). Control of asymmetric cell division. *Curr. Opin. Cell Biol.* 31, 84–91. doi: 10.1016/j.ceb.2014.09.005

Sawyer, J. K., Harris, N. J., Slep, K. C., Gaul, U., and Peifer, M. (2009). The *Drosophila* afadin homologue Canoe regulates linkage of the actin cytoskeleton to adherens junctions during apical constriction. *J. Cell Biol.* 186, 57–73. doi: 10.1083/jcb.200904001

Schneider, I. (1972). Cell lines derived from late embryonic stages of *Drosophila melanogaster*. *J. Embryol. Exp. Morphol.* 27, 353–365.

Segalen, M., Johnston, C. A., Martin, C. A., Dumortier, J. G., Prehoda, K. E., David, N. B., et al. (2010). The Fz-Dsh planar cell polarity pathway induces oriented cell division via Mud/NuMA in *Drosophila* and *Zebrafish*. *Dev. Cell.* 19, 740–752. doi: 10.1016/j.devcel.2010.10.004

Shimono, Y., Rikitake, Y., Mandai, K., Mori, M., and Takai, Y. (2012). Immunoglobulin superfamily receptors and adherens junctions. *Subcell. Biochem.* 60, 137–170. doi: 10.1007/978-94-007-4186-7_7

Siegrist, S. E., and Doe, C. Q. (2005). Microtubule-induced Pins/Galphai cortical polarity in *Drosophila neuroblasts*. *Cell* 123, 1323–1335. doi: 10.1016/j.cell.2005.09.043

Siller, K. H., Cabernard, C., and Doe, C. Q. (2006). The NuMA-related Mud protein binds Pins and regulates spindle orientation in *Drosophila neuroblasts*. *Nat. Cell Biol.* 8, 594–600. doi: 10.1038/ncb1412

Sommer, C., and Gerlich, D. W. (2013). Machine learning in cell biology - teaching computers to recognize phenotypes. *J. Cell Sci.* 126(Pt 24), 5529–5539. doi: 10.1242/jcs.123604

Thery, M. (2010). Micropatterning as a tool to decipher cell morphogenesis and functions. *J. Cell Sci.* 123(Pt 24), 4201–4213. doi: 10.1242/jcs.075150

Thery, M., Jimenez-Dalmaroni, A., Racine, V., Bornens, M., and Julicher, F. (2007). Experimental and theoretical study of mitotic spindle orientation. *Nature* 447, 493–496. doi: 10.1038/nature05786

Thery, M., Racine, V., Pepin, A., Piel, M., Chen, Y., Sibarita, J. B., et al. (2005). The extracellular matrix guides the orientation of the cell division axis. *Nat. Cell Biol.* 7, 947–953. doi: 10.1038/ncb1307

Thery, M., Racine, V., Piel, M., Pepin, A., Dimitrov, A., Chen, Y., et al. (2006). Anisotropy of cell adhesive microenvironment governs cell internal organization and orientation of polarity. *Proc. Natl. Acad. Sci. U.S.A.* 103, 19771–19776. doi: 10.1073/pnas.0609267103

Vendel, K. J. A., Tschirpke, S., Shamsi, F., Dogterom, M., and Laan, L. (2019). Minimal in vitro systems shed light on cell polarity. *J. Cell Sci.* 132:jcs217554. doi: 10.1242/jcs.217554

Wee, B., Johnston, C. A., Prehoda, K. E., and Doe, C. Q. (2011). Canoe binds RanGTP to promote Pins(TPR)/Mud-mediated spindle orientation. *J. Cell Biol.* 195, 369–376. doi: 10.1083/jcb.201102130

Wei, S. Y., Escudero, L. M., Yu, F., Chang, L. H., Chen, L. Y., Ho, Y. H., et al. (2005). Echinoid is a component of adherens junctions that cooperates with DE-Cadherin to mediate cell adhesion. *Dev. Cell.* 8, 493–504. doi: 10.1016/j.devcel.2005.03.015

Witte, K., Strickland, D., and Glotzer, M. (2017). Cell cycle entry triggers a switch between two modes of Cdc42 activation during yeast polarization. *eLife* 6:e26722. doi: 10.7554/eLife.26722

Zieske, K., and Schwille, P. (2014). Reconstitution of self-organizing protein gradients as spatial cues in cell-free systems. *eLife* 3:e03949. doi: 10.7554/eLife.03949

Conflict of Interest: The author declares that the research was conducted in the absence of any commercial or financial relationships that could be construed as a potential conflict of interest.

frontiers in Cell and Developmental Biology

CORRECTION
published: 22 June 2021
doi: 10.3389/fcell.2021.705599

Corrigendum: A Cell Adhesion-Based Reconstitution Method for Studying Cell Polarity

*Christopher A. Johnston**

Department of Biology, University of New Mexico, Albuquerque, NM, United States

Keywords: cell polarity, spindle orientation, mitosis, reconstitution, neuroblast

A Corrigendum on

A Cell Adhesion-Based Reconstitution Method for Studying Cell Polarity
by Johnston, C. A. (2020). Front. Cell Dev. Biol. 8:598492. doi: 10.3389/fcell.2020.598492

In the original article, there was an error. The restriction enzymes that are to be used when cloning target genes of interest into the Ed-modified pMT/V5-His plasmid were incorrectly described as "5'-*Bam*HI and 3'-*Xho*I" instead of "5'-*Bgl*II and 3'-*Sal*I."

A correction has been made to the legend and image of **Figure 1B** as published and the corrected **Figure 1** appears below.

A correction has been made to **Stepwise Procedures, Molecular Cloning of Ed Fusion Constructs**:

"Expression of Ed fusion constructs in S2 cells is achieved using the copper inducible metallothionein promotor within the pMT expression vector (Thermo Fisher). Cloning and construction of pMT:Ed plasmids has been previously detailed (Johnston et al., 2009). We have generated plasmids that yield either GFP- or FLAG-tagged versions of the Ed fusion, with the general structure of Ed:GFP-X, where X represents the desired cloned gene of interest (**Figure 1**). Both plasmids are linearized using 5′-*Bgl*II and 3′-*Sal*I restriction digest, which can be ligated with identically digested inserts or those digested with isocaudameric enzymes such as 5′-*Bam*HI and 3′-*Xho*I. Cloning should be done using standard molecular techniques and verified using Sanger sequencing methods."

The author apologizes for this error and state that this does not change the scientific conclusions of the article in any way. The original article has been updated.

REFERENCES

Johnston, C. A., Hirono, K., Prehoda, K. E., and Doe, C. Q. (2009). Identification of an Aurora-A/PinsLINKER/Dlg spindle orientation pathway using induced cell polarity in S2 cells. *Cell* 138, 1150–1163. doi: 10.1016/j.cell.2009.07.041

OPEN ACCESS

Edited and reviewed by:
Zhiyi Lv,
Ocean University of China, China

***Correspondence:**
Christopher A. Johnston
johnstca@unm.edu

Specialty section:
This article was submitted to Signaling, a section of the journal Frontiers in Cell and Developmental Biology

Received: *05 May 2021*
Accepted: *24 May 2021*
Published: *22 June 2021*

Citation:
Johnston CA (2021) Corrigendum: A Cell Adhesion-Based Reconstitution Method for Studying Cell Polarity. Front. Cell Dev. Biol. 9:705599. doi: 10.3389/fcell.2021.705599

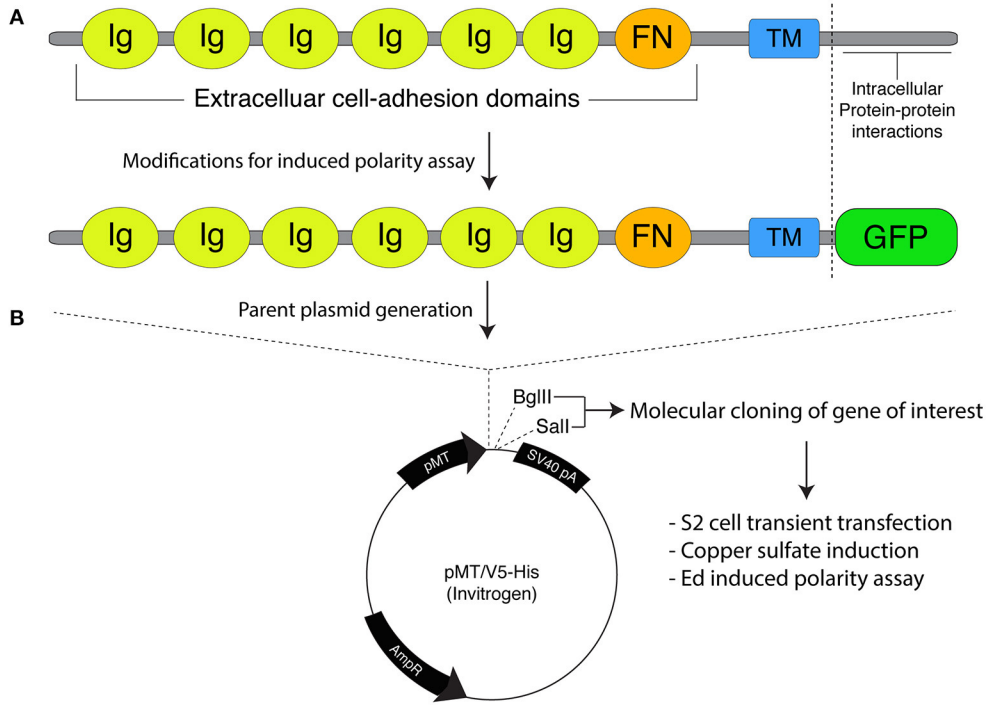

FIGURE 1 | Molecular framework for the Echinoid-based polarity reconstitution system. **(A) Top:** Domain architecture of the full-length Ed protein depicts an extracellular region containing several Immunoglobulin (Ig; yellow) and Fibronectin (FN; orange) cell adhesion domains that participate in formation of cell clusters. The transmembrane (TM; blue) region allows for insertion as an integral plasma membrane protein. The C-terminal tail (sequence following vertical dash line) resides intracellularly and is responsible for protein-protein interactions that participate in maintenance of adherens junction function and signaling. **Bottom:** Cloning of Ed for use in the induced polarity assay omits most of the intracellular tail to avoid interactions with known binding partners. This sequence is replaced with an in-frame green fluorescence protein (GFP; green) coding sequence. **(B)** The modified Ed:GFP sequence (with GFP replacing native C-terminal sequence) is cloned into the pMT/V5-His plasmid followed by 5′-*Bgl*II and 3′-*Sal*I cloning sites. Standard molecular cloning can easily generate Ed:GFP fusions to ostensibly any gene or sequence fragment the user wishes to examine. Cells are then transiently transfected with the cloned plasmid, and Ed:GFP fusion proteins are expressed using copper sulfate activation of the pMT promotor (see "Stepwise procedures").

frontiers in Cell and Developmental Biology

REVIEW
published: 30 October 2020
doi: 10.3389/fcell.2020.597446

Polarity Establishment and Maintenance in Ascidian Notochord

*Hongzhe Peng[1], Runyu Qiao[1] and Bo Dong[1,2,3]**

[1] Sars-Fang Centre, MoE Key Laboratory of Marine Genetics and Breeding, College of Marine Life Sciences, Ocean University of China, Qingdao, China, [2] Laboratory for Marine Biology and Biotechnology, Qingdao National Laboratory for Marine Science and Technology, Qingdao, China, [3] Institute of Evolution and Marine Biodiversity, Ocean University of China, Qingdao, China

Cell and tissue polarity due to the extracellular signaling and intracellular gene cascades, in turn, signals the directed cell behaviors and asymmetric tissue architectures that play a crucial role in organogenesis and embryogenesis. The notochord is a characteristic midline organ in chordate embryos that supports the body structure and produces positioning signaling. This review summarizes cellular and tissue-level polarities during notochord development in ascidians. At the early stage, planar cell polarity (PCP) is initialized, which drives cell convergence extension and migration to form a rod-like structure. Subsequently, the notochord undergoes a mesenchymal-epithelial transition, becoming an unusual epithelium in which cells have two opposing apical domains facing the extracellular lumen deposited between adjacent notochord cells controlled by apical-basal (AB) polarity. Cytoskeleton distribution is one of the main downstream events of cell polarity. Some cytoskeleton polarity patterns are a consequence of PCP: however, an additional polarized cytoskeleton, together with Rho signaling, might serve as a guide for correct AB polarity initiation in the notochord. In addition, the notochord's mechanical properties are associated with polarity establishment and transformation, which bridge signaling regulation and tissue mechanical properties that enable the coordinated organogenesis during embryo development.

Keywords: notochord, planar cell polarity, apical-basal polarity, initiation of AB polarity, lumen formation

OPEN ACCESS

Edited by:
Yi Wu,
UConn Health, United States

Reviewed by:
Ana Carmena,
Consejo Superior de Investigaciones Científicas (CSIC), Spain
Sally Ann Moody,
George Washington University, United States

***Correspondence:**
Bo Dong
bodong@ouc.edu.cn

Specialty section:
This article was submitted to Signaling, a section of the journal Frontiers in Cell and Developmental Biology

Received: *21 August 2020*
Accepted: *12 October 2020*
Published: *30 October 2020*

Citation:
Peng H, Qiao R and Dong B (2020) Polarity Establishment and Maintenance in Ascidian Notochord. Front. Cell Dev. Biol. 8:597446. doi: 10.3389/fcell.2020.597446

INTRODUCTION

Cell proliferation, migration, and deformation; extracellular matrix (ECM) secretion; and cell–cell junction formation and remodeling are basic processes in tissue and organ architecture establishment during embryogenesis. However, these processes are not always isotropic, and anisotropic processes lead to spatial differences in cell shape and structure, directed cell behaviors (e.g., migration, mitosis, adhesion, secretion, and signaling transition), and asymmetric subcellular structures (e.g., organelle localization and cytoskeleton distribution) all of which generate what is called "polarity" (Dhonukshe, 2013; Wolpert, 2013). Polarity widely exists during the entire lifespan and at all levels of an organism. At the tissue level, polarity appears as asymmetric differentiation forming distinct cell types and/or the mechanically anisotropic tissues. For the whole embryo, polarity manifests as the formation of orientated body axis and the asymmetric location of organs.

Polarity is regulated by signaling pathways that respond to chemical stimulations such as morphogens (Turing, 1952; Pickett et al., 2019) or physical stimulation like light

(Brownlee and Bouget, 1998) from the extracellular space, where oriented signals are sent, except a small part of spontaneous random cell polarization (Wedlich-Soldner and Li, 2003). Extracellular signals transmit through paracrine pathways mediated by morphogen concentration gradient signaling, such as Wnt signaling (Ukita et al., 2009), Notch signaling (Hermann et al., 2000; Kato, 2011), Hedgehog signaling (Choi and Harfe, 2011; Hu et al., 2017), and transforming growth factor beta signaling (bone morphogenetic protein, activin) (Ninomiya, 2004; Eom et al., 2011). In addition, cells also receive orientation signals through contacts, such as cell–cell adhesion (Nance, 2014) or cell-ECM network like basement membrane adhesion (Marsden and DeSimone, 2003). These extracellular signals provide directional information, which induces asymmetric distribution of protein complexes or subcellular organelles, establishing intracellular polarity (Pickett et al., 2019). There are two main intracellular polarity signal systems, apical-basal (AB) polarity mediated by the Par/atypical protein kinase C (aPKC) complex (Assémat et al., 2008), and planar cell polarity (PCP), mediated by Frizzled (Fz, also called Fzd in vertebrate)- Flamingo (Fmi, also known as starry night in Drosophila and Celsr in vertebrate)- Disheveled (Dsh, also called Dvl in vertebrate)- Diego (Dgo, also called Diversin or Inversin in vertebrate), and Van Gogh (Vang, also known as strabismus in Drosophila and Vangl in vertebrate)- Flamingo (Fmi)- Prickle (Pk, also known as prickle-spiny legs in Drosophila) complexes (Adler, 2012; Yang and Mlodzik, 2015). Both intracellular polarity signal systems coexist in cells and sometimes cooperate too (Djiane et al., 2005; Wu and Mlodzik, 2009), contributing to the formation and maintenance of multidimensional polarity.

Polarity establishment is necessary for morphogenesis, by which three-dimensional (3D) complex architectures emerge from symmetric, simple structures. Tissue and organ specialization and cell fate depend on the direction and position information. For example, anterior-posterior (AP) axis formation regulates somite differentiation (Bénazéraf and Pourquié, 2013), while left-right (LR) axis formation regulates the asymmetry location and differentiation of the brain, heart, and gut (Bisgrove et al., 2000; Hashimoto and Hamada, 2010; Grimes, 2019). The body plan symmetry of animals is diversified including spherical symmetry, radial symmetry, biradial symmetry, and bilateral symmetry (Holló, 2015). In bilaterally symmetric animals, some inner organs, such as the heart and gut, in the symmetric body plan show LR asymmetry (Raya and Belmonte, 2006).

Of multi-leveled polarities, tissue polarity, formed from cell polarity (Mlodzik, 2002) and manifesting as tissue mechanical property and tissue movement, epitomizes the polarity phenomena and plays an important role in developmental processes.

THE NOTOCHORD

The notochord is a characteristic rod-like midline organ in chordate embryos that supports the body structure and produces signaling (Stemple, 2005; Corallo et al., 2015). Notochord evolution has three stages: muscle-like axochord (Lauri et al., 2014; Brunet et al., 2015), rigid cell cord, and osseous vertebral column. A notochord-like muscle structure has been reported in annelids (Lauri et al., 2014) indicating that the notochord originates from muscle (Lauri et al., 2014; Brunet et al., 2015). In hemichordatas, the lowest chordates, the stomochord, a notochord primordium, appears (Balser and Ruppert, 1990). In amphioxus, a cephalochordate, the notochord is present throughout the body during the entire lifespan as the body's main support structure (Feng et al., 2016). In urochordates, such as ascidians, the notochord only exists in the tail part in swimming larvae and disappears after metamorphosis (Cloney, 1982; Matsunobu and Sasakura, 2015). In cyclostomes, cartilaginous tissue appears around the notochord (Ota and Kuratani, 2007). In higher chordates, such as fish and mouse, the notochord exists centrally in the embryonic and larval body, and it is replaced by the spine in adults (Wopat et al., 2018; Bagwell et al., 2020). The notochord is converted into the nucleus pulposus in fully formed intervertebral discs, which protect the vertebrae from rubbing against each other (McCann et al., 2011).

POLARITIES IN *Ciona* NOTOCHORD

Ascidian is a basic group in chordate, with the notochord at larval stage. It is becoming an ideal model in marine invertebrates' morphogenesis (Lv et al., 2019). During notochord development in *Ciona*, diverse polarity patterns are built and play an important role in asymmetric structure formation and directional movement of notochord cells. First, notochord cells intercalate to form a rod-like structure along the midline of the body through convergence extension (CE) process regulated by a medial-lateral (ML)-oriented PCP (**Figure 1A**; Munro and Odell, 2002). During CE, ventrally polarized cytoskeleton contractility induces the notochord and the tail to bend ventrally and elongate posteriorly within the chorion (**Figure 1B**). Next, mesenchymal-epithelial transition (MET) occurs, in which notochord cells become epithelial-like with AB polarity (**Figures 1C,D**). The PCP direction changes from ML to the one-dimensional (1D) AP axis (Kourakis et al., 2014). During the period, notochord cells secret the ECM into the basal, building a notochord sheath, and also into the apical surfaces, forming the extracellular lumen for cavitation (**Figure 1E**), which provides sufficient stiffness to support the body (Keller, 2006; Yasuoka, 2020). Polarity plays an essential role in all these processes. This review focuses on MET of notochord cells and polarity establishment and maintenance during this process.

ESTABLISHMENT OF AB POLARITY IN *Ciona* NOTOCHORD

A rod-like notochord appears after cell intercalation, in which PCP signaling sends polar signals parallel to the AP axis (Kourakis et al., 2014). The notochord elongates and undergoes MET, establishing AB polarity (Dong et al., 2009; Denker et al., 2013). The MET includes two main steps: (1) apical domains

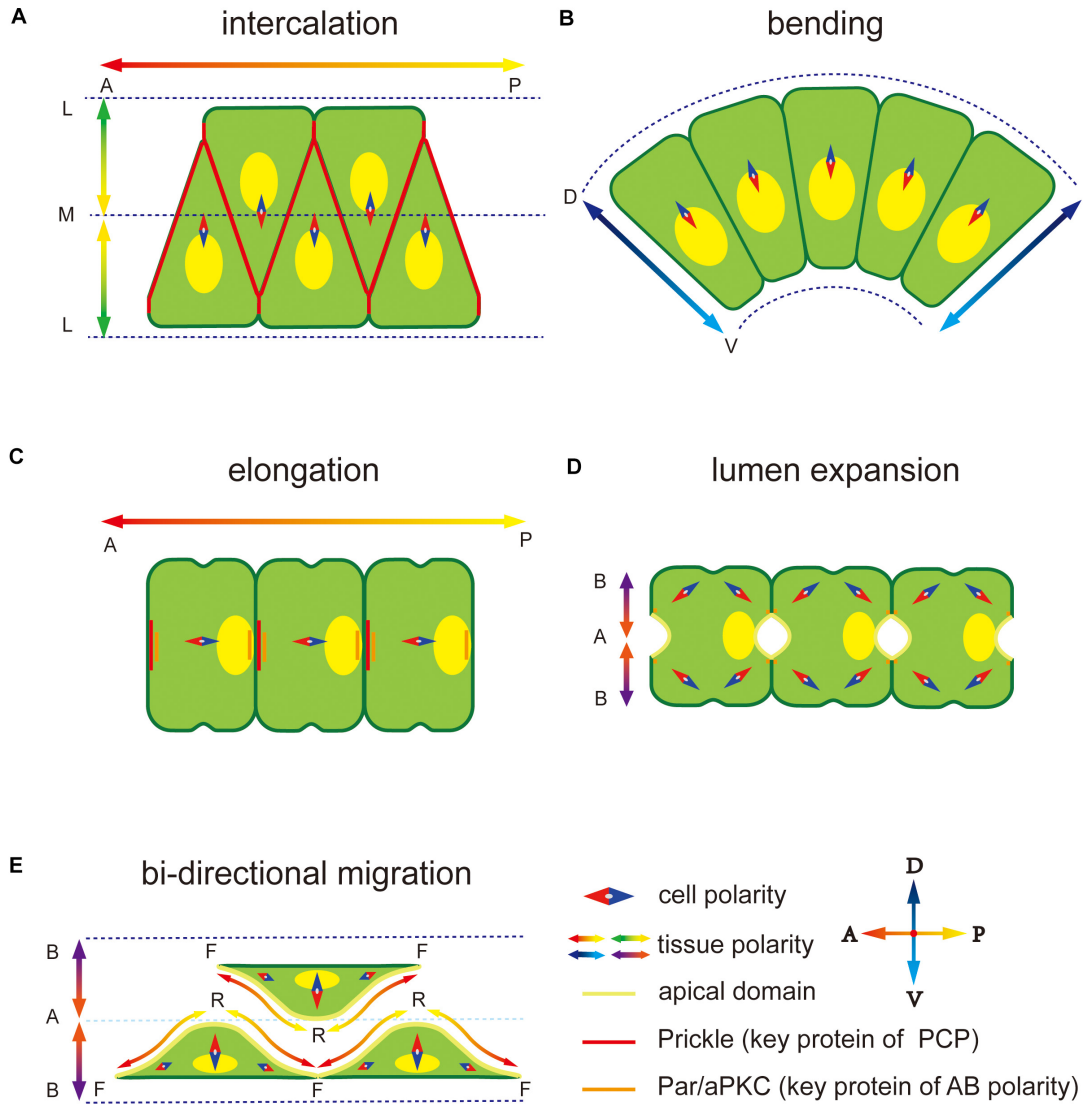

FIGURE 1 | Polarity at different notochord development stages in *Ciona*. **(A)** Notochord cells form a mediolateral (ML) polarity to drive the migration to the midline during convergence and extension. The notochord elongates parallel to the anterior-posterior (AP) axis regulated by embryonic AP polarity signaling. The key PCP component protein Prickle is located at the notochord cell–cell contact domain. **(B)** Notochord cells form a dorsal-ventral (DV) polarity to abend tissue toward the ventral side. **(C)** After cell intercalation, the PCP direction changes from ML to 1D AP axis. The Prickle relocates at the anterior edge of each notochord cell. **(D)** Apical-basal (AB) polarity is built to induces extracellular lumen formation. Two apical domains appear in one notochord cell. **(E)** Notochord cells migrate bidirectionally to induce the lumen connection. Adjacent notochord cells flatten opposite to each other along the notochord sheath.

initially appear at the center of two opposite lateral domains of each notochord cell; (2) extracellular lumen is deposited outside of apical domains and expanded continuedly (Denker and Jiang, 2012). The Par3-Par6-aPKC polarity complex is essential for AB polarity formation in epithelial cells (Assémat et al., 2008; Dhonukshe, 2013; Wen and Zhang, 2018). In *Ciona* notochord, Par3, Par6, and aPKC co-localize at the AP polar edges of notochord cells. Inhibition of Par3 function causes loss of the polarized localization of Par6 and aPKC, and the lumen cannot form, suggesting that Par3 might be the signaling upstream to guide Par/aPKC and AB polarity formation. It has been known that knockdown of *Par3* caused mislocalization of Par6 and aPKC, and blocked the AB polarity formation. However, mislocalization of Par6 using an aPKC binding dominant negative (PAR-6 ΔaPKC-BD) (Suzuki et al., 2001) did not affect the localization of Par3. While, overexpression of myristoylated aPKC (myr-aPKC), which leads to the mislocalization of aPKC, caused the mislocalization of Par6. However, the localization of Par3 was unaffected (Denker et al., 2013). These results indicate that Par3 is upstream of aPKC and Par6, while the localization of Par6 depends on aPKC in *Ciona* notochord. The upstream signaling that induces the Par3 polar localization is still unknown. Some studies in *Caenorhabditis elegans* and *Drosophila* suggest that the

localization of Par/aPKC complex is regulated by centrosome (Feldman and Priess, 2012). Engulfment and cell mobility (ELMO) family proteins might be involved in the regulatory process (Schmidt et al., 2018). With the development, ECM components are secreted out, forming the extracellular lumen at the anterior and posterior edges of notochord cells, and the notochord cell surface is separated into apical (facing the lumen), lateral (contact between neighboring cells), and basal membrane domains. After lumen formation, the Par3-Par6-aPKC polar complex localizes at the boundary between apical and lateral membranes to form a ring-like localization (Denker et al., 2013; Smith, 2018). Initially, each cell forms two apical domains in the notochord in *Ciona*, which then eventually merge into one (**Figures 1D,E**; Dong et al., 2009). During this process, notochord cells are regulated by polar signaling from both PCP and AB polarity that induces many proteins, such as cytoskeleton and cell junction proteins, toward polar localization. A contractile ring appears at the anterior side of each notochord cell and then moves to the equator to provide the force required for cell elongation (Dong et al., 2011). Zonula Occludens 1 (ZO-1), as part of the tight junction, co-localizes with the Par3-Par6-aPKC polar complex and they work together to occlude the lumen cavity (Denker et al., 2013). Solute Carrier 26aα (SLC26aα), a transmembrane transport protein locates at the apical membrane to control the osmotic pressure in the lumen cavity (Deng et al., 2013).

The relationship between PCP and AB polarities, that is, whether and how they cross-talk, is still unclear. There exist three possible ways of communication: (1) Key PCP and AB polar proteins might interact directly. This type of cross-talk between PCP and AB polarities has been identified in the *Drosophila* eye, in which aPKC inhibits PCP activity by Fz1 phosphorylation (Djiane et al., 2005; Wu and Mlodzik, 2009). In *Ciona* notochord cell, Prickle and Par/aPKC complex are overlapped at the presumptive anterior apical domain (Jiang et al., 2005; Denker et al., 2013), offering the possibility for their direct interaction. (2) Notochord cells receive signals from neighboring cells. In intercalation abnormal mutant *Ciona* embryos, a notochord cell is usually in contact with more than two adjacent cells, and apical domains can be observed at each cell–cell contact (Denker et al., 2013), confirming that the AB polarity of notochord cells is affected by neighboring cells. When cell ablation removes the posterior neighboring cell, the notochord cell loses the posterior location of the nuclei. In addition, nucleus in the 40th notochord cell, which is the last cell in notochord tissue, locates in the anterior part of the cell (Kourakis et al., 2014). Both the observed facts indicate that maintenance of PCP signaling is posterior cell dependent. (3) ECM components mediate the interaction between PCP and AB polarities. Disruption of PCP signaling causes the mislocation of ECM component at the cell–cell interface (Veeman et al., 2007), suggesting that localization of basal ECM is PCP dependent. In addition, in zebrafish and *Xenopus*, disruption of the function of notochord sheath protein components, such as laminin or collagen, leads to abnormal notochord and vacuole morphogenesis (Parsons et al., 2002; Pagnon-Minot et al., 2008; Buisson et al., 2014; Manninen, 2015).

POLARIZED ECM SECRETION IN THE NOTOCHORD

Notochord tissue in different species has a few common features, such as the notochord sheath (closed tube component of the ECM) and the lumen cavity formed by distinct ways. In *Ciona*, notochord cells form an extracellular lumen through MET, surrounded by a single layer of notochord cells and an ECM notochord sheath (Dong et al., 2009). In zebrafish, some notochord cells form a layer of outer notochord sheath cells along the notochord sheath while other cells move to an inner cell core, and vacuoles are formed within each cell (Ellis et al., 2013a,b; Corallo et al., 2015). In amniotes, such as chicken and mice, vacuolated notochord cells are surrounded by an acellular sheath (Choi et al., 2008; Ward et al., 2018).

Notochord sheath formation is oriented by secretion of the polarized basal surface ECM. In *Xenopus*, the chordamesoblast forms radial polarization induced by surrounding tissues and then secretes fibronectin at the basement surface, forming a fibronectin layer between the mesoderm and surrounding tissues. Disruption of the Pk and/or Stbm/Fz function leads to failure of basal ECM secretion (Goto et al., 2005), indicating that the Wnt/PCP signaling pathway is essential for basal ECM secretion. Similarly, failure of laminin (polarized ECM component) secretion is found in *Pk* mutant *Ciona* embryos (Veeman et al., 2007; Veeman and McDonald, 2016), indicating that a conserved regulatory mechanism underlies basal ECM secretion. In addition to the Wnt/PCP signaling pathway, other signaling pathways, such as hedgehog, might also be involved in notochord sheath formation (Choi and Harfe, 2011).

In addition to basal ECM secretion, apical ECM secretion is also found sometimes (Mizotani et al., 2018; Bhattachan et al., 2020), which forms extracellular pocket lumens. During this process, notochord polarity moves from PCP to AB polarity (Dong et al., 2009). Both PCP an AB polarities and basal vesical trafficking are required for apical ECM secretion (Mizotani et al., 2018).

CYTOSKELETON POLARITIES IN *Ciona* NOTOCHORD MORPHOGENESIS

The cytoskeleton, including the microtubule, actin filaments, and intermediate filaments, is a group of fibriform intracellular proteins that form a skeleton network to maintain the cell shape and movement (Pegoraro et al., 2017). Cytoskeleton polarity, such as asymmetry distribution; oriented arrangement; and polar crosslinking, cooperation, disassociation, and rearrangement, plays an important role in cell asymmetry structures and behaviors. A polarized cytoskeleton is the main cause of an unbalanced bioforce. In contrast, a cytoskeleton is highly dynamic. It can be sensitively regulated and under the control of cell polarity (Raman et al., 2018). Therefore, cytoskeleton polarity is an important pathway to externalize intracellular polar signaling.

Cytoskeleton polarity plays an important role in diverse notochord morphogenesis, including the ascidian notochord. At

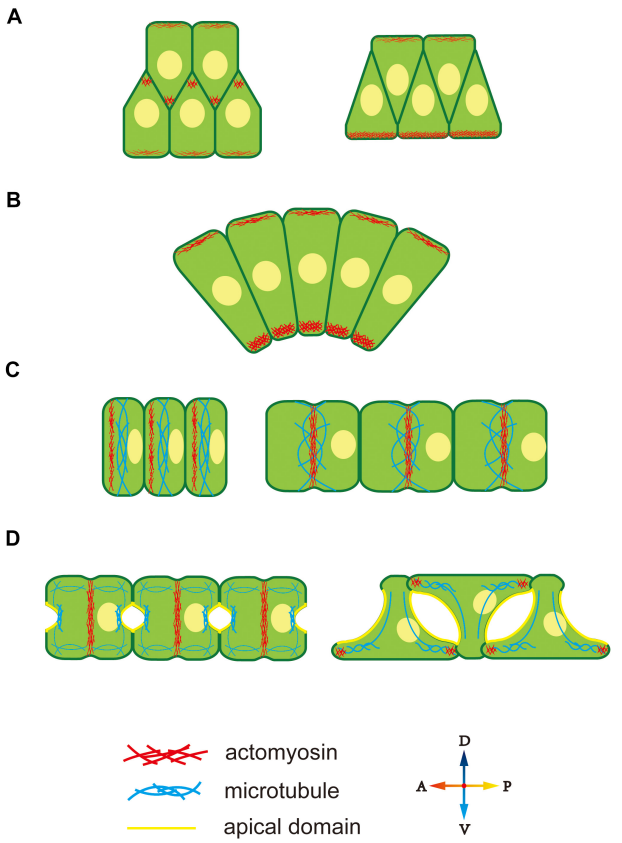

FIGURE 2 | Cytoskeleton polarity during notochord development in *Ciona*. **(A)** F-actin accumulates at the lamellipodium tip, providing migrating forces for cell intercalation. **(B)** Ventrally accumulated actomyosin contractility provides unbalanced force to drive notochord bending. **(C)** An actomyosin contractile ring forms at the anterior edge and moves to the equator of notochord cells. Actomyosin ring contraction elongates notochord cells. Microtubules are perpendicular to the AP axis within notochord cells. **(D)** During lumen expansion, microtubules accumulate at the apical domain, and along with bidirectional migration, they rotate 90° and form oriented bundles toward the leading edges of tractive lamellipodia-like protrusions. An actomyosin contractile ring also exists during lumen expansion and then disappears. At bidirectional migration, F-actin moves to the tip of lamellipodia-like protrusions.

the early stage of notochord development in *Ciona* notochord, cytoskeleton distribution is regulated by the PCP signaling pathway (Sasakura and Makabe, 2001; Niwano et al., 2009), which induces accumulation of midline-oriented F-actin at the membrane cortex, forming cell protrusions (**Figure 2A**) (Munro and Odell, 2002). These protrusions generate a mechanical force to drive cell extension and migration across the surfaces of neighbor notochord cells toward the midline. Disruption of the function of PCP components, causes notochord cells to move in random directions instead of toward the midline (Jiang et al., 2005).

During CE, the notochord bends ventrally to adapt to the limited space inside the chorion. During this process, both actin and myosin II present an obviously ventral-polarized distribution in notochord cells. The dorsal-ventral (DV) polarity of the cytoskeleton in the notochord is observed during cell intercalation (**Figure 2A**). At this stage, notochord cells are arranged in two rows, while, actomyosin accumulates at the ventral cortex of the ventral row, that is, the ventral boundary of notochord tissue (**Figure 2A**, right panel). The polarized actomyosin generates a mechanical force that, along with the faster dorsal epidermis proliferation, drives notochord bending, therefore, embryonic tail bends. The most obvious actomyosin polarity appears at the anterior part of the notochord, where the bending angle is largest (**Figure 2B**). The cytoskeleton DV polarity can only be found in the ventral row during cell intercalation. However, when notochord cells in the dorsal row migrate across the ventral row, they immediately get DV polarity, indicating that the dorsal and ventral rows of notochord cell populations build DV polarity at different time and that establishment of cytoskeleton DV polarity in notochord cells depends on whether the cells are in contact with the ventral boundary of notochord tissue. The signaling pathway that controls DV-polarized cytoskeleton is unclear. The ECM protein laminin localizes dorsally (Veeman et al., 2007), while the apical cell polarity molecule aPKC localized ventrally (Oda-Ishii et al., 2010), which might provide a polarizing signal for polarized actomyosin enrichment. The aPKC has been demonstrated to phosphorylate Lgl to inhibit its interaction with myosin II (Betschinger et al., 2003), providing a cue for further study on the mechanism how D-V polarity influences cell behavior.

After CE, F-actin, and non-muscle myosin present as an actomyosin contractile ring perpendicular to the AP axis to drive notochord cell elongation (Dong et al., 2011; Sehring et al., 2014; Lu et al., 2019). The actomyosin contractile ring first appears at the anterior edge of the notochord and then migrates toward the equator (**Figure 2C**). Positioning of the actomyosin contractile ring is regulated by a "tug-of-war" mechanism between PCP signaling and actomyosin contractility. Inhibition of contractility causes the return of contractile ring to the anterior side, while disruption of both PCP and contractility causes random positioning of contractile ring, indicating that the PCP determines the initial ring position and contractility drives the ring to move to the equator (Sehring et al., 2015). More actomyosin accumulates at the anterior edge compared to the posterior membrane (Newman-Smith et al., 2015). The anterior actomyosin cytoskeleton and core PCP component mutually co-localize at the anterior membrane domain. They interact and maintain the stable 1D PCP along the AP axis. The cytoskeleton is controlled by cell polarity; conversely, cytoskeleton polarity regulates the localization of key polarity-signaling molecules.

After notochord cell elongation, an extracellular lumen forms and then expands between adjacent notochord cells (Dong et al., 2009). This process begins with PCP-AB polarity transition (Denker et al., 2013). The mechanism underlying polarity transition is unclear, but cytoskeleton polarity is likely involved. AB polarity formation in *Drosophila* depends on the F-actin cytoskeleton (Schmidt et al., 2018; Sokac and Wieschaus, 2008a,b). In notochord cells in *Ciona*, a polarized microtubule network is seen toward the apical membrane, which might signal AB polarity formation (**Figure 2D**). Cortical actin and ERM are found to be essential for lumen formation (Dong et al., 2011).

This cytoskeleton network might function as a vesicle-trafficking track to secret the ECM into the extracellular lumen (Mizotani et al., 2018; Bhattachan et al., 2020).

When the lumen expands to a specific volume, notochord cells begin to migrate bidirectionally and flatten (**Figure 2D**). Lamellipodia-like protrusions, whose formation depends on the F-actin network, provide the mechanical force for migration (Dong et al., 2011). Disruption of F-actin polymerization causes the protrusions to disappear and notochord cells to lose migration ability. At the stage of protrusion formation, the microtubule cytoskeleton rotates 90° and forms oriented bundles toward the leading edges of tractive lamellipodia (Dong et al., 2011). Inhibiting microtubule assembling leads to abnormal the location and number of cell protrusions, indicating that polarized microtubule provides directional information for notochord cell migration.

POLARITY SIGNALING REGULATES MECHANICAL PROPERTIES OF THE NOTOCHORD TISSUE

Development is a coordinated multi-tissue-reshaping and movement process. It is also a process of biomechanical force generation, conduction, and release. During development, different tissues have distinct mechanical properties, leading to different reshaping and migratory patterns. A tissue, as a type of specific biomaterial, has autokinetic movement ability, which is a characteristic of life. Therefore a tissue's mechanical properties include not only a shape-changing ability under force, such as bending, stretching, compressing, and twisting, which are described by materials science, but also a regulatory ability to magnify, locate, and orientate bioforces (Mammoto and Ingber, 2010). The tissue's mechanical properties are determined by diverse bioforces generated by subcellular or supracellular structures, such as the cytoskeleton, nuclei, ECM, and cell junctions (Ingber, 2006). Polarity, as dynamic signaling, drives a change in a tissue's mechanical properties by regulating these subcellular or supracellular structures to match embryo developmental processes. Therefore, polarity can serve as a bridge connecting signaling regulation and tissue mechanical properties and coordinate organogenesis during embryo development.

The notochord, as a center pillar-like structure is the main support organ of chordate embryo development (Corallo et al., 2015). In addition, the notochord is a typical polarity-induced organ, and many polarity regulatory pathways are involved in notochord formation. Therefore, the notochord is an important model to study how polarity regulates a tissue's mechanical properties.

At the intercellular level, polarity regulates not match with the properties cell's mechanical properties by affecting the cytoskeleton, nuclei position, or oriented vesicle transport. The cytoskeleton, as an intracellular support structure, is the main cause of an unbalanced bioforce. A polarity signal, such as a PCP signal, regulates the Rho signal pathway to affect cytoskeleton distribution (Nishimura et al., 2012), while cytoskeleton localization and orientation creates cells' mechanical properties (Hefele et al., 2004; Shin et al., 2007). As described earlier, F-actin accumulates at the tip of the lamellipodium to force cell migration toward the midline during cell intercalation (**Figure 3Ai**). In notochord cells in *Ciona*, the ventrally accumulated actomyosin contracts to generate a force that bends the notochord (**Figure 3Aii**). Actomyosin contractile rings localize at the middle of the cells to drive cell elongation (**Figure 3Aiii**). Therefore, cytoskeleton localization affects cells' mechanical properties, while polarized oriented microtubule bundles help lumen expansion and protrusion formation, indicating how cytoskeleton orientation changes cells' mechanical properties (Dong et al., 2011).

The asymmetric position of nuclei also regulates cells' mechanical properties (Calero-Cuenca et al., 2018). During notochord cell elongation in *Ciona* embryos, PCP signaling drives the posterior location of the nuclei in notochord cells (**Figure 3Aiii**) (Jiang et al., 2005; Kourakis et al., 2014). However, the underlying mechanism is still unclear and might be related to the notochords' mechanical properties. In amoeboid migration of immune or lobopodial cells, the nucleus' position affects mechanical properties, such as strength and migration ability (Petrie et al., 2014; Salvermoser et al., 2018; Renkawitz et al., 2019).

In addition, polarity controls polarized membrane vesicle trafficking, which in turn affects cells' mechanical properties. During notochord lumen expansion in *Ciona*, vesicles are transported toward the apical domain to supply the apical membrane and release the membrane tension from continuous lumen expansion (**Figure 3Biv**) (Mizotani et al., 2018; Bhattachan et al., 2020).

At the supracellular level, polarity can regulate oriented ECM secretion, which directly affects cells' mechanical properties by forming a crosslinked network to provide enough strength and elasticity or indirectly regulates by contributing to lumen formation (Loganathan et al., 2020). In the notochord in *Ciona*, basal ECM secretion forms a basal lamina-like notochord sheath (**Figure 3Bv**) (Wei et al., 2017). In addition, some of the ECM has high hydrophilicity, significantly increasing osmotic pressure (Lu et al., 2006). Polarity signaling controls the fixed-point release of the ECM to control osmotic pressure variation in specific areas to influence extracellular liquid flow (**Figure 3Cvi**). There is a lot of ECM in the notochord lumen in *Ciona*, which is secreted by the apical membrane to increase osmotic pressure. Apical lumen expansion together with the basal notochord sheath, forms a fiber-wound cylinder hydrostatic skeleton. Since it is difficult to compress the liquid limen, this structure impacts a higher strength to the notochord than the limit of ECM's and notochord cells' mechanical properties (Adams et al., 1990; Stemple, 2005; Yasuoka, 2020). In addition, the flexibility of this fiber-wound cylinder structure is higher compared to cell reshaping and ECM remodeling. Therefore, it facilitates dynamic regulation of the notochord to adapt to faster embryo development. In *Ciona*, the notochord forms a connected single lumen. In contract, in zebrafish, the notochord forms multiple, discontinuous intracellular vacuoles (Ellis et al., 2013a,b; Corallo et al., 2015). The high connectivity of the lumen might be beneficial by dispersing the strength through lumen matrix flow, which impacts to the notochord greater impact resistance.

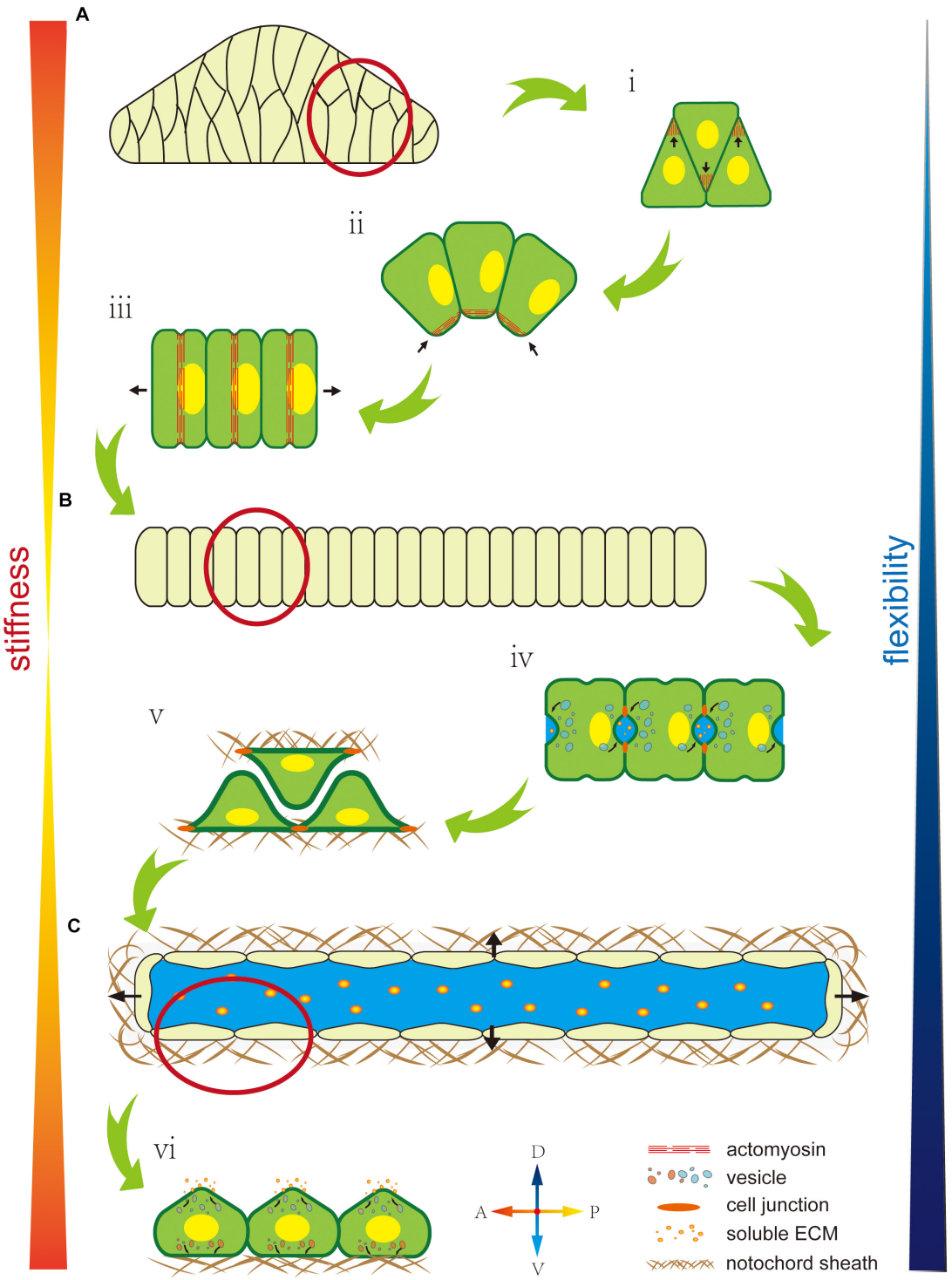

FIGURE 3 | Mechanical properties of the notochord are regulated by cell polarity. **(A)** The early notochord is a short, thick, stiff, rod-like structure made up of a multiline of cells. **(i)** Polarized F-actin drives cells to migrate and intercalate to form a single line. **(ii)** Ventrally polarized actomyosin drives notochord bending toward the ventral side. **(iii)** An equator-localized contractile ring drives notochord cell elongation. **(B)** The notochord forms as a long, thin, single cell-line cord. Its stiffness is low but flexibility is high, which facilitates rapid embryonic development in the narrow space inside the chorion. **(iv)** AB polarity is built during extracellular lumen formation. **(v)** Notochord cells migrate bidirectionally along the notochord sheath. **(vi)** Notochord cells form an endothelial-like single layer. **(C)** A single lumen-filled notochord tube increases tissue stiffness and flexibility, which enables the swimming of *Ciona* larva in seawater.

However, this structure cannot control the shape locally. The evolutionary trend from a single lumen to multiple disconnected vacuoles might compromise the notochord stiffness but impart tissue flexibility, which makes the notochord adapt to the more complex developmental processes in vertebrates.

SUMMARY AND PERSPECTIVE

Ciona notochord is composing of 40 cells with diverse polarities phenomena during development, being an ideal simple model for polarity study. Besides, the *Ciona* genome is single-copy, which benefits to elucidate the molecular mechanism for polarity establishment and maintenance. Because of the specifically evolutionary position in animal phylogenetic taxa, the knowledge achieved from *Ciona* notochord polarity can be used for reference toward both invertebrate and vertebrate.

Although the *Ciona* notochord model is simple for polarity study, there still remains several challenge questions need to be answered in the future. For example, what is the signaling contributing to the establishment of the initial AB polarity? Who mediates the interaction and transition between PCP and AB polarity? How do polarities coordinate the concerted and coherent development in multiple tissues?

Par/aPKC complex contributes to the establishment of AB polarity in notochord cell. However, the signaling for the establishment of initial AB polarity is still unknown. It has been indicated that Rho signaling mediated centrosome and microtubule play an important role in the initial localization of the key component proteins of AB polarity. Further study to reveal the controlling signals for the localization of Par/aPKC complex in *Ciona* notochord cells will provide cues to understand how AB polarity is initially established in a cell.

The crosstalk between PCP and AB polarity is also worth further exploring to learn about how the different polarity systems are coordinated. Several ways including the interaction between PCP and AB polarity components, cell–cell contact, and cell-basement membrane contact are candidate pathways to mediate such crosstalk between PCP and AB polarity. However, the molecular mechanisms underlying these possibilities are unknown. Investigation in a structurally simple and single gene copy notochord system will benefit to answer the question.

Polarity plays an important role in coordination of multiple tissue development by controlling tissue mechanical property. For example, when flat cell sheets bundle to form a biological tube, polarity regulates an asymmetry cell wedge or drives cell directional intercalate, leading to the bending movement through the mechanical property change in different parts of the cell flat sheet (Nielsen et al., 2020). Compared with the anatomically complex of vertebrate, *Ciona* embryonic tail is structurally simple, providing an excellent model to understand how polarity signaling coordinates the multiple tissue development.

AUTHOR CONTRIBUTIONS

BD and HP conceived and wrote the manuscript. HP prepared the figures. RQ provided critical editing and input. All authors contributed to the article and approved the submitted version.

FUNDING

BD was supported by the National Key Research and Development Program of China (2019YFE0190900), the National Natural Science Foundation of China (31771649), the Marine S&T Fund of Shandong Province for Pilot National Laboratory for Marine Science and Technology (Qingdao) (2018SDKJ0302-1).

ACKNOWLEDGMENTS

We thank members of the Dong Laboratory, including Zhiyi Lv, Xiuxia Yang, and Wenjie Shi for their critical reading and invaluable comments on the manuscript.

REFERENCES

Adams, D. S., Keller, R., and Koehl, M. A. (1990). The mechanics of notochord elongation, straightening and stiffening in the embryo of *Xenopus laevis*. *Development* 110, 115–130.

Adler, P. N. (2012). The frizzled/stan pathway and planar cell polarity in the *Drosophila* wing. *Curr. Top. Dev. Biol.* 101, 1–31. doi: 10.1016/b978-0-12-394592-1.00001-6

Assémat, E., Bazellières, E., Pallesi-Pocachard, E., Le Bivic, A., and Massey-Harroche, D. (2008). Polarity complex proteins. *Biochim. Biophys. Acta* 1778, 614–630.

Bagwell, J., Norman, J., Ellis, K., Peskin, B., Hwang, J., Ge, X., et al. (2020). Notochord vacuoles absorb compressive bone growth during zebrafish spine formation. *eLife* 9:e51221.

Balser, E. J., and Ruppert, E. E. (1990). Structure, ultrastructure, and function of the preoral heart-kidney in *Saccoglossus kowalevski* (Hemichordata, Enteropneusta) including new data on the stomochord. *Acta Zool.* 71, 235–249. doi: 10.1111/j.1463-6395.1990.tb01082.x

Bénazéraf, B., and Pourquié, O. (2013). Formation and segmentation of the vertebrate body axis. *Annu. Rev. Cell Dev. Biol.* 29, 1–26. doi: 10.1146/annurev-cellbio-101011-155703

Betschinger, J., Mechtler, K., and Knoblich, J. A. (2003). The Par complex directs asymmetric cell division by phosphorylating the cytoskeletal protein Lgl. *Nature* 422, 326–330. doi: 10.1038/nature01486

Bhattachan, P., Rae, J., Yu, H., Jung, W., Wei, J., Parton, R. G., et al. (2020). Ascidian caveolin induces membrane curvature and protects tissue integrity and morphology during embryogenesis. *FASEB J.* 34, 1345–1361. doi: 10.1096/fj.201901281r

Bisgrove, B. W., Essner, J. J., and Yost, H. J. (2000). Multiple pathways in the midline regulate concordant brain, heart and gut left-right asymmetry. *Development* 127, 3567–3579.

Brownlee, C., and Bouget, F. (1998). Polarity determination in fucus: from zygote to multicellular embryo. *Semin. Cell Dev. Biol.* 9, 179–185. doi: 10.1006/scdb.1997.0212

Brunet, T., Lauri, A., and Arendt, D. (2015). Did the notochord evolve from an ancient axial muscle? The axochord hypothesis. *Bioessays* 37, 836–850. doi: 10.1002/bies.201500027

Buisson, N., Sirour, C., Moreau, N., Denker, E., Le Bouffant, R., Goullancourt, A., et al. (2014). An adhesome comprising laminin, dystroglycan and myosin IIA is required during notochord development in *Xenopus laevis*. *Development* 141, 4569–4579. doi: 10.1242/dev.116103

Calero-Cuenca, F. J., Janota, C. S., and Gomes, E. R. (2018). Dealing with the nucleus during cell migration. *Curr. Opin. Cell Biol.* 50, 35–41. doi: 10.1016/j.ceb.2018.01.014

Choi, K., Cohn, M. J., and Harfe, B. D. (2008). Identification of nucleus pulposus precursor cells and notochordal remnants in the mouse: implications for disk degeneration and chordoma formation. *Dev. Dyn.* 237, 3953–3958. doi: 10.1002/dvdy.21805

Choi, K. S., and Harfe, B. D. (2011). Hedgehog signaling is required for formation of the notochord sheath and patterning of nuclei pulposi within the intervertebral discs. *Proc. Natl. Acad. Sci. U.S.A.* 108, 9484–9489. doi: 10.1073/pnas.1007566108

Cloney, R. A. (1982). Ascidian larvae and the events of metamorphosis. *Am. Zool.* 22, 817–826. doi: 10.1093/icb/22.4.817

Corallo, D., Trapani, V., and Bonaldo, P. (2015). The notochord: structure and functions. *Cell. Mol. Life Sci.* 72, 2989–3008. doi: 10.1007/s00018-015-1897-z

Deng, W., Nies, F., Feuer, A., Bocina, I., Oliver, D., and Jiang, D. (2013). Anion translocation through an Slc26 transporter mediates lumen expansion during tubulogenesis. *Proc. Natl. Acad. Sci. U.S.A.* 110, 14972–14977. doi: 10.1073/pnas.1220884110

Denker, E., and Jiang, D. (2012). *Ciona intestinalis* notochord as a new model to investigate the cellular and molecular mechanisms of tubulogenesis. *Semin. Cell Dev. Biol.* 23, 308–319. doi: 10.1016/j.semcdb.2012.03.004

Denker, E., Bocina, I., and Jiang, D. (2013). Tubulogenesis in a simple cell cord requires the formation of Bi-apical cells through two discrete par domains. *Development* 140, 2985–2996. doi: 10.1242/dev.092387

Dhonukshe, P. (2013). "Polarity, developmental," in *Brenner's Encyclopedia of Genetics*, 2nd Edn, eds S. Maloy and K. Hughes (Cambridge, MA: Academic Press), 378–382.

Djiane, A., Yogev, S., and Mlodzik, M. (2005). The apical determinants aPKC and dPatj regulate frizzled-dependent planar cell polarity in the *Drosophila* eye. *Cell* 121, 621–631. doi: 10.1016/j.cell.2005.03.014

Dong, B., Horie, T., Denker, E., Kusakabe, T., Tsuda, M., Smith, W. C., et al. (2009). Tube formation by complex cellular processes in *Ciona intestinalis* notochord. *Dev. Biol.* 330, 237–249. doi: 10.1016/j.ydbio.2009.03.015

Dong, B., Deng, W., and Jiang, D. (2011). Distinct cytoskeleton populations and extensive crosstalk control *Ciona* notochord tubulogenesis. *Development* 138, 1631–1641. doi: 10.1242/dev.057208

Ellis, K., Bagwell, J., and Bagnat, M. (2013a). Notochord vacuoles are lysosome-related organelles that function in axis and spine morphogenesis. *J. Cell Biol.* 200, 667–679. doi: 10.1083/jcb.201212095

Ellis, K., Hoffman, B. D., and Bagnat, M. (2013b). The vacuole within: how cellular organization dictates notochord function. *Bioarchitecture* 3, 64–68. doi: 10.4161/bioa.25503

Eom, D. S., Amarnath, S., Fogel, J. L., and Agarwala, S. (2011). Bone morphogenetic proteins regulate neural tube closure by interacting with the apicobasal polarity pathway. *Development* 138, 3179–3188. doi: 10.1242/dev.058602

Feldman, J. L., and Priess, J. R. (2012). A role for the centrosome and PAR-3 in the hand-off of MTOC function during epithelial polarization. *Curr. Biol.* 22, 575–582. doi: 10.1016/j.cub.2012.02.044

Feng, Y., Li, J., and Xu, A. (2016). "*Amphioxus* as a model for understanding the evolution of vertebrates," in *Amphioxus Immunity*, ed. A. Xu (Cambridge, MA: Academic Press), 1–13. doi: 10.1016/b978-0-12-849903-0.00001-4

Goto, T., Davidson, L., Asashima, M., and Keller, R. (2005). Planar cell polarity genes regulate polarized extracellular matrix deposition during frog gastrulation. *Curr. Biol.* 15, 787–793. doi: 10.1016/j.cub.2005.03.040

Grimes, D. T. (2019). Making and breaking symmetry in development, growth and disease. *Development* 146:dev170985. doi: 10.1242/dev.170985

Hashimoto, M., and Hamada, H. (2010). Translation of anterior–posterior polarity into left–right polarity in the mouse embryo. *Curr. Opin. Genet. Dev.* 20, 433–437. doi: 10.1016/j.gde.2010.04.002

Hefele, J. A., Unterseher, F., Giehl, K., Schambony, A., Wedlich, D., and De Robertis, E. M. (2004). Paraxial protocadherin coordinates cell polarity during convergent extension via Rho A and JNK. *EMBO J.* 23, 3259–3269. doi: 10.1038/sj.emboj.7600332

Hermann, G. J., Leung, B., and Priess, J. R. (2000). Left-right asymmetry in *C. elegans* intestine organogenesis involves a LIN-12/Notch signaling pathway. *Development* 127, 3429–3440.

Holló, G. (2015). A new paradigm for animal symmetry. *Interface Focus* 5, 1–10.

Hu, G., Li, G., Wang, H., and Wang, Y. (2017). Hh gene participates in the left-right asymmetry development of amphioxus by controlling Cer expression. *Development* 144, 4694–4703. doi: 10.1242/dev.157172

Ingber, D. E. (2006). Cellular mechanotransduction: putting all the pieces together again. *FASEB J.* 20, 811–827. doi: 10.1096/fj.05-5424rev

Jiang, D., Munro, E. M., and Smith, W. C. (2005). Ascidian prickle regulates both mediolateral and anterior-posterior cell polarity of notochord cells. *Curr. Biol.* 15, 79–85. doi: 10.1016/j.cub.2004.12.041

Kato, Y. (2011). The multiple roles of Notch signaling during left-right patterning. *Cell. Mol. Life Sci.* 68, 2555–2567. doi: 10.1007/s00018-011-0695-5

Keller, R. (2006). Mechanisms of elongation in embryogenesis. *Development* 133, 2291–2302. doi: 10.1242/dev.02406

Kourakis, M. J., Reeves, W., Newman-Smith, E., Maury, B., Abdul-Wajid, S., and Smith, W. C. (2014). A one-dimensional model of PCP signaling: polarized cell behavior in the notochord of the ascidian *Ciona*. *Dev. Biol.* 395, 120–130. doi: 10.1016/j.ydbio.2014.08.023

Lauri, A., Brunet, T., Handberg-Thorsager, M., Fischer, A. H. L., Simakov, O., Steinmetz, P. R. H., et al. (2014). Development of the annelid axochord: insights into notochord evolution. *Science* 345, 1365–1368. doi: 10.1126/science.1253396

Loganathan, R., Little, C. D., and Rongish, B. J. (2020). Extracellular matrix dynamics in tubulogenesis. *Cell. Signal.* 72:109619. doi: 10.1016/j.cellsig.2020.109619

Lu, Q., Bhattachan, P., and Dong, B. (2019). Ascidian notochord elongation. *Dev. Biol.* 448, 147–153. doi: 10.1016/j.ydbio.2018.11.009

Lu, Y., Parker, K. H., and Wang, W. (2006). Effects of osmotic pressure in the extracellular matrix on tissue deformation. *Philos. Trans. R. Soc. A Math. Phys. Eng. Sci.* 364, 1407–1422. doi: 10.1098/rsta.2006.1778

Lv, Z., Lu, Q., and Dong, B. (2019). Morphogenesis: a focus on marine invertebrates. *Mar. Life Sci. Technol.* 1, 28–40. doi: 10.1007/s42995-019-00016-z

Mammoto, T., and Ingber, D. E. (2010). Mechanical control of tissue and organ development. *Development* 137, 1407–1420. doi: 10.1242/dev.024166

Manninen, A. (2015). Epithelial polarity – generating and integrating signals from the ECM with integrins. *Exp. Cell Res.* 334, 337–349. doi: 10.1016/j.yexcr.2015.01.003

Marsden, M., and DeSimone, D. W. (2003). Integrin-ECM interactions regulate cadherin-dependent cell adhesion and are required for convergent extension in *Xenopus*. *Curr. Biol.* 13, 1182–1191. doi: 10.1016/s0960-9822(03)00433-0

Matsunobu, S., and Sasakura, Y. (2015). Time course for tail regression during metamorphosis of the ascidian *Ciona intestinalis*. *Dev. Biol.* 405, 71–81. doi: 10.1016/j.ydbio.2015.06.016

McCann, M. R., Tamplin, O. J., Rossant, J., and Seguin, C. A. (2011). Tracing notochord-derived cells using a Noto-cre mouse: implications for intervertebral disc development. *Dis. Models Mech.* 5, 73–82. doi: 10.1242/dmm.008128

Mizotani, Y., Suzuki, M., Hotta, K., Watanabe, H., Shiba, K., Inaba, K., et al. (2018). 14-3-3εa directs the pulsatile transport of basal factors toward the apical domain for lumen growth in tubulogenesis. *Proc. Natl. Acad. Sci. U.S.A.* 115, E8873–E8881.

Mlodzik, M. (2002). "Tissue polarity in the retina," in *Results and Problems in Cell Differentiation*, Vol. 37, ed. K. Moses (Berlin: Springer), 89–106. doi: 10.1007/978-3-540-45398-7_7

Munro, E. M., and Odell, G. M. (2002). Polarized basolateral cell motility underlies invagination and convergent extension of the ascidian notochord. *Development* 129, 13–24.

Nance, J. (2014). Getting to know your neighbor: cell polarization in early embryos. *J. Cell Biol.* 206, 823–832. doi: 10.1083/jcb.201407064

Newman-Smith, E., Kourakis, M. J., Reeves, W., Veeman, M., and Smith, W. C. (2015). Reciprocal and dynamic polarization of planar cell polarity core components and myosin. *eLife* 4:e05361.

Nielsen, B. F., Nissen, S. B., Sneppen, K., Mathiesen, J., and Trusina, A. (2020). Model to link cell shape and polarity with organogenesis. *iScience* 23:100830. doi: 10.1016/j.isci.2020.100830

Ninomiya, H. (2004). Antero-posterior tissue polarity links mesoderm convergent extension to axial patterning. *Nature* 430, 364–367. doi: 10.1038/nature02620

Nishimura, T., Honda, H., and Takeichi, M. (2012). Planar cell polarity links axes of spatial dynamics in neural-tube closure. *Cell* 149, 1084–1097. doi: 10.1016/j.cell.2012.04.021

Niwano, T., Takatori, N., Kumano, G., and Nishida, H. (2009). Wnt5 is required for notochord cell intercalation in the ascidian *Halocynthia roretzi*. *Biol. Cell* 101, 645–659. doi: 10.1042/bc20090042

Oda-Ishii, I., Ishii, Y., and Mikawa, T. (2010). Eph regulates dorsoventral asymmetry of the notochord plate and convergent extension-mediated notochord formation. *PLoS One* 5:e13689. doi: 10.1371/journal.pone.0013689

Ota, K. G., and Kuratani, S. (2007). Cyclostome embryology and early evolutionary history of vertebrates. *Integr. Comp. Biol.* 47, 329–337. doi: 10.1093/icb/icm022

Pagnon-Minot, A., Malbouyres, M., Haftek-Terreau, Z., Kim, H. R., Sasaki, T., Thisse, C., et al. (2008). Collagen XV, a novel factor in zebrafish notochord differentiation and muscle development. *Dev. Biol.* 316, 21–35. doi: 10.1016/j.ydbio.2007.12.033

Parsons, M. J., Pollard, S. M., Saúde, L., Feldman, B., Coutinho, P., Elizabeth, M. A. H., et al. (2002). Zebrafish mutants identify an essential role for laminins in notochord formation. *Development* 129, 3137–3146.

Pegoraro, A. F., Janmey, P., and Weitz, D. A. (2017). Mechanical properties of the cytoskeleton and cells. *Cold Spring Harb. Perspect. Biol.* 9:a022038. doi: 10.1101/cshperspect.a022038

Petrie, R. J., Koo, H., and Yamada, K. M. (2014). Generation of compartmentalized pressure by a nuclear piston governs cell motility in a 3D matrix. *Science* 345, 1062–1065. doi: 10.1126/science.1256965

Pickett, M. A., Naturale, V. F., and Feldman, J. L. (2019). A polarizing issue: diversity in the mechanisms underlying apico-basolateral polarization in vivo. *Annu. Rev. Cell Dev. Biol.* 35, 285–308. doi: 10.1146/annurev-cellbio-100818-125134

Raman, R., Pinto, C. S., and Sonawane, M. (2018). Polarized organization of the cytoskeleton: regulation by cell polarity proteins. *J. Mol. Biol.* 430, 3565–3584. doi: 10.1016/j.jmb.2018.06.028

Raya, Á., and Belmonte, J. C. I. (2006). Left–right asymmetry in the vertebrate embryo: from early information to higher-level integration. *Nat. Rev. Genet.* 7, 283–293. doi: 10.1038/nrg1830

Renkawitz, J., Kopf, A., Stopp, J., de Vries, I., Driscoll, M. K., Merrin, J., et al. (2019). Nuclear positioning facilitates amoeboid migration along the path of least resistance. *Nature* 568, 546–550. doi: 10.1038/s41586-019-1087-5

Salvermoser, M., Begandt, D., Alon, R., and Walzog, B. (2018). Nuclear deformation during neutrophil migration at sites of inflammation. *Front. Immunol.* 9:2680. doi: 10.3389/fimmu.2018.02680

Sasakura, Y., and Makabe, K. W. (2001). Ascidian Wnt-5 gene is involved in the morphogenetic movement of notochord cells. *Dev. Growth Differ.* 43, 573–582. doi: 10.1046/j.1440-169x.2001.00602.x

Schmidt, A., Lv, Z., and Großhans, J. (2018). ELMO and sponge specify subapical restriction of canoe and formation of the subapical domain in early *Drosophila* embryos. *Development* 145:dev157909. doi: 10.1242/dev.157909

Sehring, I. M., Dong, B., Denker, E., Bhattachan, P., Deng, W., Mathiesen, B. T., et al. (2014). An equatorial contractile mechanism drives cell elongation but not cell division. *PLoS Biol.* 12:e1001781. doi: 10.1371/journal.pbio.1001781

Sehring, I. M., Recho, P., Denker, E., Kourakis, M., Mathiesen, B., Hannezo, E., et al. (2015). Assembly and positioning of actomyosin rings by contractility and planar cell polarity. *eLife* 4:e09206.

Shin, J. H., Tam, B. K., Brau, R. R., Lang, M. J., Mahadevan, L., and Matsudaira, P. (2007). Force of an actin spring. *Biophys. J.* 92, 3729–3733. doi: 10.1529/biophysj.106.099994

Smith, W. C. (2018). Cellular processes of notochord formation. *Adv. Exp. Med. Biol.* 1029, 165–177. doi: 10.1007/978-981-10-7545-2_15

Sokac, A. M., and Wieschaus, E. (2008a). Local actin-dependent endocytosis is zygotically controlled to initiate Drosophila cellularization. *Dev. Cell* 14, 775–786. doi: 10.1016/j.devcel.2008.02.014

Sokac, A. M., and Wieschaus, E. (2008b). Zygotically controlled F-actin establishes cortical compartments to stabilize furrows during *Drosophila* cellularization. *J. Cell Sci.* 121, 1815–1824. doi: 10.1242/jcs.025171

Stemple, D. L. (2005). Structure and function of the notochord: an essential organ for chordate development. *Development* 132, 2503–2512. doi: 10.1242/dev.01812

Suzuki, A., Yamanaka, T., Hirose, T., Manabe, N., Mizuno, K., Shimizu, M., et al. (2001). Atypical protein kinase C is involved in the evolutionarily conserved par protein complex and plays a critical role in establishing epithelia-specific junctional structures. *J. Cell Biol.* 152, 1183–1196. doi: 10.1083/jcb.152.6.1183

Turing, A. M. (1952). The chemical basis of morphogenesis. *Philos. Trans. R. Soc. Lond. B* 237, 37–72.

Ukita, K., Hirahara, S., Oshima, N., Imuta, Y., Yoshimoto, A., Jang, C., et al. (2009). Wnt signaling maintains the notochord fate for progenitor cells and supports the posterior extension of the notochord. *Mech. Dev.* 126, 791–803. doi: 10.1016/j.mod.2009.08.003

Veeman, M. T., and McDonald, J. A. (2016). Dynamics of cell polarity in tissue morphogenesis: a comparative view from *Drosophila* and *Ciona*. *F1000Res.* 5:1084. doi: 10.12688/f1000research.8011.1

Veeman, M. T., Nakatani, Y., Hendrickson, C., Ericson, V., Lin, C., and Smith, W. C. (2007). Chongmague reveals an essential role for laminin-mediated boundary formation in chordate convergence and extension movements. *Development* 135, 33–41. doi: 10.1242/dev.010892

Ward, L., Pang, A. S. W., Evans, S. E., and Stern, C. D. (2018). The role of the notochord in amniote vertebral column segmentation. *Dev. Biol.* 439, 3–18. doi: 10.1016/j.ydbio.2018.04.005

Wedlich-Soldner, R., and Li, R. (2003). Spontaneous cell polarization: undermining determinism. *Nat. Cell Biol.* 5, 267–270. doi: 10.1038/ncb0403-267

Wei, J., Wang, G., Li, X., Ren, P., Yu, H., and Dong, B. (2017). Architectural delineation and molecular identification of extracellular matrix in ascidian embryos and larvae. *Biol. Open* 6, 1383–1390. doi: 10.1242/bio.026336

Wen, W., and Zhang, M. (2018). Protein complex assemblies in epithelial cell polarity and asymmetric cell division. *J. Mol. Biol.* 430, 3504–3520. doi: 10.1016/j.jmb.2017.09.013

Wolpert, L. (2013). Cell polarity. *Philos. Trans. R. Soc. Lond. B Biol. Sci.* 368:20130419.

Wopat, S., Bagwell, J., Sumigray, K. D., Dickson, A. L., Huitema, L. F. A., Poss, K. D., et al. (2018). Spine patterning is guided by segmentation of the notochord sheath. *Cell Rep.* 22, 2026–2038. doi: 10.1016/j.celrep.2018.01.084

Wu, J., and Mlodzik, M. (2009). A quest for the mechanism regulating global planar cell polarity of tissues. *Trends Cell Biol.* 19, 295–305. doi: 10.1016/j.tcb.2009.04.003

Yang, Y., and Mlodzik, M. (2015). Wnt-frizzled/planar cell polarity signaling: cellular orientation by facing the wind (Wnt). *Annu. Rev. Cell Dev. Biol.* 31, 623–646. doi: 10.1146/annurev-cellbio-100814-125315

Yasuoka, Y. (2020). Morphogenetic mechanisms forming the notochord rod: the turgor pressure-sheath strength model. *Dev. Growth Differ.* 62, 379–390. doi: 10.1111/dgd.12665

Conflict of Interest: The authors declare that the research was conducted in the absence of any commercial or financial relationships that could be construed as a potential conflict of interest.

frontiers in Cell and Developmental Biology

MINI REVIEW
published: 23 December 2020
doi: 10.3389/fcell.2020.619958

Planar Cell Polarity and E-Cadherin in Tissue-Scale Shape Changes in *Drosophila* Embryos

Deqing Kong and Jörg Großhans*

Department of Biology, Philipps-University Marburg, Marburg, Germany

Planar cell polarity and anisotropic cell behavior play critical roles in large-scale epithelial morphogenesis, homeostasis, wound repair, and regeneration. Cell–Cell communication and mechano-transduction in the second to minute scale mediated by E-cadherin complexes play a central role in the coordination and self-organization of cellular activities, such as junction dynamics, cell shape changes, and cell rearrangement. Here we review the current understanding in the interplay of cell polarity and cell dynamics during body axis elongation and dorsal closure in *Drosophila* embryos with a focus on E-cadherin dynamics in linking cell and tissue polarization and tissue-scale shape changes.

Keywords: *Drosophila* embryonic epithelium, DE-cadherin, planar polarity, non-muscle myosin-II, tissue-scale shape changes

OPEN ACCESS

Edited by:
Yi Wu,
UCONN Health, United States

Reviewed by:
Jun Zhou,
German Cancer Research Center (DKFZ), Germany
Ana Carmena,
Consejo Superior de Investigaciones Científicas (CSIC), Spain

****Correspondence:***
Deqing Kong
deqing.kong@biologie.uni-marburg.de

Specialty section:
This article was submitted to Signaling, a section of the journal Frontiers in Cell and Developmental Biology

Received: *21 October 2020*
Accepted: *07 December 2020*
Published: *23 December 2020*

Citation:
Kong D and Großhans J (2020) Planar Cell Polarity and E-Cadherin in Tissue-Scale Shape Changes in Drosophila Embryos. Front. Cell Dev. Biol. 8:619958. doi: 10.3389/fcell.2020.619958

INTRODUCTION

Epithelia constitute the surface of organs in multicellular organisms and the units of many morphogenetic processes. Epithelial cells adhere to one another to form two-dimensional sheets and constitute permeability barriers for compartmentalization of the body, which is essential for the physiology and protection of the organs and even the whole organisms. Despite their physical integrity and stability, epithelial sheets are intrinsically dynamic and able to restructure in a time scale as fast as minutes (Gumbiner, 1992; Leptin, 1994; Lye and Sanson, 2011; Lv et al., 2019). During morphogenesis, epithelia undergo tissue-scale morphology changes, such as extension, closure, invagination, tubulation, and wrapping. Underlying those morphogenetic processes are cellular activities such as junction remodeling, cell shape changes, and cell rearrangement.

Planar polarity is based on molecular asymmetries within the epithelial sheet and cells and impinges on the cellular activities leading to tissue-scale shape changes. Cell junctions are at the center of the transition from cells to tissue. The mechanical link between is constituted by adherens junctions with E-cadherin (E-cad)–catenin complexes as the central component. Together with numerous associated proteins varying between cell types and developmental stages, the E-cad complex provides a mechanical link between the actomyosin networks of adjacent cells and coordinates their activities via mechanotransduction (Maître and Heisenberg, 2013; Leckband and de Rooij, 2014; Charras and Yap, 2018).

In this review, we will focus on recent progress in two processes of *Drosophila* embryogenesis, i.e., germband extension and dorsal closure. With these two case studies, we will discuss how cell and tissue polarization are coordinated to give rise to tissue-scale changes in visible morphology.

DROSOPHILA EMBRYONIC EPITHELIUM

The first epitheliogenesis, termed cellularization, in *Drosophila* development is initiated when the zygotic genome is activated at the transition from syncytial to cellular morphology (Schmidt and Grosshans, 2018). Cell polarization and epithelial sheet formation are intrinsically linked during cellularization. As the plasma membrane ingresses, the cell cortex becomes polarized as visible by segregation of cortical markers. Initially assembling into spot junctions distributed along the lateral furrow, the E-cad–catenin complex coalesces into unmatured adherens junctions at the typical subapical position only by the end of cellularization. During gastrulation, the epithelial epidermis undergoes stage and position-dependent morphogenetic movements, such as tissue invagination (Leptin, 2005; Martin, 2020), folding (Wang et al., 2012), convergent extension (Kong et al., 2017; Paré and Zallen, 2020), compartmental boundaries formation (Sharrock and Sanson, 2020), and dorsal closure (Hayes and Solon, 2017; Kiehart et al., 2017) to name the most prominent ones.

DE-CADHERIN AND ADHERENS JUNCTIONS

Drosophila E-cadherin (DE-cadherin, DE-cad), known as Shotgun (Shg) in *Drosophila*, was identified as Armadillo (β-catenin) associated glycoprotein (Oda et al., 1994) and by the zygotic lethal mutation *shotgun* (Tepass et al., 1996; Uemura et al., 1996). Similar to classical cadherins in vertebrates, DE-cad is a single-transmembrane protein with seven cadherin repeats at its extracellular N-terminal region, followed by a cysteine-rich region, an EGF-like region and a laminin G domain. The cytoplasmic part contains binding sites for p120-catenin (Myster et al., 2003) and β-catenin (Pai et al., 1996), which leads to the assembly of the stereotypic cadherin–catenin complex at the core of adherens junctions (**Figure 1A**). DE-cad is proteolytically cleaved at its cysteine-rich region into two fragments after translation. The two fragments remain associated, however, via non-covalent interactions to form the mature protein (Oda and Tsukita, 1999). E-cad molecules undergo stable Ca^{2+}-dependent homotypic interactions in trans between adjacent cells (Oda et al., 1994). The mammalian E-cad contains five cadherin repeats at its N-terminal portion. Of these, the most N-terminal-most cadherin domain engages in homophilic binding. In *Drosophila*, the four N-terminal-most cadherin domains have been reported to mediate the trans interaction (**Figure 1B**) (Nishiguchi et al., 2016). Beside the polypeptide backbone, post-translational modifications, such as glycosylation and phosphorylation, are essential for the functions of DE-cad and epithelial morphogenesis (Zhang et al., 2014; Chen et al., 2017).

In the fertilized egg and syncytial stage, DE-cad is more or less uniformly distributed within the plasma membrane and intracellular vesicles. The first junctions involving DE-cad are observed during cellularization (Cox et al., 1996; Müller and Wieschaus, 1996). Generic adherens junctions at a subapical position with an F-actin belt form and mature during late cellularization and gastrulation (stage 7–9), when the DE-cad density increases and coalesces into clusters and stable microdomains (Harris and Peifer, 2004; Cavey et al., 2008; Truong Quang et al., 2013). Beside the Ca^{2+}-dependent interactions in trans, E-cadherin molecules bind to each other in cis within the same lipid bilayer to form super-molecular clusters (**Figure 1B**). Similar to mammalian cells (Engl et al., 2014; Wu et al., 2015), the DE-cad clusters require interactions with F-actin (Truong Quang et al., 2013). Non-muscle Myosin-II (Myosin-II) dependent tensile forces promote DE-cad clustering at cell contacts (Kale et al., 2018). However, the detailed mechanisms by which the cell cortex impinges on the DE-cad clusters remain elusive. *In vitro* studies revealed a function of the intracellular cadherin–catenin complex as a force sensor. Mechanical forces from actin cytoskeleton induce long-lived bonds in the cadherin-catenin complex (Buckley et al., 2014) and promote binding of the actin-binding protein Vinculin to α-catenin. In this way, a self-reinforcing system is established to strengthen the linkage between E-cad clusters and the actin cytoskeleton.

Armadillo is the *Drosophila* homolog of β-catenin, whose 13 copies of so-called Armadillo repeats are its characteristic feature (Peifer and Wieschaus, 1990). The N-terminal region and the first Armadillo repeat bind to α-catenin, while Armadillo repeats 3–8 are necessary and sufficient for DE-cad binding (Orsulic and Peifer, 1996; Pai et al., 1996), thus generating a bridge between the plasma membrane with E-cad and α-catenin with F-actin.

Within α-catenin, the VH1 domain mediates the interaction with ß-catenin (Oda et al., 1993; Pai et al., 1996) and the VH3 domain, binding to F-actin (Pokutta et al., 2008). Vertebrate α-catenin undergoes a reversible force-dependent change between two stable conformations (Choi et al., 2012; Rangarajan and Izard, 2012; Yao et al., 2014; Charras and Yap, 2018; Ishiyama et al., 2018). In the open conformation, when force is applied, α-catenin is bound on the one side to the Cadherin complex and the other side via the central mechanosensitive modulatory (M) domain to the D1 domain of Vinculin, thus bridging adherens junctions and F-actin. In contrast, when no force is applied, α-catenin changes into closed conformation with an inaccessible M-domain. In the closed conformation, α-catenin binds only to the Cadherin complex but not to Vinculin and its associated F-actin (**Figure 1A**). In *Drosophila* embryos, Vinculin colocalizes with E-cad (Kale et al., 2018), which is promoted by intracellular contracting forces and reduced following tissue relaxation (Kong et al., 2019).

p120-catenin is involved in endocytosis of the dynamic E-cadherin and Bazooka complexes in *Drosophila* embryos (Bulgakova and Brown, 2016). Binding of p120-catenin also appears to be mechanosensitive as recent research from *Drosophila* wing epithelium. In this system, p120-catenin is involved in E-cadherin turnover and epithelial viscoelasticity (Iyer et al., 2019). The numerous proteins associated with adherens junctions beyond the core complex have been discussed and reviewed by Harris (2012), for example.

In summary, adherens junctions with the E-cad–catenin complex at its core link the actin cytoskeletons of two neighboring cells in an epithelium (**Figure 1**). Spatial and

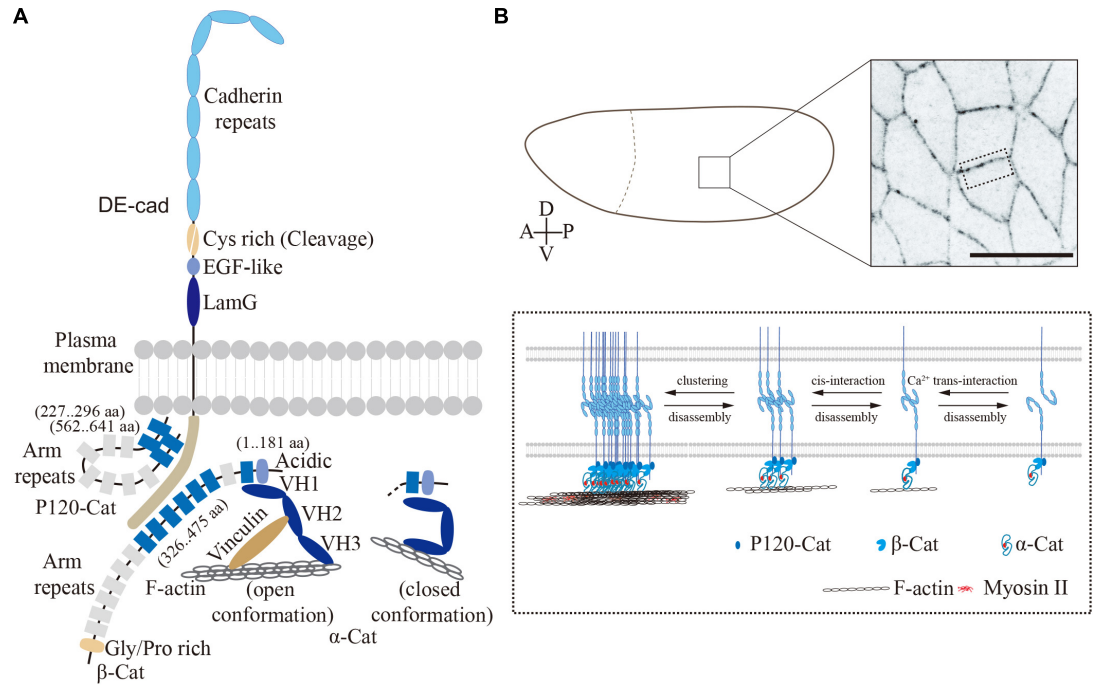

FIGURE 1 | *Drosophila* embryonic epithelium. **(A)** The cadherin–catenin complex in *Drosophila* (modified from Harris, 2012). The single-transmembrane protein, DE-cadherin mediates cell–cell adhesion through homophilic interactions between its extracellular domain. In contrast, its cytoplasmic domain binding with p120-catenin, β-catenin, and α-catenin as cadherin–catenin complex forms the core of adherens junctions. Protein domains and interacting regions are indicated. **(B)** Confocal image of lateral epithelium from an embryo expressing E-Cad-GFP, scale bar is 10 μm. The close-up view on the bottom shows the adherens junctions and DE-cad clusters in *Drosophila* epithelium. DE-cad forms the adherens junctions via homophilic binding of N-terminal-most four extracellular cadherin domains, while the cytoplasmic domain binding with actomyosin network via Arm/ß-catenin and α-catenin.

temporal modulation of the complexes is a central feature of dynamic epithelia during embryogenesis.

GERMBAND EXTENSION: FROM ANTERIOR–POSTERIOR PATTERN TO PLANAR POLARITY TO CELL INTERCALATION

Drosophila germband extension serves as a paradigm for axis elongation by convergence and extension of an epithelial sheet (**Figures 2A–C**) (Kong et al., 2017). During germband extension, the lateral epidermis increases its length more than two-fold along the anterior–posterior (AP) axis, while correspondingly narrowing along the dorsal–ventral (DV) axis. The elongation of the tissue is largely due to polarized cell rearrangement by neighbor exchanges (**Figures 2A–C**) (Irvine and Wieschaus, 1994), whose key process is junction remodeling similar to a topological T1 transition (**Figure 2C**) (Weaire and Rivier, 1984). T1 transitions consist of two phases: (1) collapse of a junction (DV orientation, AP interfaces) leading to fusion of two 3x vertices into a single 4x vertex and (2) expansion of a new junction in perpendicular orientation (AP direction, DV interfaces) creating two new 3x vertices out of the transient 4x vertex (**Figure 2C**) (Bertet et al., 2004). A complex variant of T1 transitions, rosettes, are observed later in germband extension when multiple junctions collapse simultaneously to generate multiple fold vertices (rosette), which subsequently resolved by the formation of multiple new junctions (**Figure 2C**) (Blankenship et al., 2006).

Myosin-II and the junction-associated actomyosin network on the one side and Baz/PAR-3 and adherens junction proteins on the other side show a complementary and polarized distribution at the junctions and thus reflect a planar polarity (**Figure 2B**) (Bertet et al., 2004; Zallen and Wieschaus, 2004; Blankenship et al., 2006). Myosin-II and F-actin, enriched at AP interfaces, generate contractile forces leading to junction collapse (Bertet et al., 2004; Zallen and Wieschaus, 2004; Blankenship et al., 2006; Rauzi et al., 2008; Fernandez-Gonzalez et al., 2009). The force is probably generated by a flow of contractile filaments away from the adherens junctions at the apical cortex (medial). In an isotropic case, this leads to apical contractions (Martin et al., 2009; Kong et al., 2019). In the planar polarized situation of the lateral epidermis, the force acts in an anisotropic fashion mainly on the junctions with a DV orientation to induce a junction collapse (Rauzi et al., 2010).

The cortical and junctional actomyosin network is the force-generating machinery in the cell. Myosin-II exists as an inactive hexametric complex, consisting of two heavy chains, two essential light chains (ELC) and two regulatory light chains (RLC) (Hartman and Spudich, 2012). The Rho signaling pathway

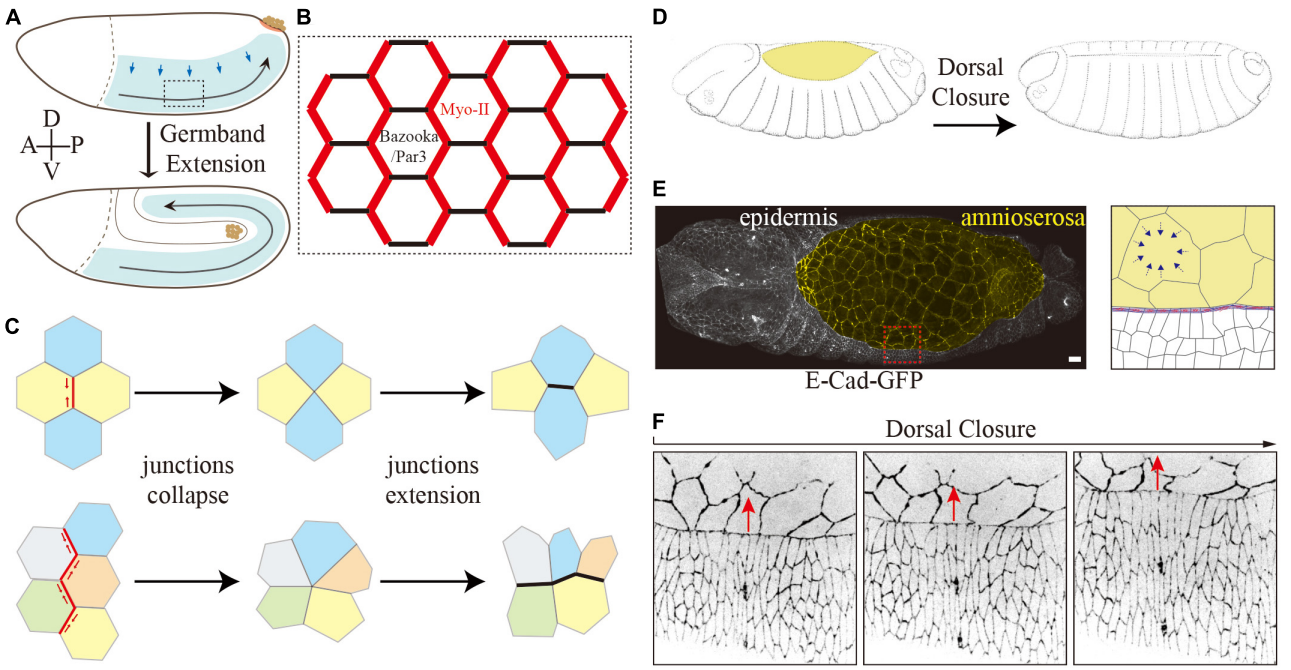

FIGURE 2 | Two tissue-scale shapes change events during *Drosophila* embryogenesis. **(A–C)** Germband extension. **(A)** Schematic drawing of germband extension. **(B)** Polarized planer polarity of the lateral epidermis during germband extension. Myosin-II is enriched explicitly at AP interfaces, and Bazooka/PAR-3 is enriched at DV interfaces conversely in the intercalating cells. **(C)** Schematic representation of a simple and rosette-type T1 transition. **(D–F)** Dorsal closure. Schematic drawing of dorsal closure. Images modified from Hartenstein (1993) **(D)**. It involves two different types of epithelial tissues and their coordination: amnioserosa (yellow) and epidermal cells **(E)**. Confocal image of an embryo expressing E-Cad-GFP. The magnified view on the right shows the interface of amnioserosa and epidermal cells. The blue arrows indicate cell contraction. The leading edge cells polarize by the accumulation of filamentous actin and myosin II at the epidermis–amnioserosa interface in the form of an F-actin cable. **(F)** Time series of an embryo expressing E-Cad-GFP shows the shape of surrounding epidermal cells elongates along the dorsal–ventral axis during dorsal closure. The red arrows indicate the movements of epidermal cells during dorsal closure.

is essential for this polarization in the lateral epidermis and Myosin-II activity. Myosin-II is activated by phosphorylation of the RLCs by Rho-kinase (Rok) among other protein kinases. During germband extension, Rok is enriched at AP interface (de Matos Simões et al., 2010), and activated by the G protein-coupled receptor (GPRC)-Rho1 signaling (Kerridge et al., 2016), involving Dp114RhoGEF and the subunits of trimeric G proteins, Gβ13F/Gγ1 (De Las Bayonas et al., 2019). The asymmetry in Rho1 and Rok activation leads to polarized Myosin-II activation at AP junctions (de Matos Simões et al., 2010; Simões et al., 2014). Ligands of the FGF family control the assembly of rosette-like mechanosensory organs in the migrating lateral line primordium of the zebrafish (Lecaudey et al., 2008; Nechiporuk and Raible, 2008). It was revealed that Fgfr-Ras-MAPK signaling is required for apical constriction via apical positioning of Rho-associated kinase (Harding and Nechiporuk, 2012), which could be a potential further mechanism for acto-myosin activation during *Drosophila* germband extension. In parallel Rho1 also activates the formin Diaphanous (Dia), which initiates DE-cad endocytosis leading to depletion of α-catenin (Levayer et al., 2011) and Baz/PAR-3 at AP interface (de Matos Simões et al., 2010; Simões et al., 2014).

The initial signal for polarization is provided by the striped expression of anteroposterior patterning genes (Irvine and Wieschaus, 1994). The striped and staggered expression of the primary pair-rule genes, *runt*, *eve*, and *paired* imposes a planar polarity on the tissue, which guides the orientation of T1 transitions and thus the directionality of cell intercalation. AP patterning of *Drosophila* embryo is controlled by a hierarchical genetic cascade starting with localized maternal determinants to the zygotic gap, pair-rule, and segment polarity genes (Nasiadka et al., 2002). The link between patterning genes and planar cell polarity is mediated by members of the Toll receptor (protein) family (Paré et al., 2014). The staggered expression of primary pair-rule genes induces a corresponding stripe-like expression of Toll-2, 6, 8 (Eldon et al., 1994; Kambris et al., 2002). Heterophilic interfaces at the AP interfaces between these Toll-2,6,8 proteins, lacking at DV interfaces, induce specific signaling different between AP and DV interfaces (Paré et al., 2014; Tetley et al., 2016). The molecular link between Toll receptors and Myo-II may be provided by the adhesion GPCR Cirl, which can bind to Toll-8 (Lavalou et al., 2020). The Toll-8-Cirl complex self-organizes to generate local asymmetric interfaces which are essential for planar polarizations of contractile interfaces. In addition to Toll-Rho signaling, the classical planar polarity system involving Frizzled and which mediates planar polarity in wings and eye imaginal discs may also be involved in germband extension (Yang and Mlodzik, 2015). Although Frizzled was reported to be enriched on vertical junctions during cell intercalation (Warrington et al., 2013), neither the

Frizzled nor the major Wnt effector Disheveled appears to be required for germ-band extension (Zallen and Wieschaus, 2004; Warrington et al., 2013).

DORSAL CLOSURE

Dorsal closure is another prominent morphogenetic process in *Drosophila* embryogenesis (**Figures 2D–F**) (Hayes and Solon, 2017; Kiehart et al., 2017). Dorsal closure involves two types of epithelial tissues and their coordination, i.e., the squamous amnioserosa and the columnar dorsal–lateral epidermis. After germband retraction, the extraembryonic amnioserosa bridges the left and right sheets of the dorsal epidermis (**Figure 2E**). Within about 4 h, the two lateral epidermal sheets on both sides of the embryo move toward the dorsal midline while the amnioserosa retreats and finally disappears (**Figure 2D**). The mechanical forces for the directed movement are provided from both tissues and their interface. The squamous amnioserosa cells display pulsatile isotropic contractions which lead to very regular oscillations of the cross-sectional area. On the tissue scale, the oscillations balance out each other due to their asynchrony during the stationary phase preceding dorsal closure. During dorsal closure, however, the contractions take over and lead to a gradual decrease of the total area of the amnioserosa. The decreasing area is compensated or promoted by the movement of the adjacent epidermis. Given several recent excellent reviews on the role of the amnioserosa cells (Hayes and Solon, 2017; Kiehart et al., 2017; Perez-Vale and Peifer, 2020), we will focus on the surrounding epidermis for the closure process in the following paragraphs.

The interface between the two tissues plays an important role. The dorsal-most epidermal cells, the leading edge cells, polarize by an accumulation of F-actin at the interface between their dorsal edge and the amnioserosa interface, which generates a prominent and contractile F-actin cable (**Figure 2E**) (Young et al., 1993; Kiehart et al., 2000). Meanwhile, the leading edge cells dramatically elongate along the DV direction as if they were pulled by the amnioserosa (**Figure 2F**) (Jacinto et al., 2002). This notion has remained untested. Both models are conceivable. In the passive model, the elongation of epidermal cells is due to pulling by the amnioserosa cell/actin cable contractions. In the active model, the epidermal cells elongate by an autonomous mechanism within the epidermis and thus generate a pushing force. A combination of both models would also be possible.

Tissue restricted Myo-II depletion in the amnioserosa or surrounding epidermis revealed that the Myo-II dependent contractions within the amnioserosa tissue but not actin cable are required for dorsal closure (Pasakarnis et al., 2016). However, the kinetics of the overall closure process appeared slower when Myo-II was depleted in the epidermis. Myo-II depletion in epidermis affects the contractility of all cells of the epidermis, not only the leading edge cells and the actin cable. Yet unidentified autonomous mechanisms could be affected within the epidermis. It is worth noting that Myo-II depletion specifically within the amnioserosa, also affected the actin cable structure (Pasakarnis et al., 2016). In these embryos, the actin cable initially formed but the cable structure disassembled partially during dorsal closure. These observations suggest a role of amnioserosa cell contractions for the cable structure. The elongation of epidermal cells might be due to pulling by the actin cable tension. The tension along the actin cable increases steadily over time, as revealed by the recoil velocity following UV laser-induced junction cutting (Saias et al., 2015). Opposing a role of the actin cable comes from the analysis of *Zasp52* mutants embryos, which lack any actin cable but undergo an apparently normal dorsal closure (Ducuing and Vincent, 2016). Interestingly, the elongation of epidermal cells is still observed in *Zasp52* mutants. These observations suggest that the elongation of epidermal cells is not only due to pulling by the actin cable.

ADHERENS JUNCTIONS AT THE LEADING EDGE CELLS

Although the amnioserosa cells behave isotropically with respect to their oscillations, the cell junctions at the interface are polarized as seen not only by the actin cable but also by the junction and junction-associated proteins. The epidermis connects with amnioserosa cells via E-cad and integrin-mediated adhesions (Narasimha and Brown, 2004). Reduced E-cad levels impair cell contacts between leading edge cells and amnioserosa (Gorfinkiel and Arias, 2007). Correspondingly interface defects within the actin cable and edge cells of the amnioserosa were observed in α-*catenin* mutant embryos, in which the actin-binding domain was specifically deleted (Jurado et al., 2016). Further actin-binding proteins associated with adherens junctions were recently identified to localize at the interface. Although Canoe and Polychaetoid are not essential for the actin cable, the architecture and morphology of leading-edge cells were impaired in embryos depleted for those proteins (Manning et al., 2019). The Ajuba LIM protein (Jub), a force-sensitive protein, is enriched at the interface, and loss of Jub enhances dorsal closure defects in mutants defective for cell adhesion (Razzell et al., 2018). This protein accumulates at adherens junctions under tension and acts as a critical component of a negative-feedback loop, which stabilizes and distributes tension at adherens junctions at the interface (Rauskolb et al., 2019). These studies strongly suggest that adherens junctions have fundamental functions in adapting to mechanical forces and coordinate the tissue and cell interactions leading to morphogenesis.

CONCLUSION AND REMARKS

Within the lateral epidermis during gastrulation, the AP patterning system establishes a system of planar cell polarity, which polarizes junctional and cytoskeletal dynamics and subsequently directs cell rearrangement for the tissue-scale changes in morphology. The finding that members of the Toll-family of membrane receptors are involved in the polarization of the tissue has started to open the black box of molecular links between the transcriptional patterning machinery for axis formation and the cell biological machinery of contractile

actomyosin clusters and cell adhesion complexes (Paré et al., 2014; Tetley et al., 2016; Lavalou et al., 2020). E-cad adhesion complexes are at the core of mechanical coordination between neighbors in epithelia. Its potential functions and the interactions with contractile actomyosin networks and other interaction partners provide ample options for fine-tuning sensory and signaling functions.

Yet missing is an integrative systems-type analysis involving mechanisms of coordination among the direct neighbors but also long-ranging influences to second and third neighbors. Analysis of the temporal and spatial coordination of the identified contractile and adhesive activities will be needed for the step from understanding the individual events such as a junction collapse to the tissue-scale shape changes during morphogenesis. *Drosophila* embryos provide a suitable and highly tractable system to study such questions *in vivo*.

Beyond the individual tissue, polarized and anisotropic tensions from the neighboring tissues have a potentially big impact on morphogenetic processes. The anisotropic tension by the posterior midgut during gastrulation pulls on the lateral epidermis, which is visible by a corresponding AP stretching of the cells during the onset of germband extension (Lye et al., 2015). This anisotropic tension with a gradual increase toward the posterior tip of the embryos transiently orientates newly formed junctions (Collinet et al., 2015). During germband extension cell stretching is diminished by cell rearrangement, even though the polarized tension remains on the tissue scale (Collinet et al., 2015; Lye et al., 2015). For a full understanding, it needs to be investigated whether and how E-Cad complexes and its interacting partners are involved in the coordination of local and tissue-scale forces during epithelium morphogenesis.

Similar tissue interactions are essential for the morphogenesis of the amnioserosa and dorsal closure. The two sheets of the dorsal epidermis are exposed to an anisotropic tension from the pulsating and contracting amnioserosa as well as the contractile actin cable. Cell elongation occurs not only in the leading edge cells but also in the further distant second and third and so forth neighbors in the epidermis (**Figure 2F**). It has remained unclear to which degree the elongation of the epidermal cells contributes to the closure process. How does the dorsal epidermis respond to and coordinate the polarized anisotropic tension with the cell shape changes? Adherens junctions and the binding proteins could be the potential candidates. For example, Arf-GEF Steppke is recruited to the myosin-rich adherens junction via coiled-coil heterodimerization with an adaptor protein, where the complex downregulates junctional tension and facilitates tissue stretching (West et al., 2017; Zheng et al., 2019). It is worth expanding the research focus from the amnioserosa and actin cable to the surrounding epidermis. As stated above the numerous proteins and processes associated with E-cad core complexes provide ample options for regulation and fine-tuning of morphogenetic processes.

AUTHOR CONTRIBUTIONS

DK wrote the manuscript and drew the figures. JG revised the manuscript. JG and DK conceived the study and edited the manuscript. Both authors contributed to the article and approved the submitted version.

FUNDING

This work was supported by Deutsche Forschungsgemeinschaft (GR1945/10-1 and GR1945/10-2).

REFERENCES

Bertet, C., Sulak, L., and Lecuit, T. (2004). Myosin-dependent junction remodelling controls planar cell intercalation and axis elongation. *Nature* 429, 667–671. doi: 10.1038/nature02590

Blankenship, J. T., Backovic, S. T., Sanny, J. S., Weitz, O., and Zallen, J. A. (2006). Multicellular rosette formation links planar cell polarity to tissue morphogenesis. *Dev. Cell* 11, 459–470. doi: 10.1016/j.devcel.2006.09.007

Buckley, C. D., Tan, J., Anderson, K. L., Hanein, D., Volkmann, N., Weis, W. I., et al. (2014). Cell adhesion. The minimal cadherin-catenin complex binds to Actin filaments under force. *Science* 346:1254211. doi: 10.1126/science.1254211

Bulgakova, N. A., and Brown, N. H. (2016). *Drosophila* p120-catenin is crucial for endocytosis of the dynamic E-cadherin-Bazooka complex. *J. Cell Sci.* 129, 477–482. doi: 10.1242/jcs.177527

Cavey, M., Rauzi, M., Lenne, P. F., and Lecuit, T. (2008). A two-tiered mechanism for stabilization and immobilization of E-cadherin. *Nature* 453, 751–756. doi: 10.1038/nature06953

Charras, G., and Yap, A. S. (2018). Tensile forces and mechanotransduction at cell-cell junctions. *Curr. Biol.* 28, R445–R457.

Chen, Y. J., Huang, J., Huang, L., Austin, E., and Hong, Y. (2017). Phosphorylation potential of *Drosophila* E-Cadherin intracellular domain is essential for development and adherens junction biosynthetic dynamics regulation. *Development* 144, 1242–1248. doi: 10.1242/dev.141598

Choi, H. J., Pokutta, S., Cadwell, G. W., Bobkov, A. A., Bankston, L. A., Liddington, R. C., et al. (2012). αE-catenin is an autoinhibited molecule that *Coactivates vinculin*. *Proc. Natl. Acad. Sci. U.S.A.* 109, 8576–8581. doi: 10.1073/pnas.1203906109

Collinet, C., Rauzi, M., Lenne, P. F., and Lecuit, T. (2015). Local and tissue-scale forces drive oriented junction growth during tissue extension. *Nat. Cell Biol.* 17, 1247–1258. doi: 10.1038/ncb3226

Cox, R. T., Kirkpatrick, C., and Peifer, M. (1996). Armadillo is required for adherens junction assembly, cell polarity, and morphogenesis during *Drosophila embryogenesis*. *J. Cell Biol.* 134, 133–148. doi: 10.1083/jcb.134.1.133

De Las Bayonas, A. G., Philippe, J. M., Lellouch, A. C., and Lecuit, T. (2019). Distinct RhoGEFs activate apical and junctional contractility under control of G proteins during epithelial morphogenesis. *Curr. Biol.* 29, 3370–3385.e7.

de Matos Simões, M., Blankenship, J. T., Weitz, O., Farrell, D. L., Tamada, M., Fernandez-Gonzalez, R., et al. (2010). Rho-kinase directs Bazooka/Par-3 planar polarity during *Drosophila* axis elongation. *Dev. Cell* 19, 377–388. doi: 10.1016/j.devcel.2010.08.011

Ducuing, A., and Vincent, S. (2016). The actin cable is dispensable in directing dorsal closure dynamics but neutralizes mechanical stress to prevent scarring in the *Drosophila embryo*. *Nat. Cell Biol.* 18, 1149–1160. doi: 10.1038/ncb3421

Eldon, E., Kooyer, S., D'Evelyn, D., Duman, M., Lawinger, P., Botas, J., et al. (1994). The *Drosophila* 18 wheeler is required for morphogenesis and has striking similarities to Toll. *Development* 120, 885–899.

Engl, W., Arasi, B., Yap, L. L., Thiery, J. P., and Viasnoff, V. (2014). Actin dynamics modulate mechanosensitive immobilization of E-cadherin at adherens junctions. *Nat. Cell Biol.* 16, 587–594.

Fernandez-Gonzalez, R., Simoes Sde, M., Röper, J. C., Eaton, S., and Zallen, J. A. (2009). Myosin II dynamics are regulated by tension in intercalating cells. *Dev. Cell* 17, 736–743. doi: 10.1016/j.devcel.2009.09.003

Gorfinkiel, N., and Arias, A. M. (2007). Requirements for adherens junction components in the interaction between epithelial tissues during dorsal closure in *Drosophila*. *J. Cell Sci.* 120, 3289–3298. doi: 10.1242/jcs.010850

Gumbiner, B. M. (1992). Epithelial morphogenesis. *Cell* 69, 385–387.

Harding, M. J., and Nechiporuk, A. V. (2012). Fgfr-Ras-MAPK signaling is required for apical constriction via apical positioning of Rho-associated kinase during mechanosensory organ formation. *Development* 139, 3130–3135. doi: 10.1242/dev.082271

Harris, T. J. (2012). Adherens junction assembly and function in the *Drosophila embryo*. *Int. Rev. Cell Mol. Biol.* 293, 45–83. doi: 10.1016/b978-0-12-394304-0.00007-5

Harris, T. J., and Peifer, M. (2004). Adherens junction-dependent and -independent steps in the establishment of epithelial cell polarity in *Drosophila*. *J. Cell Biol.* 167, 135–147. doi: 10.1083/jcb.200406024

Hartenstein, V. (1993). *Atlas of Drosophila Development*. Cold Spring Harbor, NJ: Cold Spring Harbor Laboratory Press.

Hartman, M. A., and Spudich, J. A. (2012). The myosin superfamily at a glance. *J. Cell Sci.* 125, 1627–1632. doi: 10.1242/jcs.094300

Hayes, P., and Solon, J. (2017). *Drosophila* dorsal closure: an orchestra of forces to zip shut the embryo. *Mech. Dev.* 144, 2–10. doi: 10.1016/j.mod.2016.12.005

Irvine, K. D., and Wieschaus, E. (1994). Cell intercalation during *Drosophila germband* extension and its regulation by pair-rule segmentation genes. *Development* 120, 827–841.

Ishiyama, N., Sarpal, R., Wood, M. N., Barrick, S. K., Nishikawa, T., Hayashi, H., et al. (2018). Force-dependent allostery of the α-catenin actin-binding domain controls adherens junction dynamics and functions. *Nat. Commun.* 9:5121.

Iyer, K. V., Piscitello-Gómez, R., Paijmans, J., Jülicher, F., and Eaton, S. (2019). Epithelial viscoelasticity is regulated by mechanosensitive E-cadherin turnover. *Curr. Biol.* 29, 578–591.e575.

Jacinto, A., Wood, W., Woolner, S., Hiley, C., Turner, L., Wilson, C., et al. (2002). Dynamic analysis of actin cable function during *Drosophila* dorsal closure. *Curr. Biol.* 12, 1245–1250. doi: 10.1016/s0960-9822(02)00955-7

Jurado, J., de Navascués, J., and Gorfinkiel, N. (2016). α-Catenin stabilizes cadherin-catenin complexes and modulates actomyosin dynamics to allow pulsatile apical contraction. *J. Cell Sci.* 129, 4496–4508. doi: 10.1242/jcs.193268

Kale, G. R., Yang, X., Philippe, J. M., Mani, M., Lenne, P. F., and Lecuit, T. (2018). Distinct contributions of tensile and shear stress on E-cadherin levels during morphogenesis. *Nat. Commun.* 9:5021.

Kambris, Z., Hoffmann, J. A., Imler, J.-L., and Capovilla, M. (2002). Tissue and stage-specific expression of the Tolls in *Drosophila embryos*. *Gene Express. Patt.* 2, 311–317. doi: 10.1016/s1567-133x(02)00020-0

Kerridge, S., Munjal, A., Philippe, J. M., Jha, A., de las Bayonas, A. G., Saurin, A. J., et al. (2016). Modular activation of Rho1 by GPCR signalling imparts polarized myosin II activation during morphogenesis. *Nat. Cell Biol.* 18, 261–270. doi: 10.1038/ncb3302

Kiehart, D. P., Crawford, J. M., Aristotelous, A., Venakides, S., and Edwards, G. S. (2017). Cell Sheet Morphogenesis: dorsal closure in *Drosophila melanogaster* as a model system. *Annu. Rev. Cell Dev. Biol.* 33, 169–202. doi: 10.1146/annurev-cellbio-111315-125357

Kiehart, D. P., Galbraith, C. G., Edwards, K. A., Rickoll, W. L., and Montague, R. A. (2000). Multiple forces contribute to cell sheet morphogenesis for dorsal closure in *Drosophila*. *J. Cell Biol.* 149, 471–490. doi: 10.1083/jcb.149.2.471

Kong, D., Lv, Z., Haring, M., Lin, B., Wolf, F., and Grosshans, J. (2019). In vivo optochemical control of cell contractility at single-cell resolution. *EMBO Rep.* 20:e47755.

Kong, D., Wolf, F., and Grosshans, J. (2017). Forces directing germ-band extension in *Drosophila embryos*. *Mech. Dev.* 144, 11–22. doi: 10.1016/j.mod.2016.12.001

Lavalou, J., Mao, Q., Harmansa, S., Kerridge, S., Lellouch, A. C., Philippe, J.-M., et al. (2020). Formation of polarized contractile interfaces by self-organized Toll-8/Cirl GPCR asymmetry. *bioRxiv* [Preprint], doi: 10.1101/2020.03.16.993758

Lecaudey, V., Cakan-Akdogan, G., Norton, W. H. J., and Gilmour, D. (2008). Dynamic Fgf signaling couples morphogenesis and migration in the *Zebrafish* lateral line primordium. *Development* 135, 2695–2705. doi: 10.1242/dev.025981

Leckband, D. E., and de Rooij, J. (2014). Cadherin adhesion and mechanotransduction. *Annu. Rev. Cell Dev. Biol.* 30, 291–315. doi: 10.1146/annurev-cellbio-100913-013212

Leptin, M. (1994). Morphogenesis. Control of epithelial cell shape changes. *Curr. Biol.* 4, 709–712. doi: 10.1016/s0960-9822(00)00156-1

Leptin, M. (2005). Gastrulation movements: the logic and the nuts and bolts. *Dev. Cell* 8, 305–320. doi: 10.1016/j.devcel.2005.02.007

Levayer, R., Pelissier-Monier, A., and Lecuit, T. (2011). Spatial regulation of Dia and Myosin-II by RhoGEF2 controls initiation of E-cadherin endocytosis during epithelial morphogenesis. *Nat. Cell Biol.* 13, 529–540. doi: 10.1038/ncb2224

Lv, Z., Lu, Q., and Dong, B. (2019). Morphogenesis: a focus on marine invertebrates. *Mar. Life Sci. Technol.* 1, 28–40. doi: 10.1007/s42995-019-00016-z

Lye, C. M., Blanchard, G. B., Naylor, H. W., Muresan, L., Huisken, J., Adams, R. J., et al. (2015). Mechanical coupling between endoderm invagination and axis extension in *Drosophila*. *PLoS Biol.* 13:e1002292. doi: 10.1371/journal.pbio.1002292

Lye, C. M., and Sanson, B. (2011). Tension and epithelial morphogenesis in *Drosophila* early embryos. *Curr. Top. Dev. Biol.* 95, 145–187. doi: 10.1016/b978-0-12-385065-2.00005-0

Maître, J. L., and Heisenberg, C. P. (2013). Three functions of cadherins in cell adhesion. *Curr. Biol.* 23, R626–R633.

Manning, L. A., Perez-Vale, K. Z., Schaefer, K. N., Sewell, M. T., and Peifer, M. (2019). The *Drosophila* Afadin and ZO-1 homologues canoe and polychaetoid act in parallel to maintain epithelial integrity when challenged by Adherens junction remodeling. *Mol. Biol. Cell* 30, 1938–1960. doi: 10.1091/mbc.e19-04-0209

Martin, A. C. (2020). The physical mechanisms of *Drosophila* gastrulation: mesoderm and endoderm invagination. *Genetics* 214, 543–560. doi: 10.1534/genetics.119.301292

Martin, A. C., Kaschube, M., and Wieschaus, E. F. (2009). Pulsed contractions of an actin-myosin network drive apical constriction. *Nature* 457, 495–499. doi: 10.1038/nature07522

Müller, H. A., and Wieschaus, E. (1996). armadillo, bazooka, and stardust are critical for early stages in formation of the zonula adherens and maintenance of the polarized blastoderm epithelium in *Drosophila*. *J. Cell Biol.* 134, 149–163. doi: 10.1083/jcb.134.1.149

Myster, S. H., Cavallo, R., Anderson, C. T., Fox, D. T., and Peifer, M. (2003). *Drosophila* p120catenin plays a supporting role in cell adhesion but is not an essential adherens junction component. *J. Cell Biol.* 160, 433–449. doi: 10.1083/jcb.200211083

Narasimha, M., and Brown, N. H. (2004). Novel Functions for Integrins in Epithelial Morphogenesis. *Curr. Biol.* 14, 381–385. doi: 10.1016/j.cub.2004.02.033

Nasiadka, A., Dietrich, B. H., and Krause, H. M. (2002). Anterior-posterior patterning in the *Drosophila embryo*. *Adv. Dev. Biol. Biochem.* 12, 155–204. doi: 10.1016/s1569-1799(02)12027-2

Nechiporuk, A., and Raible, D. W. (2008). FGF-dependent mechanosensory organ patterning in *Zebrafish*. *Science* 320, 1774–1777. doi: 10.1126/science.1156547

Nishiguchi, S., Yagi, A., Sakai, N., and Oda, H. (2016). Divergence of structural strategies for homophilic E-cadherin binding among bilaterians. *J. Cell Sci.* 129, 3309–3319. doi: 10.1242/jcs.189258

Oda, H., and Tsukita, S. (1999). Nonchordate classic cadherins have a structurally and functionally unique domain that is absent from chordate classic cadherins. *Dev. Biol.* 216, 406–422. doi: 10.1006/dbio.1999.9494

Oda, H., Uemura, T., Harada, Y., Iwai, Y., and Takeichi, M. (1994). A *Drosophila* homolog of cadherin associated with armadillo and essential for embryonic cell-cell adhesion. *Dev. Biol.* 165, 716–726. doi: 10.1006/dbio.1994.1287

Oda, H., Uemura, T., Shiomi, K., Nagafuchi, A., Tsukita, S., and Takeichi, M. (1993). Identification of a *Drosophila* homologue of alpha-catenin and its association with the armadillo protein. *J. Cell Biol.* 121, 1133–1140. doi: 10.1083/jcb.121.5.1133

Orsulic, S., and Peifer, M. (1996). An in vivo structure-function study of armadillo, the beta-catenin homologue, reveals both separate and overlapping regions of the protein required for cell adhesion and for wingless signaling. *J. Cell Biol.* 134, 1283–1300. doi: 10.1083/jcb.134.5.1283

Pai, L. M., Kirkpatrick, C., Blanton, J., Oda, H., Takeichi, M., and Peifer, M. (1996). *Drosophila* alpha-catenin and E-cadherin bind to distinct regions of *Drosophila* armadillo. *J. Biol. Chem.* 271, 32411–32420.

Paré, A. C., Vichas, A., Fincher, C. T., Mirman, Z., Farrell, D. L., Mainieri, A., et al. (2014). A positional Toll receptor code directs convergent extension in *Drosophila*. *Nature* 515, 523–527. doi: 10.1038/nature13953

Paré, A. C., and Zallen, J. A. (2020). Cellular, molecular, and biophysical control of epithelial cell intercalation. *Curr. Top. Dev. Biol.* 136, 167–193. doi: 10.1016/bs.ctdb.2019.11.014

Pasakarnis, L., Frei, E., Caussinus, E., Affolter, M., and Brunner, D. (2016). Amnioserosa cell constriction but not epidermal actin cable tension autonomously drives dorsal closure. *Nat. Cell Biol.* 18, 1161–1172. doi: 10.1038/ncb3420

Peifer, M., and Wieschaus, E. (1990). The segment polarity gene armadillo encodes a functionally modular protein that is the *Drosophila* homolog of human plakoglobin. *Cell* 63, 1167–1176. doi: 10.1016/0092-8674(90)90413-9

Perez-Vale, K. Z., and Peifer, M. (2020). Orchestrating morphogenesis: building the body plan by cell shape changes and movements. *Development* 147:dev191049. doi: 10.1242/dev.191049

Pokutta, S., Drees, F., Yamada, S., Nelson, W. J., and Weis, W. I. (2008). Biochemical and structural analysis of alpha-catenin in cell-cell contacts. *Biochem. Soc. Trans.* 36, 141–147. doi: 10.1042/bst0360141

Rangarajan, E. S., and Izard, T. (2012). The cytoskeletal protein α-catenin unfurls upon binding to vinculin. *J. Biol. Chem.* 287, 18492–18499. doi: 10.1074/jbc.m112.351023

Rauskolb, C., Cervantes, E., Madere, F., and Irvine, K. D. (2019). Organization and function of tension-dependent complexes at adherens junctions. *J. Cell Sci.* 132:jcs224063. doi: 10.1242/jcs.224063

Rauzi, M., Lenne, P. F., and Lecuit, T. (2010). Planar polarized actomyosin contractile flows control epithelial junction remodelling. *Nature* 468, 1110–1114. doi: 10.1038/nature09566

Rauzi, M., Verant, P., Lecuit, T., and Lenne, P. F. (2008). Nature and anisotropy of cortical forces orienting *Drosophila* tissue morphogenesis. *Nat. Cell Biol.* 10, 1401–1410. doi: 10.1038/ncb1798

Razzell, W., Bustillo, M. E., and Zallen, J. A. (2018). The force-sensitive protein Ajuba regulates cell adhesion during epithelial morphogenesis. *J. Cell Biol.* 217, 3715–3730. doi: 10.1083/jcb.201801171

Saias, L., Swoger, J., D'Angelo, A., Hayes, P., Colombelli, J., Sharpe, J., et al. (2015). Decrease in cell volume generates contractile forces driving dorsal closure. *Dev. Cell* 33, 611–621. doi: 10.1016/j.devcel.2015.03.016

Schmidt, A., and Grosshans, J. (2018). Dynamics of cortical domains in early *Drosophila* development. *J. Cell Sci.* 131:jcs212795.

Sharrock, T. E., and Sanson, B. (2020). Cell sorting and morphogenesis in early *Drosophila embryos*. *Semin. Cell Dev. Biol.* 107, 147–160. doi: 10.1016/j.semcdb.2020.07.010

Simões, S. M., Mainieri, A., and Zallen, J. A. (2014). Rho GTPase and Shroom direct planar polarized actomyosin contractility during convergent extension. *J. Cell Biol.* 204, 575–589. doi: 10.1083/jcb.201307070

Tepass, U., Gruszynski-DeFeo, E., Haag, T. A., Omatyar, L., Török, T., and Hartenstein, V. (1996). shotgun encodes *Drosophila* E-cadherin and is preferentially required during cell rearrangement in the neurectoderm and other morphogenetically active epithelia. *Genes Dev.* 10, 672–685. doi: 10.1101/gad.10.6.672

Tetley, R. J., Blanchard, G. B., Fletcher, A. G., Adams, R. J., and Sanson, B. (2016). Unipolar distributions of junctional myosin II identify cell stripe boundaries that drive cell intercalation throughout *Drosophila* axis extension. *eLife* 5:e12094.

Truong Quang, B. A., Mani, M., Markova, O., Lecuit, T., and Lenne, P. F. (2013). Principles of E-cadherin supramolecular organization in vivo. *Curr. Biol.* 23, 2197–2207. doi: 10.1016/j.cub.2013.09.015

Uemura, T., Oda, H., Kraut, R., Hayashi, S., Kotaoka, Y., and Takeichi, M. (1996). Zygotic *Drosophila* E-cadherin expression is required for processes of dynamic epithelial cell rearrangement in the *Drosophila embryo*. *Genes Dev.* 10, 659–671. doi: 10.1101/gad.10.6.659

Wang, Y. C., Khan, Z., Kaschube, M., and Wieschaus, E. F. (2012). Differential positioning of adherens junctions is associated with initiation of epithelial folding. *Nature* 484, 390–393. doi: 10.1038/nature10938

Warrington, S. J., Strutt, H., and Strutt, D. (2013). The Frizzled-dependent planar polarity pathway locally promotes E-cadherin turnover via recruitment of RhoGEF2. *Development* 140, 1045–1054. doi: 10.1242/dev.088724

Weaire, D., and Rivier, N. (1984). Soap, cells and statistics—random patterns in two dimensions. *Contemp. Phys.* 25, 59–99. doi: 10.1080/00107518408210979

West, J. J., Zulueta-Coarasa, T., Maier, J. A., Lee, D. M., Bruce, A. E. E., Fernandez-Gonzalez, R., et al. (2017). An actomyosin-Arf-GEF negative feedback loop for tissue elongation under stress. *Curr. Biol.* 27, 2260–2270.e2265.

Wu, Y., Kanchanawong, P., and Zaidel-Bar, R. (2015). Actin-delimited adhesion-independent clustering of E-cadherin forms the nanoscale building blocks of adherens junctions. *Dev. Cell* 32, 139–154. doi: 10.1016/j.devcel.2014.12.003

Yang, Y., and Mlodzik, M. (2015). Wnt-Frizzled/planar cell polarity signaling: cellular orientation by facing the wind (Wnt). *Annu. Rev. Cell Dev. Biol.* 31, 623–646. doi: 10.1146/annurev-cellbio-100814-125315

Yao, M., Qiu, W., Liu, R., Efremov, A. K., Cong, P., Seddiki, R., et al. (2014). Force-dependent conformational switch of α-catenin controls vinculin binding. *Nat. Commun.* 5:4525.

Young, P. E., Richman, A. M., Ketchum, A. S., and Kiehart, D. P. (1993). Morphogenesis in *Drosophila* requires nonmuscle myosin heavy chain function. *Genes Dev.* 7, 29–41. doi: 10.1101/gad.7.1.29

Zallen, J. A., and Wieschaus, E. (2004). Patterned gene expression directs bipolar planar polarity in *Drosophila*. *Dev. Cell* 6, 343–355. doi: 10.1016/s1534-5807(04)00060-7

Zhang, Y., Kong, D., Reichl, L., Vogt, N., Wolf, F., and Großhans, J. (2014). The glucosyltransferase Xiantuan of the endoplasmic reticulum specifically affects E-Cadherin expression and is required for gastrulation movements in *Drosophila*. *Dev. Biol.* 390, 208–220. doi: 10.1016/j.ydbio.2014.03.007

Zheng, S., West, J. J., Yu, C. G., and Harris, T. J. C. (2019). Arf-GEF localization and function at myosin-rich adherens junctions via coiled-coil heterodimerization with an adaptor protein. *Mol. Biol. Cell* 30, 3090–3103. doi: 10.1091/mbc.e19-10-0566

Conflict of Interest: The authors declare that the research was conducted in the absence of any commercial or financial relationships that could be construed as a potential conflict of interest.

frontiers in Cell and Developmental Biology

REVIEW
published: 18 January 2021
doi: 10.3389/fcell.2020.619869

Mechanochemical Control of Symmetry Breaking in the *Caenorhabditis elegans* Zygote

Wan Jun Gan[1]* *and Fumio Motegi*[1,2,3,4]*

[1] Temasek Life-Sciences Laboratory, Singapore, Singapore, [2] Department of Biological Sciences, National University of Singapore, Singapore, Singapore, [3] Mechanobiology Institute, National University of Singapore, Singapore, Singapore, [4] Institute of Genetic Medicine, Hokkaido University, Sapporo, Japan

Cell polarity is the asymmetric organization of cellular components along defined axes. A key requirement for polarization is the ability of the cell to break symmetry and achieve a spatially biased organization. Despite different triggering cues in various systems, symmetry breaking (SB) usually relies on mechanochemical modulation of the actin cytoskeleton, which allows for advected movement and reorganization of cellular components. Here, the mechanisms underlying SB in *Caenorhabditis elegans* zygote, one of the most popular models to study cell polarity, are reviewed. A zygote initiates SB through the centrosome, which modulates mechanics of the cell cortex to establish advective flow of cortical proteins including the actin cytoskeleton and partitioning defective (PAR) proteins. The chemical signaling underlying centrosomal control of the Aurora A kinase–mediated cascade to convert the organization of the contractile actomyosin network from an apolar to polar state is also discussed.

Keywords: symmetry breaking, polarization, cortical contractility, Aurora-A, *Caenorhabditis elegans*

OPEN ACCESS

Edited by:
Zhiyi Lv,
Ocean University of China, China

Reviewed by:
Bruce Bowerman,
University of Oregon, United States
Reinhard Christoph Dechant,
ETH Zürich, Switzerland
Josana Rodriguez,
Newcastle University, United Kingdom
Tony Harris,
University of Toronto, Canada

***Correspondence:**
Wan Jun Gan
ganwanjun@tll.org.sg;
wgan6649@alumni.sydney.edu.au
Fumio Motegi
fmotegi@tll.org.sg;
motegi@igm.hokudai.ac.jp

Specialty section:
This article was submitted to Signaling, a section of the journal Frontiers in Cell and Developmental Biology

Received: *21 October 2020*
Accepted: *08 December 2020*
Published: *18 January 2021*

Citation:
Gan WJ and Motegi F (2021) Mechanochemical Control of Symmetry Breaking in the Caenorhabditis elegans Zygote. Front. Cell Dev. Biol. 8:619869. doi: 10.3389/fcell.2020.619869

INTRODUCTION

Multiple tissues are generated during the development of multicellular organisms. The morphogenesis of these tissues is characterized by spatially biased rearrangement of cells along the major body axes. These complex tissues originate from the single-celled zygote, which is formed following fertilization of an oocyte with a sperm. The fertilized zygote initially exhibits no predetermined spatial asymmetry and initiates spatial differences in the shape, structure, and function between the opposite poles. The first step of this process is called symmetry breaking (SB), during which the uniformity of the zygote is disrupted to generate a spatially biased cellular structure. Under most physiological conditions, the zygote responds to local transient "cues" and amplifies microscopic inhomogeneity into stable macroscopic asymmetry. A cue can be a localized landmark either inherited from the oocyte, spontaneously produced by the zygote, or a type of extrinsic stimulus (Li and Bowerman, 2010). The *Caenorhabditis elegans* zygote serves as a useful model organism to understand the mechanism(s) underlying SB. Similar to mammalian oocytes (Santella et al., 1992), the *C. elegans* oocyte is formed without predetermined polarity or extracellular stimuli. Upon entering the reproductive organ known as the spermatheca, the shape of an oocyte is transformed from cuboidal to ovoid (McCarter et al., 1999). A sperm usually enters the oocyte from its leading edge of entering the spermatheca. Shortly after fertilization, the zygote begins to form an extracellular matrix known as eggshell, which provides physical protection to the zygote shape (Olson et al., 2012). The zygote then undergoes polarization,

which leads to spatial segregation of the actin cytoskeleton and the presence of conserved signaling proteins in a head-to-tail orientation.

MECHANOCHEMICAL POLARIZATION OF THE *CAENORHABDITIS ELEGANS* ZYGOTE

Upon entry of the sperm, the zygote undergoes two rounds of meiosis to reduce the number of duplicated maternal chromosomes (Schneider and Bowerman, 2003; Johnston et al., 2006). The excess chromosomes are expelled from the zygote near the pole proximal to the maternal nucleus (Schneider and Bowerman, 2003). Shortly after the completion of meiosis, the zygote starts dynamic cycles of contraction and relaxation of the cell cortex, which is the layer greatly enriched with the actin cytoskeleton underneath the plasma membrane (**Figure 1A**) (Schneider and Bowerman, 2003; Michaux et al., 2018). The actin cytoskeleton is mainly composed of actin filaments and several actin-binding proteins, including non–muscle myosin II (NMYII). The actin filaments are bundled and cross-linked into a complex network structure at the cortex (termed *cortical actomyosin network*) (Chugh and Paluch, 2018). NMYII is an actin filament–crosslinking protein and acts as a molecular motor driven by adenosine triphosphate (ATP). The catalytic cycles of ATP hydrolysis and the mechanical steps of attachment and detachment of NMYII with cross-linked actin filaments generate contractile forces to its associated structure, thereby inducing contraction and relaxation cycles at the cortex (Hill and Strome, 1988; Chugh and Paluch, 2018; Michaux et al., 2018). The formation and contraction of the cortical network are regulated by Rho-type small GTPase (RHO-1 in *C. elegans* and RhoA in mammals), which hydrolyzes the nucleotide guanosine triphosphate (GTP) to guanosine diphosphate (GDP) (Agarwal and Zaidel-Bar, 2019). RHO-1 is inactive when bound to GDP and active when bound to GTP. RHO-1 is inactivated by stimulating the rate of GTP hydrolysis via GTPase-activating proteins (GAPs), whereas RHO-1 is activated by exchanging GDP with GTP via guanine nucleotide exchange factors (GEFs). Dynamic turnover of RHO-1 between the two states has been correlated with the cyclic contraction and relaxation behaviors of the actomyosin-enriched cortex (Nishikawa et al., 2017; Michaux et al., 2018). The cortex also contains conserved regulators of cell polarity, known as partitioning defective (PAR) proteins. Six PAR proteins (PAR-1 to PAR-6) have been identified in *C. elegans* by genetic screening (Morton et al., 1992, 2002; Levitan et al., 1994; Etemad-Moghadam et al., 1995; Guo and Kemphues, 1995; Watts et al., 1996). Four of the PAR proteins (PAR-1, PAR-2, PAR-3, and PAR-6) are asymmetrically distributed throughout the zygote: PAR-1 and PAR-2 are localized at the posterior cortex, whereas PAR-3 and PAR-6 are enriched at the anterior cortex (Etemad-Moghadam et al., 1995; Guo and Kemphues, 1995; Boyd et al., 1996; Watts et al., 1996). Later studies found that protein kinase C (PKC-3) and cell division control protein 42 homolog (CDC-42) are localized at the anterior cortex (Tabuse et al., 1998; Hung and Kemphues, 1999), and lethal giant larvae-1, LGL-1, and the CDC-42 GAP, CHIN-1, at the posterior cortex (Beatty et al., 2010, 2013; Hoege et al., 2010; Kumfer et al., 2010). PAR-3, PAR-6, PKC-3, and CDC-42 are referred to as anteriorly localizing PAR proteins (aPARs), and PAR-1 and PAR-2 as posteriorly localizing PAR proteins (pPARs). Prior to SB of the zygote, all PAR proteins are symmetrically distributed. PAR-3, PAR-6, and PKC-3 are distributed throughout the cortex, whereas PAR-1, PAR-2, and CHIN-1 are homogeneously present in the cytoplasm (**Figure 1A**) (Etemad-Moghadam et al., 1995; Guo and Kemphues, 1995; Boyd et al., 1996; Watts et al., 1996; Beatty et al., 2013).

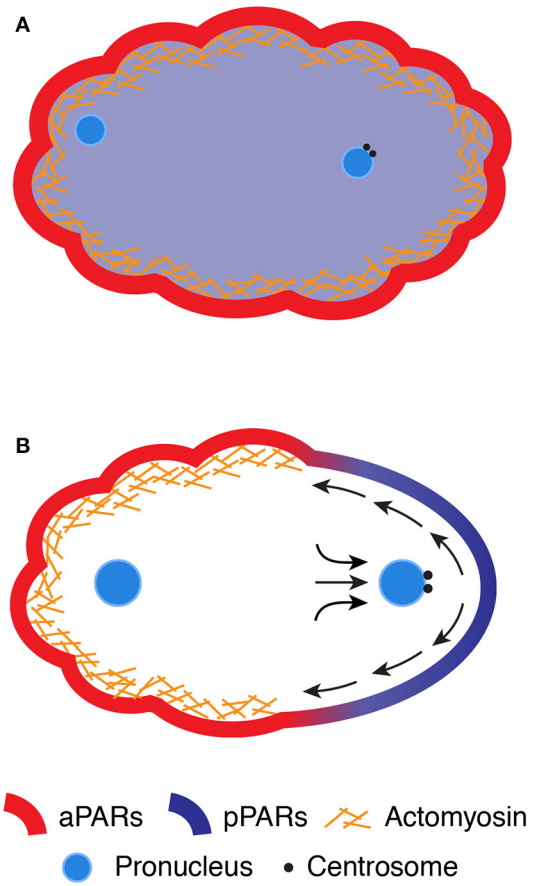

FIGURE 1 | SB in the *C. elegans* zygote. **(A)** The cell cortex enriches of the contractile actomyosin network, which exhibits dynamic cycles of contraction and relaxation, whereas the maternal and paternal chromosomes decondense into pronuclei in the cytoplasm. The aPARs are distributed evenly along the cortex, whereas the pPARs are localized throughout the cytoplasm. **(B)** While the paternal pronucleus approaches the posterior pole, centrosomes send unknown signals to the cortex to initiate SB. The contractile actomyosin network and aPARs are segregated toward the anterior pole via cortical flow, whereas the pPARs are translocated from the cytoplasm to the smoothing posterior pole of the zygote.

Shortly after meiotic exit, the zygote begins to establish distinct cortical domains with different cortical contractile properties and PAR protein concentrations (**Figure 1B**). The zygote initially develops actomyosin-based contractility

throughout the cortex, which generates forces for the formation of characteristic ruffles on the cell surface (Nishikawa et al., 2017; Michaux et al., 2018). At the onset of polarization (i.e., SB), the zygote locally ceases cortical contraction and forms a smooth-shaped noncontractile cortical domain, which expands from the future posterior pole to half of the cortex. The expansion of the smooth domain coincides with the flow of yolk granules beneath the cortex toward the anterior pole (Hird and White, 1993). The formation of cortical ruffles and the cortical flow can be blocked by the loss of cortical contractility [via inhibition of either NMYII (NMY-2 and myosin light chain-4) (Guo and Kemphues, 1996; Shelton et al., 1999) or the actin polymerizing factor formin (cytokinesis defect-1, CYK-1) (Severson et al., 2002; Hirani et al., 2019)], indicating a critical role of actomyosin-based contractility in this process. These findings imply that contractile asymmetry may induce the establishment of a high-to-low gradient in mechanical tension at the cortex along the anteroposterior axis, which leads to a flow of the actomyosin network toward the anterior pole. However, ultraviolet laser-based ablation experiments revealed the lack of a cortical tension gradient along the anteroposterior axis and instead supported an alternative model in which such contractile asymmetry could mediate asymmetry in hydrodynamic forces within the cortical layer (Kruse et al., 2005; Mayer et al., 2010). A model of hydrodynamic forces depends on the balance of forces applied to the cortex including actomyosin contractile forces and friction caused by compression or expansion of viscoelastic materials on the cortex. Theoretical consideration of the hydrodynamic forces can better explain the flow and density of actomyosin network during polarization (Mayer et al., 2010). However, the physical properties of the cortex, such as hydrodynamic forces, viscosity, and elasticity, have not yet been directly measured during SB.

Simultaneously with the establishment of contractile asymmetry, aPARs (PAR-3, PAR-6, aPKC, and CDC-42) become enriched at the anterior high-contractility domain, whereas pPARs (PAR-1 and PAR-2) translocate from the cytoplasm to the posterior low-contractility domain (**Figure 1B**). The boundary between the high- and low-contractility domains corresponds precisely with that between the aPAR and pPAR domains (Schenk et al., 2010; Goehring et al., 2011a). Consistent with the tight link between cortical contractility and the PAR domains, live cell imaging experiments revealed the comigratory behaviors of NMYII foci and PAR-6 at the cortex during polarization (Munro et al., 2004). These observations suggest that aPAR is stably embedded within the actomyosin-enriched cortical layer and thus passively transported by the advected flow of the actomyosin network (Munro et al., 2004). This model is also supported by theoretical modeling, which proposes that the velocity of cortical flow is sufficient to passively redistribute freely diffusing aPARs along the anteroposterior axis (Munro et al., 2004). Such advected movement of aPARs depletes aPARs from the posterior pole, allowing pPARs to translocate from the cytoplasm to the posterior domain (Motegi et al., 2011). Once aPARs and pPARs establish cortical asymmetry, both complexes are mutually excluded from the cortex via antagonistic phosphorylation reactions (see the review by Lang and Munro, 2017). Thus, polarization of the *C. elegans* zygote can be understood as a combination of mechanical forces by rearrangement of the cortical actomyosin network with chemical reactions between the aPAR and pPAR complexes.

INDUCTION OF SB BY THE CENTROSOME

In parallel, the mechanism employed by the zygote for SB in the actomyosin network was investigated. Most genes that contribute to polarization of the zygote (i.e., PAR genes) were found to carry recessive maternal-effect embryonic-lethal mutations. These maternally provided factors are believed to sense the entry or location of paternally provided factors, as the polarization cascade is initiated by sperm entry (Goldstein and Hird, 1996). A sperm normally enters an oocyte from the side opposing the nucleus. Shortly after the completion of meiosis II, the paternal pronucleus appears near the pole opposite of the maternal pronucleus (Goldstein and Hird, 1996). The paternal pronucleus is associated with the centrosome, an organelle that serves as the main microtubule-organizing center during mitosis. The centrosome is removed from the oocyte, but maintained in sperm and thus is a paternally provided factor in the fertilized zygote (Cowan and Hyman, 2004). The loss of centrosomes, but not paternal chromosomes, during spermatogenesis compromises polarization of the zygote, indicating that the centrosomes and/or associated factors are indispensable for zygote polarization (Sadler and Shakes, 2000). Consistent with the role of centrosomes in polarity induction, SB in cortical contractility will occur from the cortex closest to the position of the centrosomes in the zygote (Bienkowska and Cowan, 2012). Even in mutant zygotes with the centrosomes located near the maternal pronucleus during meiosis, SB is always triggered from the cortex proximally to the centrosomes, which results in the establishment of a reversed pattern of cortical flow and PAR distribution (Goldstein and Hird, 1996; Kimura and Kimura, 2020). These findings indicate that zygote polarization is induced by centrosomes.

Each centrosome contains two centrioles that harbor a matrix of proteins, known as pericentriolar material (PCM) (Chrétien et al., 1997). The PCM then recruits "client" proteins to stimulate nucleation of the microtubules, thereby forming the microtubule-organizing center (Woodruff et al., 2017). This recruitment process, known as centrosome maturation, is generally stimulated during mitosis. Genetic mutations that result in defective centrosome maturation, such as those of the PCM core proteins spindle-defective protein SPD-2 (O'Connell et al., 2000), SPD-5 (Hamill et al., 2002), and the cyclin-dependent kinase 2 (CDK-2)/cyclin E (Cowan and Hyman, 2006) complex, failed to polarize cortical contractility and PAR distribution. Ablation of the centrosomes just prior to the onset of SB also blocked the establishment of asymmetric cortical domains (Cowan and Hyman, 2004). This evidence indicates that the centrosome is the cue triggering SB. Notably, centrosomes distant from the cortex can also induce SB (Bienkowska and Cowan, 2012), suggesting that the "cue" generated by the centrosomes can be transmitted to the cortex through the cytoplasm.

CENTROSOMAL AURORA A KINASE (AIR-1) INHIBITS CORTICAL CONTRACTILITY AT THE POSTERIOR POLE

Three recent studies have proposed that AIR-1 plays a key role in centrosome-mediated SB (Kapoor and Kotak, 2019; Klinkert et al., 2019; Zhao et al., 2019). AIR-1 is a highly conserved serine/threonine kinase that is recruited to the centrosome and stimulates centrosome maturation during mitosis (Schumacher et al., 1998). *C. elegans* zygotes depleted of AIR-1 exhibit defects in the recruitment of PCM, including SPD-2 and SPD-5, microtubule assembly at the centrosomes, and the establishment of cortical polarity (Schumacher et al., 1998). Similar to AIR-1–depleted zygotes, zygotes depleted of either SPD-2 or SPD-5 failed to trigger SB in the actomyosin network (O'Connell et al., 2000; Hamill et al., 2002). AIR-1 is essential to recruit SPD-2 and SPD-5 to centrosomes and vice versa, suggesting that AIR-1, SPD-2, and SPD-5 are engaged with a positive feedback to stimulate centrosome maturation and SB. Such interlinks among the PCM proteins (deletion of one dissociates the assembly of many others) complicate the identification of the specific SB cue conveyed by the PCM.

Three recent studies all demonstrated that AIR-1 is essential for SB in the contractile actomyosin network. A specific role of AIR-1 in reorganization of the actin cytoskeleton was highlighted from the cortical distribution of NMYII in zygotes depleted of AIR-1 after SB (during late prophase) (Kapoor and Kotak, 2019; Klinkert et al., 2019; Zhao et al., 2019). In contrast to control zygotes (such as those depleted of SPD-5), AIR-1–depleted zygotes showed abnormal maintenance of higher activity of RHO-1 (Kapoor and Kotak, 2019; Klinkert et al., 2019; Zhao et al., 2019). This observation implies a unique role of AIR-1 in the inhibition of the cortical actomyosin network, possibly via suppression of RHO-1 activation. Expression of GFP-tagged AIR-1 was able to restore centrosome maturation but unable to rescue SB in zygotes depleted of endogenous AIR-1, highlighting a specific requirement of AIR-1 in SB (Zhao et al., 2019). To support a role of AIR-1 nearby the cortex, Zhao et al. (2019) demonstrated that artificial targeting of AIR-1 to the polar cortex in SB-defective zygotes induced SB in both cortical NMYII and PAR-6. These results delineate a SB cascade in which AIR-1 acts as the centrosomal cue that locally inhibits the actomyosin contractility at the cortex proximal to the centrosome. The downstream signaling of AIR-1 to inhibit formation of a contractile actomyosin network remains unclear. Thus, several models of the inhibition of the formation of a contractile actomyosin network by the transmission of signals facilitated by AIR-1 from the centrosome to the cortex during SB have been proposed (**Figure 2**).

The first possibility is that AIR-1 diffuses from the centrosome to the cortex and directly phosphorylates a cortical substrate that controls RHO-1 activity. The RhoGEF ECT-2, which activates RHO-1 and stimulates cortical contractility during polarization, is a candidate substrate of AIR-1. ECT-2 contains a lipid-binding motif at the C-terminal region and localizes to the cortex in the *C. elegans* zygote. During SB, ECT-2 is locally excluded from the cortex proximal to the centrosome, but not from the posterior pole of zygotes with nonfunctional centrosomes (i.e., those depleted of either AIR-1 or SPD-5) (Kapoor and Kotak, 2019; Zhao et al., 2019). Kapoor and Kotak (2019) also suggested the serine-rich protein NOP-1, which promotes RHO-1–dependent stimulation of cortical contractility, as another candidate. Indeed, loss of NOP-1 reduced or abolished cortical flow during polarization and prevented a subset of zygotes from establishing polarized PAR domains (Tse et al., 2012). However, at present, there is no direct evidence of interactions among AIR-1, ECT-2, and NOP-1 to confirm these hypotheses.

As a second possibility, AIR-1 could activate a substrate that promotes inactivation of RHO-1. As a potential candidate, RhoGAPs stimulate hydrolysis of the RHO-1 GTPase. RhoGAP domain-containing protein RGA-3, RGA-4, and cytokinesis defect CYK-4 have been characterized as RhoGAPs that act on RHO-1 in *C. elegans*. RGA-3 and RGA-4 have high similarity and are likely to function in a redundant manner. Codepletion of RGA-3 and RGA-4 causes hyperactivation of RHO-1 and hypercontractility but does not block cortical flow during polarization (Schmutz et al., 2007; Schonegg et al., 2007). In contrast to RGA-3 and RGA-4, CYK-4 is required for reorganization of the actomyosin network during SB and cytokinesis (Jantsch-Plunger et al., 2000; Jenkins et al., 2006). Jenkins et al. showed that depletion of CYK-4 blocked SB in the actomyosin network and cortical PAR distribution in 33–50% of zygotes (Jenkins et al., 2006). Notably, the contribution

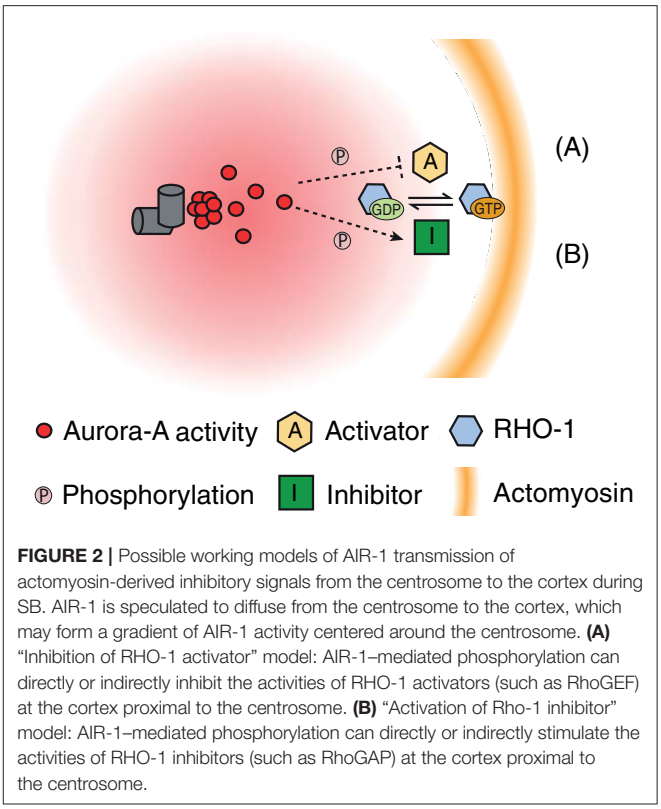

FIGURE 2 | Possible working models of AIR-1 transmission of actomyosin-derived inhibitory signals from the centrosome to the cortex during SB. AIR-1 is speculated to diffuse from the centrosome to the cortex, which may form a gradient of AIR-1 activity centered around the centrosome. **(A)** "Inhibition of RHO-1 activator" model: AIR-1–mediated phosphorylation can directly or indirectly inhibit the activities of RHO-1 activators (such as RhoGEF) at the cortex proximal to the centrosome. **(B)** "Activation of Rho-1 inhibitor" model: AIR-1–mediated phosphorylation can directly or indirectly stimulate the activities of RHO-1 inhibitors (such as RhoGAP) at the cortex proximal to the centrosome.

of CYK-4 to SB is strictly paternal (Jenkins et al., 2006), indicating that CYK-4 provided by sperm triggers SB. Consistent with this paternal contribution, immunostaining revealed that CYK-4 was enriched around the sperm pronucleus (Jenkins et al., 2006). These findings support a model in which CYK-4 acts as a GAP that inactivates RHO-1 at the cortex around the sperm pronucleus during SB. However, this model is contradictory to the findings of several recent studies, which demonstrated that a function of CYK-4 is the local stimulation of RHO-1 activity during cytokinesis. CYK-4 can directly interact with RhoGEF ECT-2 and promote RHO-1 activation at the cleavage furrow during cytokinesis (Zhang and Glotzer, 2015; Gómez-Cavazos et al., 2020). Given that CYK-4 carrying the E448K mutation in the GAP domain has no effect on SB, the GAP activity of CYK-4 might be dispensable during SB (Tse et al., 2012). It is paradoxical that without GAP activity during SB, CYK-4 can serve as an inhibitor of RHO-1, but this does not exclude the possibility that CYK-4 may require other associated proteins or posttranscriptional modifications to sense centrosomal AIR-1 and inhibit cortical contractility. The hypothesis of CYK-4 as downstream target of AIR-1 warrants further investigations.

Although AIR-1 is proposed to diffuse from the centrosome and induce SB at the cortex, the possible involvement of a secondary "messenger" protein that links centrosomal AIR-1 to cortical RHO-1 regulators cannot be ruled out. Microtubules are obvious candidates in this case. Indeed, AIR-1 can indirectly associate with microtubules in a manner dependent on TPXL-1 (*C. elegans* ortholog of targeting protein for *Xenopus* Klp2-like) and colocalize with astral and cortical microtubules (Mangal et al., 2018; Klinkert et al., 2019). However, at present, there is a lack of direct evidence for a role of microtubules in the polarization of the actomyosin networks. Severe depletion of microtubule assembly by RNA interference of tubulin-encoding genes or treatment with nocodazole caused only marginal or no delay on the onset of SB (Strome and Wood, 1983; Cowan and Hyman, 2004; Sonneville and Gönczy, 2004). AIR-1 may also target proteins that control intracellular trafficking linking the centrosome to the cortex. Several proteins involved in intracellular trafficking, such as polarity and osmotic sensitivity defect POD-1 and POD-2, can contribute to SB in the *C. elegans* zygote. POD-1 and POD-2 belong to the coronin family of actin-binding proteins, which connect the actin cytoskeleton to microtubules to regulate intracellular trafficking. Mutations to pod-1 or pod-2 in the zygote result in defective distribution of cortical PARs independent of functions in the regulation of cellular osmolarity (Rappleye et al., 1999; Tagawa et al., 2001).

To understand the complete signaling cascade of centrosome-mediated SB, it is vital to identify potential AIR-1 substrates and other effector proteins. Characterization of this signaling cascade will address several unresolved questions about the mechanism underlying SB, such as "How does the centrosome and centrosome-derived active form of AIR-1 transmit SB signals to the cortex through the cytoplasm?" "How does the centrosome inhibit cortical contractility?" and "Is there any feedback from the actin cytoskeleton to centrosomal AIR-1?" Perhaps unbiased biochemical approaches, such as *in vivo* protein-proximity labeling and comparative mass spectroscopy analysis, can help to further delineate the SB cascade and address these important questions.

TEMPORAL CONTROL OF SB: SUPPRESSION OF PREMATURE POLARIZATION

SB usually occurs shortly after the completion of meiosis. The timing of SB should be controlled in the zygote because intracellular conditions must be prepared prior to polarization. Wallenfang and Seydoux (2000) reported that PAR proteins can respond to centrosome-independent cues and establish asymmetric cortical domains during meiosis (in zygotes arrested at meiosis). Such meiotic PAR polarization is dependent on microtubules and the formation of meiotic spindles. These observations raised the question as to why the meiotic spindle is unable to trigger polarization under physiological conditions. It has been proposed that premature polarization may be suppressed because of the inefficient ability of the meiotic spindles to induce SB. However, a recent study by Reich et al. (2019) proposed an alternative model in which premature polarization is suppressed by two cell-cycle regulators (i.e., Polo and AIR-1 kinases) during meiosis. Depletion of either Polo or AIR-1 resulted in premature loading of PAR-3 and PAR-6 to the cortex, not only in the fertilized zygote, but also in the oocyte. Given that PAR-3 and PAR-6 can be directly phosphorylated by Polo and AIR-1 in *C. elegans* and *Drosophila melanogaster*, these kinases may directly suppress premature loading of the PAR proteins to the cortex and limit reactivity of the cortex to noncentrosomal SB cues (Wirtz-Peitz et al., 2008; Dickinson et al., 2017). Therefore, these two kinases may perform dual functions in SB: suppression during meiosis and later triggering during mitosis.

However, it remains unclear how the function of these kinases is switched toward SB during oocyte-to-zygote transition, which coincides with the transition from meiosis to mitosis. Activation of the centrosome via centrosome maturation is also suppressed during meiosis but induced during mitosis. It is tempting to speculate that cell cycle–dependent signaling molecules, such as cell cycle–dependent kinases and cyclins, may play direct roles in regulating the activity and/or specificity of Polo and AIR-1. Alternatively, cell cycle–dependent signaling cascades may indirectly control the locations of active Polo and AIR-1 via activation of centrosome maturation. In *C. elegans*, CDK-2 and cyclin E play essential roles in centrosome maturation, as well as SB in zygotes (Cowan and Hyman, 2006). Hence, future investigations of the relationship between CDK-2 and cyclin E, and Polo and AIR-1 kinases are warranted to clarify these hypothetical models and provide a complete view of the cell cycle–dependent control of SB.

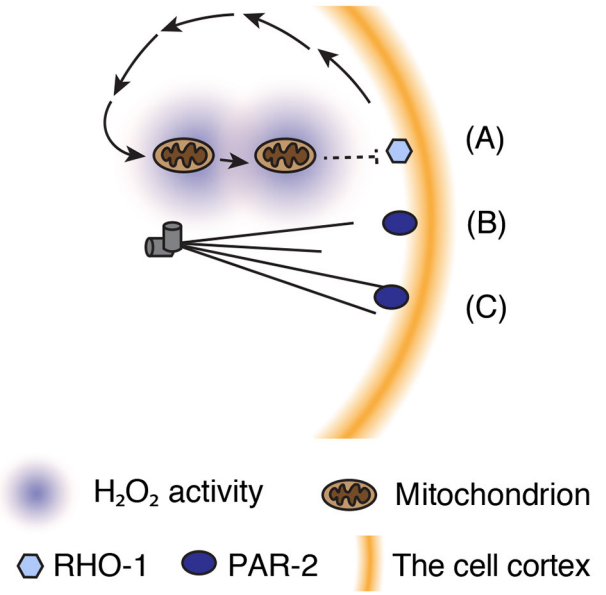

FIGURE 3 | Parallel mechanisms amplify SB to achieve asymmetric patterning of actomyosin and PAR proteins. **(A)** Asymmetric distribution of mitochondria in the cytosol generates H_2O_2 gradient, which may oxidize RHO-1 to inhibit its activity. **(B)** Microtubule binding regulates PAR-2 localization onto the posterior domain. **(C)** Membrane curvature facilitates PAR-2 cortical localization and concentration at the posterior pole.

SB IS FACILITATED BY MULTIPLE MECHANOCHEMICAL FEEDBACK CASCADES

In most SB events, the cell responds to certain cues and amplifies initial transient bias into more stable cellular-scale asymmetry. Recent studies of *C. elegans* zygotes have highlighted several mechanochemical feedback cascades that amplify SB initiated by the centrosome and facilitate stable patterning of the actin cytoskeleton and PAR proteins in the cortex (**Figure 3**).

Centrosome-mediated SB establishes directed (posterior-to-anterior) flow of cortical proteins. Given that the cortex and cytoplasm are physically connected, a physical force that drives cortical flow creates a hydrodynamic force that moves the cytoplasm in an opposite (anterior-to-posterior) direction. Although the physiological function of cytoplasmic flow in cell polarization remains unclear, a recent study proposed that cytoplasmic flow and intracellular hydrogen peroxide (H_2O_2) facilitate polarization of cortical contractility (De Henau et al., 2020). H_2O_2 is a reactive oxygen species that is predominantly produced by the mitochondrial electron transport chain and implicated as a transmitter of redox signals. In the *C. elegans* zygote, the cytoplasmic distribution of mitochondria undergoes dynamic changes from a uniform to posteriorly enriched pattern as cortical and cytoplasmic flows emerge during SB (De Henau et al., 2020). Measurements of intracellular H_2O_2 levels with a biosensor revealed local enrichment of H_2O_2 at the posterior pole during SB (De Henau et al., 2020). The gradient of H_2O_2 is built up from an actomyosin-dependent flow that redistributes cytoplasmic mitochondria toward the posterior pole (De Henau et al., 2020). Lowering H_2O_2 production by either the paternal or maternal mitochondria delays the timing of SB (De Henau et al., 2020), indicating a role of H_2O_2 in ensuring efficient SB. Remarkably, optogenetic manipulation of mitochondria localization toward the pole opposite to the centrosome (in an SB-defective zygote) reversed the pattern of polarization (De Henau et al., 2020). These findings support a model in which H_2O_2 contributes to SB either downstream or in parallel with the centrosomal AIR-1–mediated cascade. However, it remains unclear how H_2O_2 can inhibit the RHO-1–mediated cortical contraction cascade. RHO-1 itself can be a downstream target of redox signaling, as RHO-1 has two highly conserved cysteine residues for oxidation (Heo and Campbell, 2005; De Henau et al., 2020). Hence, further studies are needed to clarify the target molecule(s) of redox signals and possible relationships with the centrosomal AIR-1–mediated cascade.

Despite the role of AIR-1 in mediating SB in cortical contractility, PAR-2 can be translocated to the polar cortex during mitosis even in zygotes depleted of AIR-1 (Kapoor and Kotak, 2019; Klinkert et al., 2019; Zhao et al., 2019). In AIR-1–depleted zygotes, PAR-2 accumulates at the anterior pole or both poles, but at a significantly slower rate than that of wild-type zygotes. Recruitment of PAR-2 to the polar cortex in the absence of a functional centrosome can be mediated via microtubule-containing structures, such as the astral microtubules of meiotic spindles and meiotic spindle remnants at the anterior pole (Wallenfang and Seydoux, 2000). Binding to microtubules protects PAR-2 from PKC-3-mediated phosphorylation and exclusion from the cortex, leading to the stabilization of cortical PAR-2 (Motegi et al., 2011). Once translocated to the cortex, PAR-2 recruits PAR-1 kinase, while excluding anterior PAR proteins from the cortex, in order to establish a low-contractility cortical domain (Ramanujam et al., 2018).

Recruitment of PAR-2 to the polar cortex in the absence of functional centrosomes can also be stimulated by the macroscopic geometry of the cell, particularly the curvature of the plasma membrane. In zygotes with nonfunctional centrosomes, PAR-2 tends to appear at the high-curvature polar cortex. To test the hypothesis that PAR-2 preferentially associates with the high-curvature cortex, Klinkert et al. (2019) squeezed zygotes into triangular microwells and sharpened the curved regions of the cortex. Under wild-type conditions, PAR-2 was localized along one side of the cortex in half of the zygotes and was distributed at one of the triangular corners in the other half (Klinkert et al., 2019). In contrast, AIR-1–depleted zygotes preferentially positioned PAR-2 at the corner with the highest curvature (Klinkert et al., 2019). This behavior of PAR-2 was independent of the functions of centrosomes and microtubules, indicating that the curvature of the plasma membrane can be viewed as a novel factor that contributes to polarity establishment even in the absence of centrosomes and microtubules. PAR-2 has a phosphoinositide-binding domain and can be oligomerized at the cortex. Similar to proteins containing a bin-amphiphysin-rvs (BAR) domain, the oligomerized form of PAR-2 may form a "bended" shape that preferentially adopts to a plasma membrane

with high curvature (Ford et al., 2002; Peter et al., 2004; Miller et al., 2015; Zeno et al., 2018). PAR-2 may sense the specific composition and/or density of phosphoinositides that accumulate at the high-curvature cortex. Hence, it would be informative to elucidate the structural features of oligomerized PAR-2 and reconstruct the curvature-sensing capability of PAR-2 with the use of synthetic liposomes.

ENSURING THE POSITION OF THE CENTROSOME FOR EFFICIENT SB

In addition to the aforementioned mechanisms that initiate and facilitate SB, the *C. elegans* zygote utilizes other mechanisms to maintain a complex consisting of the paternal pronucleus and centrosomes closer to the cortex prior to SB (**Figure 4**). Several studies have demonstrated that premature movement and mispositioning of the centrosomes away from the cortex can disrupt polarity, indicating that the proximity between the centrosomes and cortex is critical for efficient SB. This concept was first proposed from genetic studies of *pam-1* mutant zygotes, which exhibited both centrosome mispositioning and defects in the onset of SB (Lyczak et al., 2006; Fortin et al., 2010). Although the *pam-1* mutant zygotes exhibited pleiotropic phenotypes including prolonged meiotic exit, the defect in SB in *pam-1* mutant zygotes was rescued when the position of centrosomes was restricted near the posterior cortex (via inhibition of dynein) (Fortin et al., 2010). This finding suggests a role of PAM-1 in the control of SB through suppression of premature movement of the centrosomes away from the cortex. However, the molecular details of how PAM-1 prevents premature movement of the centrosome are currently unclear.

The second line of evidence was obtained from investigations of centrosome positioning in mutant zygotes with improperly assembled cytoplasmic microtubules. The loss of either γ-tubulin, a tubulin subtype that contributes to nucleation of microtubules at the microtubule minus end, or Ran GTPase dramatically reduced the assembly of microtubules in the cytoplasm (Bienkowska and Cowan, 2012). Reduction in the density of cytoplasmic microtubules inhibits cortically biased movement of the centrosome, resulting in an increased distance from the centrosome to the cortex (Bienkowska and Cowan, 2012). In γ-tubulin–depleted zygotes, the proximity between the centrosome and cortex is closely correlated to the time required for SB, indicating that the efficiency of SB is ensured through constraining centrosome movement by cytoplasmic microtubules.

In the *C. elegans* embryo, the position of the centrosome is also influenced by physical attachment to the nuclear envelope, which is mediated by a member of the hook protein family, zygote defective protein 12 (ZYG-12) (Malone et al., 2003). ZYG-12 is expressed as three distinct isoforms: A, B, and C. ZYG-12 A is associated with the centrosome, in a microtubule-dependent manner, whereas ZYG-12 B and C are enriched in the nuclear envelope, in a SUN-1 protein-dependent manner. The self-binding of ZYG-12 links centrosomal ZYG-12 A to nuclear ZYG-12 B and C (Malone et al., 2003; Minn et al., 2009). In ZYG-12–depleted zygotes, the centrosome is physically separated from the paternal pronucleus and positioned away from the cortex (Malone et al., 2003). Although cortical polarity can be established during mitosis in *zyg-12* mutant zygotes, the kinetics and efficiency of SB have not been investigated.

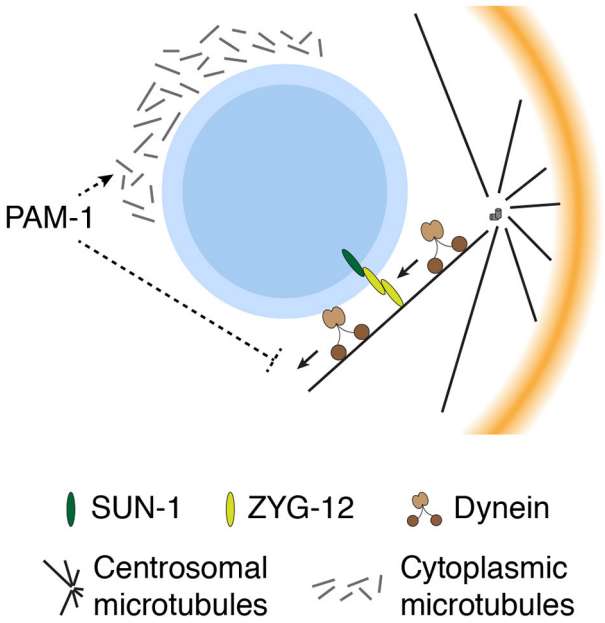

FIGURE 4 | Multiple mechanisms constrain movement of the pronucleus–centrosome complex near the cortex for efficient SB. Cytoplasmic microtubules prevent premature movement of the pronucleus–centrosome complex away from the cortex, whereas ZYG-12 physically links the centrosomes to the pronucleus. PAM-1 may contribute to the formation of cytoplasmic microtubules or suppress dynein-dependent movement of the pronucleus–centrosome complex prior to SB.

The position of the centrosome prior to SB is also influenced by cytoplasmic streaming during meiosis. From fertilization to SB, circular cytoplasmic streaming facilitates uncontrolled drifting of the paternal centrosome–pronucleus complex, which occurs orthogonally to the anteroposterior axis in a manner dependent on microtubules and the microtubule motor protein kinesin-1 (Kimura et al., 2017). During cytoplasmic streaming, kinesin-1 transports a network of endoplasmic reticula toward the plus end of the microtubule (Kimura et al., 2017). If by chance cytoplasmic streaming moves the centrosome–pronucleus complex away from the sperm-entry site toward the opposite pole, where the maternal pronucleus is generally located, the centrosome can induce SB at the cortex opposite to the sperm-entry site (Kimura and Kimura, 2020). These observations confirmed that the position of the centrosome at the time of SB, but not the sperm-entry site, specifies the anteroposterior axis.

CONCLUSION AND PERSPECTIVES

Overall, studies of the *C. elegans* zygote have revealed the molecular mechanisms that control SB and the establishment of cell polarity, which include PAR proteins and their regulators.

The versatility of the PAR cascade in cell polarization reflects a conserved mechanism that orchestrates the establishment of distinct cortical domains in many types of polarized cells. In addition to PAR proteins, the actin cytoskeleton and RhoA GTPase play crucial roles in SB. The cortical actomyosin network is engaged with cycles of contraction and relaxation before SB, but the cortical PAR proteins remain distributed throughout the cortex, indicating the robustness of the apolar state to prevent random polarization. A recent study reported the involvement of the Polo and AIR-1 kinases in suppression of premature polarization. However, a key to understand this process is whether these kinases have any influence on either the PAR proteins or actin cytoskeleton. Similar to other types of polarized cells, such as neurons and immune cells, SB in the *C. elegans* zygote relies on a localized signaling center that transmits "symmetry breaking signal(s)" to induce local changes in the organization of the cortical actomyosin network. Recent studies identified AIR-1 as the long-sought-after "cue," which is concentrated by the centrosome to inhibit cortical contractility. Given that activated AIR-1 should trigger SB, it is important to identify the associated activators and substrates. Of equal interest is how the function of AIR-1 switches from prevention of premature polarization to induction of SB during oocyte-to-zygote transition. Recent studies have reported mechanochemical coupling between cytoplasmic flow and redox signaling and that recruitment of PAR-2 to the polar cortex is dependent on the curvature of the plasma membrane. Further investigations will undoubtedly shed light on the molecular basis of these positive feedback loops.

The *C. elegans* zygote is so far the most well-studied system to investigate the intrinsic pathways in SB. In contrast, other model systems including mammalian embryos have highlighted distinct intrinsic pathways that facilitate efficient SB. Mouse preimplantation embryo becomes polarized by segregating PAR proteins along inside–outside orientation at the 8-cell stage. A single cell isolated from the 8-cell stage embryo is capable of polarizing actomyosin contractility and PAR proteins at the cortex in a cell-autonomous manner (Anani et al., 2014; Maître et al., 2016). Asymmetry in cortical contractility in turn directs internalization of a lower-contractile cell in the 16-cell stage embryo (Maître et al., 2016). How SB is induced in the 8-cell stage embryo remains not fully understood. Distinct from *C. elegans* zygote, the cells of the mouse embryo lack centrosomes, suggesting an involvement of other intracellular structures in SB. Interestingly, these cells maintain their cytokinetic bridge structure (also known as midbody) even after cell division and position them toward the outer side of the cortex (Zenker et al., 2017). This bridge structure serves as scaffold for the accumulation of microtubule-associated proteins such as CAMSAP3, thereby acting as a noncentrosomal microtubule-organizing center during interphase (Zenker et al., 2017). The volume of the bridge structure is asymmetric between two daughter cells, resulting in asymmetry in transport of key proteins required for cell polarity to the outer cortex (Zenker et al., 2017). It remains unknown how the bridge structure acquires asymmetric properties after cell division. Recent study of *C. elegans* gastrulation revealed a role of Aurora-B kinase in polarizing the midbody toward the apical cortex and establishing the apical cortical domain (Bai et al., 2020). These findings suggest that mouse embryo may utilize the bridge structure as an intracellular signaling center for cell polarity kinase(s). Recent study also highlighted a role of intermediate filaments including keratins in the induction of cell polarity in mouse embryos (Lim et al., 2020). Keratins function as asymmetrically inherited factors and stabilize the outer cortical domain via interaction with the actin cortex. Asymmetric inheritance of keratins to the outer cells requires the outer cortical domain proteins such as PARD6B and the actin cytoskeleton (Lim et al., 2020), suggesting that keratins may be involved in a positive feedback with these proteins and otherwise may not be the most upstream factor in the SB cascade. SB in mouse embryo is also ensured by extrinsic stimuli including cadherin-based adhesions (Shirayoshi et al., 1983) and mechanical forces through physical attachment with neighboring cells (Samarage et al., 2015; Korotkevich et al., 2017). Therefore, distinct from *C. elegans* zygote, mammalian embryos utilize a combination of intrinsic and extrinsic pathways to ensure efficient SB during embryogenesis.

Understanding the mechanism underlying cell polarization has been a long-standing problem in cell and developmental biology. Particularly, our knowledge of SB induction is far less comprehensive. Recent advancement in imaging technologies and artificial manipulation of cellular signaling has revealed novel mechanistic insights into SB. It is reasonable to employ computer-assisted approaches to achieve quantitative explanations from these insights. Several mathematical models have already contributed to our understanding of the basic principles in *C. elegans* SB (Tostevin and Howard, 2008; Dawes and Munro, 2011; Goehring et al., 2011b; Kravtsova and Dawes, 2014; Gross et al., 2019; Geßele et al., 2020). Further comprehensive assessment and modeling of the concentration, diffusion, and complex composition of the actin cytoskeleton and PAR proteins will be useful to decipher the complex molecular behaviors into simple principles that govern the spatial organization of a cell. In conclusion, utilization of the *C. elegans* zygote as a model to study the mechanochemical reactions underlying SB and polarization has yielded valuable insights into the biophysical basis of the signaling cascades and has advanced the discovery of novel functions of proteins in various developmental contexts.

AUTHOR CONTRIBUTIONS

WG and FM prepared, wrote, and revised the manuscript together. All authors contributed to the article and approved the submitted version.

FUNDING

This study was supported by the Singapore National Research Foundation [NRF_NRFF2012-08 (FM)] and the

Strategic Japan-Singapore Cooperative Research Program by the Japan Science and Technology Agency and the Singapore Agency for Science, Technology, and Research [1514324022 (FM)].

ACKNOWLEDGMENTS

We thank members in the Motegi lab for helpful comments on the manuscript.

REFERENCES

Agarwal, P., and Zaidel-Bar, R. (2019). Principles of actomyosin regulation *in vivo*. *Trends Cell Biol.* 29, 150–163. doi: 10.1016/j.tcb.2018.09.006

Anani, S., Bhat, S., Honma-Yamanaka, N., Krawchuk, D., and Yamanaka, Y. (2014). Initiation of Hippo signaling is linked to polarity rather than to cell position in the pre-implantation mouse embryo. *Development* 141, 2813–2824. doi: 10.1242/dev.107276

Bai, X., Melesse, M., Sorensen Turpin, C. G., Sloan, D. E., Chen, C. Y., Wang, W. C., et al. (2020). Aurora B functions at the apical surface after specialized cytokinesis during morphogenesis in C. *elegans. Development* 147:dev18109. doi: 10.1242/dev.181099

Beatty, A., Morton, D., and Kemphues, K. (2010). The C. elegans homolog of Drosophila Lethal giant larvae functions redundantly with PAR-2 to maintain polarity in the early embryo. *Development* 137, 3995–4004. doi: 10.1242/dev.056028

Beatty, A., Morton, D. G., and Kemphues, K. (2013). PAR-2, LGL-1 and the CDC-42 GAP CHIN-1 act in distinct pathways to maintain polarity in the *C. elegans* embryo. *Development* 140, 2005–2014. doi: 10.1242/dev.088310

Bienkowska, D., and Cowan, C. R. (2012). Centrosomes can initiate a polarity axis from any position within one-cell *C. elegans* embryos. *Curr. Biol.* 22, 583–589. doi: 10.1016/j.cub.2012.01.064

Boyd, L., Guo, S., Levitan, D., Stinchcomb, D. T., and Kemphues, K. J. (1996). PAR-2 is asymmetrically distributed and promotes association of P granules and PAR-1 with the cortex in *C. elegans* embryos. *Development* 122, 3075–3084.

Chrétien, D., Buendia, B., Fuller, S. D., and Karsenti, E. (1997). Reconstruction of the centrosome cycle from cryoelectron micrographs. *J. Struct. Biol* 120, 117–133. doi: 10.1006/jsbi.1997.3928

Chugh, P., and Paluch, E. K. (2018). The actin cortex at a glance. *J. Cell Sci.* 131:jcs186254. doi: 10.1242/jcs.186254

Cowan, C. R., and Hyman, A. A. (2004). Centrosomes direct cell polarity independently of microtubule assembly in *C. elegans* embryos. *Nature* 431, 92–96. doi: 10.1038/nature02825

Cowan, C. R., and Hyman, A. A. (2006). Cyclin E–Cdk2 temporally regulates centrosome assembly and establishment of polarity in Caenorhabditis elegans embryos. *Nat. Cell Biol.* 8, 1441–1447. doi: 10.1038/ncb1511

Dawes, A. T., and Munro, E. M. (2011). PAR-3 oligomerization may provide an actin-independent mechanism to maintain distinct par protein domains in the early *Caenorhabditis elegan*s embryo. *Biophys. J.* 101, 1412–1422. doi: 10.1016/j.bpj.2011.07.030

De Henau, S., Pagès-Gallego, M., Pannekoek, W. J., and Dansen, T. B. (2020). Mitochondria-derived H(2)O(2) promotes symmetry breaking of the *C. elegans* zygote. *Dev. Cell* 53, 263–271.e266. doi: 10.1016/j.devcel.2020.03.008

Dickinson, D. J., Schwager, F., Pintard, L., Gotta, M., and Goldstein, B. (2017). A single-cell biochemistry approach reveals PAR complex dynamics during cell polarization. *Dev. Cell* 42, 416–434.e411. doi: 10.1016/j.devcel.2017.07.024

Etemad-Moghadam, B., Guo, S., and Kemphues, K. J. (1995). Asymmetrically distributed PAR-3 protein contributes to cell polarity and spindle alignment in early *C. elegans* embryos. *Cell* 83, 743–752. doi: 10.1016/0092-8674(95)90187-6

Ford, M. G., Mills, I. G., Peter, B. J., Vallis, Y., Praefcke, G. J., Evans, P. R., et al. (2002). Curvature of clathrin-coated pits driven by epsin. *Nature* 419, 361–366. doi: 10.1038/nature01020

Fortin, S. M., Marshall, S. L., Jaeger, E. C., Greene, P. E., Brady, L. K., Isaac, R. E., et al. (2010). The PAM-1 aminopeptidase regulates centrosome positioning to ensure anterior-posterior axis specification in one-cell *C. elegans* embryos. *Dev. Biol.* 344, 992–1000. doi: 10.1016/j.ydbio.2010.06.016

Geßele, R., Halatek, J., Würthner, L., and Frey, E. (2020). Geometric cues stabilise long-axis polarisation of PAR protein patterns in *C. elegans. Nat. Commun.* 11:539. doi: 10.1038/s41467-020-14317-w

Goehring, N. W., Hoege, C., Grill, S. W., and Hyman, A. A. (2011a). PAR proteins diffuse freely across the anterior-posterior boundary in polarized *C. elegans* embryos. *J. Cell Biol.* 193, 583–594. doi: 10.1083/jcb.201011094

Goehring, N. W., Trong, P. K., Bois, J. S., Chowdhury, D., Nicola, E. M., Hyman, A. A., et al. (2011b). Polarization of PAR proteins by advective triggering of a pattern-forming system. *Science* 334, 1137–1141. doi: 10.1126/science.1208619

Goldstein, B., and Hird, S. N. (1996). Specification of the anteroposterior axis in *Caenorhabditis elegans*. *Development* 122, 1467–1474.

Gómez-Cavazos, J. S., Lee, K. Y., Lara-González, P., Li, Y., Desai, A., Shiau, A. K., et al. (2020). A Non-canonical BRCT-phosphopeptide recognition mechanism underlies RhoA activation in cytokinesis. *Curr. Biol.* 30, 3101–3115.e3111. doi: 10.1016/j.cub.2020.05.090

Gross, P., Kumar, K. V., Goehring, N. W., Bois, J. S., Hoege, C., Jülicher, F., et al. (2019). Guiding self-organized pattern formation in cell polarity establishment. *Nat. Phys.* 15, 293–300. doi: 10.1038/s41567-018-0358-7

Guo, S., and Kemphues, K. J. (1995). par-1, a gene required for establishing polarity in *C. elegans* embryos, encodes a putative Ser/Thr kinase that is asymmetrically distributed. *Cell* 81, 611–620. doi: 10.1016/0092-8674(95)90082-9

Guo, S., and Kemphues, K. J. (1996). A non-muscle myosin required for embryonic polarity in Caenorhabditis elegans. *Nature* 382, 455–458. doi: 10.1038/382455a0

Hamill, D. R., Severson, A. F., Carter, J. C., and Bowerman, B. (2002). Centrosome maturation and mitotic spindle assembly in *C. elegans* require SPD-5, a protein with multiple coiled-coil domains. *Dev. Cell* 3, 673–684. doi: 10.1016/S1534-5807(02)00327-1

Heo, J., and Campbell, S. L. (2005). Mechanism of redox-mediated guanine nucleotide exchange on redox-active Rho GTPases. *J. Biol. Chem.* 280, 31003–31010. doi: 10.1074/jbc.M504768200

Hill, D. P., and Strome, S. (1988). An analysis of the role of microfilaments in the establishment and maintenance of asymmetry in *Caenorhabditis elegans* zygotes. *Dev. Biol.* 125, 75–84. doi: 10.1016/0012-1606(88)90060-7

Hirani, N., Illukkumbura, R., Bland, T., Mathonnet, G., Suhner, D., Reymann, A.-C., et al. (2019). Anterior-enriched filopodia create the appearance of asymmetric membrane microdomains in polarizing *C. elegans* zygotes. *J. Cell Sci.* 132:jcs230714. doi: 10.1242/jcs.230714

Hird, S. N., and White, J. G. (1993). Cortical and cytoplasmic flow polarity in early embryonic cells of Caenorhabditis elegans. *J. Cell Biol.* 121, 1343–1355. doi: 10.1083/jcb.121.6.1343

Hoege, C., Constantinescu, A. T., Schwager, A., Goehring, N. W., Kumar, P., and Hyman, A. A. (2010). LGL can partition the cortex of one-cell Caenorhabditis elegans embryos into two domains. *Curr. Biol.* 20, 1296–1303. doi: 10.1016/j.cub.2010.05.061

Hung, T. J., and Kemphues, K. J. (1999). PAR-6 is a conserved PDZ domain-containing protein that colocalizes with PAR-3 in *Caenorhabditis elegans* embryos. *Development* 126, 127–135.

Jantsch-Plunger, V. A., Gönczy, P., Romano, A., Schnabel, H., Hamill, D., Schnabel, R., et al. (2000). CYK-4: A Rho family gtpase activating protein (GAP) required for central spindle formation and cytokinesis. *J. Cell Biol.* 149, 1391–1404. doi: 10.1083/jcb.149.7.1391

Jenkins, N., Saam, J. R., and Mango, S. E. (2006). CYK-4/GAP Provides a localized cue to initiate anteroposterior polarity upon fertilization. *Science* 313, 1298–1301. doi: 10.1126/science.1130291

Johnston, W. L., Krizus, A., and Dennis, J. W. (2006). The eggshell is required for meiotic fidelity, polar-body extrusion and polarization of the *C. elegans* embryo. *BMC Biol.* 4:35. doi: 10.1186/1741-7007-4-35

Kapoor, S., and Kotak, S. (2019). Centrosome Aurora A regulates RhoGEF ECT-2 localisation and ensures a single PAR-2 polarity axis in *C. elegans* embryos. *Development* 146:dev174565. doi: 10.1242/dev.174565

Kimura, K., and Kimura, A. (2020). Cytoplasmic streaming drifts the polarity cue and enables posteriorization of the *Caenorhabditis elegans* zygote

at the side opposite of sperm entry. *Mol. Biol. Cell* 31, 1765–1773. doi: 10.1091/mbc.E20-01-0058

Kimura, K., Mamane, A., Sasaki, T., Sato, K., Takagi, J., Niwayama, R., et al. (2017). Endoplasmic-reticulum-mediated microtubule alignment governs cytoplasmic streaming. *Nat. Cell Biol.* 19, 399–406. doi: 10.1038/ncb3490

Klinkert, K., Levernier, N., Gross, P., Gentili, C., von Tobel, L., Pierron, M., et al. (2019). Aurora A depletion reveals centrosome-independent polarization mechanism in *Caenorhabditis elegans*. *Elife* 8:e44552. doi: 10.7554/eLife.44552.034

Korotkevich, E., Niwayama, R., Courtois, A., Friese, S., Berger, N., Buchholz, F., et al. (2017). The apical domain is required and sufficient for the first lineage segregation in the mouse embryo. *Dev. Cell* 40, 235–247.e237. doi: 10.1016/j.devcel.2017.01.006

Kravtsova, N., and Dawes, A. T. (2014). Actomyosin regulation and symmetry breaking in a model of polarization in the early *Caenorhabditis elegans* embryo : symmetry breaking in cell polarization. *Bull. Math. Biol.* 76, 2426–2448. doi: 10.1007/s11538-014-0016-x

Kruse, K., Joanny, J. F., Jülicher, F., Prost, J., and Sekimoto, K. (2005). Generic theory of active polar gels: a paradigm for cytoskeletal dynamics. *Eur. Phys. J. E Soft Matter* 16, 5–16. doi: 10.1140/epje/e2005-00002-5

Kumfer, K. T., Cook, S. J., Squirrell, J. M., Eliceiri, K. W., Peel, N., O'Connell, K. F., et al. (2010). CGEF-1 and CHIN-1 regulate CDC-42 activity during asymmetric division in the *Caenorhabditis elegans* embryo. *Mol. Biol. Cell* 21, 266–277. doi: 10.1091/mbc.e09-01-0060

Lang, C. F., and Munro, E. (2017). The PAR proteins: from molecular circuits to dynamic self-stabilizing cell polarity. *Development* 144, 3405–3416. doi: 10.1242/dev.139063

Levitan, D. J., Boyd, L., Mello, C. C., Kemphues, K. J., and Stinchcomb, D. T. (1994). par-2, a gene required for blastomere asymmetry in *Caenorhabditis elegans*, encodes zinc-finger and ATP-binding motifs. *Proc. Natl. Acad. Sci. U. S. A.* 91, 6108–6112. doi: 10.1073/pnas.91.13.6108

Li, R., and Bowerman, B. (2010). Symmetry breaking in biology. *Cold Spring Harb. Perspect. Biol.* 2:a003475. doi: 10.1101/cshperspect.a003475

Lim, H. Y. G., Alvarez, Y. D., Gasnier, M., Wang, Y., Tetlak, P., Bissiere, S., et al. (2020). Keratins are asymmetrically inherited fate determinants in the mammalian embryo. *Nature* 585, 404–409. doi: 10.1038/s41586-020-2647-4

Lyczak, R., Zweier, L., Group, T., Murrow, M. A., Snyder, C., Kulovitz, L., et al. (2006). The puromycin-sensitive aminopeptidase PAM-1 is required for meiotic exit and anteroposterior polarity in the one-cell Caenorhabditis elegans embryo. *Development* 133, 4281–4292. doi: 10.1242/dev.02615

Maître, J.-L., Turlier, H., Illukkumbura, R., Eismann, B., Niwayama, R., Nédélec, F., et al. (2016). Asymmetric division of contractile domains couples cell positioning and fate specification. *Nature* 536, 344–348. doi: 10.1038/nature18958

Malone, C. J., Misner, L., Le Bot, N., Tsai, M. C., Campbell, J. M., Ahringer, J., et al. (2003). The *C. elegans* hook protein, ZYG-12, mediates the essential attachment between the centrosome and nucleus. *Cell* 115, 825–836. doi: 10.1016/S0092-8674(03)00985-1

Mangal, S., Sacher, J., Kim, T., Osório, D. S., Motegi, F., Carvalho, A. X., et al. (2018). TPXL-1 activates Aurora A to clear contractile ring components from the polar cortex during cytokinesis. *J. Cell Biol.* 217, 837–848. doi: 10.1083/jcb.201706021

Mayer, M., Depken, M., Bois, J. S., Jülicher, F., and Grill, S. W. (2010). Anisotropies in cortical tension reveal the physical basis of polarizing cortical flows. *Nature* 467, 617–621. doi: 10.1038/nature09376

McCarter, J., Bartlett, B., Dang, T., and Schedl, T. (1999). On the control of oocyte meiotic maturation and ovulation in Caenorhabditis elegans. *Dev. Biol.* 205, 111–128. doi: 10.1006/dbio.1998.9109

Michaux, J. B., Robin, F. B., McFadden, W. M., and Munro, E. M. (2018). Excitable RhoA dynamics drive pulsed contractions in the early *C. elegans* embryo. *J. Cell Biol.* 217, 4230–4252. doi: 10.1083/jcb.201806161

Miller, S. E., Mathiasen, S., Bright, N. A., Pierre, F., Kelly, B. T., Kladt, N., et al. (2015). CALM regulates clathrin-coated vesicle size and maturation by directly sensing and driving membrane curvature. *Dev. Cell* 33, 163–175. doi: 10.1016/j.devcel.2015.03.002

Minn, I. L., Rolls, M. M., Hanna-Rose, W., and Malone, C. J. (2009). SUN-1 and ZYG-12, mediators of centrosome-nucleus attachment, are a functional SUN/KASH pair in *Caenorhabditis elegans*. *Mol. Biol. Cell* 20, 4586–4595. doi: 10.1091/mbc.e08-10-1034

Morton, D. G., Roos, J. M., and Kemphues, K. J. (1992). par-4, a gene required for cytoplasmic localization and determination of specific cell types in Caenorhabditis elegans embryogenesis. *Genetics* 130, 771–790.

Morton, D. G., Shakes, D. C., Nugent, S., Dichoso, D., Wang, W., Golden, A., et al. (2002). The Caenorhabditis elegans par-5 gene encodes a 14-3-3 protein required for cellular asymmetry in the early embryo. *Dev. Biol.* 241, 47–58. doi: 10.1006/dbio.2001.0489

Motegi, F., Zonies, S., Hao, Y., Cuenca, A. A., Griffin, E., and Seydoux, G. (2011). Microtubules induce self-organization of polarized PAR domains in *Caenorhabditis elegans* zygotes. *Nat. Cell Biol.* 13, 1361–1367. doi: 10.1038/ncb2354

Munro, E., Nance, J., and Priess, J. R. (2004). Cortical flows powered by asymmetrical contraction transport PAR proteins to establish and maintain anterior-posterior polarity in the early *C. elegans* embryo. *Dev. Cell* 7, 413–424. doi: 10.1016/j.devcel.2004.08.001

Nishikawa, M., Naganathan, S. R., Jülicher, F., and Grill, S. W. (2017). Controlling contractile instabilities in the actomyosin cortex. *Elife* 6:e19595. doi: 10.7554/eLife.19595

O'Connell, K. F., Maxwell, K. N., and White, J. G. (2000). The spd-2 gene is required for polarization of the anteroposterior axis and formation of the sperm asters in the Caenorhabditis elegans zygote. *Dev. Biol.* 222, 55–70. doi: 10.1006/dbio.2000.9714

Olson, S. K., Greenan, G., Desai, A., Müller-Reichert, T., and Oegema, K. (2012). Hierarchical assembly of the eggshell and permeability barrier in *C. elegans*. *J. Cell Biol.* 198, 731–748. doi: 10.1083/jcb.201206008

Peter, B. J., Kent, H. M., Mills, I. G., Vallis, Y., Butler, P. J., Evans, P. R., et al. (2004). BAR domains as sensors of membrane curvature: the amphiphysin BAR structure. *Science* 303, 495–499. doi: 10.1126/science.1092586

Ramanujam, R., Han, Z., Zhang, Z., Kanchanawong, P., and Motegi, F. (2018). Establishment of the PAR-1 cortical gradient by the aPKC-PRBH circuit. *Nat. Chem. Biol.* 14, 917–927. doi: 10.1038/s41589-018-0117-1

Rappleye, C. A., Paredez, A. R., Smith, C. W., McDonald, K. L., and Aroian, R. V. (1999). The coronin-like protein POD-1 is required for anterior-posterior axis formation and cellular architecture in the nematode caenorhabditis elegans. *Genes Dev.* 13, 2838–2851. doi: 10.1101/gad.13.21.2838

Reich, J. D., Hubatsch, L., Illukkumbura, R., Peglion, F., Bland, T., Hirani, N., et al. (2019). Regulated activation of the PAR polarity network ensures a timely and specific response to spatial cues. *Curr. Biol.* 29, 1911–1923.e1915. doi: 10.1016/j.cub.2019.04.058

Sadler, P. L., and Shakes, D. C. (2000). Anucleate *Caenorhabditis elegans* sperm can crawl, fertilize oocytes and direct anterior-posterior polarization of the 1-cell embryo. *Development* 127, 355–366. Available online at: https://dev.biologists.org/content/develop/127/2/355.full.pdf

Samarage, C. R., White, M. D., Álvarez, Y. D., Fierro-González, J. C., and Henon, Y., Jesudason, E.C., et al. (2015). Cortical tension allocates the first inner cells of the mammalian embryo. *Dev. Cell* 34, 435–447. doi: 10.1016/j.devcel.2015.07.004

Santella, L., Alikani, M., Talansky, B. E., Cohen, J., and Dale, B. (1992). Is the human oocyte plasma membrane polarized? *Hum. Reprod.* 7, 999–1003. doi: 10.1093/oxfordjournals.humrep.a137788

Schenk, C., Bringmann, H., Hyman, A. A., and Cowan, C. R. (2010). Cortical domain correction repositions the polarity boundary to match the cytokinesis furrow in *C. elegans* embryos. *Development* 137, 1743–1753. doi: 10.1242/dev.040436

Schmutz, C., Stevens, J., and Spang, A. (2007). Functions of the novel RhoGAP proteins RGA-3 and RGA-4 in the germ line and in the early embryo of *C. elegans*. *Development* 134, 3495–3505. doi: 10.1242/dev.000802

Schneider, S. Q., and Bowerman, B. (2003). Cell Polarity and the Cytoskeleton in the *Caenorhabditis elegans* Zygote. *Ann. Rev. Genet.* 37, 221–249. doi: 10.1146/annurev.genet.37.110801.142443

Schonegg, S., Constantinescu, A. T., Hoege, C., and Hyman, A. A. (2007). The Rho GTPase-activating proteins RGA-3 and RGA-4 are required to set the initial size of PAR domains in *Caenorhabditis elegans* one-cell embryos. *Proc. Natl. Acad. Sci. U. S. A.* 104, 14976–14981. doi: 10.1073/pnas.0706941104

Schumacher, J. M., Ashcroft, N., Donovan, P. J., and Golden, A. (1998). A highly conserved centrosomal kinase, AIR-1, is required for accurate cell cycle

progression and segregation of developmental factors in *Caenorhabditis elegans* embryos. *Development* 125, 4391–4402.

Severson, A. F., Baillie, D. L., and Bowerman, B. (2002). A Formin Homology protein and a profilin are required for cytokinesis and Arp2/3-independent assembly of cortical microfilaments in *C. elegans*. *Curr. Biol.* 12, 2066–2075. doi: 10.1016/S0960-9822(02)01355-6

Shelton, C. A., Carter, J. C., Ellis, G. C., and Bowerman, B. (1999). The Nonmuscle myosin regulatory light chain gene mlc-4 is required for cytokinesis, anterior-posterior polarity, and body morphology during *Caenorhabditis elegans* embryogenesis. *J. Cell Biol.* 146, 439–451. doi: 10.1083/jcb.146.2.439

Shirayoshi, Y., Okada, T. S., and Takeichi, M. (1983). The calcium-dependent cell-cell adhesion system regulates inner cell mass formation and cell surface polarization in early mouse development. *Cell* 35 (3 Pt 2), 631–638. doi: 10.1016/0092-8674(83)90095-8

Sonneville, R., and Gönczy, P. (2004). zyg-11 and cul-2 regulate progression through meiosis II and polarity establishment in *C. elegans*. *Development* 131, 3527–3543. doi: 10.1242/dev.01244

Strome, S., and Wood, W. B. (1983). Generation of asymmetry and segregation of germ-line granules in early *C. elegans* embryos. *Cell* 35, 15–25. doi: 10.1016/0092-8674(83)90203-9

Tabuse, Y., Izumi, Y., Piano, F., Kemphues, K. J., Miwa, J., and Ohno, S. (1998). Atypical protein kinase C cooperates with PAR-3 to establish embryonic polarity in *Caenorhabditis elegans*. *Development* 125, 3607–3614.

Tagawa, A., Rappleye, C. A., and Aroian, R. V. (2001). Pod-2, along with pod-1, defines a new class of genes required for polarity in the early *Caenorhabditis elegans* embryo. *Dev. Biol.* 233, 412–424. doi: 10.1006/dbio.2001.0234

Tostevin, F., and Howard, M. (2008). Modeling the establishment of PAR protein polarity in the one-cell *C. elegans* embryo. *Biophys. J.* 95, 4512–4522. doi: 10.1529/biophysj.108.136416

Tse, Y. C., Werner, M., Longhini, K. M., Labbe, J. C., Goldstein, B., and Glotzer, M. (2012). RhoA activation during polarization and cytokinesis of the early *Caenorhabditis elegans* embryo is differentially dependent on NOP-1 and CYK-4. *Mol. Biol. Cell* 23, 4020–4031. doi: 10.1091/mbc.e12-04-0268

Wallenfang, M. R., and Seydoux, G. (2000). Polarization of the anterior-posterior axis of *C. elegans* is a microtubule-directed process. *Nature* 408, 89–92. doi: 10.1038/35040562

Watts, J. L., Etemad-Moghadam, B., Guo, S., Boyd, L., Draper, B. W., Mello, C. C., et al. (1996). par-6, a gene involved in the establishment of asymmetry in early *C. elegans* embryos, mediates the asymmetric localization of PAR-3. *Development* 122, 3133–3140.

Wirtz-Peitz, F., Nishimura, T., and Knoblich, J. A. (2008). Linking cell cycle to asymmetric division: Aurora-A phosphorylates the Par complex to regulate Numb localization. *Cell* 135, 161–173. doi: 10.1016/j.cell.2008.07.049

Woodruff, J. B., Ferreira Gomes, B., Widlund, P. O., Mahamid, J., Honigmann, A., and Hyman, A. A. (2017). The centrosome is a selective condensate that nucleates microtubules by concentrating tubulin. *Cell* 169, 1066–1077.e1010. doi: 10.1016/j.cell.2017.05.028

Zenker, J., White, M. D., Templin, R. M., Parton, R. G., Thorn-Seshold, O., Bissiere, S., et al. (2017). A microtubule-organizing center directing intracellular transport in the early mouse embryo. *Science* 357, 925–928. doi: 10.1126/science.aam9335

Zeno, W. F., Baul, U., Snead, W. T., DeGroot, A. C. M., Wang, L., Lafer, E. M., et al. (2018). Synergy between intrinsically disordered domains and structured proteins amplifies membrane curvature sensing. *Nat. Commun.* 9:4152. doi: 10.1038/s41467-018-06532-3

Zhang, D., and Glotzer, M. (2015). The RhoGAP activity of CYK-4/MgcRacGAP functions non-canonically by promoting RhoA activation during cytokinesis. *Elife* 4:e08898. doi: 10.7554/eLife.08898.031

Zhao, P., Teng, X., Tantirimudalige, S. N., Nishikawa, M., Wohland, T., Toyama, Y., et al. (2019). Aurora-A breaks symmetry in contractile actomyosin networks independently of its role in centrosome maturation. *Dev. Cell* 48, 631–645.e636. doi: 10.1016/j.devcel.2019.02.012

Conflict of Interest: The authors declare that the research was conducted in the absence of any commercial or financial relationships that could be construed as a potential conflict of interest.

frontiers in Cell and Developmental Biology

REVIEW
published: 21 January 2021
doi: 10.3389/fcell.2020.632253

PLK-1 Regulation of Asymmetric Cell Division in the Early *C. elegans* Embryo

Amelia J. Kim† *and Erik E. Griffin**†

Department of Biological Sciences, Dartmouth College, Hanover, NH, United States

PLK1 is a conserved mitotic kinase that is essential for the entry into and progression through mitosis. In addition to its canonical mitotic functions, recent studies have characterized a critical role for PLK-1 in regulating the polarization and asymmetric division of the one-cell *C. elegans* embryo. Prior to cell division, PLK-1 regulates both the polarization of the PAR proteins at the cell cortex and the segregation of cell fate determinants in the cytoplasm. Following cell division, PLK-1 is preferentially inherited to one daughter cell where it acts to regulate the timing of centrosome separation and cell division. PLK1 also regulates cell polarity in asymmetrically dividing *Drosophila* neuroblasts and during mammalian planar cell polarity, suggesting it may act broadly to connect cell polarity and cell cycle mechanisms.

Keywords: PLK1 (Polo-like Kinase 1), *C. elegans*, asymmetric cell division (ACD), cell polarity, PAR proteins

OPEN ACCESS

Edited by:
Yi Wu,
UCONN Health, United States

Reviewed by:
Monica Gotta,
Université de Genève, Switzerland
Ana Carmena,
Instituto de Neurociencias de Alicante (IN), Spain

****Correspondence:***
Erik E. Griffin
erik.e.griffin@dartmouth.edu

†ORCID:
Amelia J. Kim
orcid.org/0000-0002-4178-699X
Erik E. Griffin
orcid.org/0000-0001-9958-2466

Specialty section:
This article was submitted to Signaling, a section of the journal Frontiers in Cell and Developmental Biology

Received: *22 November 2020*
Accepted: *21 December 2020*
Published: *21 January 2021*

Citation:
Kim AJ and Griffin EE (2021) PLK-1 Regulation of Asymmetric Cell Division in the Early C. elegans Embryo. Front. Cell Dev. Biol. 8:632253. doi: 10.3389/fcell.2020.632253

INTRODUCTION

Asymmetric cell division is a process in which a dividing cell gives rise to daughter cells with differing fate, size and/or function. In bacteria and yeast, asymmetric divisions are widespread and give rise to cells that differ in morphology, function or replicative capacity (Macara and Mili, 2008; Kysela et al., 2013). In metazoans, asymmetric divisions contribute to the diversification of cell types during embryonic development and are also required to maintain tissue homeostasis in adults, for example through the continued asymmetric division of stem cells (Knoblich, 2010). While diverse molecular mechanisms control asymmetric divisions in unicellular and multicellular organisms (Macara and Mili, 2008), coordination between cell polarization and cell cycle progression lies at the heart of each asymmetric division: factors are polarized prior to cell division such that they are partitioned unequally to the daughter cells upon cytokinesis (Li, 2013; Venkei and Yamashita, 2018). Therefore, understanding the interplay between cell polarization, cell cycle and cell division mechanisms is central to understanding how cells divide asymmetrically (Knoblich, 2010; Noatynska et al., 2010).

Polo-like kinase 1 (PLK1) is a conserved and essential mitotic kinase that regulates centrosome duplication and maturation, mitotic entry, bipolar spindle formation, chromosome segregation, and cytokinesis (Barr et al., 2004; Petronczki et al., 2008; Archambault and Glover, 2009; Pintard and Archambault, 2018). PLK1 activity is relatively low during interphase and increases at the G2/M transition before falling again after anaphase. Abnormally high PLK1 activity during G2 and M-phase is associated with tumorigenesis, and has therefore been extensively studied as a target for cancer therapeutics (Strebhardt and Ullrich, 2006). In addition to its canonical mitotic functions, important roles for PLK1 in asymmetric cell division have been characterized. In this review, we focus on the role of PLK-1 during the asymmetric division of the one-cell *C. elegans*

embryo (zygote). We describe the mechanisms by which PLK-1 both regulates the polarization of the worm zygote and as well as the ways in which the asymmetric inheritance of PLK-1 contributes to differences between daughter cells at the two-cell stage.

OVERVIEW OF PLK1 STRUCTURE AND REGULATION

polo was first identified in *Drosophila* (Sunkel and Glover, 1988) and its homologs include *S. cerevisiae* Cdc5, *S. pombe* Plo1, *C. elegans* PLK-1 and human PLK1 (Archambault and Glover, 2009). PLK1 contains an N-terminal Serine/Threonine kinase domain that is highly conserved among polo-like kinases and is similar to those in Aurora kinases and calcium/calmodulin-dependent kinases (Zitouni et al., 2014). PLK1 kinase activity is stimulated by phosphorylation of the activation loop in the PLK1 kinase domain by Aurora A kinase, which depends on the Aurora A cofactor Bora (Jang et al., 2002; Macurek et al., 2008; Seki et al., 2008; Tavernier et al., 2015b) (**Figure 1**). The C-terminus features a non-catalytic Polo box domain (PBD) that binds phosphopeptides generated by either PLK1 itself (self-primed) or by other kinases (non-self primed) (Zitouni et al., 2014) (**Figure 1**). The interaction between the PBD and various binding partners guides PLK1 localization to different cellular structures such as the centrosome, kinetochores, nuclear envelope and midbody (Lee et al., 1998; Elia et al., 2003). Additionally, the interaction between the PBD and its binding partners relieves the autoinhibition of PLK1 kinase activity by the intramolecular interaction between the PBD and the kinase domain, thereby coupling PLK1 localization with its activation toward specific substrates (Elia et al., 2003; Lowery et al., 2005; Zitouni et al., 2014) (**Figure 1**).

INTRODUCTION TO THE ASYMMETRIC DIVISION OF THE *C. ELEGANS* EMBRYO

The one-cell *C. elegans* embryo undergoes an asymmetric division to give rise to an anterior daughter cell named AB and a posterior daughter cell named P1. AB and P1 differ in several respects: AB gives rise exclusively to somatic lineages whereas P1 gives rise to both somatic and germline lineages, AB is larger than P1, and AB divides roughly 2 min before P1 with a mitotic spindle oriented orthogonally to the P1 spindle (Rose and Gonczy, 2014; Griffin, 2015). All aspects of this asymmetric division depend on the polarization of the embryo by the conserved PAR polarity regulators.

The PAR proteins include the Anterior PAR proteins (aPARs) PAR-3, PAR-6 and PKC-3/aPKC and the Posterior PAR proteins (pPARs) PAR-1 and PAR-2. The aPARs and pPARs antagonize each other's cortical association such that any region of the cortex is typically occupied by either the aPARs or the pPARs, but not both (Lang and Munro, 2017). The PAR proteins are deposited in the oocyte and remain symmetrically distributed as the oocyte matures and as the newly fertilized embryo completes meiosis II. Upon the completion of meiosis, several symmetry breaking cues at the posterior pole combine to trigger the precisely timed, robust, and rapid polarization of the embryo (Goldstein and Hird, 1996). These cues include microtubules and Aurora A kinase activity that emanates from the sperm-donated centrosome at the posterior end (Tsai and Ahringer, 2007; Motegi et al., 2011; Klinkert et al., 2019; Zhao et al., 2019) and redox signaling from mitochondria near the posterior cortex (De Henau et al., 2020). These cues trigger the establishment of polarity, which takes roughly 10 min and results in the concentration of the aPARs at the anterior cortex and the pPARs at the posterior cortex. During polarity establishment, anteriorly-directed cortical actomyosin flows help to sweep the cortical aPARs out of the posterior domain, thereby allowing pPARs to load from the cytoplasm onto the posterior cortex (Cheeks et al., 2004; Munro et al., 2004; Goehring et al., 2011; Gubieda et al., 2020). These asymmetries are maintained for ∼10 min until the embryo divides. From their polarized domains, the PAR proteins regulate the polarization of both cortical and cytoplasmic factors along the anterior/posterior (A/P) axis that result in the differences in size, fate, spindle orientation and cell division timing between AB and P1.

Consistent with its canonical role in the cell cycle, PLK-1 regulates meiotic and mitotic progression in the *C. elegans* zygote (Chase et al., 2000), including by promoting nuclear envelope breakdown (Rahman et al., 2015, 2020; Martino et al., 2017; Velez-Aguilera et al., 2020) and centrosome maturation (Woodruff et al., 2015). Here, we focus on PLK-1's contributions to the asymmetric division of the zygote as both a regulator at multiple stages of the zygote polarization and as a factor whose asymmetric inheritance contributes directly to differences between AB and P1 (**Figures 2A,B**). It is important to keep in mind that because complete depletion of PLK-1 activity results in sterility, the early embryonic functions of PLK-1 described below reflect the phenotypes of embryos partially depleted of PLK-1 activity.

PLK-1 REGULATES POLARIZATION OF THE *C. ELEGANS* ZYGOTE

PLK-1 Suppresses Premature Polarization During Meiosis

The *C. elegans* oocyte remains apolar as it matures, is fertilized and completes two meiotic divisions. In the maturing oocyte, the pPARs occupy the cell cortex and the aPARs are restricted to the cytoplasm. By anaphase II of meiosis, the PAR proteins have switched locations with the aPARs at the cell cortex and the pPARs restricted to the cytoplasm (Reich et al., 2019), positioning them to respond to the posterior symmetry breaking cues upon the completion of meiosis (**Figure 2B**). PLK-1 and Aurora A (AIR-1) suppress the premature cortical loading of the anterior PARs, thereby ensuring polarization is only established following the completion of meiosis. Depletion of either AIR-1 or PLK-1 results in the premature cortical localization of aPARs and the restriction of the pPARs to the cytoplasm in oocytes and meiotic embryos. This recruitment of the aPARs to the cortex "activates" the PAR polarity system prematurely (**Figure 2B**),

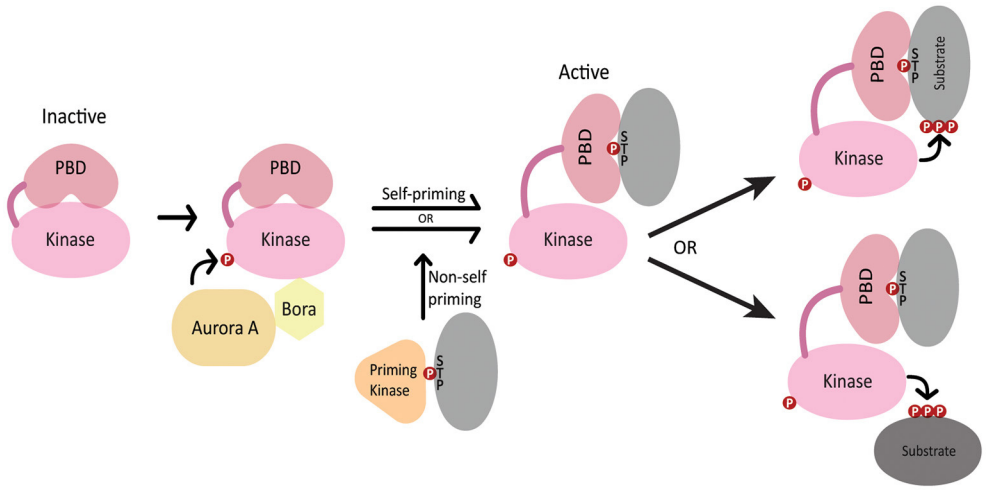

FIGURE 1 | Regulation of PLK1 activation and localization. In the inactive state, the kinase domain activation loop is not phosphorylated and the PBD domain autoinhibits the kinase domain. Aurora A and SPAT/Bora stimulate kinase activity through phosphorylation of the PLK1 activation loop. The PBD domain binds phosphopeptides generated by PLK1 (self-primed) or by a priming kinase (non-self-primed), which relieves autoinhibition of the kinase domain. The PBD interacts either with PLK1 substrates or localizes PLK-1 in proximity to its substrates.

such that normally cryptic symmetry breaking cues present in the meiotic embryo, including regions of high membrane curvature and microtubules associated with the meiotic spindle, can trigger polarization before the completion of meiosis (Wallenfang and Seydoux, 2000; Kapoor and Kotak, 2019; Klinkert et al., 2019; Reich et al., 2019; Zhao et al., 2019). As a result, *air-1* and *plk-1* depleted embryos display a range of polarity defects, including bipolarity, reversed polarity and mispositioned PAR domains (Noatynska et al., 2010; Klinkert et al., 2019; Reich et al., 2019; Zhao et al., 2019). Suppressing activation of the PAR system until after the completion of meiosis ensures the embryo only polarizes in response to the multiple coordinate symmetry breaking cues from the posterior end, resulting in the rapid and highly stereotyped establishment of the anterior/posterior polarity axis.

In the future, it will be important to determine whether PLK-1 and/or AIR-1 is the principal inhibitor of PAR network activation. Depletion of SPAT/Bora, which facilitates the activation of PLK-1 by AIR-1, results in similar polarity defects as depletion of either AIR-1 or PLK-1 (Noatynska et al., 2010). This observation is consistent with PLK-1 acting downstream of AIR-1 to suppress activation of the PAR network. Additionally, it will be important to identify the relevant substrates and mechanisms that suppress activation. As discussed in the next section, PLK-1 phosphorylates PAR-3 to suppress its cortical localization in mitotic one-cell embryos (Dickinson et al., 2017), suggesting this could be one possible mechanism by which PLK-1 might suppress aPAR cortical loading in oocytes and meiotic embryos.

PLK-1 Disassembles PAR-3 Clusters During Polarity Maintenance

Polarity establishment coincides with the dramatic flow of the contractile actomyosin cortex from the posterior toward the anterior (**Figure 2B**). These actomyosin flows help move the aPARs out of the posterior, clearing the way for pPARs to load from the cytoplasm onto the posterior cortex (Munro et al., 2004; Goehring et al., 2011). During actomyosin flows, the aPARs colocalize in prominent cortical clusters that stabilize their cortical association and help entrain them within actomyosin flows, thereby promoting segregation to the anterior (Tabuse et al., 1998; Hung and Kemphues, 1999; Beers and Kemphues, 2006; Sailer et al., 2015; Dickinson et al., 2017; Rodriguez et al., 2017; Wang et al., 2017). PAR-3 is critical for aPAR clustering: PAR-3 forms clusters in the absence of either PKC-3 or PAR-6, is required for PKC-3 clustering and contains an oligomerization domain that mediates its clustering (Dickinson et al., 2017; Rodriguez et al., 2017; Wang et al., 2017). Actomyosin flows cease when they reach roughly the midpoint of the A/P axis and shortly thereafter PAR-3 clusters disperse as the embryo enters mitosis and the maintenance phase of polarization.

The assembly of PAR-3 into cortical clusters is inhibited by PLK-1. In *plk-1(RNAi)* embryos, PAR-3 clusters form prematurely (before symmetry breaking), potentially reflecting the premature activation of the PAR network in meiotic embryos discussed above (Dickinson et al., 2017; Reich et al., 2019) (**Figure 2B**). Additionally, PAR-3 clusters fail to disassemble during maintenance phase in *plk-1* mutant embryos. The PAR-3 N-terminus contains two putative PBD binding motifs, both of which are required for the PLK-1 PBD domain to bind PAR-3 in a yeast two-hybrid assay. This interaction also depends on the phosphopeptide-binding motif in the PLK-1 PBD domain, suggesting that priming phosphorylation of PAR-3 stimulates an interaction between PLK-1 and PAR-3 (Dickinson et al., 2017). PAR-3 contains two putative PLK-1 phosphorylation sites (Thr32 and Thr89), one of which was shown to be phosphorylated by PLK-1 *in vitro*. Importantly,

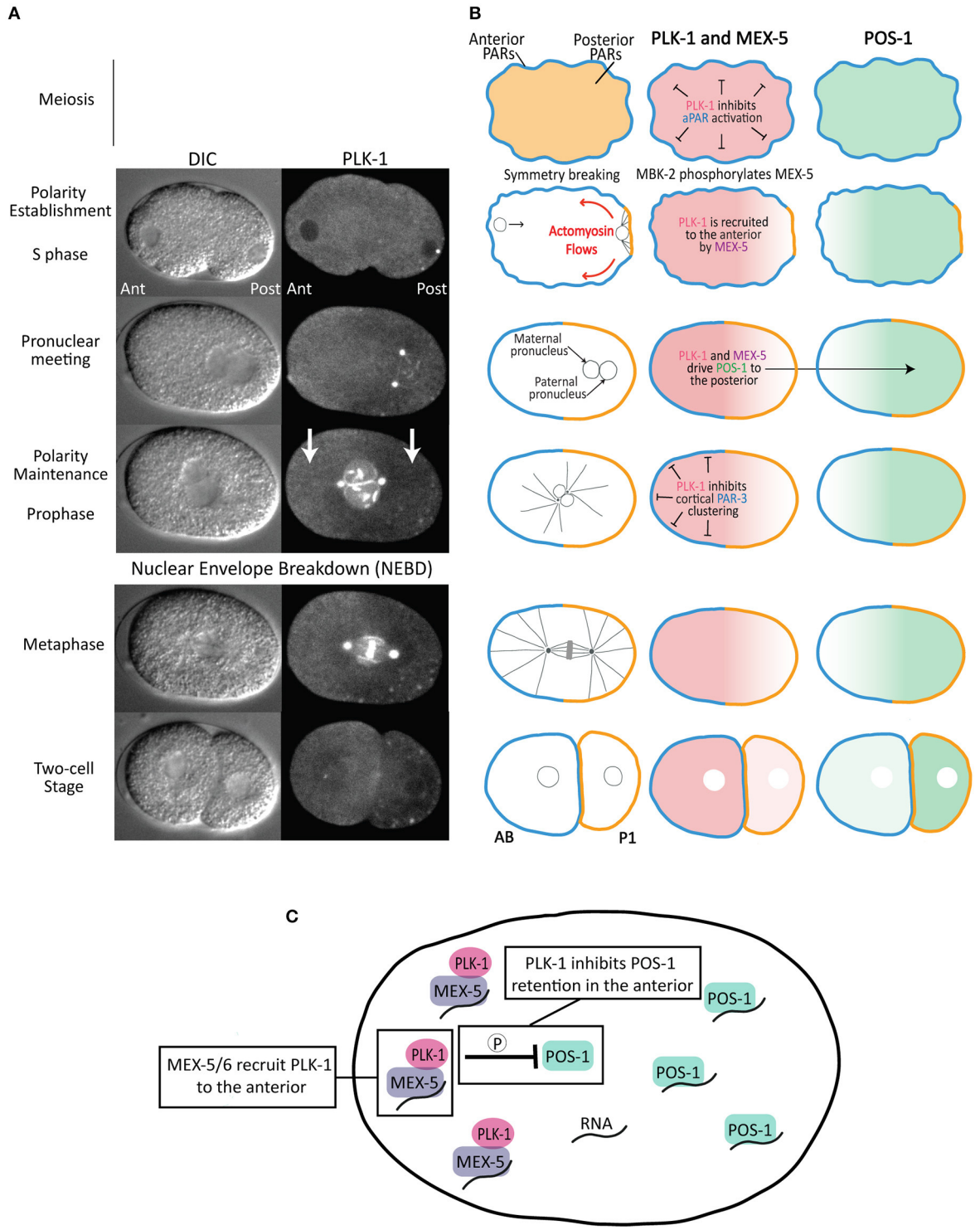

FIGURE 2 | Asymmetric division of the *C. elegans* zygote. **(A)** DIC and fluorescence images of a one-cell embryo expressing PLK-1::sGFP (Martino et al., 2017) from polarity establishment through its asymmetric division. Note that, in addition to its localization to the nuclear envelope, centrosomes and chromosomes, there is a cytoplasmic pool that is enriched in the anterior cytoplasm relative to the posterior cytoplasm (indicated by white arrows). **(B)** Schematics of aPAR (blue), pPAR (yellow), PLK-1, MEX-5 and POS-1 localization during the asymmetric division of the zygote. The stages are as indicated in **(A)**. The left panels indicate the position of the maternal and paternal pro-nuclei (black circles), microtubules (black lines) and chromosomes (gray) in the mitotic spindle. **(C)** Model for the mechanism by which MEX-5 and PLK-1 regulate POS-1 segregation. MEX-5 and PLK-1 are retained in the anterior cytoplasm, likely through the association of MEX-5 with RNA. PLK-1 phosphorylates POS-1 to inhibit its retention in the anterior. As a consequence, POS-1 enriches in the posterior cytoplasm, presumably on RNA. This model predicts POS-1 dephosphorylation is required for its retention in the posterior.

phosphomimetic substitutions at these residues prevent both PAR-3 oligomerization and PAR-3 localization to the cell cortex (Dickinson et al., 2017). Taken together, these data suggest that relatively low levels of PLK-1 activity during interphase allows PAR-3 cluster formation and entrainment in actomyosin flows during polarity establishment. PLK-1 activity increases at the transition from establishment to maintenance phase, at which point PLK-1 phosphorylates PAR-3 to disperse aPAR clusters (**Figure 2B**). This dispersal makes PAR-3 insensitive to subsequent actomyosin flows during cytokinesis (Dickinson et al., 2017). In the future, it will be interesting to learn how PLK-1 activity toward PAR-3 is coordinated with the transition from polarity establishment to polarity maintenance. For example, the global increase in PLK-1 activity as the embryo enters mitosis could trigger PAR-3 cluster disassembly. Alternately, there may be unknown mechanisms that temporally control PLK-1 activity specifically toward PAR-3. Consistent with the latter possibility, PLK-1 acts prior to maintenance phase to drive the segregation of the cytoplasmic fate determinant POS-1, as discussed below (Han et al., 2018).

PLK-1 Controls Segregation of POS-1

A key output of the PAR polarity system is to control the segregation of cytoplasmic cell fate determinants along the A/P axis of the one-cell embryo, leading to the preferential partitioning of somatic factors to AB and germline factors to P1 (**Figure 2B**). The polarization of cytoplasmic proteins is not caused by local protein degradation or local protein synthesis, but rather by their preferential retention in either the anterior or posterior cytoplasm, which leads to their accumulation in that cytoplasmic domain (Tenlen et al., 2008; Daniels et al., 2009, 2010; Griffin et al., 2011; Wu et al., 2015, 2018). The posterior kinase PAR-1 inhibits the retention of its substrate the RNA-binding protein MEX-5 in the posterior cytoplasm, leading to MEX-5 segregation to the anterior cytoplasm (Pagano et al., 2007; Tenlen et al., 2008; Griffin et al., 2011). In turn, MEX-5, along with the highly similar protein MEX-6 (MEX-5/6 hereafter), controls the segregation of germline factors to the posterior cytoplasm by inhibiting their retention in the anterior (Schubert et al., 2000) (**Figure 2B**). For example, MEX-5/6 inhibit the retention of the RNA-binding protein POS-1 in the anterior, leading to the progressive accumulation of POS-1 in the posterior (Farley et al., 2008; Wu et al., 2015; Han et al., 2018). Both the retention of MEX-5 (and presumably MEX-6) in the anterior and the retention of POS-1 in the posterior depends on their ability to bind RNA (Griffin et al., 2011; Han et al., 2018), suggesting they may accumulate on RNA in the anterior and posterior cytoplasm, respectively (**Figure 2C**).

The ability of MEX-5/6 to drive POS-1 segregation to the posterior depends on PLK-1. The priming kinase MBK-2 phosphorylates MEX-5 and MEX-6 (on MEX-5 residue Thr186), generating a binding site for the PBD domain of PLK-1 (Nishi et al., 2008). MBK-2 becomes active upon the completion of meiosis, suggesting the interaction between MEX-5 and PLK-1 is likely coupled to this transition and to the onset of polarization (Stitzel et al., 2006, 2007; Maruyama et al., 2007; Cheng et al., 2009). As a consequence of its interaction with MEX-5/6, the cytoplasmic pool of PLK-1 becomes enriched in the anterior cytoplasm (Nishi et al., 2008) (**Figures 2A,B**). In addition, binding to MEX-5 increases PLK-1 kinase activity *in vitro*, likely by relieving PLK-1 autoinhibition by the PBD domain (Nishi et al., 2008). Similar to *mex-5/6* mutant embryos, POS-1 segregation fails in embryos in which PLK-1 has been depleted, in which PLK-1 kinase activity has been inhibited or in embryos in which the interaction between PLK-1 and MEX-5 has been disrupted through mutation of the priming phosphorylation site on MEX-5 (Thr186) (Han et al., 2018). *In vitro*, PLK-1 phosphorylates a cluster of residues in the POS-1 C-terminal region. *In vivo*, a non-phosphorylatable allele of POS-1 fails to segregate because it is inappropriately retained in the anterior cytoplasm. In contrast, a phosphomimetic allele of POS-1 fails to segregate because it is not retained in the posterior cytoplasm (Han et al., 2018). These data suggest MEX-5/PLK-1 complexes in the anterior cytoplasm phosphorylate POS-1 to inhibit its retention in the anterior (**Figure 2C**). Because RNA-binding is required for MEX-5 retention in the anterior and for POS-1 retention in the posterior, one possibility is that MEX-5 recruits PLK-1 to RNA in the anterior where it is positioned to inhibit POS-1 retention on RNA. In contrast to PLK-1 regulation of PAR-3 disassembly, PLK-1 regulates POS-1 segregation throughout both polarity establishment and maintenance phases, suggesting that at least the cytoplasmic pool of PLK-1 is active during interphase.

POS-1 is one of a collection of germline RNA-binding proteins that segregate to the posterior cytoplasm in response to MEX-5/6 (Schubert et al., 2000). Many of these germline proteins concentrate in germ granules (called P granules in *C. elegans*) which are non-membranous, phase-separated condensates composed primarily of RNA and RNA-binding proteins (Updike and Strome, 2010; Seydoux, 2018). The relatively high concentration of MEX-5/6 in the anterior cytoplasm causes P granules to disassemble, whereas P granules assemble and grow in the posterior cytoplasm (Brangwynne et al., 2009). One mechanism that disassembles P granules in the anterior is the sequestration of RNA by MEX-5/6, which starves P granule proteins of the RNA they need to assemble in granules (Saha et al., 2016; Smith et al., 2016). Interestingly, there is genetic evidence that PLK-1 may also act with MEX-5/6 to stimulate P granule disassembly: both depletion of PLK-1 by RNAi and mutation of the PLK-1 binding site on MEX-5 results in the inappropriate stabilization of P granules in the anterior cytoplasm (Nishi et al., 2008; Wu et al., 2019). Whether PLK-1 plays a direct role in P granule disassembly, for example by inhibiting P granule assembly through direct phosphorylation of P granule protein(s), awaits further study.

PLK-1 ASYMMETRY CONTRIBUTES TO DIFFERENCES BETWEEN AB AND P1

In addition to the role of PLK-1 in regulating asymmetries before the division of the one cell embryo, the asymmetric inheritance of PLK-1 following cell division also contributes to differences in the timing of centrosome separation and cell division between AB and P1. The preferential inheritance of PLK-1 to AB derives from

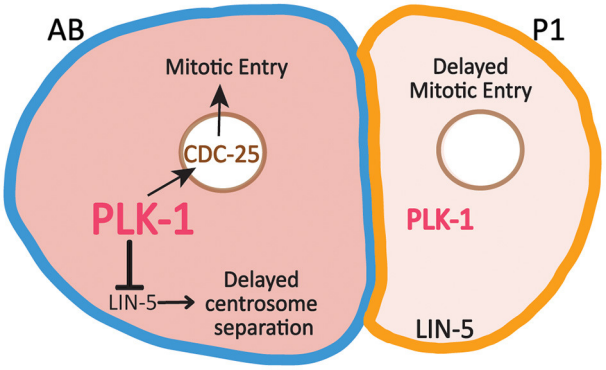

FIGURE 3 | Asymmetric inheritance of PLK-1 contributes to differences in the timing of cell division and centrosome separation between AB and P1. Relatively high levels of PLK-1 in AB promotes mitotic entry by increasing nuclear levels of CDC25, which contributes to the faster cell division timing in AB relative to P1. PLK-1 also acts to reduce cortical LIN-5 levels in AB, which delays centrosome separation in AB.

the interaction between PLK-1 and MEX-5 and the resultant enrichment of PLK-1 in the anterior cytoplasm before cell division (Nishi et al., 2008).

PLK-1 Regulation of Cell Division Asymmetry

As in many animal embryos, *C. elegans* development begins with a series of rapid, reductive cleavages that alternate between interphase and mitosis and lack G1 and G2 phases. Beginning at the two-cell stage, cells in the germline P lineage divide more slowly than their somatic sister cells. For example, P1 divides roughly 2 min after AB (Noatynska et al., 2013; Tavernier et al., 2015a) as a result of the combined effect of differences in the activities of several cell cycle regulators. Part of the cell division asynchrony is due to delayed DNA replication in P1 and the preferential activation of the ATL-1/CHK-1 DNA replication checkpoint in P1, which delays P1's entry into mitosis (Brauchle et al., 2003; Benkemoun et al., 2014). In addition, the preferential inheritance of both PLK-1 and cyclin B3 promotes the advanced timing of AB division (Budirahardja and Gönczy, 2008; Rivers et al., 2008; Michael, 2016). PLK-1 promotes mitotic entry in part through phosphorylation and activation of CDC25. Indeed, the enrichment of PLK-1 in AB correlates with higher levels of nuclear CDC25 in AB than in P1 (Rivers et al., 2008) (**Figure 3**). Partial depletion of either PLK-1 or CDC25 causes a more substantial delay in the division of P1 than the division of AB, consistent with the idea that the low levels of PLK-1 and CDC25 in P1 are limiting (Budirahardja and Gönczy, 2008; Rivers et al., 2008).

PLK-1 Regulation of Centrosome Separation in AB

In addition to promoting mitotic entry, the enrichment of PLK-1 in AB also delays centrosome separation in AB relative to P1 (**Figure 3**). LIN-5 (the *C. elegans* NUMA ortholog) is a dynein binding protein present in the cytoplasm and at the cell cortex. PLK-1 acts to reduce the cortical levels of LIN-5 in AB relative to P1 (Bondaz et al., 2019). LIN-5 promotes the separation of centrosomes by exerting force on centrosomes through astral microtubules that reach the cortex. As a result of the differences in cortical LIN-5 levels, centrosome separation is delayed in AB relative to P1. Embryos depleted of KLP-7 (the *C. elegans* MCAK ortholog) are particularly sensitive to the low levels of cortical LIN-5 in AB and therefore exhibit enhanced delay in the timing of centrosome in AB. This delay can be suppressed through depletion in PLK-1 which increases cortical LIN-5 levels in AB (Bondaz et al., 2019). In mammalian cells, PLK1 regulates cortical NUMA levels directly, suggesting PLK-1 may directly target LIN-5 in AB to reduce its cortical association (Kiyomitsu and Cheeseman, 2012; Sana et al., 2018).

CONCLUSION

In addition to its role in the asymmetric division of the *C. elegans* zygote, PLK1 also contributes to asymmetric division and cell polarization in other cell types. During the asymmetric division of *Drosophila* neuroblasts, the asymmetric localization of cortical cell fate determinants is regulated by Polo (the *C. elegans* ortholog of PLK-1). The membrane-associated proteins Pros, Numb, Miranda and Partner of Numb (Pon) are uniformly distributed during interphase. During late prophase, Polo directly phosphorylates Pon, leading to the asymmetric localization of PON and its binding partner Numb to the basal cortex (Wang et al., 2007). In *polo* mutants, Pon and Numb are not asymmetrically localized to basal cortex, causing a failure of asymmetric division that leads to neuroblast over-proliferation. Additionally, increased Polo activity at the daughter centrosomes relative to mother centrosomes is essential for the retention of the daughter centrosome in the neuroblast cell following cell division (Januschke et al., 2013; Conduit et al., 2014; Gallaud et al., 2020). The extent to which the resulting asymmetric inheritance of mother and daughter centrosomes regulates the fate of apical and basal daughter cells remains an open area of investigation. Similarly, during the asymmetric division of *S. cerevisiae* cells, increased Cdc5 activity at the mother centrosome (spindle pole body) is essential for its asymmetric inheritance to the newly born daughter cell (Maekawa et al., 2017). Non-random inheritance of mother and daughter centrosomes is widespread and may contribute to the partitioning of aging/rejuvenation programs between daughter cells or in the asymmetric inheritance of centrosome-associated fate determinants (Macara and Mili, 2008; Pelletier and Yamashita, 2012; Manzano-Lopez et al., 2019; Sunchu and Cabernard, 2020). PLK1 has also been shown to regulate planar cell polarity in mammalian epithelial cells through phosphorylation of CELSR-1 (Flamingo in *Drosophila*), which triggers CELSR-1 clearance from the cell surface as cells prepare to undergo cytokinesis (Shrestha et al., 2015). These studies, along with the numerous ways in which PLK-1 regulates the asymmetric division of the *C. elegans* zygote, raise the possibility that PLK1 may act broadly and in diverse ways to control both cell polarization and cell cycle progression. In the future, it will be interesting to learn in which contexts PLK1's role in cell polarization is coordinated with its role in cell cycle progression and in which contexts PLK1 acts independently in these two processes.

AUTHOR CONTRIBUTIONS

All authors listed have made a substantial, direct and intellectual contribution to the work, and approved it for publication.

FUNDING

This work was supported by NIH Grants Nos. R01GM110194 and R35GM136302 to EG.

REFERENCES

Archambault, V., and Glover, D. M. (2009). Polo-like kinases: conservation and divergence in their functions and regulation. *Nat. Rev. Mol. Cell Biol.* 10, 265–275. doi: 10.1038/nrm2653

Barr, F. A., Sillje, H. H., and Nigg, E. A. (2004). Polo-like kinases and the orchestration of cell division. *Nat. Rev. Mol. Cell Biol.* 5, 429–440. doi: 10.1038/nrm1401

Beers, M., and Kemphues, K. (2006). Depletion of the co-chaperone CDC-37 reveals two modes of PAR-6 cortical association in *C. elegans* embryos. *Development* 133, 3745–3754. doi: 10.1242/dev.02544

Benkemoun, L., Descoteaux, C., Chartier, N. T., Pintard, L., and Labbe, J.-C. (2014). PAR-4/LKB1 regulates DNA replication during asynchronous division of the early *C. elegans* embryo. *J. Cell Biol.* 205, 447–455. doi: 10.1083/jcb.201312029

Bondaz, A., Cirillo, L., Meraldi, P., and Gotta, M. (2019). Cell polarity-dependent centrosome separation in the *C. elegans* embryo. *J. Cell Biol.* 218, 4112–4126. doi: 10.1083/jcb.201902109

Brangwynne, C. P., Eckmann, C. R., Courson, D. S., Rybarska, A., Hoege, C., Gharakhani, J., et al. (2009). Germline P granules are liquid droplets that localize by controlled dissolution/condensation. *Science* 324, 1729–1732. doi: 10.1126/science.1172046

Brauchle, M., Baumer, K., and Gönczy, P. (2003). Differential activation of the DNA replication checkpoint contributes to asynchrony of cell division in *C. elegans* embryos. *Curr. Biol.* 13, 819–827. doi: 10.1016/S0960-9822(03)00295-1

Budirahardja, Y., and Gönczy, P. (2008). PLK-1 asymmetry contributes to asynchronous cell division of *C. elegans* embryos. *Development* 135, 1303–1313. doi: 10.1242/dev.019075

Chase, D., Serafinas, C., Ashcroft, N., Kosinski, M., Longo, D., Ferris, D. K., et al. (2000). The polo-like kinase PLK-1 is required for nuclear envelope breakdown and the completion of meiosis in *Caenorhabditis elegans*. *Genesis* 26, 26–41. doi: 10.1002/(SICI)1526-968X(200001)26:1<26::AID-GENE6>3.0.CO;2-O

Cheeks, R. J., Canman, J. C., Gabriel, W. N., Meyer, N., Strome, S., and Goldstein, B. (2004). *C. elegans* PAR proteins function by mobilizing and stabilizing asymmetrically localized protein complexes. *Curr. Biol.* 14, 851–862. doi: 10.1016/j.cub.2004.05.022

Cheng, K. C.-C., Klancer, R., Singson, A., and Seydoux, G. (2009). Regulation of MBK-2/DYRK by CDK-1 and the pseudophosphatases EGG-4 and EGG-5 during the oocyte-to-embryo transition. *Cell* 139, 560–572. doi: 10.1016/j.cell.2009.08.047

Conduit, P. T., Feng, Z., Richens, J. H., Baumbach, J., Wainman, A., Bakshi, S. D., et al. (2014). The centrosome-specific phosphorylation of Cnn by Polo/Plk1 drives Cnn scaffold assembly and centrosome maturation. *Dev. Cell* 28, 659–669. doi: 10.1016/j.devcel.2014.02.013

Daniels, B. R., Dobrowsky, T. M., Perkins, E. M., Sun, S. X., and Wirtz, D. (2010). MEX-5 enrichment in the *C. elegans* early embryo mediated by differential diffusion. *Development* 137, 2579–2585. doi: 10.1242/dev.051326

Daniels, B. R., Perkins, E. M., Dobrowsky, T. M., Sun, S. X., and Wirtz, D. (2009). Asymmetric enrichment of PIE-1 in the *Caenorhabditis elegans* zygote mediated by binary counterdiffusion. *J. Cell Biol.* 184, 473–479. doi: 10.1083/jcb.200809077

De Henau, S., Pages-Gallego, M., Pannekoek, W. J., and Dansen, T. B. (2020). Mitochondria-derived H_2O_2 promotes symmetry breaking of the *C. elegans* zygote. *Dev. Cell* 53, 263–271. doi: 10.1016/j.devcel.2020.03.008

Dickinson, D. J., Schwager, F., Pintard, L., Gotta, M., and Goldstein, B. (2017). A single-cell biochemistry approach reveals PAR complex dynamics during cell polarization. *Dev. Cell.* 42, 416–434. doi: 10.1016/j.devcel.2017.07.024

Elia, A. E., Rellos, P., Haire, L. F., Chao, J. W., Ivins, F. J., Hoepker, K., et al. (2003). The molecular basis for phosphodependent substrate targeting and regulation of Plks by the Polo-box domain. *Cell* 115, 83–95. doi: 10.1016/S0092-8674(03)00725-6

Farley, B. M., Pagano, J. M., and Ryder, S. P. (2008). RNA target specificity of the embryonic cell fate determinant POS-1. *RNA* 14, 2685–2697. doi: 10.1261/rna.1256708

Gallaud, E., Ramdas Nair, A., Horsley, N., Monnard, A., Singh, P., Pham, T. T., et al. (2020). Dynamic centriolar localization of Polo and Centrobin in early mitosis primes centrosome asymmetry. *PLoS Biol.* 18:e3000762. doi: 10.1371/journal.pbio.3000762

Goehring, N. W., Trong, P. K., Bois, J. S., Chowdhury, D., Nicola, E. M., Hyman, A. A., et al. (2011). Polarization of PAR proteins by advective triggering of a pattern-forming system. *Science* 334, 1137–1141. doi: 10.1126/science.1208619

Goldstein, B., and Hird, S. N. (1996). Specification of the anteroposterior axis in *Caenorhabditis elegans*. *Development* 122, 1467–1474.

Griffin, E. E. (2015). Cytoplasmic localization and asymmetric division in the early embryo of *Caenorhabditis elegans*. Wiley Interdiscip. *Rev. Dev. Biol.* 4, 267–282. doi: 10.1002/wdev.177

Griffin, E. E., Odde, D. J., and Seydoux, G. (2011). Regulation of the MEX-5 gradient by a spatially segregated kinase/phosphatase cycle. *Cell* 146, 955–968. doi: 10.1016/j.cell.2011.08.012

Gubieda, A. G., Packer, J. R., Squires, I., Martin, J., and Rodriguez, J. (2020). Going with the flow: insights from *Caenorhabditis elegans* zygote polarization. *Philos. Trans. R. Soc. Lond. B. Biol. Sci.* 375:20190555. doi: 10.1098/rstb.2019.0555

Han, B., Antkowiak, K. R., Fan, X., Rutigliano, M., Ryder, S. P., and Griffin, E. E. (2018). Polo-like kinase couples cytoplasmic protein gradients in the *C. elegans* zygote. *Curr Biol.* 28, 60–69. doi: 10.1016/j.cub.2017.11.048

Hung, T. J., and Kemphues, K. J. (1999). PAR-6 is a conserved PDZ domain-containing protein that colocalizes with PAR-3 in *Caenorhabditis elegans* embryos. *Development* 126, 127–135.

Jang, Y. J., Ma, S., Terada, Y., and Erikson, R. L. (2002). Phosphorylation of threonine 210 and the role of serine 137 in the regulation of mammalian polo-like kinase. *J. Biol. Chem.* 277, 44115–44120. doi: 10.1074/jbc.M202172200

Januschke, J., Reina, J., Llamazares, S., Bertran, T., Rossi, F., Roig, J., et al. (2013). Centrobin controls mother-daughter centriole asymmetry in *Drosophila* neuroblasts. *Nat. Cell Biol.* 15, 241–248. doi: 10.1038/ncb2671

Kapoor, S., and Kotak, S. (2019). Centrosome Aurora A regulates RhoGEF ECT-2 localisation and ensures a single PAR-2 polarity axis in *C. elegans* embryos. *Development* 146:dev174565. doi: 10.1242/dev.174565

Kiyomitsu, T., and Cheeseman, I. M. (2012). Chromosome- and spindle-pole-derived signals generate an intrinsic code for spindle position and orientation. *Nat. Cell Biol.* 14, 311–317. doi: 10.1038/ncb2440

Klinkert, K., Levernier, N., Gross, P., Gentili, C., von Tobel, L., Pierron, M., et al. (2019). Aurora A depletion reveals centrosome-independent polarization mechanism in *Caenorhabditis elegans*. *Elife* 8:e44552. doi: 10.7554/eLife.44552

Knoblich, J. A. (2010). Asymmetric cell division: recent developments and their implications for tumour biology. *Nat. Rev. Mol. Cell Biol.* 11, 849–860. doi: 10.1038/nrm3010

Kysela, D. T., P.,Brown, J. B., Huang, K. C., and Brun, Y. V. (2013). Biological consequences and advantages of asymmetric bacterial *Growth* 67, 417–435. doi: 10.1146/annurev-micro-092412-155622

Lang, C. F., and Munro, E. (2017). The PAR proteins: from molecular circuits to dynamic self-stabilizing cell polarity. *Development* 144, 3405–3416. doi: 10.1242/dev.139063

Lee, K. S., Grenfell, T. Z., Yarm, F. R., and Erikson, R. L. (1998). Mutation of the polo-box disrupts localization and mitotic functions of the mammalian polo kinase Plk. *Proc. Natl. Acad. Sci. U.S.A.* 95, 9301–9306. doi: 10.1073/pnas.95.16.9301

Li, R. (2013). The art of choreographing asymmetric cell division. *Dev. Cell.* 25, 439–450. doi: 10.1016/j.devcel.2013.05.003

Lowery, D. M., Lim, D., and Yaffe, M. B. (2005). Structure and function of Polo-like kinases. *Oncogene* 24, 248–259. doi: 10.1038/sj.onc.1208280

Macara, I., and Mili, S. (2008). Polarity and differential inheritance—universal attributes of life? *Cell* 135, 801–812. doi: 10.1016/j.cell.2008.11.006

Macurek, L., Lindqvist, A., Lim, D., Lampson, M. A., Klompmaker, R., Freire, R., et al. (2008). Polo-like kinase-1 is activated by aurora A to promote checkpoint recovery. *Nature* 455, 119–123. doi: 10.1038/nature07185

Maekawa, H., Neuner, A., Ruthnick, D., Schiebel, E., Pereira, G., and Kaneko, Y. (2017). Polo-like kinase Cdc5 regulates Spc72 recruitment to spindle pole body in the methylotrophic yeast *Ogataea polymorpha*. *Elife* 6:e24340. doi: 10.7554/eLife.24340

Manzano-Lopez, J., Matellan, L., Alvarez-Llamas, A., Blanco-Mira, J. C., and Monje-Casas, F. (2019). Asymmetric inheritance of spindle microtubue-organizing centers preserves replicative *lifespan* 21, 952–965. doi: 10.1038/s41556-019-0364-8

Martino, L., Morchoisne-Bolhy, S., Cheerambathur, D. K., Van Hove, L., Dumont, J., Joly, N., et al. (2017). Channel nucleoporins recruit PLK-1 to nuclear pore complexes to direct nuclear envelope breakdown in *C. elegans*. *Dev. Cell*. 43, 157–171. doi: 10.1016/j.devcel.2017.09.019

Maruyama, R., Velarde, N. V., Klancer, R., Gordon, S., Kadandale, P., Parry, J. M., et al. (2007). EGG-3 regulates cell-surface and cortex rearrangements during egg activation in *Caenorhabditis elegans*. *Curr. Biol*. 17, 1555–1560. doi: 10.1016/j.cub.2007.08.011

Michael, W. M. (2016). Cyclin CYB-3 controls both S-phase and mitosis and is asymmetrically distributed in the early *C. elegans embryo*. *Development*. 143, 3119–3127. doi: 10.1242/dev.141226

Motegi, F., Zonies, S., Hao, Y., Cuenca, A. A., Griffin, E., and Seydoux, G. (2011). Microtubules induce self-organization of polarized PAR domains in *Caenorhabditis elegans* zygotes. *Nat. Cell Biol*. 13, 1361–1367. doi: 10.1038/ncb2354

Munro, E., Nance, J., and Priess, J. R. (2004). Cortical flows powered by asymmetrical contraction transport PAR proteins to establish and maintain anterior-posterior polarity in the early *C. elegans* embryo. *Dev. Cell*. 7, 413–424. doi: 10.1016/j.devcel.2004.08.001

Nishi, Y., Rogers, E., Robertson, S. M., and Lin, R. (2008). Polo kinases regulate *C. elegans* embryonic polarity via binding to DYRK2-primed MEX-5 and MEX-6. *Development* 135, 687–697. doi: 10.1242/dev.013425

Noatynska, A., Panbianco, C., and Gotta, M. (2010). SPAT-1/Bora acts with Polo-like kinase 1 to regulate PAR polarity and cell cycle progression. *Development* 137, 3315–3325. doi: 10.1242/dev.055293

Noatynska, A., Tavernier, N., Gotta, M., and Pintard, L. (2013). Coordinating cell polarity and cell cycle progression: what can we learn from flies and worms? *Open Biol*. 3:130083. doi: 10.1098/rsob.130083

Pagano, J. M., Farley, B. M., Mccoig, L. M., and Ryder, S. P. (2007). Molecular basis of RNA recognition by the embryonic polarity determinant MEX-5. *J. Biol. Chem*. 282, 8883–8894. doi: 10.1074/jbc.M700079200

Pelletier, L., and Yamashita, Y. M. (2012). Centrosome asymmetry and inheritance during animal development. *Curr Opin Cell BioI*. 24, 541–546. doi: 10.1016/j.ceb.2012.05.005

Petronczki, M., Lenart, P., and Peters, J. M. (2008). Polo on the rise-from mitotic entry to cytokinesis with Plk1. *Dev. Cell*. 14, 646–659. doi: 10.1016/j.devcel.2008.04.014

Pintard, L., and Archambault, V. (2018). A unified view of spatio-temporal control of mitotic entry: polo kinase as the key. *Open Biol*. 8:180114. doi: 10.1098/rsob.180114

Rahman, M., Chang, I. Y., Harned, A., Maheshwari, R., Amoateng, K., Narayan, K., and Cohen-Fix, O. (2020). *C. elegans* pronuclei fuse after fertilization through a novel membrane structure. *J. Cell Biol*. 219:e201909137. doi: 10.1083/jcb.201909137

Rahman, M. M., Munzig, M., Kaneshiro, K., Lee, B., Strome, S., Muller-Reichert, T., and Cohen-Fix, O. (2015). *Caenorhabditis elegans* polo-like kinase PLK-1 is required for merging parental genomes into a single nucleus. *Mol. Biol. Cell*. 26, 4718–4735. doi: 10.1091/mbc.E15-04-0244

Reich, J. D., Hubatsch, L., Illukkumbura, R., Peglion, F., Bland, T., Hirani, N., et al. (2019). Regulated activation of the PAR polarity network ensures a timely and specific response to spatial cues. *Curr. Biol*. 29, 1911–1923. doi: 10.1016/j.cub.2019.04.058

Rivers, D. M., Moreno, S., Abraham, M., and Ahringer, J. (2008). PAR proteins direct asymmetry of the cell cycle regulators Polo-like kinase and Cdc25. *J. Cell Biol*. 180, 877–885. doi: 10.1083/jcb.200710018

Rodriguez, J., Peglion, F., Martin, J., Hubatsch, L., Reich, J., Hirani, N., et al. (2017). aPKC cycles between functionally distinct PAR protein assemblies to drive cell polarity. *Dev. Cell*. 42, 400–415. doi: 10.1016/j.devcel.2017.07.007

Rose, L., and Gonczy, P. (2014). "Polarity establishment, asymmetric division and segregation of fate determinants in early *C. elegans* embryos," in *WormBook*, ed The *C. elegans* Research Community (WormBook). Avalable online at: http://www.wormbook.org (accessed December 30, 2014)

Saha, S., Weber, C. A., Nousch, M., Adame-Arana, O., Hoege, C., Hein, M. Y., et al. (2016). Polar positioning of phase-separated liquid compartments in cells regulated by an mRNA competition mechanism. *Cell* 166, 1572–1584. doi: 10.1016/j.cell.2016.08.006

Sailer, A., Anneken, A., Li, Y., Lee, S., and Munro, E. (2015). Dynamic opposition of clustered proteins stabilizes cortical polarity in the *C. elegans* zygote. *Dev. Cell*. 35, 131–142. doi: 10.1016/j.devcel.2015.09.006

Sana, S., Keshri, R., Rajeevan, A., Kappor, S., and Kotak, S. (2018). PLK1 regulates spindle orientation by phosphorylating NuMA in human cells. *Life Sci. Alliance*. 1:e201800223. doi: 10.26508/lsa.201800223

Schubert, C. M., Lin, R., de Vries, C. J., Plasterk, R. H., and Priess, J. R. (2000). MEX-5 and MEX-6 function to establish soma/germline asymmetry in early *C. elegans* embryos. *Mol Cell*. 5, 671–682. doi: 10.1016/S1097-2765(00)80246-4

Seki, A., Coppinger, J. A., Jang, C. Y., Yates, J. R., and Fang, G. (2008). Bora and the kinase Aurora a cooperatively activate the kinase Plk1 and control mitotic entry. *Science* 320, 1655–1658. doi: 10.1126/science.1157425

Seydoux, G. (2018). The P Granules of *C. elegans*: a genetic model for the study of RNA-protein condensates. *J. Mol. Biol*. 430, 4702–4710. doi: 10.1016/j.jmb.2018.08.007

Shrestha, R., Little, K. A., Tamayo, J. V., Li, W., Perlman, D. H., and Devenport, D. (2015). Mitotic control of planar cell polarity by Polo-like kinase 1. *Dev. Cell*. 33, 522–534. doi: 10.1016/j.devcel.2015.03.024

Smith, J., Calidas, D., Schmidt, H., Lu, T., Rasoloson, D., and Seydoux, G. (2016). Spatial patterning of P granules by RNA-induced phase separation of the intrinsically-disordered protein MEG-3. *Elife* 5:e21337. doi: 10.7554/eLife.21337

Stitzel, M. L., K. C.-,Cheng, C., and Seydoux, G. (2007). Regulation of MBK-2/Dyrk kinase by dynamic cortical anchoring during the oocyte-to-zygote transition. *Curr. Biol*. 17, 1545–1554. doi: 10.1016/j.cub.2007.08.049

Stitzel, M. L., Pellettieri, J., and Seydoux, G. (2006). The *C. elegans* DYRK kinase MBK-2 marks oocyte proteins for degradation in response to meiotic maturation. *Curr. Biol*. 16, 56–62. doi: 10.1016/j.cub.2005.11.063

Strebhardt, K., and Ullrich, A. (2006). Targeting polo-like kinase 1 for cancer therapy. *Nat. Rev. Cancer*. 6:321–330. doi: 10.1038/nrc1841

Sunchu, B., and Cabernard, C. (2020). Principles and mechanisms of asymmetric cell division. *Development* 147:dev167650. doi: 10.1242/dev.167650

Sunkel, C. E., and Glover, D. M. (1988). Polo, a mitotic mutant of Drosophila displaying abnormal spindle poles. *J. Cell Sci*. 89, 25–38.

Tabuse, Y., Izumi, Y., Piano, F., Kemphues, K. J., Miwa, J., and Ohno, S. (1998). Atypical protein kinase C cooperates with PAR-3 to establish embryonic polarity in *Caenorhabditis elegans*. *Development* 125, 3607–3614.

Tavernier, N., Labbe, J. C., and Pintard, L. (2015a). Cell cycle timing regulation during asynchronous divisions of the early *C. elegans* embryo. *Exp. Cell Res*. 337, 243–248. doi: 10.1016/j.yexcr.2015.07.022

Tavernier, N., Noatynska, A., Panbianco, C., Martino, L., Van Hove, L., Schwager, F., et al. (2015b). Cdk1 phosphorylates SPAT-1/Bora to trigger PLK-1 activation and drive mitotic entry in *C. elegans* embryos. *J. Cell Biol*. 208, 661–669. doi: 10.1083/jcb.201408064

Tenlen, J. R., Molk, J. N., London, N., Page, B. D., and Priess, J. R. (2008). MEX-5 asymmetry in one-cell *C. elegans* embryos requires PAR-4- and PAR-1-dependent phosphorylation. *Development* 135, 3665–3675. doi: 10.1242/dev.027060

Tsai, M. C., and Ahringer, J. (2007). Microtubules are involved in anterior-posterior axis formation in *C. elegans* embryos. *J. Cell Biol*. 179, 397–402. doi: 10.1083/jcb.200708101

Updike, D., and Strome, S. (2010). P granule assembly and function in *Caenorhabditis elegans* germ cells. *J. Androl*. 31, 53–60. doi: 10.2164/jandrol.109.008292

Velez-Aguilera, G., Nkombo Nkoula, S., Ossareh-Nazari, B., Link, J., Paouneskou, D., Van Hove, L., et al. (2020). PLK-1 promotes the merger of the parental

genome into a single nucleus by triggering lamina disassembly. *Elife* 9:e59510. doi: 10.7554/eLife.59510

Venkei, Z. G., and Yamashita, Y. M. (2018). Emerging mechanisms of asymmetric stem cell division. *J. Cell Biol.* 217, 3785–3795. doi: 10.1083/jcb.201807037

Wallenfang, M. R., and Seydoux, G. (2000). Polarization of the anterior-posterior axis of *C. elegans* is a microtubule-directed process. *Nature* 408, 89–92. doi: 10.1038/35040562

Wang, H., Ouyang, Y., Somers, W. G., Chia, W., and Lu, B. (2007). Polo inhibits progenitor self-renewal and regulates Numb asymmetry by phosphorylating Pon. *Nature* 449, 96–100. doi: 10.1038/nature06056

Wang, S. C., T., Low, Y. F., Nishimura, Y., Gole, L., Yu, W., et al. (2017). Cortical forces and CDC-42 control clustering of PAR proteins for *Caenorhabditis elegans* embryonic polarization. *Nat. Cell Biol.* 19, 988–995. doi: 10.1038/ncb3577

Woodruff, J. B., Wueseke, O., Viscardi, V., Mahamid, J., Ochoa, S. D., Bunkenborg, J., et al. (2015). Centrosomes. Regulated assembly of a supramolecular centrosome scaffold *in vitro*. *Science* 348, 808–812. doi: 10.1126/science.aaa3923

Wu, Y., Han, B., Gauvin, T. J., Smith, J., Singh, A., and Griffin, E. E. (2019). Single-molecule dynamics of the P granule scaffold MEG-3 in the *Caenorhabditis elegans* zygote. *Mol. Biol. Cell.* 30, 333–345. doi: 10.1091/mbc.E18-06-0402

Wu, Y., Han, B., Li, Y., Munro, E., Odde, D. J., and Griffin, E. E. (2018). Rapid diffusion-state switching underlies stable cytoplasmic gradients in the *Caenorhabditis elegans* zygote. *Proc. Natl. Acad. Sci. U.S.A.* 115, E8440–E8449. doi: 10.1073/pnas.1722162115

Wu, Y., Zhang, H., and Griffin, E. E. (2015). Coupling between cytoplasmic concentration gradients through local control of protein mobility in the *Caenorhabditis elegans* zygote. *Mol. Biol. Cell.* 26, 2963–2970. doi: 10.1091/mbc.E15-05-0302

Zhao, P., Teng, X., Tantirimudalige, S. N., Nishikawa, M., Wohland, T., Toyama, Y., et al. (2019). Aurora-A breaks symmetry in contractile actomyosin networks independently of its role in centrosome maturation. *Dev. Cell.* 48, 631–645 e636. doi: 10.1016/j.devcel.2019.02.012

Zitouni, S., Nabais, C., Jana, S. C., Guerrero, A., and Bettencourt-Dias, M. (2014). Polo-like kinases: structural variations lead to multiple functions. *Nat. Rev. Mol. Cell Biol.* 15, 433–452. doi: 10.1038/nrm3819

Conflict of Interest: The authors declare that the research was conducted in the absence of any commercial or financial relationships that could be construed as a potential conflict of interest.

frontiers in Cell and Developmental Biology

BRIEF RESEARCH REPORT
published: 28 January 2021
doi: 10.3389/fcell.2020.625717

Haspin Modulates the G2/M Transition Delay in Response to Polarization Failures in Budding Yeast

*Martina Galli†‡, Laura Diani†, Roberto Quadri†, Alessandro Nespoli, Elena Galati, Davide Panigada, Paolo Plevani and Marco Muzi-Falconi**

Dipartimento di Bioscienze, Università degli Studi di Milano, Milano, Italy

OPEN ACCESS

Edited by:
Benjamin Lin,
New York University, United States

Reviewed by:
Duncan Clarke,
University of Minnesota Twin Cities, United States
Yanchang Wang,
Florida State University, United States

***Correspondence:**
Marco Muzi-Falconi
marco.muzifalconi@unimi.it

†These authors have contributed equally to this work

‡Present address:
Martina Galli,
Istituto FIRC di Oncologia Molecolare, Milano, Italy

Specialty section:
This article was submitted to Signaling, a section of the journal Frontiers in Cell and Developmental Biology

Received: *03 November 2020*
Accepted: *28 December 2020*
Published: *28 January 2021*

Citation:
Galli M, Diani L, Quadri R, Nespoli A, Galati E, Panigada D, Plevani P and Muzi-Falconi M (2021) Haspin Modulates the G2/M Transition Delay in Response to Polarization Failures in Budding Yeast. Front. Cell Dev. Biol. 8:625717. doi: 10.3389/fcell.2020.625717

Symmetry breaking by cellular polarization is an exquisite requirement for the cell-cycle of *Saccharomyces cerevisiae* cells, as it allows bud emergence and growth. This process is based on the formation of polarity clusters at the incipient bud site, first, and the bud tip later in the cell-cycle, that overall promote bud emission and growth. Given the extreme relevance of this process, a surveillance mechanism, known as the morphogenesis checkpoint, has evolved to coordinate the formation of the bud and cell cycle progression, delaying mitosis in the presence of morphogenetic problems. The atypical protein kinase haspin is responsible for histone H3-T3 phosphorylation and, in yeast, for resolution of polarity clusters in mitosis. Here, we report a novel role for haspin in the regulation of the morphogenesis checkpoint in response to polarity insults. Particularly, we show that cells lacking the haspin ortholog Alk1 fail to achieve sustained checkpoint activation and enter mitosis even in the absence of a bud. In *alk1*Δ cells, we report a reduced phosphorylation of Cdc28-Y19, which stems from a premature activation of the Mih1 phosphatase. Overall, the data presented in this work define yeast haspin as a novel regulator of the morphogenesis checkpoint in *Saccharomyces cerevisiae,* where it monitors polarity establishment and it couples bud emergence to the G2/M cell cycle transition.

Keywords: polarization, mitosis, actin cytoskeleton, cell cycle, *Saccharomyces cerevisiae*, morphogenesis checkpoint

INTRODUCTION

The yeast *Saccharomyces cerevisiae* reproduces through a budding process in which the daughter cell growth is promoted prior to anaphase, thus defining the orientation of the future mitotic spindle. This process starts in G1, when a cluster of proteins collectively known as the polarisome is built up at the presumptive bud site to drive symmetry breaking from an otherwise round cell. A major player in this polarization step is the small GTPase Cdc42, which oversees every step of the polarization process ranging from actin organization, to septin deposition and vesicle delivery (Etienne-Manneville, 2004). Cdc42 is regulated by an intricate mechanism to timely promote polarity onset and bud emergence and later in the cell-cycle polarity dispersion and cytokinesis. The main determinants of Cdc42 activation are the essential GEF Cdc24, whose

differential localization directs when and where polarity clusters are established (Zheng et al., 1994; Caviston et al., 2002), and its GDI (Rdi1) and GAPs (Rga1, Rga2, Bem2, and Bem3) (Pierce and Clark, 1981; Marquitz et al., 2002; Smith et al., 2002; Tiedje et al., 2008). In particular, localized recruitment and activity of Cdc24 is essential to promote symmetry breaking and the consequent bud emergence. Given the absolute requirement for a bud to the cell-cycle of budding yeast, it is not surprising that a surveillance mechanism, known as the morphogenesis checkpoint exists to delay mitotic progression in presence of polarization insults that impair bud emergence and growth (Lew and Reed, 1995a; McMillan et al., 1998). This pathway acts through an inhibitory phosphorylation of Cdc28 on Y19, which is catalyzed by the kinase Swe1 (Gould and Nurse, 1989; Harvey et al., 2005) (Wee1 in higher eukaryotes) and reverted by the phosphatase Mih1 (Russell and Nurse, 1986, 1987; Dunphy and Kumagai, 1991; Gautier et al., 1991) (Cdc25). In case of altered polarization, and thus impaired budding, the morphogenesis checkpoint provides the cells the chance to achieve an efficient polarity establishment and bud emergence before entering mitosis. Once a proper cellular morphogenesis is restored, Swe1 is degraded and Mih1 removes Cdc28-Y19 phosphorylation allowing completion of the cell cycle (Sia, 1998; McMillan et al., 2002; Kellogg, 2003; Asano et al., 2005; McNulty and Lew, 2005; Raspelli et al., 2011; Anastasia et al., 2012; King et al., 2013). In contrast with this wt scenario, mutants defective for the morphogenesis checkpoint undergo mitosis even in the presence of non-polarized, unbudded cells; resulting in nuclear division within a single cell compartment (Russell et al., 1989; Booher et al., 1993; Lew and Reed, 1995a; Sia et al., 1996; McMillan et al., 1998; Harvey and Kellogg, 2003; Keaton and Lew, 2006). Most works have focused on the ability of the morphogenesis checkpoint to inhibit mitotic entry. However, activation of this process was also found to cause delays later during mitosis, primarily in metaphase, through inhibition of APC/C activity (Barral et al., 1999; Sreenivasan and Kellogg, 1999; Theesfeld et al., 1999; Carroll et al., 2005; Chiroli et al., 2007; Lianga et al., 2013). A further complication comes from evidence in budding yeast showing that the deletion of *MIH1* induces only mild delays in mitotic entry and anaphase onset, suggesting the possible contribution of other phosphatases (Russell et al., 1989; Rudner et al., 2000; Pal et al., 2008; Lianga et al., 2013). This hypothesis was confirmed by the discovery that Mih1, Ptp1, and $PP2A^{Rts1}$ act redundantly to regulate the spatial and temporal reactivation of Cdc28, collaborating to its stepwise triggering prior to anaphase onset (Kennedy et al., 2016). Swe1 and Mih1 are temporally and spatially modulated by various factors. The regulatory circuits monitoring their activity involve Hsl1, Hsl7, Cla4, and Cdc5, which promote Swe1 phosphorylation at the septin ring (Barral et al., 1999; Longtine et al., 2000; Crutchley et al., 2009). Hyper-phosphorylated Swe1 is ubiquitinated by the Met30/SCF complex, which targets it for Cdc34-dependent proteolysis (Kaiser et al., 1998). Mih1, on the other hand, undergoes dramatic changes in phosphorylation throughout the cell cycle in a Cdc28 and casein kinase 1-dependent manner (Pal et al., 2008). Though the contribution of Mih1 phosphorylation to its activity is still debated, there are reports showing that during the G2/M transition Mih1 is dephosphorylated and activated by Cdc55-dependent PP2A phosphatase (Carroll et al., 2005; Wicky et al., 2011).

Haspin is an atypical serine/threonine atypical kinase that phosphorylates H3-T3 during metaphase, promoting the recruitment of the chromosomal passenger complex (CPC) at kinetochores (Tanaka et al., 1999; Higgins, 2001a,b; Kelly et al., 2010; Wang et al., 2010). Accordingly, depletion of haspin in mammalian cells prevents proper chromosome positioning at the metaphase plate, eventually blocking cell-cycle progression in mitosis (Dai and Higgins, 2005; Dai et al., 2005, 2006; Yamagishi et al., 2010). Haspin activity is cell-cycle dependent, with the protein being held in an inactive state during interphase through folding of an autoinhibitory domain onto the catalytic one (Kelly et al., 2010). This autoinhibition is relieved during mitosis by Cyclin-dependent kinase 1 (CDK1)-mediated phosphorylation at haspin N-terminus, followed by further phosphorylations at multiple sites by the Polo-like kinase 1 (Plk1). These Plk1-dependent modifications trigger haspin activity, resulting in phosphorylation of H3-T3 (Ghenoiu et al., 2013; Zhou et al., 2014). The genome of *Saccharomyces cerevisiae* encodes for two haspin paralogues, Alk1 and Alk2 (Nespoli et al., 2006), whose levels peak in mitosis and G2-phase, respectively, and that are phosphorylated during the cell cycle (Spellman et al., 1998; Nespoli et al., 2006). We previously reported that Alk1 and Alk2 are critical to efficiently disperse polarity clusters in mitosis (Quadri et al., 2020a), preventing cell death in case of transient mitotic delays (Panigada et al., 2013). In agreement with Alk1 and Alk2 being, at least partly, redundant, these phenotypes have been observed in double deleted strains, with single mutants behaving as their wt counterparts.

Here we report that budding yeast haspin homolog Alk1 exerts an independent function, playing a critical role in the regulation of the G2/M transition in response to morphogenetic stress. Cells deleted for *ALK1* are indeed defective in the morphogenesis checkpoint and are characterized by a premature Cdc28-Y19 dephosphorylation. Intriguingly, the phenotypes of *alk1*Δ mutants are suppressed by concomitant deletion of *ALK2*. Accordingly, we show evidence for a precocious and higher inhibition of Cdc28 in *alk2*Δ strains, supporting a role for Alk2 in quenching of the morphogenesis checkpoint.

RESULTS

Haspin Regulates Cell-Cycle Progression Upon Defective Polarization

The atypical protein kinase haspin has been shown to be involved in the promotion of a proper alignment of the chromosomes on the metaphase plate (Dai and Higgins, 2005; Dai et al., 2005; Kelly et al., 2010; Wang et al., 2010, 2011; Yamagishi et al., 2010) and in cell polarity (Panigada et al., 2013; Quadri et al., 2020a,b). To expand our comprehension of haspin and identify other possible functions, we tested the sensitivity of haspin-lacking cells to a set of non-genotoxic compounds. Interestingly, we found that the deletion of *ALK1*, but not of *ALK2,* suppressed the sensitivity of yeast cells to the actin depolymerizing drug LatA (**Figure 1A**).

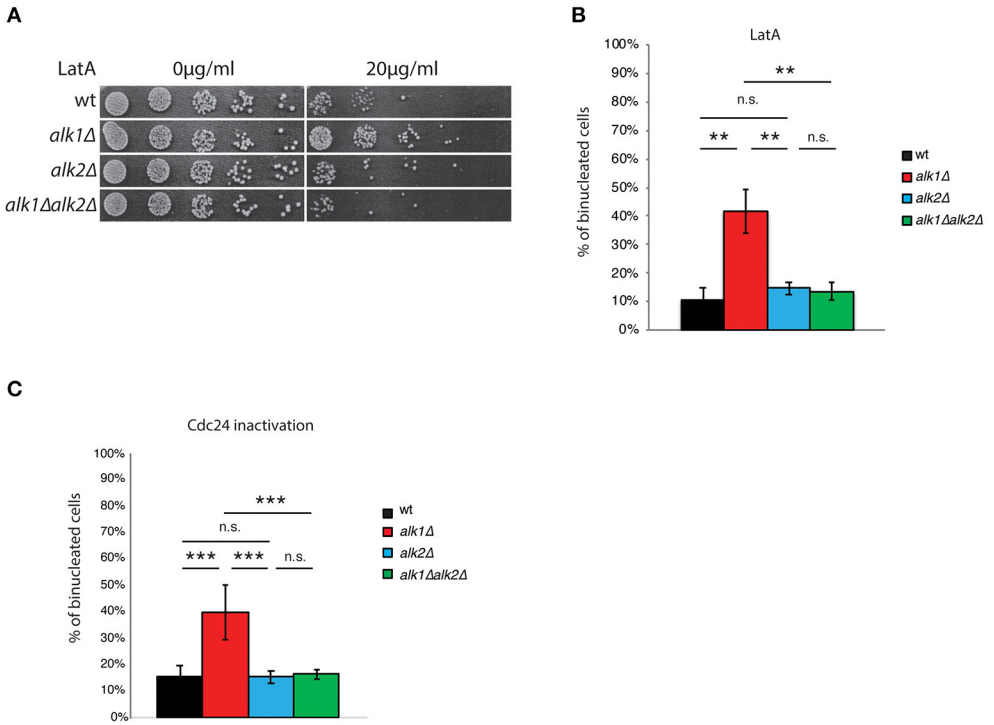

FIGURE 1 | Haspin mutants show altered response to polarity failures. **(A)** Serial dilutions of cultures of the indicated strains were spotted on either DMSO or LatA containing plates. After 24 h incubation at 28°C plates were imaged. **(B)** Cells of the indicated strains expressing Tub1-GFP were arrested in G1 with mating pheromone and then released in the presence of 100 µM LatA. After 4 h cells were fixed and analyzed for nuclear division by fluorescence microscopy. **(C)** Cells were arrested in G1 at the permissive temperature (25°C), shifted for 45' at the restrictive temperature (37°C) and then released at 37°C. After 2 h, samples were fixed and analyzed for nuclear division, as above. Error bars in **(B,C)** represent standard deviation, statistical significance was measured by *T*-test, ns: not significant, $^{**}p < 0.01$, $^{***}p < 0.005$.

Such suppression required the activity of Alk2, indeed the concomitant deletion of *ALK2* restored the LatA sensitivity of *alk1*Δ mutants to that of control strains (**Figure 1A**).

LatrunculinA is a powerful natural toxin that, by binding actin monomers, prevents their polymerization (Spector et al., 1983; Ayscough et al., 1997). In budding yeast, a deficient organization of the actin cytoskeleton impairs, among other processes bud emission. Cells thus arrest of cell-cycle progression as single cells with and undivided nucleus through activation of the morphogenesis checkpoint (Lew, 2003). To better characterize the influence of *ALK1* on the cellular response to LatA treatment, we analyzed nuclear division following exposure to LatA in control cells or cells lacking Alk1, Alk2, or both. Tub1-GFP expressing cells were synchronized in G1 with mating pheromone and then released into fresh medium containing 100 µM LatA. Nuclear dynamics was monitored 4 h after the release, scoring the percentage of cells with two nuclei and the presence of anaphase spindles. As shown in **Figure 1B**; **Supplementary Figures 1A,B**, LatA treatment prevents anaphase in wt strains, where a marginal fraction (11%) of cells becomes binucleated in these conditions. In agreement with the phenotype observed by drop assays, *alk1*Δ cells exhibited a reduced response to LatA treatment, as seen by nuclear division (42% binucleated cells) and spindle elongation (29% anaphase spindles). Deletion of *ALK2*, which does not significantly alter the cellular sensitivity to LatA of control strains, rescues the defects observed in *alk1*Δ cells.

To test whether the observed phenotypes were specific to LatA treatment or a common feature of haspin mutants upon G1 polarization defects, we employed a genetic approach to interfere with bud emission. Cdc24 is the main guanine nucleotide exchange factor (GEF) for Cdc42, the master regulator of cellular polarity in budding yeast (Adams et al., 1990; Zheng et al., 1994; Bi et al., 2000). Among the plethora of processes directly regulated by Cdc42 are polarity establishment, actin dynamics and bud emergence, and hence impaired Cdc42 activity during G1 ultimately leads to the activation of the morphogenesis checkpoint as a consequence of polarity impairments (Miller and Johnson, 1997). We thus exploited a *cdc24-1* mutant that upon shift to restrictive temperature is unable to sustain polarization, thus triggering the morphogenesis checkpoint (Sloat et al., 1981).

First, we verified whether, as observed upon LatA treatment, loss of *ALK1* improved the fitness of *cdc24-1* strains upon polarization defects. To this end, we tested the growth of *cdc24-1* and *cdc24-1alk1*Δ strains at permissive (25°C), semi-permissive (32°C) or restrictive (37°C) temperatures. As shown in **Supplementary Figure 1C**, loss of *ALK1* promoted the growth of cells with impaired Cdc24 activity at 32°C, confirming an

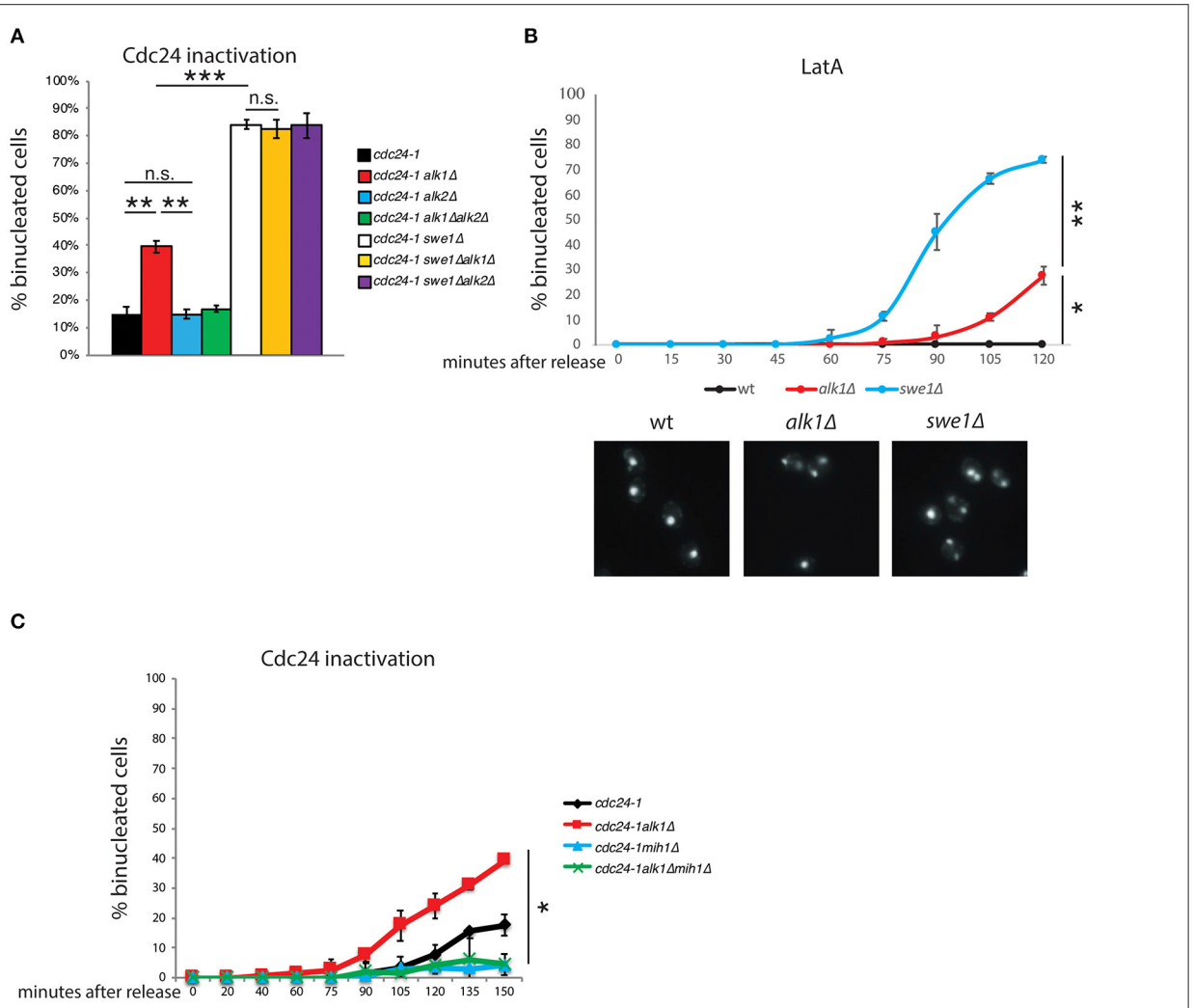

FIGURE 2 | Alk1 regulates cell cycle progression through Mih1. Cells of the indicated strains were arrested in G1 at 25°C and held at 37°C for further 45' before being released at 37°C. After 2 h samples were taken and nuclear segregation was evaluated by fluorescence microscopy **(A)** For wt, *alk1*Δ, *alk2*Δ and *alk1*Δ*alk2*Δ, the mean value was calculated on data from experiment in **Figure 1C** combined with new biological replicates performed together with the other indicated strains. **(B)** Cells of the indicated strains were synchronized in G1 and treated with LatA. Following release, samples were taken to monitor nuclear division by fluorescence microscopy. Representative images at the 120' time point are shown **(C)** Cells were treated as in A, taking samples at the indicated time points to monitor nuclear segregation or cell-cycle progression (**Supplementary Figure 2**). Error bars represent standard deviation, statistical significance was measured by *T*-test, ns: not significant, $*p < 0.05$, $**p < 0.01$, $***p < 0.005$.

improved fitness of cells lacking Alk1 in presence of polarization insults. We then monitored Alk1 contribution to nuclear segregation upon chronic exposure to Cdc24 inactivation. Wild-type, *alk1*Δ, *alk*Δ, and *alk1*Δ *alk2*Δ cells in *cdc24-1* background were grown at 25°C (permissive temperature), arrested in G1 with α-factor and shifted at 37°C (non-permissive temperature) for the last 45 min of the treatment, in order to deplete Cdc24 activity before budding onset. Cells were then released from the G1 arrest into fresh medium at 37°C to promote cell cycle progression in presence of budding defects. The kinetics of nuclear division was analyzed by fluorescence microscopy. As shown in **Figure 1C**, cells expressing wild-type haspin delay anaphase onset so that only a small fraction (15%) of the population underwent nuclear division at 120' when budding is defective due to mutated *CDC24*. Consistently with what observed with LatA, in *cdc24-1alk1*Δ strains the mitotic delay is defective and binucleated cells reach 40% by 2 h after the G1 release. This phenotype is again suppressed by concomitant loss of Alk2.

Up to now, most of the roles played by haspin are exerted through phosphorylation of H3-T3. Thus, we verified whether the phenotypes observed upon loss of Alk1 could be ascribed to altered histone phosphorylation. To this end, we incubated wt, *H3-T3A* and *alk1*Δ*H3-T3A* strains with 100μM Lat A for 4 h and then calculated the percentage of binucleated non-budded cells. As shown in **Supplementary Figure 1D,** loss of histone phosphorylation *per se* does not lead to unscheduled nuclear division in these conditions, suggesting that, whatever the role

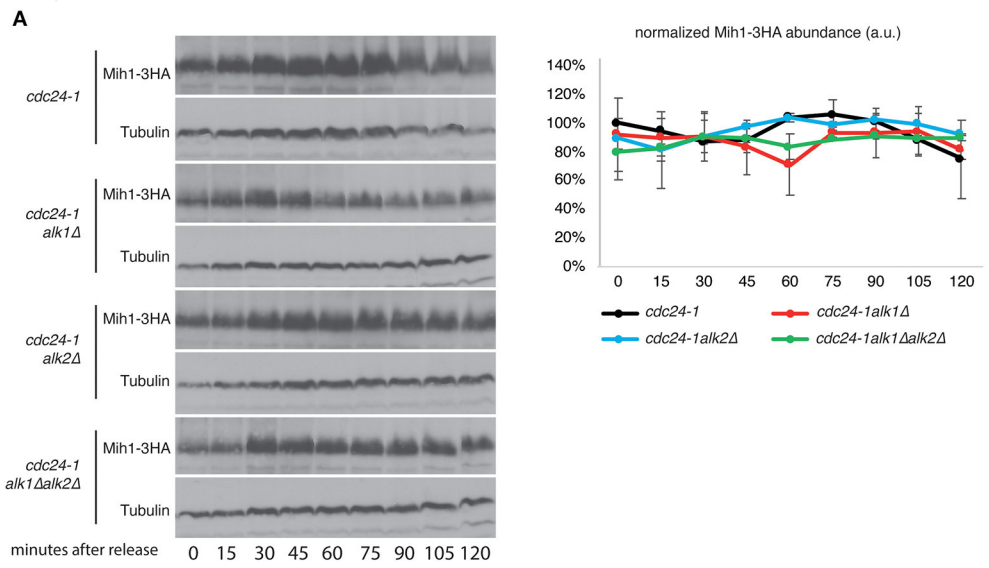

FIGURE 3 | Alk1 does not modulate Mih1 post-translational modifications. **(A)** Cells of the indicated strains were synchronized in G1 at permissive temperature and held at 37°C for further 45' before being released into the cell cycle at restrictive temperature. Samples were taken every 15' to follow protein levels and modifications by western blot. The graph shows the relative Mih1-3HA abundance normalized on tubulin levels. Error bars represent standard deviation.

played by haspin in this pathway, it is not dependent on H3-T3 phosphorylation.

Overall, these observations indicate that yeast *ALK1* plays a role in the cellular response to polarization insults in the early stages of the cell cycle. Surprisingly, this function is not shared between haspin paralogues. Indeed, our results suggest a role for Alk1 in promoting of the morphogenesis checkpoint, while Alk2 seems to have an opposite role.

Alk1 Regulates Cell Cycle Progression Through Mih1 Inactivation

In budding yeast, budding impairments trigger a surveillance mechanism, known as the morphogenesis checkpoint, which delays mitotic entry (Lew and Reed, 1995a; McMillan et al., 1998). Swe1 kinase phosphorylates Cdc28-Y19 (Gould and Nurse, 1989; Harvey et al., 2005), inhibiting its function and preventing entry into mitosis. The phosphatase Mih1 is largely responsible for the removal of the phosphate group, releasing the cell cycle arrest (Sia et al., 1996; Harvey and Kellogg, 2003). The premature resumption of cell cycle progression observed in *alk1*Δ cells suggests that Alk1 may positively modulate Swe1 or act as an inhibitor of Mih1, preventing the G2/M transition in the presence of polarity problems. Similarly, Alk2 could act on Swe1 or Mih1 with an opposite role. To obtain clearer insights on the possible interplay between haspin and Swe1 in the control of Cdc28 activity we analyzed different mutants in a *cdc24-1* background, following the release from a G1 arrest at the restrictive temperature. We then assessed how loss of *ALK1* or *ALK2* affected the nuclear segregation of cells lacking *SWE1*. As shown in **Figure 2A**, loss of Alk1 or Alk2 does not further worsen or ameliorate the defects of *swe1*Δ mutants, suggesting that haspin is indeed involved in the regulation of the morphogenesis checkpoint (see **Supplementary Figure 2A** for cell-cycle analysis). We then compared the kinetics of nuclear division in *ALK1* and *SWE1* mutants following LatA treatment in G1 (**Figure 2B**). Interestingly, we found that, besides being defective compared to control cells, nuclear segregation in *alk1*Δ strains is delayed compared to that of cells completely lacking Swe1 kinase, suggesting defects in sustained morphogenesis checkpoint activity. If the morphogenetic insult is prolonged, in the absence of both Alk1 or Swe1, cells fail to arrest and undergo multiple rounds of DNA replication as nuclear division even in the absence of a bud, leading to the formation of polynucleated cells (**Supplementary Figure 2B**).

In the presence of polarity insults that trigger the morphogenesis checkpoint, Mih1 is expected to be inactive (Harrison et al., 2001; Ciliberto et al., 2003). Thus, two possibilities can explain the observed defects in Alk1 mutants: loss of Alk1 either causes a failure in sustaining Swe1 activity or it promotes unscheduled Mih1 activation. If the loss of *ALK1* results in the unscheduled activation of Mih1, deletion of *MIH1* should suppress the phenotypes of Alk1-lacking cells. On the other hand, if *ALK1* deletion causes defective Swe1 activity, the concomitant loss of Mih1 would not impact *alk1*Δ phenotypes since Mih1 should be inactive in these conditions. As shown in **Figure 2C** (see **Supplementary Figure 2C** for cell-cycle analysis), while loss of Alk1 led to an anticipated nuclear division, additional deletion of *MIH1* restored normal anaphase kinetics, confirming the epistatic relation between Alk1 and Mih1. Noteworthy, *MIH1* deletion alone do not affect anaphasic nuclei at 90'-105'-120' after the release, when *alk1*Δ strains already exhibit nuclear segregation, confirming that the phosphatase is inactive in control cells. This observation further supports the proposed unscheduled activation of Mih1 upon loss of Alk1.

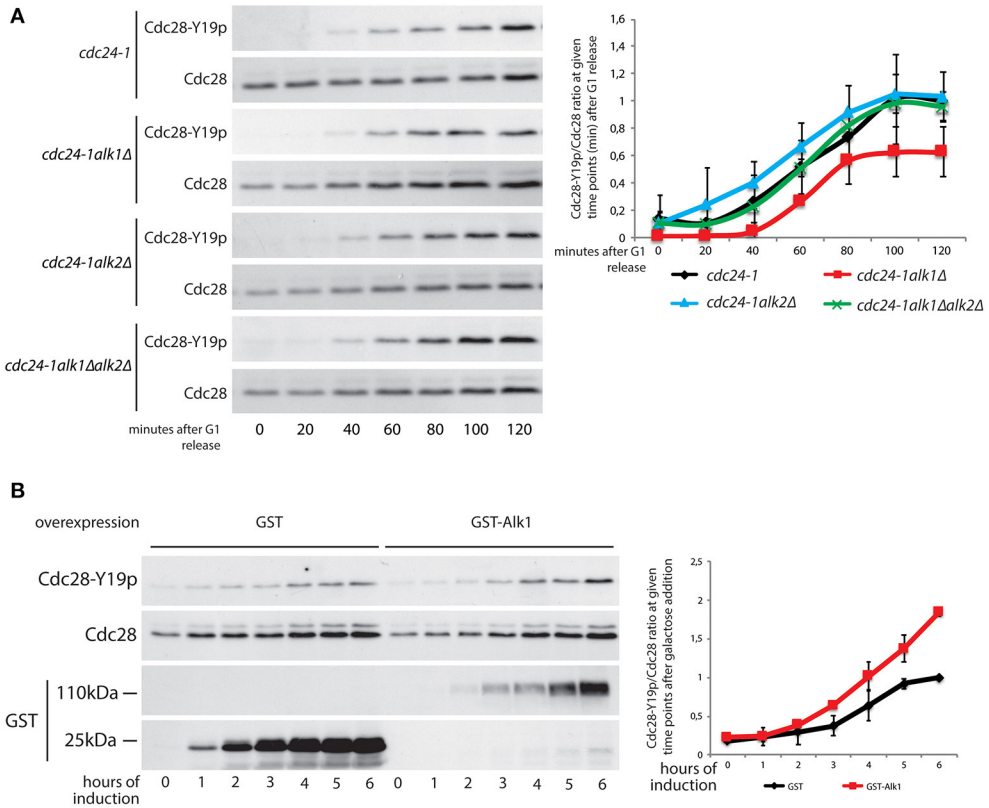

FIGURE 4 | Alk1 is required for sustained Cdc28-Y19 phosphorylation. **(A)** Cells of the indicated strains were synchronized in G1 at permissive temperature and held at 37°C for further 45' before being released into the cell cycle at restrictive temperature. Samples were taken every 20' to follow protein levels by western blot using antibodies for total Cdc28 and phosphospecific antibodies for Cdc28-Y19p. The right panel reports the quantification of the phosphorylation signals normalized over the total Cdc28. Error bars represent standard deviation **(B)** Logarithmically growing cells, bearing the pGAL-*GST* or pGAL-*GST-ALK1* constructs, were incubated in the presence of 2% galactose to induce protein overexpression. Samples were taken every hour to monitor protein levels. Western blotting was performed with antibodies for total Cdc28 and phosphospecific antibodies for Cdc28-Y19p. Expression levels of GST and GST-Alk1 were analyzed with anti GST antibodies. The graph shows the ratio between phosphorylated Cdc28-Y19 and total Cdc28, error bars represent standard deviation.

This regulation is unlikely to be direct. Indeed, no physical interaction between Alk1 and Mih1 (nor Swe1) was detected by two-hybrid (**Supplementary Figure 3A**; a strain expressing LexA-p53 and B42-3HA-SV40 was used as a positive control). The morphogenesis checkpoint main regulators, Mih1 and Swe1 are both tightly controlled in a posttranslational manner which involves several kinases and phosphorylation events (Pal et al., 2008). We then hypothesized that Alk1 and Alk2 could exert their role in this pathway by regulating Mih1 phosphorylations. However, we did not observe significant differences in both Mih1 and Swe1 protein levels or posttranslational modifications in haspin mutants (**Figure 3A**; **Supplementary Figure 3B**).

Alk1 and Alk2 Modulate Cdc28-Y19 Phosphorylation Upon Defective Budding

Previous results show an interplay between yeast haspin and the morphogenesis checkpoint in case of unpolarized cells. To directly address haspin involvement in the activation and maintenance of this checkpoint we monitored the impact of haspin loss on the kinetics of Cdc28-Y19 phosphorylation in synchronized cultures. *cdc24-1, cdc24-1alk1*Δ, *cdc24-1alk2*Δ, and *cdc24-1alk1*Δ*alk2*Δ strains were arrested in G1, shifted to non-permissive temperature to deplete Cdc24 activity and released in pheromone-free medium, taking samples at different time points. The levels of phosphorylated Cdcd28-Y19 were measured with phosphospecific antibodies and fluorescence-based analysis. As shown in **Figure 4A**, (see **Supplementary Figure 4A** for cell cycle analysis) loss of Alk1 does not impede Cdc28-Y19 phosphorylation, but it prevents its accumulation after ∼1 h from the release. Again, removal of Alk2 restores a wt inactivation of Cdc28 in *alk1*Δ cells. To reinforce the notion that Alk1 is a positive regulator of the morphogenesis checkpoint, we exploited a reversed approach, where we overexpressed the kinase and monitored the accumulation of Cdc28-Y19p. As shown in **Figure 4B**; **Supplementary Figure 4B**, increased *ALK1* levels indeed caused elevated levels of phosphorylated Cdc28-Y19 with no evident effect on cell-cycle progression, further supporting our conclusions.

DISCUSSION

A proper timing between different developmental events is fundamental for successful cell-cycle completion and proliferation of every organism. In *Saccharomyces cerevisiae*, cell division occurs by budding and this requires that a daughter cell is formed prior to anaphase. It is the mother-bud axis, pre-defined in G1 by setting up polarity clusters, that will determine the direction of spindle elongation. In this scenario, failures in symmetry breaking and cellular polarization impede bud emission and lead to a cell-cycle arrest with replicated DNA in a single nucleus (Lew and Reed, 1995b). The molecular mechanism that couples nuclear dynamics and budding is known as morphogenesis checkpoint, a network able to perceive defects in bud formation and to transduce this stimulus in an inhibitory phosphorylation of CDK1 (Cdc28-Y19p) (Sia et al., 1996). Two proteins act as master regulators of the morphogenesis checkpoint, the kinase Swe1 and the phosphatase Mih1 (WEE1 and CDC25 in higher eukaryotes, respectively); the concerted activity of these players directly regulate Cdc28-Y19 phosphorylation (Booher et al., 1993; Sia et al., 1996).

The atypical kinase haspin targets H3-T3 and has been ascribed with several roles in nuclear dynamics, ranging from chromosome cohesion to chromatin condensation, alignment at the metaphase plate and asymmetric histone inheritance (Dai and Higgins, 2005; Dai et al., 2005, 2006; Kelly et al., 2010; Wang et al., 2010, 2011; Yamagishi et al., 2010; Tran et al., 2012; Ghenoiu et al., 2013). Here we report an unprecedented involvement of budding yeast haspin paralogues Alk1 and Alk2 in the morphogenesis checkpoint. In particular Alk1 seems to play a positive role in delaying the cell cycle progression upon failures in polarity establishment and bud emergence. Indeed, cells lacking *ALK1* exhibit an abortive cell cycle arrest in response to the actin cytoskeleton poison LatA and following genetic inactivation of the polarity regulator Cdc24. This last observation excludes that the LatA sensitivity phenotype could be due to a reduced cell wall permeability of *alk1*Δ cells or to LatA specific effects. Alk2 has an opposite role and its loss is sufficient to restore normal phenotypes in Alk1 mutants. This failure in cell-cycle arrest is due to a defective inhibitory phosphorylation of Cdc28-Y19 in *alk1*Δ strains, which is again suppressed by concomitant loss of Alk2. In particular, *alk1*Δ cells are able to generate an initial, increase in levels of phosphorylated Cdc28-Y19, which however fails to accumulate to the levels of wt strains. This could be explained both by a loss in Swe1 functionality or by an unscheduled Mih1 activation.

However, deletion of *MIH1* completely suppresses the defects due to loss of *ALK1*. Notably, this suppression occurs at a stage when in wt cells Mih1 itself is inactive, clearly identifying Mih1 and not Swe1 as the branch regulated by Alk1. Our two hybrid results suggest that Alk1 does not directly interact with Mih1 or Swe1, and we found no evident contribution in terms of posttranslational modifications of Mih1 or Swe1 by Alk1.

All the proteins analyzed here are conserved in human cells, where Wee1 (Swe1) and Cdc25 (Mih1) have crucial activities

TABLE 1 | Strains and plasmids used in this work.

Name	Relevant Genotype	Source
STRAINS		
K699	*ade2-1, trp1-1, can1-100, leu2-3, his3-11,15, ura3 MATa*	K.Nasmyth
EGY42	*ura3 his3 trp1 6xLexAop-LEU2 MATa*	R.Brent
UCC1111	*adh4::URA3-TEL (VII-L) hhf1-hht1::LEU2 hhf2-hht2::MET15 [HHF2-HHT2]* MATα	Parthun's Lab (Kelly et al., 2000)
SP1791	*TUB1-GFP::HIS3 MATa*	Piatti's Lab
YPD294	*TUB1-GFP::HIS3 alk1::NATr MATa*	This work
YPD414/1A	*TUB1-GFP:HIS3 alk2::KANr MATa*	This work
YPD298	*TUB1-GFP::HIS3 alk1::NATr alk2::KANr MATa*	This work
YPD274	*cdc24-1 MATa*	This work
YPD280/9A	*cdc24-1 alk1::NATr MATa*	This work
YPD282/12A	*cdc24-1 alk2::KANr MATa*	This work
YPD282/5A	*cdc24-1 alk1::NATr alk2::KANr MATa*	This work
**YPD226	*UCC1111 [HHT2-T3A]* MATα	This work
**YRQ549	*UCC1111 alk1::KANr [HHT2-T3A]* MATα	This work
YPD458	*cdc24-1 swe1::LEU2 MATa*	This work
YPD459	*cdc24-1 alk1::NATr swe1::LEU2 MATa*	This work
YPD460	*cdc24-1 alk2::KANr swe1::LEU2 MATa*	This work
Q225	*swe1::LEU2 MATa*	This work
YPD286/10C	*cdc24-1 mih1::TRP1 MATa*	This work
YPD288/7A	*cdc24-1 alk1::NATr mih1::TRP1 MATa*	This work
*YLD123	*[pSH18-34] [B42-3HA] [LexA-ALK1] MATa*	This work
*YLD125	*[pSH18-34] [B42-3HA-MIH1] [LexA] MATa*	This work
*YLD124	*[pSH18-34] [B42-3HA-SWE1] [LexA] MATa*	This work
*YLD127	*[pSH18-34] [B42-3HA-MIH1] [LexA-ALK1] MATa*	This work
*YLD126	*[pSH18-34] [B42-3HA-SWE1] [LexA-ALK1] MATa*	This work
*YMIC1D7	*[pSH18-34] [B42-3HA-SV40] [LexA-p53] MATa*	Lab stock
YLD18/20C	*cdc24-1 MIH1-HA-TRP1 MATa*	This work
YLD19/13A	*cdc24-1 alk1::KANr MIH1-HA-TRP1 MATa*	This work
YLD20/3D	*cdc24-1 alk2::HIS3 MIH1-HA-TRP1 MATa*	This work
YLD21/10D	*cdc24-1 alk1::KANr alk2::HIS3 MIH1-HA-TRP1 MATa*	This work
YPD336/6A	*cdc24-1 SWE1-HA-URA3 MATa*	This work
YPD338/11A	*cdc24-1 alk1::KANr SWE1-HA-URA3 MATa*	This work
YPD339/9C	*cdc24-1 alk2::HIS3 SWE1-HA-URA3 MATa*	This work
YPD341/7C	*cdc24-1 alk1::KANr alk2::HIS3 SWE1-HA-URA3 MATa*	This work
YAN64-2	*[pGAL1-GST]*	This work
YAN78-1	*[pGAL1-GST-ALK1]*	This work
PLASMIDS		
pPD9	*PMP3-HHT2-T3A*	This work
pSH18-34	*8xLexAop-LacZ*	R.Brent
pJG4-5	*pGAL1-B42AD-HA*	R.Brent
pEG202	*pADH-LexA*	R.Brent
pAN5	*pEG202-ALK1*	This work
pLD22	*pJG4-5-SWE1*	This work
pLD23	*pJG4-5-MIH1*	This work
p53	*pEG202-p53*	Lab stock
TAg	*pJG4-5-SV40TAg*	Lab stock
pEG(KT)	*pGAL-GST*	Lab stock
pAN8	*pGAL-GST-ALK1*	This work

in the control of cell cycle, and their misfunction is often coupled with carcinogenesis. The mechanism by which *WEE1* and *CDC25* become deregulated during cancer development remains still unclear. Conceptually, we therefore believe that understanding haspin contribution to the Wee1/Cdc25 pathway can shed light in long term on mechanisms underlying tumor development. The mechanism linking haspin to the morphogenesis checkpoint is still elusive. Both Swe1 and Mih1 are subjected to extensive phosphorylation, and it has been technically very challenging to link haspin activity to it. The involvement of H3-T3 phosphorylation is unlikely as this PTM is restricted to mitosis, while the morphogenesis checkpoint arrests cells at the G2/M transition. This suggest that other still unidentified haspin targets may be relevant to this pathway.

METHODS

Yeast Strains and Plasmids

Yeast strains used in this study are isogenic to W303 apart from those used in two-hybrid assays, marked with *, which are isogenic to EGY48, and those marked with **, which are isogenic to UCC1111, and are listed in **Table 1**. Conditions for yeast cell cultures used have been previously described (Rose et al., 1990). When indicated the cultures were synchronized in G1 by 2 μg/ml α-factor as previously described (Foiani et al., 1994). Standard molecular genetics techniques were used to construct plasmids and strains. In particular, PCR-based genotyping were used to confirm gene disruption and tagging (Longtine et al., 1998).

Latrunculin a Treatment

Cells were grown in YPD medium, synchronized in G1 with α-factor (2 μg/ml) and released in the presence of LatA (SIGMA L5163) 100 μM for 240 min. Cells were then harvested for protein extraction or fixed for microscopy analysis.

Spindle Elongation and Nuclear Division Analysis

Cells carrying *TUB1-GFP* were fixed with formaldehyde (3.7%) and washed three times with PBS. GFP was visualized by fluorescence microscopy with a Leica DMRA2 widefield fluorescence microscope equipped with a CCD camera (Leica DC 300F). For the analysis of nuclear division cells were fixed with ethanol, washed three times in PBS and DNA was stained with DAPI. Labeled-DNA was visualized by fluorescence microscopy as described above. Images were processed by ImageJ (Schindelin et al., 2012). Nuclear division pattern was evaluated by scoring for unbudded cells showing a single nucleus or two nuclei. At least 300 cells were categorized per sample across three experimental repeats to calculate a mean and a standard deviation.

Morphogenesis Checkpoint Assays

To evaluate morphogenesis checkpoint activation cells carrying *cdc24-1* temperature-sensitive allele were grown at 25°C (permissive temperature), arrested in G1 with α-factor (2 μg/ml), shifted for 45 min at 37°C (non-permissive temperature) and released at 37°C. At indicated time points, samples were collected, fixed in ethanol and stained with DAPI. Nuclear division was evaluated as described above. Trichloroacetic acid protein extraction was used to evaluate Cdc28-Y19 phosphorylation by Western blot. The ratio between Cdc28-Y19 phosphorylation and total Cdc28 was performed on protein levels of three independent experiments.

Western Blot

To analyze proteins during kinetic experiments samples were collected at given time points and exposed to trichloroacetic acid precipitation (Muzi Falconi et al., 1993). Protein extracts were then resolved by SDS- PAGE and analyzed by Western blot using proper antibodies. Anti-HA antibodies (12CA5) were used as previously described (Sabbioneda et al., 2007). Anti-phospho-Cdc2 (Tyr15) (#9111, Cell Signaling), anti-Cdc2 (ab17) (#ab18-100, Abcam) and anti-GST (#27-4577-01V, GE Healthcare) were used with standard techniques. Images were taken with a ChemidocTouch Imaging System (Bio-Rad) and processed with ImageLab and ImageJ.

Two-Hybrid

EGY42 cells were transformed with the indicated plasmids (pEG202, pJG4-5 and their derivatives expressing fusions with Alk1, Mih1, or Swe1). Fusion proteins were checked by western blots. The *lacZ* reporter is harbored on the pSH18-34 plasmid. Relevant strains were patched on selective raffinose/galactose-containing plates supplemented with 0.195 nM X-Gal, 23.1mM NaH_2PO_4 and 21.1mM Na_2HPO_4. Pictures were taken after overnight incubation at 28°C.

Cell Cycle Analysis With FACScan

Samples were taken at given time points, fixed with ethanol and processed with RNase A and Proteinase K. Cells were then stained with 1 μM SytoxGreen and DNA content was determined using a FACScan cytofluorimeter.

DATA AVAILABILITY STATEMENT

The raw data supporting the conclusions of this article will be made available by the authors, without undue reservation.

AUTHOR CONTRIBUTIONS

MG, LD, RQ, MM-F, and PP planned the experimental approach, revised the experiments and analyzed the data. MG, RQ, and MM-F wrote the manuscript. MG, LD, RQ, AN, and DP performed the experiments. EG and DP contributed to experimental procedures and discussion. All authors contributed to the article and approved the submitted version.

FUNDING

MM-F lab is supported by grants from AIRC (n.21806) and MIUR (PRIN). RQ was supported by and AIRC fellowship (n. 17919).

ACKNOWLEDGMENTS

We sincerely thank Marco Geymonat and Simonetta Piatti for useful discussion and donating strains. The authors acknowledge the support from the University of Milan through the APC initiative.

SUPPLEMENTARY MATERIAL

The Supplementary Material for this article can be found online at: https://www.frontiersin.org/articles/10.3389/fcell.2020.625717/full#supplementary-material

REFERENCES

Adams, A. E. M., Johnson, D. I., Longnecker, R. M., Sloat, B. F., and Pringle, J. R. (1990). CDC42 and CDC43, two additional genes involved in budding and the establishment of cell polarity in the yeast *Saccharomyces cerevisiae*. *J. Cell Biol.* 111, 131–42. doi: 10.1083/jcb.111.1.131

Anastasia, S. D., Nguyen, D. L., Thai, V., Meloy, M., MacDonough, T., and Kellogg, D. R. (2012). A link between mitotic entry and membrane growth suggests a novel model for cell size control. *J. Cell Biol.* 197, 89–104. doi: 10.1083/jcb.201108108

Asano, S., Park, J. E., Sakchaisri, K., Yu, L.-R., Song, S., Supavilai, P., et al. (2005). Concerted mechanism of Swe1/Wee1 regulation by multiple kinases in budding yeast. *EMBO J.* 24, 2194–204. doi: 10.1038/sj.emboj.7600683

Ayscough, K. R., Stryker, J., Pokala, N., Sanders, M., Crews, P., and Drubin, D. G. (1997). High rates of actin filament turnover in budding yeast roles for actin in establishment maintenance of cell polarity revealed using the actin inhibitor latrunculin-A. *J. Cell Biol.* 137, 399–416. doi: 10.1083/jcb.137.2.399

Barral, Y., Parra, M., Bidlingmaier, S., and Snyder, M. (1999). Nim1-related kinases coordinate cell cycle progression with the organization of the peripheral cytoskeleton in yeast. *Genes Dev.* 13, 176–87. doi: 10.1101/gad.13.2.176

Bi, E., Chiavetta, J. B., Chen, H., Chen, G.-C., Chan, C. S. M., and Pringle, J. R. (2000). Identification of novel, evolutionarily conserved Cdc42p-interacting proteins and of redundant pathways linking Cdc24p and Cdc42p to actin polarization in *yeast. Mol. Biol. Cell* 11, 773–793. doi: 10.1091/mbc.11.2.773

Booher, R. N., Deshaies, R. J., and Kirschner, M. W. (1993). Properties of Saccharomyces cerevisiae wee1 and its differential regulation of p34CDC28 in response to G1 and G2 cyclins. *EMBO J.* 12, 3417–3426. doi: 10.1002/j.1460-2075.1993.tb06016.x

Carroll, C. W., Enquist-Newman, M., and Morgan, D. O. (2005). The APC subunit Doc1 promotes recognition of the substrate destruction box. *Curr. Biol.* 15, 11–18. doi: 10.1016/j.cub.2004.12.066

Caviston, J. P., Tcheperegine, S. E., and Bi, E. (2002). Singularity in budding: a role for the evolutionarily conserved small GTPase Cdc42p. *Proc. Natl. Acad. Sci. U.S.A.* 99,12185–12190. doi: 10.1073/pnas.182370299

Chiroli, E., Rossio, V., Lucchini, G., and Piatti, S. (2007). The budding yeast PP2ACdc55 protein phosphatase prevents the onset of anaphase in response to morphogenetic defects. *J. Cell Biol.* 177, 599–611. doi: 10.1083/jcb.200609088

Ciliberto, A., Novak, B., and Tyson, J. J. (2003). Mathematical model of the morphogenesis checkpoint in budding yeast. *J. Cell Biol.* 163, 1243–1254. doi: 10.1083/jcb.200306139

Crutchley, J., King, K. M., Keaton, M. A., Szkotnicki, L., Orlando, D. A., Zyla, T. R., et al. (2009). Molecular dissection of the checkpoint kinase *Hsl1p*. *Mol Biol Cell* 20, 1926–1936. doi: 10.1091/mbc.e08-08-0848

Dai, J., and Higgins, J. M. G. (2005). Haspin: a mitotic histone kinase required for metaphase chromosome alignment. *Cell Cycle* 4, 665–668. doi: 10.4161/cc.4.5.1683

Dai, J., Sullivan, B. A., and Higgins, J. M. G. (2006). Regulation of mitotic chromosome cohesion by haspin and aurora B. *Dev. Cell.* 11, 741–750. doi: 10.1016/j.devcel.2006.09.018

Dai, J., Sultan, S., Taylor, S. S., and Higgins, J. M. G. (2005). The kinase haspin is required for mitotic histone H3 Thr 3 phosphorylation and normal metaphase chromosome alignment. *Genes Dev.* 19, 472–488. doi: 10.1101/gad.1267105

Dunphy, W. G., and Kumagai, A. (1991). The cdc25 protein contains an intrinsic phosphatase activity. *Cell* 67, 189–196. doi: 10.1016/0092-8674(91)90582-J

Etienne-Manneville, S. (2004). Cdc42–the centre of polarity. *J. Cell Sci.* 117, 1291–1300. doi: 10.1242/jcs.01115

Foiani, M., Marini, F., Gamba, D., Lucchini, G., and Plevani, P. (1994). The B subunit of the DNA polymerase alpha-primase complex in *Saccharomyces cerevisiae* executes an essential function at the initial stage of DNA replication. *Mol. Cell Biol.* 14, 923–33. doi: 10.1128/MCB.14.2.923

Gautier, J., Solomon, M. J., Booher, R. N., Bazan, J. F., and Kirschner, M. W. (1991). cdc25 is a specific tyrosine phosphatase that directly activates p34cdc2. *Cell* 67, 197–211. doi: 10.1016/0092-8674(91)90583-K

Ghenoiu, C., Wheelock, M. S., and Funabiki, H. (2013). Autoinhibition and polo-dependent multisite phosphorylation restrict activity of the histone H3 kinase haspin to mitosis. *Mol. Cell.* 52, 734–745. doi: 10.1016/j.molcel.2013.10.002

Gould, K. L., and Nurse, P. (1989). Tyrosine phosphorylation of the fission yeast cdc2+ protein kinase regulates entry into mitosis. *Nature* 342, 39–45. doi: 10.1038/342039a0

Harrison, J. C., Bardes, E. S. G., Ohya, Y., and Lew, D. J. (2001). A role for the Pkc1p/Mpk1p kinase cascade in the morphogenesis checkpoint. *Nat. Cell Biol.* 3, 417–420. doi: 10.1038/35070104

Harvey, S. L., Charlet, A., Haas, W., Gygi, S. P., and Kellogg, D. R. (2005). Cdk1-dependent regulation of the mitotic inhibitor Wee1. *Cell* 122, 407–420. doi: 10.1016/j.cell.2005.05.029

Harvey, S. L., and Kellogg, D. R. (2003). Conservation of mechanisms controlling entry into mitosis: budding yeast wee1 delays entry into mitosis and is required for cell size control. *Curr. Biol.* 13, 264–275. doi: 10.1016/S0960-9822(03)00049-6

Higgins, J. M. (2001a). Haspin-like proteins: a new family of evolutionarily conserved putative eukaryotic protein kinases. *Protein Sci.* 10, 1677–1684. doi: 10.1110/ps.49901

Higgins, J. M. G. (2001b). The Haspin gene: location in an intron of the Integrin alphaE gene, associated transcription of an Integrin alphaE-derived RNA and expression in diploid as well as haploid cells. *Gene* 267, 55–69. doi: 10.1016/S0378-1119(01)00387-0

Kaiser, P., Sia, R. A. L., Bardes, E. G. S., and Lew, D. J. (1998). & Reed SI. Cdc34 and the F-box protein Met30 are required for degradation of the Cdk-inhibitory kinase Swe1. *Genes Dev.* 12, 2587–2597. doi: 10.1101/gad.12.16.2587

Keaton, M. A., and Lew, D. J. (2006). Eavesdropping on the cytoskeleton: progress and controversy in the yeast morphogenesis checkpoint. *Curr. Opin. Microbiol.* 9, 540–546. doi: 10.1016/j.mib.2006.10.004

Kellogg, D. R. (2003). Wee1-dependent mechanisms required for coordination of cell growth and cell division. *J. Cell Sci.* 116, 4883–4890. doi: 10.1242/jcs.00908

Kelly, A. E., Ghenoiu, C., Xue, J. Z., Zierhut, C., Kimura, H., and Funabiki, H. (2010). Survivin reads phosphorylated histone H3 threonine 3 to activate the mitotic kinase Aurora B. *Science* 330, 235–239. doi: 10.1126/science.1189505

Kelly, T. J., Qin, S., Gottschling, D. E., and Parthun, M. R. (2000). Type B histone acetyltransferase Hat1p participates in telomeric silencing. *Mol. Cell Biol.* 20, 7051–7058. doi: 10.1128/MCB.20.19.7051-7058.2000

Kennedy, E. K., Dysart, M., Lianga, N., Williams, E. C., Pilon, S., Doré C., et al. (2016). Redundant regulation of Cdk1 tyrosine dephosphorylation in *Saccharomyces cerevisiae. Genetics* 202, 903–910. doi: 10.1534/genetics.115.182469

King, K., Kang, H., Jin, M., and Lew, D. J. (2013). Feedback control of Swe1p degradation in the yeast morphogenesis checkpoint. *Mol. Biol. Cell.* 24, 914–922. doi: 10.1091/mbc.e12-11-0812

Lew, D. J. (2003). The morphogenesis checkpoint: how yeast cells watch their figures. *Curr. Opin. Cell Biol.* 15, 648–653. doi: 10.1016/j.ceb.2003.09.001

Lew, D. J., and Reed, S. I. (1995a). A cell cycle checkpoint monitors cell morphogenesis in budding yeast. *J. Cell Biol.* 129, 739–749. doi: 10.1083/jcb.129.3.739

Lew, D. J., and Reed, S. I. (1995b). Cell cycle control of morphogenesis in budding yeast. *Curr. Opin. Genet. Dev.* 5, 17–23. doi: 10.1016/S0959-437X(95)90048-9

Lianga, N., Williams, E. C., Kennedy, E. K., Doré C., Pilon, S., Girard, S. L., et al. (2013). A Wee1 checkpoint inhibits anaphase *onset*. *J. Cell Biol.* 201, 843–862. doi: 10.1083/jcb.201212038

Longtine, M. S., McKenzie, A., Demarini, D. J., Shah, N. G., Wach, A., Brachat, A., et al. (1998). Additional modules for versatile and economical PCR-based gene deletion and modification in Saccharomyces cerevisiae. *Yeast* 14, 953–961. doi: 10.1002/(SICI)1097-0061(199807)14:10<953::AID-YEA293>3.0.CO;2-U

Longtine, M. S., Theesfeld, C. L., McMillan, J. N., Weaner, E., Pringle, J. R., and Lew, D. J. (2000). Septin-dependent assembly of a cell cycle-regulatory module in *Saccharomyces cerevisiae*. *Mol. Cell Biol.* 20, 4049–4061. doi: 10.1128/MCB.20.11.4049-4061.2000

Marquitz, A. R., Harrison, J. C., Bose, I., Zyla, T. R., McMillan, J. N., and Lew, D. J. (2002). The Rho-GAP Bem2p plays a GAP-independent role in the morphogenesis checkp*oint*. *EMBO J.* 21, 4012–4025. doi: 10.1093/emboj/cdf416

McMillan, J. N., Sia, R. A. L., and Lew, D. J. (1998). A morphogenesis checkpoint monitors the actin cytoskeleton in yeast. *J. Cell Biol.* 142, 1487–1499. doi: 10.1083/jcb.142.6.1487

McMillan, J. N., Theesfeld, C. L., Harrison, J. C., Bardes, E. S. G., and Lew, D. J. (2002). Determinants of Swe1p degradation in *Saccharomyces cerevisiae*. *Mol. Biol. Cell.* 13, 3560–3575. doi: 10.1091/mbc.e02-05-0283

McNulty, J. J., and Lew, D. J. (2005). Swe1p responds to cytoskeletal perturbation, not bud size, in S. *cerevisiae*. *Curr. Biol.* 15, 2190–2198. doi: 10.1016/j.cub.2005.11.039

Miller, P. J., and Johnson, D. I. (1997). Characterization of the *Saccharomyces cerevisiae* cdc42-1ts allele and new temperature-conditional-lethal cdc42 alleles. *Yeast*. 13, 561–572. doi: 10.1002/(SICI)1097-0061(199705)13:6<561::AID-YEA114>3.0.CO;2-X

Muzi Falconi, M., Piseri, A., Ferrari, M., Lucchini, G., Plevani, P., and Foiani, M. (1993). De novo synthesis of budding yeast DNA polymerase alpha and POL1 transcription at the G1/S boundary are not required for entrance into S phase. *Proc. Natl. Acad. Sci. U.S.A.* 90, 10519–10523. doi: 10.1073/pnas.90.22.10519

Nespoli, A., Vercilio, R., di Nola, L., Diani, L., Giannattasio, M., Plevani, P., et al. (2006). Alk1 and Alk2 are two new cell cycle-regulated haspin-like proteins in budding yeast. *Cell Cycle* 5, 1464–1471. doi: 10.4161/cc.5.13.2914

Pal, G., Paraz, M. T. Z., and Kellogg, D. R. (2008). Regulation of Mih1/Cdc25 by protein phosphatase 2A and casein kinase 1. *J. Cell Biol.* 180, 931–945. doi: 10.1083/jcb.200711014

Panigada, D., Grianti, P., Nespoli, A., Rotondo, G., Gallo Castro, D., Quadri, R., et al. (2013). Yeast haspin kinase regulates polarity cues necessary for mitotic spindle positioning and is required to tolerate mitotic arrest. *Dev. Cell* 26, 1–13. doi: 10.1016/j.devcel.2013.07.013

Pierce, J., and Clark, H. (1981). Mutation of RGA1, which encodes a putative GTPase-activating protein for the polarity-establishment protein Cdc42p, activates the pheromone-response pahtway in the yeast *Saccharomyces cerevisiae*. *Genes Dev.* 506, 506–511.

Quadri, R., Galli, M., Galati, E., Rotondo, G., Gallo, G. R., Panigada, D., et al. (2020a). Haspin regulates Ras localization to promote Cdc24-driven mitotic depolarization. *Cell Discov.* 6. doi: 10.1038/s41421-020-0170-2

Quadri, R., Sertic, S., and Muzi-falconi, M. (2020b). gRASping depolarization : contribution of RAS GTPases to mitotic polarity clusters resolution. *Front. Cell Dev. Biol.* 8, 1–5. doi: 10.3389/fcell.2020.589993

Raspelli, E., Cassani, C., Lucchini, G., and Fraschini, R. (2011). Budding yeast Dma1 and Dma2 participate in regulation of Swe1 levels and localization. *Mol. Biol. Cell.* 22, 2185–2197. doi: 10.1091/mbc.e11-02-0127

Rose, M., Winston, F., and Hieter, P. (1990). *Methods in Yeast Genetics*. Cold Spring Harbor, NY: Cold Spring Harbor Laboratory Press.

Rudner, A. D., Hardwick, K. G., and Murray, A. W. (2000). Cdc28 activates exit from mitosis in budding yeast. *J. Cell Biol.* 149, 1361–1376. doi: 10.1083/jcb.149.7.1361

Russell, P., Moreno, S., and Reed, S. I. (1989). Conservation of mitotic controls in fission and budding yeasts. *Cell* 57, 295–303. doi: 10.1016/0092-8674(89)90967-7

Russell, P., and Nurse, P. (1986). cdc25+functions as an inducer in the mitotic control of fission yeast. *Cell* 45, 145–153. doi: 10.1016/0092-8674(86)90546-5

Russell, P., and Nurse, P. (1987). Negative regulation of mitosis by wee1+, a gene encoding a protein kinase homolog. *Cell* 48, 559–567. doi: 10.1016/0092-8674(87)9v0458-2

Sabbioneda, S., Bortolomai, I., Giannattasio, M., Plevani, P., and Muzi-Falconi, M. (2007). Yeast Rev1 is cell cycle regulated, phosphorylated in response to DNA damage and its binding to chromosomes is dependent upon MEC1. *DNA Repair (Amst)*. 6, 121–127. doi: 10.1016/j.dnarep.2006.09.002

Schindelin, J., Arganda-Carreras, I., Frise, E., Kayinig, V., Longair, M., Pietzsch, T., et al. (2012). Fiji: an open-source platform for biological-image analysis. *Nat. Methods* 9, 676–682. doi: 10.1038/nmeth.2019

Sia, R. A., Herald, H. A., and Lew, D. J. (1996). Cdc28 tyrosine phosphorylation and the morphogenesis checkpoint in budding yeast. *Mol. Biol Cell.* 7, 1657–1666. doi: 10.1091/mbc.7.11.1657

Sia, R. A. L. (1998). Control of Swe1p degradation by the morphogenesis checkpoint. *EMBO J.* 17, 6678–6688. doi: 10.1093/emboj/17.22.6678

Sloat, B. F., Adams, A., and Pringle, J. R. (1981). Roles of the CDC24 gene product in cellular morphogenesis during the *Saccharomyces cerevisiae* cell cycle. *J. Cell Biol.* 89, 394–405. doi: 10.1083/jcb.89.3.395

Smith, G. R., Givan, S. A., Cullen, P., and Sprague, G. F. (2002). GTPase-activating proteins for Cdc42. *Eukaryot. Cell.* 1, 469–480. doi: 10.1128/EC.1.3.469-480.2002

Spector, I., Shochet, N. R., Kashman, Y., and Groweiss, A. (1983). Latrunculins: novel marine toxins that disrupt microfilament organization in cultured cells. *Science* 219, 493–495. doi: 10.1126/science.6681676

Spellman, P. T., Sherlock, G., Zhang, M. Q., Iyer, V. R., Ander, K., Eisen, M. B., et al. (1998). Comprehensive identification of cell cycle-regulated genes of the yeast *Saccharomyces cerevisiae* by microarray hybridiz*ation*. *Mol. Biol. Cell* 9, 3273–3297. doi: 10.1091/mbc.9.12.3273

Sreenivasan, A., and Kellogg, D. (1999). The Elm1 kinase functions in a mitotic signaling network in budding yeast. *Mol. Cell Biol.* 19, 7983–7994. doi: 10.1128/MCB.19.12.7983

Tanaka, H., Yoshimura, Y., Nozaki, M., Yomogida, K., Tsuchida, J., Tosaka, Y., et al. (1999). Identification and characterization of a haploid germ cell-specific nuclear protein kinase (Haspin) in spermatid nuclei and its effects on somatic cells. *J. Biol. Chem.* 274, 17049–17057. doi: 10.1074/jbc.274.24.17049

Theesfeld, C. L., Irazoqui, J. E., Bloom, K., and Lew, D. J. (1999). The role of actin in spindle orientation changes during the *Saccharomyces cerevisiae* cell cycle. *J. Cell Biol.* 146, 1019–1032. doi: 10.1083/jcb.146.5.1019

Tiedje, C., Sakwa, I., Just, U., and Höfken, T. (2008). The Rho GDI Rdi1 regulates Rho GTPases by distinct mechanisms. *Mol. Biol. Cell.* 19, 2885–2896. doi: 10.1091/mbc.e07-11-1152

Tran, V., Lim, C., Xie, J., and Chen, X. (2012). Asymmetric division of Drosophila male germline stem cell shows asymmetric histone distribution. *Science* 338, 679–682. doi: 10.1126/science.1226028

Wang, F., Dai, J., Daum, J. R., Niedzialkowska, E., Benerjee, B., Stukenberg, P. T., et al. J., and Higgins JMG, (2010). Histone H3 Thr-3 phosphorylation by Haspin positions Aurora B at centromeres in mitosis. *Science* 330, 231–235. doi: 10.1126/science.1189435

Wang, F., Ulyanova, N., van der Waal, M. S., Patnaik, D., Lens, S. M., and Higgins, J. M. G. (2011). A positive feedback loop involving Haspin and Aurora B promotes CPC accumulation at centromeres in mitosis. *Curr. Biol.* 21, 1061–1069. doi: 10.1016/j.cub.2011.05.016

Wicky, S., Tjandra, H., Schieltz, D., Yates, J., and Kellogg, D. R. (2011). The Zds proteins control entry into mitosis and target protein phosphatase 2A to the Cdc25 phosphatase. *Mol. Biol. Cell.* 22, 20–32. doi: 10.1091/mbc.e10-06-0487

Yamagishi, Y., Honda, T., Tanno, Y., and Watanabe, Y. (2010). Two histone marks establish the inner centromere and chromosome bi-orientation. *Science* 330, 239–243. doi: 10.1126/science.1194498

Zheng, Y., Cerione, R., and Bender, A. (1994). Control of the yeast bud-site assembly GTPase Cdc42. Catalysis of guanine nucleotide exchange by Cdc24 and stimulation of GTPase activity by Bem3. *J. Biol. Chem.* 269, 2369–2372. doi: 10.1016/S0021-9258(17)41953-3

Zhou, L., Tian, X., Zhu, C., Wang, F., and Higgins, J. M. G. (2014). Polo-like kinase-1 triggers histone phosphorylation by Haspin in mitosis. *EMBO Rep*. 15, 273–281. doi: 10.1002/embr.201338080

Conflict of Interest: The authors declare that the research was conducted in the absence of any commercial or financial relationships that could be construed as a potential conflict of interest.

frontiers in Cell and Developmental Biology

ORIGINAL RESEARCH
published: 09 February 2021
doi: 10.3389/fcell.2021.619596

Differential Thresholds of Proteasome Activation Reveal Two Separable Mechanisms of Sensory Organ Polarization in *C. elegans*

*Patricia Kunz, Christina Lehmann and Christian Pohl**†*

Buchmann Institute for Molecular Life Sciences and Institute of Biochemistry II, Medical Faculty, Goethe University Frankfurt, Frankfurt, Germany

OPEN ACCESS

Edited by:
Zhiyi Lv,
Ocean University of China, China

Reviewed by:
Jeff Hardin,
University of Wisconsin-Madison, United States
Rodrigo Franco,
University of Nebraska-Lincoln, United States

***Correspondence:**
Christian Pohl
pohl@em.uni-frankfurt.de

†Present address:
Christian Pohl,
Discovery Biology – Neuroscience, AbbVie Deutschland GmbH & Co KG, Ludwigshafen, Germany

Specialty section:
This article was submitted to Signaling, a section of the journal Frontiers in Cell and Developmental Biology

Received: *20 October 2020*
Accepted: *19 January 2021*
Published: *09 February 2021*

Citation:
Kunz P, Lehmann C and Pohl C (2021) Differential Thresholds of Proteasome Activation Reveal Two Separable Mechanisms of Sensory Organ Polarization in C. elegans. Front. Cell Dev. Biol. 9:619596. doi: 10.3389/fcell.2021.619596

Cephalization is a major innovation of animal evolution and implies a synchronization of nervous system, mouth, and foregut polarization to align alimentary tract and sensomotoric system for effective foraging. However, the underlying integration of morphogenetic programs is poorly understood. Here, we show that invagination of neuroectoderm through *de novo* polarization and apical constriction creates the mouth opening in the *Caenorhabditis elegans* embryo. Simultaneously, all 18 juxta-oral sensory organ dendritic tips become symmetrically positioned around the mouth: While the two bilaterally symmetric amphid sensilla endings are towed to the mouth opening, labial and cephalic sensilla become positioned independently. Dendrite towing is enabled by the pre-polarized sensory amphid pores intercalating into the leading edge of the anteriorly migrating epidermal sheet, while apical constriction-mediated cell–cell re-arrangements mediate positioning of all other sensory organs. These two processes can be separated by gradual inactivation of the 26S proteasome activator, RPN-6.1. Moreover, RPN-6.1 also shows a dose-dependent requirement for maintenance of coordinated apical polarization of other organs with apical lumen, the pharynx, and the intestine. Thus, our data unveil integration of morphogenetic programs during the coordination of alimentary tract and sensory organ formation and suggest that this process requires tight control of ubiquitin-dependent protein degradation.

Keywords: sensory organ development, apical polarity, dendrite morphogenesis, proteasome, apical constriction, collective cell migration

INTRODUCTION

Through sensory organs, animals can receive stimuli and transduce these to the nervous system to bring about a physiological change or behavioral response (Schmidt-Rhaesa, 2007). The most common form of sensory organs is cellular extensions such as microvilli and cilia, which harbor specific mechano-, chemo-, photo-, or thermoreceptors. Nematoda like Tardigrada and Euarthropoda use cuticular ciliary receptors. In the case of nematodes, these are either cuticular extensions (bristles/bristle-like structures) or cuticular pores. The nematode *Caenorhabditis elegans* exclusively uses cuticular pores where ciliated tips of sensory neuron dendrites either end in a

cuticular channel that is connected to the exterior, project into a cuticular cavity, or end in a juxta-cuticular glial pocket (Altun and Hall, 2010).

The morphogenesis of *C. elegans* sensory organ dendrites is poorly understood. It has been initially suggested that "anterior neurons move toward the tip of the head, and the rudiments of the sensilla are formed; the neurons then move posteriorly again, sensory cell bodies laying down their dendritic processes as they go" (Sulston et al., 1983). This idea has been revisited a decade ago, and the morphogenetic mechanism of retrograde extension has been coined to describe this presumably particular mode of dendrite morphogenesis utilized here (Heiman and Shaham, 2009). In this mechanism, neurons tether their dendritic tips first anteriorly and then dendrites passively extend through the migration of posteriorly positioned neuron cell bodies in the opposite direction. It has been shown that a tight interaction between glia, their associated neurons and the surrounding epidermis is possible since both glia and neurons exhibit properties of epithelial cells that allow them to integrate into the surrounding epithelium (Low et al., 2019). Importantly, this mechanism was proposed specifically for the amphid sensilla, a bilateral pair of sensory organs both containing 12 sensory neuron dendrites (Altun and Hall, 2010). It has been suggested that although amphid sensilla dendrite morphogenesis requires anchoring of dendritic tips, the extension of dendrites is not driven by neuron migration but by towing of dendritic tips through the epidermis (Fan et al., 2019; Low et al., 2019). This is highly consistent with the timing of epidermal morphogenesis: The amphid sensory pore is embedded within the epidermis and connected to it through adherens junctions (Perkins et al., 1986). During embryonic elongation, which is driven by the epidermis, the amphid sensilla gain their specific elongated shape by establishing a connection to the epidermal sheet right before epidermal migration events occur (Fan et al., 2019). This connection is maintained during head enclosure (during which the epidermis encloses the anterior third of the embryo in a collective migration event) (Chisholm and Hardin, 2005). The connection between epidermis and dendritic tips requires DYF-7 (an extracellular protein required for anchoring), FRM-2 (a EPBL/moe/Yurt ortholog) (Low et al., 2019), SAX-7 (L1-type CAM), HMR-1 (E-cadherin), and DLG-1 (discs large) (Fan et al., 2019). In addition, it has been shown for arborized mechanosensory dendrites in *C. elegans* that the epidermis itself actively patterns dendritic morphogenesis, which, among other factors, also requires the cell adhesion molecule SAX-7 (reviewed in Yang and Chien, 2019). Taken together, the most recently proposed morphogenetic mechanism for amphid dendrites, dendrite towing, involves the neighboring tissue, the epidermis (Fan et al., 2019). This is in stark contrast to the retrograde extension mechanism proposed earlier (Heiman and Shaham, 2009). However, dendrite towing bears strong similarities to the morphogenetic mechanism described for a different sensory organ, the lateral line in zebrafish. Here, axonal growth cones co-migrate with their target cells, while their cell bodies remain stationary behind (Metcalfe, 1985). This has later been confirmed by time-lapse imaging and has been coined axon towing (Gilmour et al., 2004).

A presumably similar morphogenetic process to amphid sensilla formation has been previously described in *C. elegans*: In the male, the morphogenesis of a pair of prong-like sensory structures, called the copulatory spicules (Lints and Hall, 2009), is driven by the spicule socket cell. This socket cell guides the collective cellular movement that leads to the elongation of this sensory organ. The socket cell also creates the cuticular pore in which spicule dendrites end (Jiang and Sternberg, 1999). However, the relationship between socket cell migration and sensory dendrite elongation has not been addressed so far.

Notwithstanding a potential similarity of amphid to spicule dendrite morphogenesis, the mechanism of dendrite morphogenesis for the other 16 sensory organs of the head, the cephalic, and the inner and outer labial sensilla has not been addressed in any detail so far. It has been originally proposed that tissue folding might be involved: "a depression appears in the tip of the head; this does not involve morphogenetic cell death, and is presumably a way of providing more surface area for the sensilla" (Sulston et al., 1983). This suggests that a morphogenetic mechanism seems to be involved that can mediate tissue invagination. Tissue invagination during development often requires apical constriction as morphogenetic mechanism (Hunter and Fernandez-Gonzalez, 2017). Apical constriction can drive collective cellular re-arrangements through the polarized activation of actomyosin contractility, which has been characterized in *C. elegans* for gastrulation (Harrell and Goldstein, 2011; Pohl et al., 2012), ventral enclosure (Wernike et al., 2016), and pharynx morphogenesis (Rasmussen et al., 2012). The topological outcome of apical constriction is variable: It leads to scar-less cell internalization during gastrulation due to the lack of polarized junctions at this stage (Pohl et al., 2012), it induces cyst formation during pharynx morphogenesis (Rasmussen et al., 2012), and it often leads to the formation of tissue folds in other developing organisms (Hunter and Fernandez-Gonzalez, 2017).

During nervous system morphogenesis and dendrite morphogenesis in particular, substantial cellular remodeling has to occur. Such remodeling entails targeted degradation of proteins, protein complexes, and organelles, which can be brought about by the ubiquitin-proteasome system (UPS) or autophagy, respectively. It has been established that autophagy and the UPS are key contributors to neuron morphogenesis (Hamilton and Zito, 2013; Stavoe and Holzbaur, 2019). Inhibition of the proteasome, for instance, prevents neurite outgrowth (Laser et al., 2003) and proteasomes control axon and dendrite morphogenesis (Hamilton et al., 2012; Hsu et al., 2015). Moreover, the activity of the proteasome can be regulated by proteasome subunits that act as linking factors for the two main proteasomal subcomplexes, the 20S core and the 19S lid. It has become clear that the 19S component Rpn6/PSMD11 acts as a key regulator in this respect: Rpn6 stabilizes the otherwise weak interactions between the 19S lid and the alpha ATPase rings of the 20S proteolytic core (Pathare et al., 2012) and can be activated by stimulus-dependent phosphorylation (VerPlank et al., 2019). For instance, Rpn6-dependent regulation of proteasome activity has been documented for aging of the sub-ventricular zone (Wang et al., 2016). Looking beyond

neuro-morphogenesis, Rpn6 seems to be generally involved in developmental decisions as it is required for efficient myofibroblast differentiation (Semren et al., 2015) and has to be down-regulated during drought stress in plants (Cho et al., 2015). Moreover, null alleles of *rpn6* in Drosophila (*l(2)k00103* and *rpn62F*) support embryo development; however, hatched larvae die at early stages, and it has been argued that this is due to an additive effect on cell proliferation rather than a distinct disruption of development (Lier and Paululat, 2002). This is similar in *C. elegans*, where RNAi of *rpn-6.1* has been shown to lead to substantial lethality with only 3% of embryos hatching (Takahashi et al., 2002). Importantly, it has been shown that increased levels of RPN-6.1 can protect animals from proteotoxic stress (Vilchez et al., 2012). However, the role of *rpn-6.1* in *C. elegans* morphogenesis has not been addressed yet.

Here, we investigate the mechanism of sensory organ dendrite morphogenesis during late stages of *C. elegans* embryogenesis. Specifically, we revisit observations originally made when determining the lineage of *C. elegans* (Sulston et al., 1983). We demonstrate that the mouth forms synchronously with overt morphogenesis of pharynx and nervous system. While the pharynx constricts, mouth and neuro-ectodermal cells invaginate at the anterior tip of the embryo through apical constriction. Remarkably, tissue invagination during mouth formation leads to movement of sensory organ endings on the surface of the head to their final positions at the tip of the embryo. In case of the amphid sensory organ, dendrite elongation occurs through the previously characterized mechanism of dendrite towing. However, unlike proposed earlier, sheath and socket glia cells seem to differentially contribute to towing. For all other head sensory organs, cell shape changes through *de novo* apical polarization, and subsequent apical constriction mediates their centripetal movement and symmetric placement of their juxta-oral, anterior endings. We show that these two processes not only occur through different morphogenetic mechanisms, we also uncover that they show a differential sensitivity to reduced proteasome activity. While amphid dendrite towing is highly sensitive to depletion of the key proteasome activator, RPN-6.1, apical constriction-dependent morphogenesis of all other sensory organs is much less sensitive. We reveal that other morphogenetic processes that are sensitive to RPN-6.1 depletion also involve *de novo* apical polarization. Hence, our results show that different morphogenetic mechanisms can couple epidermal morphogenesis to dendritic patterning and that these different mechanisms can be separated through titration of proteasome activity.

MATERIALS AND METHODS

Caenorhabditis elegans Strain Maintenance

Strains used in this study were cultivated on NGM agar plates (Brenner, 1974) at 20–25°C feeding on OP50. Strain designations and genotypes are listed in **Supplementary Materials**.

Mounting of Embryos

Embryos were mounted as described previously (Dutta et al., 2015), and time-lapse analysis was performed during the stages of early lima bean to 1.5-fold elongation. For imaging of head-on view embryos, we used Cellview cell culture dishes (Greiner Bio-One GmbH, Germany). All compartments of the dish were filled with M9. Embryos were arranged in one compartment, and 1 μl diluted 45.0 μm polystyrene microspheres (Polysciences, Inc., Warrington, PA, United States) were added. Embryos were positioned head-on through moving them with an eye lash within the M9 solution.

Long-Term Imaging

Imaging was executed with a VisiScope spinning disk confocal microscope system (Visitron Systems, Puchheim, Germany). The system consists of a Leica DMI6000B inverted microscope, a Yokogawa CSU X1 scan head, and a Hamamatsu ImagEM EM-CCD. Z-sectioning was performed with a Piezo-driven motorized stage (Applied Scientific Instrumentation, Eugene, OR, United States) using a Leica HC PL APO 63X/1,4-0,6 oil objective. All acquisitions were performed at 20–23°C.

For most experiments, we collected z-stacks with 45 steps at 1.0 μm distance each with 2, 3, 4, or 5 min intervals, respectively, for a total duration of 1–3 h for acquiring early lima bean to 1.5-fold stage embryos. For imaging of the head-on-view, we used 3–4 min intervals to avoid tipping of embryos. For lineaging, we performed long-term imaging for 250 time points at 3 min intervals and with z sampling of 1 μm over a distance of 30 μm. For acquiring of embryos for one time point before and a time-lapse series after UV laser ablation, we used 2 min intervals and z sampling at 1 μm over a distance of 40–45 μm.

UV Laser Ablation

For UV Laser ablation, we used a MLC03A-DPI VS-FRAP-control and VS-Laser Control system (Visitron Systems GmbH, Puchheim, Germany). For ablation of the AM pores, we positioned the UV laser at a PAR-6:GFP marked pore with 5 ms frap time per pixel with a target area diameter matching the diameter of the pore. Epidermal ablation was executed in proximity of the AM pore at a focal layer of ABDvab-10:mCherry marked epidermal tissue with 10 ms frap time per pixel in a wider diameter then for pore ablation. The laser was controlled manually by applying 3–8 frap cycles. All UV laser ablations were performed unilaterally, leaving the other side of the embryo intact as an internal control. We only took embryos into account, which were developing after laser ablation and where the morphogenesis of the AM dendrites on the non-ablated side was not affected.

RNA Interference

We used the clone F57B9.10 from a commercially available library (Rual et al., 2004). On day 1 the clone was streaked on LB-ampicillin plates and cultured over night at 37°C. The next day a single clone was picked from the plate and cultivated over night at 37°C in LB-ampicillin. On day 3, the plasmid

was extracted, and the sequence was verified through Sanger sequencing (using forward 5′-GTTTTCCCAGTCACGACGTT-3′ and reverse primer 5′-TGGATAACCGTATTACCGCC-3′). Afterward, the plasmid was amplified by PCR with a T7 primer (5′-TAATACGACTCACTATAGGG-3′). The PCR product was purified and transcribed into dsRNA (AmpliScribe T7 High Yield, Epicentre, Madison, WI, United States). Then, we diluted the dsRNA solution to the desired concentration in DEPC-treated M9 buffer.

For dsRNA injection, we prepared 2% agarose injection pads. These pads were dried at 37°C. Injection needles were pulled from borosilicate capillaries (Kwik-Fil 1B100F-4, World Precision Instruments, Sarasota, FL, United States) with a P-97 Flaming/Brown micropipette puller (Sutter Instruments, Novato, CA, United States) to obtain tapered, closed tips. After centrifugation, 1 μl of the dsRNA solution was filled into the injection needle. Afterward, the needle tip was broken open manually and the dsRNA solution injected into the ovaries of young adult *C. elegans*. For this, animals were positioned onto an agarose pad and immersed with a drop of halocarbon oil 700 (Sigma Aldrich, Steinheim, Germany). Injection of the dsRNA was accomplished with a Leica DMIL LED microscope with a 40×/0.75 PH2 air objective and Hoffman modulation contrast (Leica Microsystems, Wetzlar, Germany), a SMX micromanipulator (Sensapex Oy, Oulu, Finland), a MINJ-1 microinjector with a MINJ-4 needle holder (Tritech Research, Inc., Los Angeles, CA, United States), and an Einhell compressor (Einhell AG, Landau, Germany). For injection, we used 50–60 psi pressure and 1–8 injection cycles per animal. Animals were recovered in a drop of M9 on an OP50 seeded plate over night at 20°C. F1 offspring from injected animals was analyzed by imaging throughout the next day. We excluded embryos with obvious abnormalities, e.g., vacuoles, loss of marker signal, or extremely strong developmental defects. These embryos accounted for ∼30% of cases. The remaining ∼70% were analyzed by microscopy. Due to incomplete penetrance, we include a detailed quantification of phenotypes.

Measurements and Lineaging

Movement of sensory organ pores was quantified in Fiji (ImageJ) (Schindelin et al., 2012) using a linear measuring tool. Specifically, we used maximum intensity *z*-stack projections of time lapse image series with a resolution of 7 pixels per μm. We measured movement length of pores or neurite tips every second or fifth time point relative to the position of the arcade cells' apical anterior front, which becomes the most anterior, trackable part of the mouth. The length of the neurites was measured from the anterior border of their cell bodies to the tip of the neurites (directly adjacent to the AM pores). The position of AM cell bodies was analyzed through measuring the distance from the middle of the AM cell body assembly to the apical anterior front of arcade cells. All measurements were normalized to the length of each individual embryo. Tracking of arcade morphogenesis and lineaging of AM organ development was performed manually, by tracking apical surfaces and cell membranes or by tracking nuclei from four-cell stage embryos in time-lapse *z*-stacks and manual highlighting tracked structures in Fiji. Statistical analysis [two-way ANOVA and two-stage linear step-up procedure (Benjamnini, Kreiger, and Yekutieli)] was performed in GraphPad Prism 9 (for details of ANOVA statistics, see **Supplementary Material**).

RESULTS

Amphid Pores Move Simultaneously With All Superficial Pores

At the tip of the *C. elegans* head, a total of 18 epithelial sense organs, composed of ciliated dendritic endings of bipolar sensory neurons ensheathed by a single sheath (proximal) and one or more socket glia (at the distal end), can be found (Altun and Hall, 2010). They comprise sensilla, symmetrically positioned around the mouth: A bilateral pair of amphid (AM) sensilla, the four-fold symmetric cephalic (CEP), and the six-fold symmetric inner (IL) and outer labial sensilla (lateral outer labial, OLL; quadrant outer labial, OLQ, which are adjacent to the CEP sensilla). Since all these sensilla require an apical lumen for the dendrite endings of sensory neurons to integrate into or penetrate through the cuticle, we reasoned that apical polarity factors (aPARs, abnormal embryonic PARtitioning of cytoplasm) should highlight them. Accordingly, we found that PAR-3 (see below; using *it298[par-3:GFP]* and PAR-6 (using different markers: *xnIs3[par-6:PAR-6:GFP]*; *it319[par-6:GFP]*; *asIx1928[par-6:mCherry:PAR-6]*) (see also **Supplementary Materials**) not only highlight apical polarization of tubular organs (intestine, rectum, excretory pore) at this stage but also highlight all socket cells (pores) of these sensilla (**Figure 1A** and **Supplementary Video 1**). Remarkably, apical polarization of all structures that open on the surface of the embryo, including the mouth (see below), bilateral anterior deirid sensilla (data not shown), the excretory pore, the rectum, and the bilateral phasmid sensilla also occur simultaneously. Sheath cells do not seem to undergo apical polarization along their extensions that ensheath sensory neuron dendrites. The posterior deirid sensilla pores are not highlighted since they are only present at the L2 larval stage (Altun and Hall, 2010). At the same time, when the elongation of the embryo starts, the AM, IL, OLQ, OLL, and CEP sensilla pores move anteriorly to become symmetrically positioned around the prospective mouth (**Figure 1A** superimposition and **Supplementary Video 1**). The amphid pores start the movement from the most posterior-lateral position and follow the other pores at a distance to reach their final position, which is posterior-lateral relative to the other sensilla pores. Together with the pores, the anterior epidermal cell hyp4 also moves anteriorly (**Figure 1A**, bottom panel), demonstrating that sensilla pore movement occurs during head enclosure (see below).

Sensory Organ Assembly Through Complex Cell Trajectories

The amphid sensillum is composed of the socket cell (AMso), the sheath cell (AMsh) and neuronal cell dendritic tips (of the ASE, ASG, ASH, ASI, ASJ, ASK, ADF, and ADL neurons). Its apical part has been shown to be completely embedded in

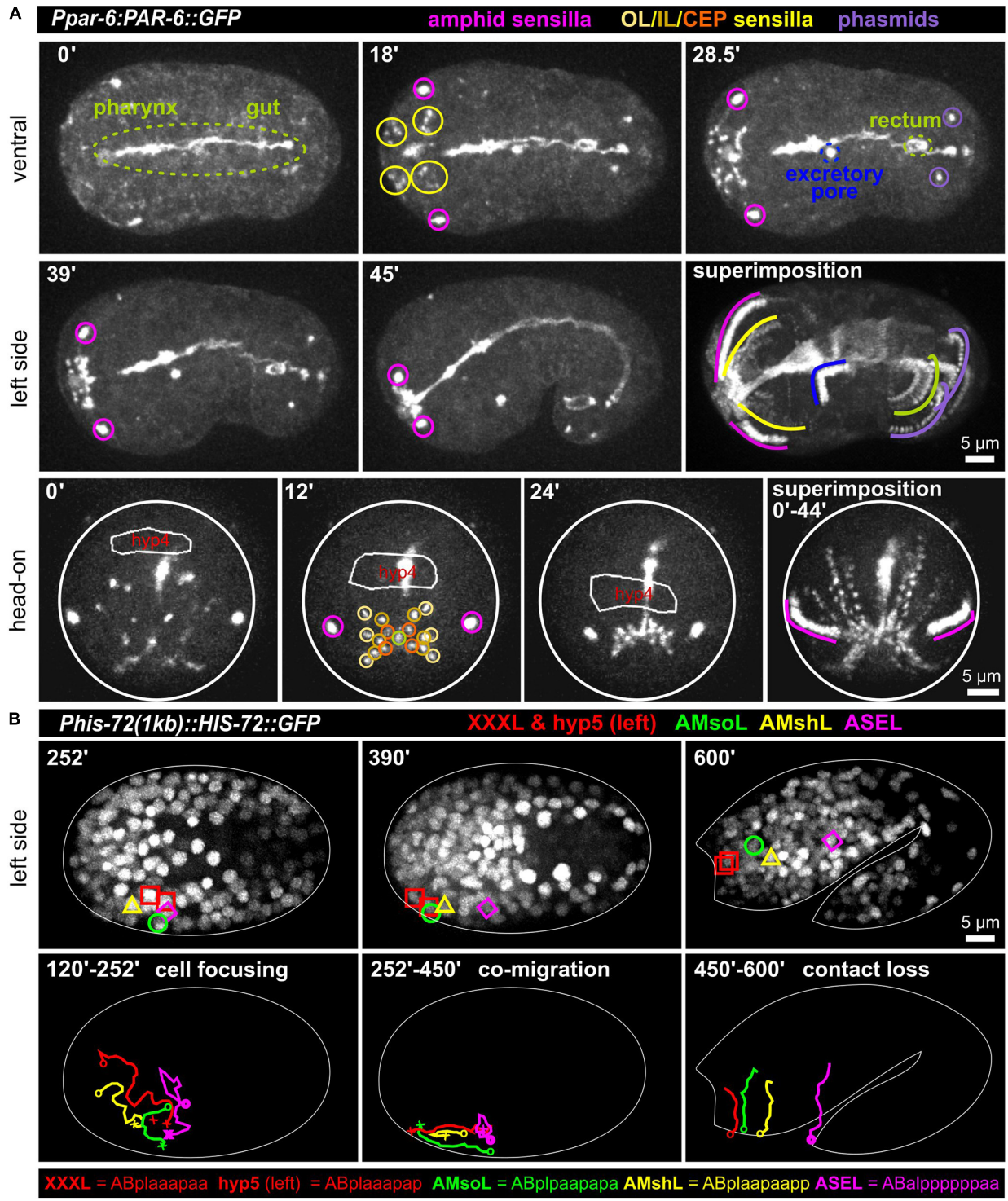

FIGURE 1 | Simultaneous polarization and movement of apical pores in *C. elegans* during embryonic elongation. **(A)** Maximum intensity projections of stacks of confocal images from time lapse recordings of ventral (top), left side (middle), and head-on (bottom) views of wt embryos expressing PAR-6:GFP, highlighting the anterior directed movements of the amphid, outer labial (OL), inner labial (IL), cephalic (CEP), and phasmid sensilla pores during lima bean to 1.5-fold stage. See also **Supplementary Video 1**. PAR-6:GFP additionally highlights pharynx, gut, rectum, and the excretory pore. In the head-on view, the anterior-most hypodermal cell is traced (hyp4, traced based on a membrane marker which is not shown for clarity). **(B)** Maximum intensity projections of stacks of confocal images from time lapse recordings of lateral (left side) views of a representative wt embryo expressing GFP-marked histones from lima bean to twofold stage. Movement of the XXXL, hyp5 (hypodermal cell), AMsoL (amphid socket left), AMshL (amphid sheath left), and ASEL (amphid neuron cell body) are lineaged. Images in panel **(B)** required time-dependent brightness adjustment due to onset and increased expression of the histone from its zygotic promoter. See also **Supplementary Video 2**.

the epidermis (and later in the cuticle). To better understand its developmental trajectory, we lineage traced AM sensillum cells (using the ASE neuron as an example for AM neurons) and the two adjacent anterior-most epidermal cells (XXX and hyp5, XXX later delaminates and forms a neuron-like cell; Altun and Hall, 2009a) during the early lima bean to the twofold stage of embryonic elongation (**Figure 1B** and **Supplementary Video 2**). We discovered complex trajectories that lead to focusing of all cells during mid-embryogenesis. After focusing, the epidermal cells hyp 5 and XXXL, AMso, and, at a small distance, AMsh move anteriorly. AMsh stops migrating already before the other cells do. Importantly, the ASE cell body does not move anteriorly with the other AM cells after focusing. Subsequently, the close contact between AM cells is lost, and, during elongation, cells adopt positions that resemble those known from larval/adult neuroanatomy. These observations show that the anterior movement of the amphid pores is coupled to the anterior migration of epidermal and socket glia cells while neuronal cells are stationary.

Coupling of Epidermal Migration and AM Pore Movement

Since AM sensilla are embedded in the epidermis, we wanted to clarify the role of head enclosure as part of the mechanism driving AM dendrite morphogenesis. Therefore, we investigated epidermal migration together with PAR-6, visualizing AM pores and the apical lumen of other pores and tubular organs. Consistent with what has been shown earlier (Fan et al., 2019; Low et al., 2019), at the beginning of the head enclosure, AM pores are forming laterally at the anterior epidermal front (**Figure 2A**, arrowheads and **Supplementary Video 3**). Together with progressive migration of the epidermal front, AM pores move anteriorly, finally reaching the prospective mouth at the end of epidermal enclosure (**Figure 2B**, arrowheads and **Supplementary Video 3**). To corroborate a physical link between epidermis and AM pores, we performed UV laser ablation of the epidermis directly adjacent to the AM pore (**Figure 2C** and **Supplementary Video 4**). We did so since our tracking analysis revealed that the epidermal hyp4 cell is among the first head epidermal cells to show marker expression from an epidermal promotor (*lin-26*; see also **Supplementary Materials**). Importantly, we designed our laser ablation experiments to not disturb epidermal migration and movement of the non-ablated AM pore on the other side of the embryo. By doing so, we found head enclosure by the epidermis to be uncoupled from AM pore movement. AM pore movement stops after ablation while epidermal migration is largely not affected (**Figures 2C,D**, yellow arrowheads and **Supplementary Video 4**). We conclude that a physical connection between the AM pore and the migrating epidermal tissue is essential for correct positioning of AM dendrite tips. However, our analysis also revealed that the movement of the remaining sensilla pores of the head is not directly coupled to the spreading of the epidermis over the head. Instead, these sensilla pores always form and move in front of the epidermal edge to obtain their final symmetric position (**Figures 2B,E** and **Supplementary Video 3**).

Coupling of Epidermis Migration to AM Dendrite Elongation

To further corroborate that AM dendritic tips move together with AM pores, we constructed strains that allowed us to monitor dendrite morphogenesis directly and together with epidermal sheet or pore movement. We found that microRNA promotor strains constructed previously (*mjIs27 [mir-124p:GFP + lin-15(+)]* and; *mjEx142 [mir-124p:mCherry];* Clark et al., 2010) are perfectly suited to monitor AM sensory organ dendrite morphogenesis. Specifically, this reporter is expressed in many AM neurons embedded in the AM pore (ASE, ASH, ASI, ASK) and AM neurons associated with the AM sheath (AWA, AWB, AWC). This reporter is also expressed in a limited set of other neurons with ciliated dendrites, an IL neuron (IL1) and – much weaker – phasmid neurons (PHA, PHB) (**Supplementary Video 5**). We found that expression of the reporter starts shortly after ciliated neurons are born, which is at the beginning of epidermal morphogenesis (ventral closure; **Figure 3**, top panel and **Supplementary Video 6**). Subsequently, when the anterior edge of the epidermis extends over the AM neuron cell bodies, dendrites and their sensory tips can be clearly discriminated (**Figure 3**, middle and bottom, arrowheads and **Supplementary Video 6**, white arrowheads). Consistent with the tracking data (**Figure 1B** and **Supplementary Video 2**) and the analysis of pore movement (**Figure 2** and **Supplementary Video 3**), we observed a coupled movement of AM pores together with AM neuron dendritic tips (**Figure 4A**, arrowheads and **Supplementary Video 5**). While pores and dendritic tips move, neuron cell bodies stay stationary (**Figure 4C**, right panel). Thus, the movement of the pore seems directly coupled to dendrite elongation, which is also apparent from quantifications of pore movement and dendrite elongation (**Figure 4C**, left and middle panel). Moreover, in contrast to AM pore movement, the pores of all other sensory organs also move at that time (**Figure 4A**, dashed lines and **Supplementary Video 6**), however, they are always ahead of the epidermal border (**Figure 2**). To corroborate the coupling of epidermal migration and dendrite elongation, we again performed UV laser ablation, in this case, we ablated one of the AM pores. Ablation caused dendrite elongation arrest while the neurites on the control side elongated normally to the prospective mouth (**Figures 4B,D** and **Supplementary Video 7**). Notably, the remaining part of the pore and dendrites stayed associated and dendrites arrested during elongation; neurons of ablated AM organs even formed commissures (**Figure 4B**, blue arrowhead and **Supplementary Video 7**). This clarifies that the ablation of epidermis or AM pores does not destroy the whole sensory organ architecture but is specific for the targeted area and does not interfere with other aspects of its development.

Taken together, we conclude that head enclosure by the epidermis, AM pore movement and the elongation of AM dendrites are connected morphogenetic processes. We infer that AM dendrites are elongated trough the migration of the epidermis-attached AM pores while all AM neural cell bodies stay stationary. These findings are generally consistent with recent reports (Fan et al., 2019; Low et al., 2019) but are difficult to

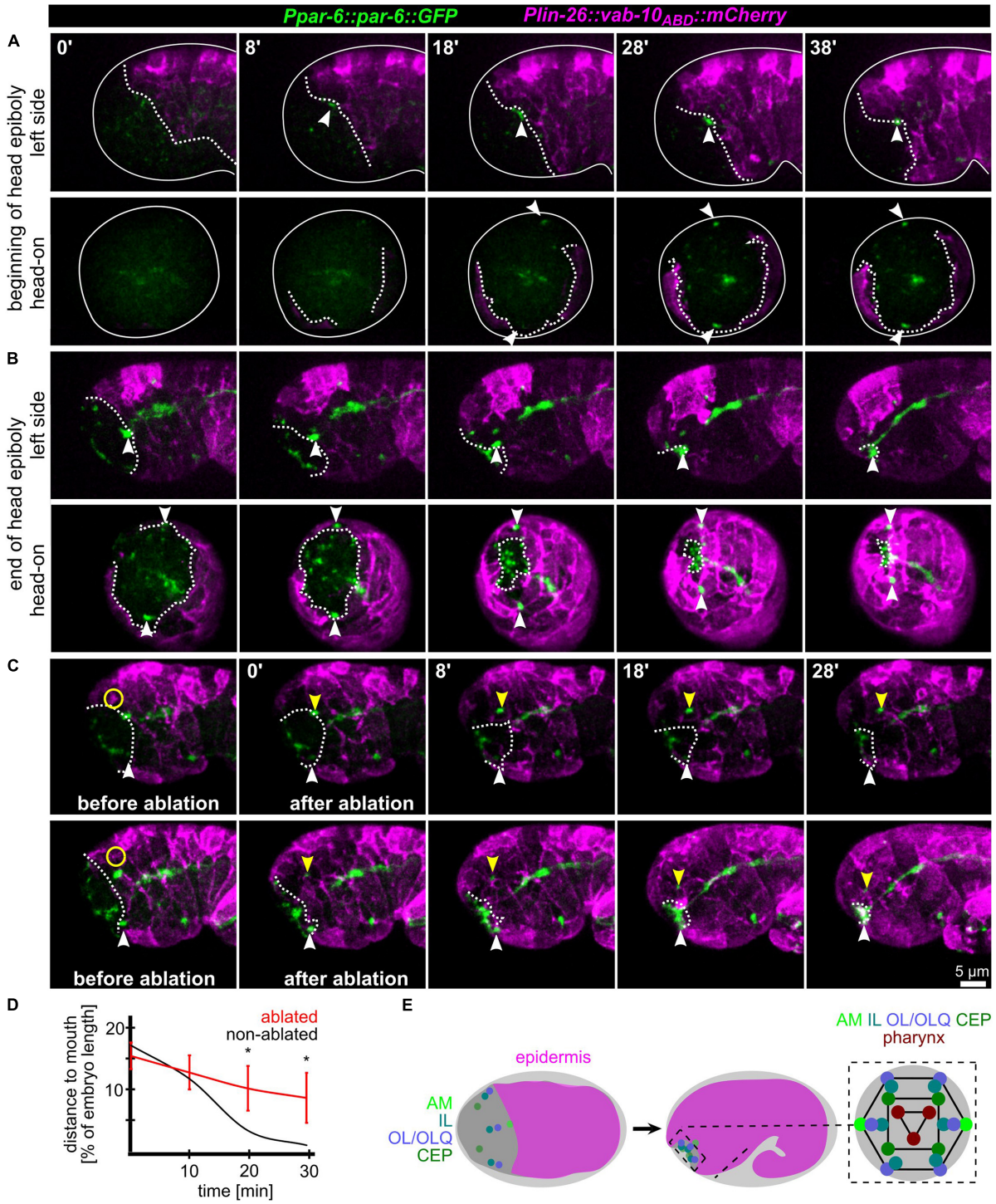

FIGURE 2 | Epidermis migration and AM pore movement. **(A)** Maximum intensity projections of stacks of confocal images from time lapse recordings of left (top) and head-on (bottom) views of epidermis movement and movement of AM pores during lima bean stage. See also **Supplementary Video 3**. **(B)** Same as panel **(A)**, however, stage is lima bean to 1.5-fold stage. **(C)** Lateral view of embryos before and after UV laser ablation of the epidermis close to the AM pore. White dashed lines highlight the epidermal front. White arrowheads point to the position of the AM pore, and yellow arrowheads mark the position of the pore close to the ablated epidermis. Yellow circle marks the position of the laser ablation. See also **Supplementary Video 4**. **(D)** Quantification of epidermis ablation experiments ($n = 4$). The relative distance of the ablated (red) and un-ablated (black) AM pores to the mouth was measured. *P*-values from a multiple unpaired t-test and with two-stage linear step-up procedure (Benjamnini, Kreiger, and Yekutieli) are shown (*≥0.05; **≥0.01). **(E)** Left and middle: Schematic depicting the spreading of the epidermis around the head (head enclosure) and the initial and final positions of the sensory organ pores. Note that only the AM pores are located at the anterior epidermal edge. Right: Schematic depicting a juxta-oral cross section that highlights the symmetry of sensory organ pores and the symmetry of the pharynx.

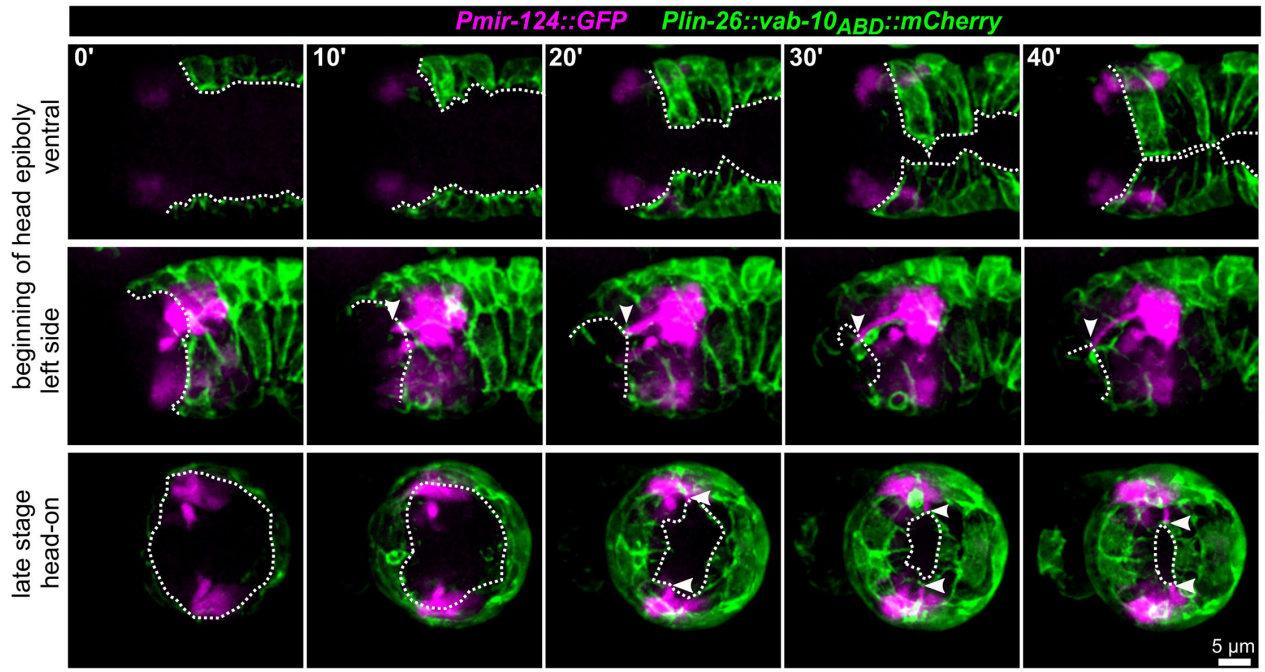

FIGURE 3 | Epidermal enclosure and AM dendrite extension. Maximum intensity projections of stacks of confocal images from time lapse recordings of ventral (top), left side (middle), and head-on (bottom) view of wt embryos from lima-bean to 1.5-old stage. AM cell bodies and dendrites are highlighted in magenta and the epidermis in green. White arrowheads point to the position of AM dendrite tips at the anterior edge of the epidermis. White dashed lines mark the anterior and ventral edges of the epidermal sheet. See also **Supplementary Video 5**.

reconcile with AM dendrite morphogenesis through retrograde extension (Heiman and Shaham, 2009).

Depletion of RPN-6 Disrupts AM Morphogenesis

It has been shown that components of the two main catabolic pathways, the UPS and autophagy, regulate transitions during *C. elegans* development (e.g., Zhang et al., 2009; Du et al., 2015). Especially, regulation of the oocyte-to-embryo transition is probably the best example for evolutionary conservation of UPS' role (Verlhac et al., 2010). Nevertheless, besides the oocyte-to-embryo transition and a thorough analysis of embryonic differentiation programs (Du et al., 2015), little is known about the role of the UPS in *C. elegans* morphogenesis. This is most likely due to targeting of the UPS having been considered to lead to pleiotropic developmental phenotypes. Motivated by pioneering work on specific roles of basal UPS factors in Drosophila neuro-morphogenesis (reviewed in Hegde and Upadhya, 2007), we decided to test roles of the UPS in *C. elegans* sensory organ morphogenesis. By happenstance, we first characterized the role of *C. elegans*' ortholog of Rpn6/PSMD11 for AM morphogenesis. RPN-6.1 is an evolutionarily highly conserved component of the 26S proteasome lid, which is crucial to connect the core and regulatory proteasomal subcomplexes (Pathare et al., 2012) and hence has been coined proteasome activator.

Even moderate depletion of RPN-6.1 by RNAi preserved expression of all markers used in this study (including apical, neuronal, and epidermal) and allowed us to rule out pleiotropic effects such as general problems in cell fate acquisition (see below). The first obvious phenotypes under these conditions are failures in AM pore movement and dendrite elongation (**Figures 5A,B** and **Supplementary Video 8**). Importantly, irrespective of impaired AM pore movement, all other sensilla pores move to the prospective mouth like in wt (**Figure 5B**, middle and bottom panel and **Supplementary Video 8**). Specifically, the AM pore on one side moves normally and its dendrite fully extends, while the AM pore on the other side of the same embryo either becomes stretched, moves only partially, dendritic tips detach from the pore (in some cases only the anterior part of an AM pore reaches the prospective mouth subsequently), or an AM pore fails to be properly established and move (**Figure 5B**, arrowheads in top panels). These phenotypes are striking in several ways: First, they reveal that the first vulnerability of embryonic development after depletion of RPN-6.1 is the proper spatiotemporal coordination of AM sensory organ morphogenesis; second, they show that titration of RPN-6.1 levels can result in stochastic, unilateral phenotypes; third, cell fates seem to be by and large unaffected, for instance, the ciliated neuron-specific marker expressed from the *mir-124* promotor does not show any changes (**Figure 5B**). Strong phenotypes after RPN-6.1 depletion include total arrest of AM pores while the pores of other sensilla still reach the prospective mouth (**Figure 5B**, middle panels). Here, AM neurites are also not migrating in a thick bundle like in wt but often show only thin and fragile connections to the AM pore. Very strong depletion

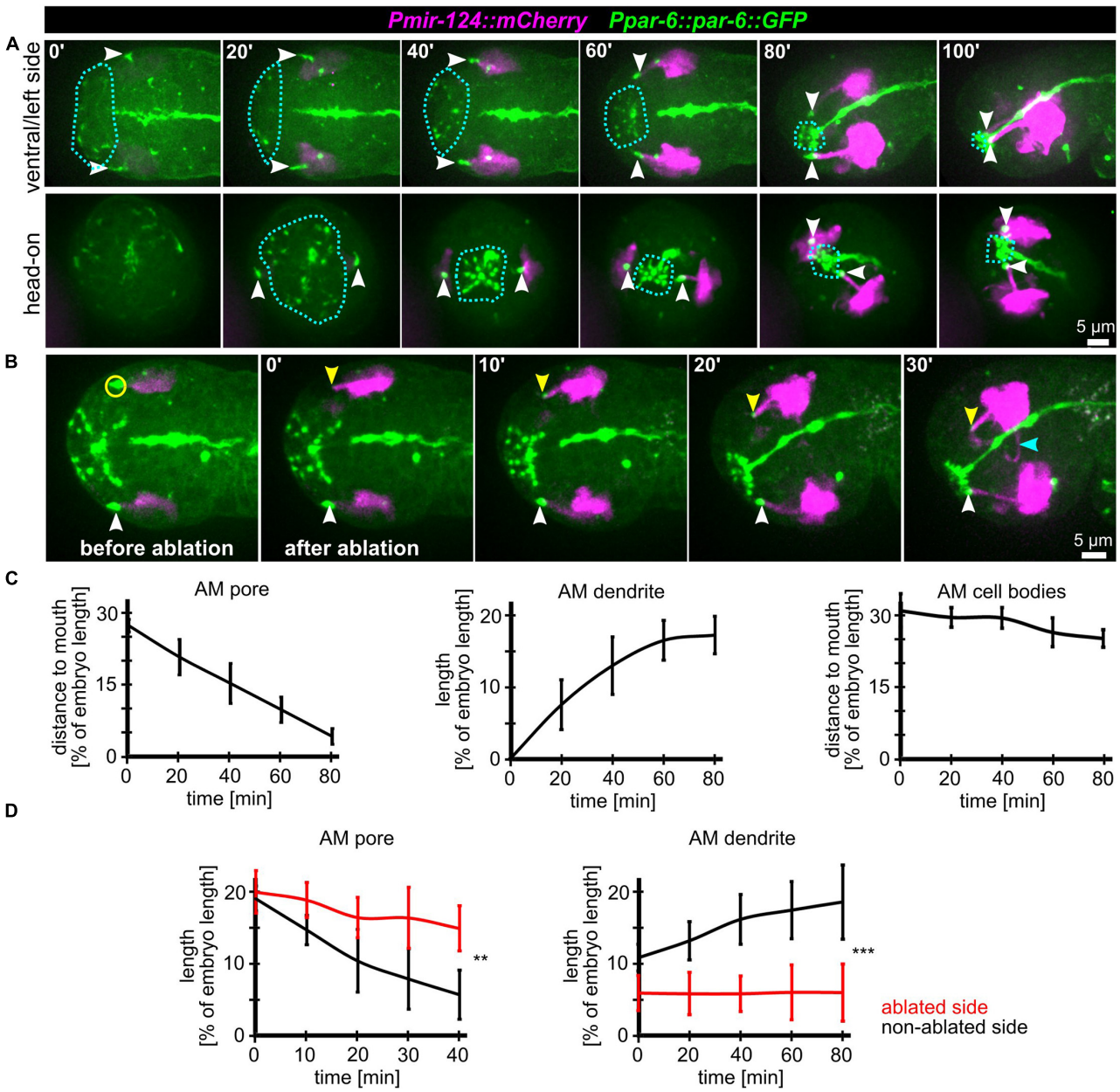

FIGURE 4 | Coupling of AM pore movement to AM dendrite elongation. **(A)** Maximum intensity projections of stacks of confocal images from time lapse recordings of ventral/left side (top) and head-on (bottom) view of wt embryos from lima-bean to 1.5-old stage. AM cell bodies and dendrites are marked in magenta, and pores and apical lumen of pharynx and intestine are marked in green. Dashed lines indicate the anterior epidermal edge. White arrowheads mark the AM pores. See also **Supplementary Video 6**. **(B)** Depictions as in A; ventral/left side view of a representative embryo before and after UV laser-ablation of one of the two AM pores. The ablated area is marked by a yellow circle, the non-ablated AM pore is marked by a white arrowhead, and the ablated AM pore is marked by a yellow arrowhead. See also **Supplementary Video 7**. **(C)** Quantifications of the distance of the AM pore to the mouth (left), AM dendrite elongation (middle) and position of the AM neuron cell bodies relative to the mouth (right) (n = 5). **(D)** Quantifications of AM pore movement (left) and AM dendrite length in embryos where one AM pore was UV laser ablated, and the pore or dendrite on the other side was measured as internal control (n = 5; ±SD; two-way ANOVA P; ** ≥ 0.01; *** ≥ 0.001).

results in a complete lack of sensilla pore movement including AM, CEP, OLQ, and IL pores (**Supplementary Video S12**). Quantification of moderate cases of RPN-6.1 depletion shows a highly significant perturbation of AM pore movement and, consistently, also a strong reduction of AM dendrite bundle extension (**Figure 5C**).

We further investigated whether the specific role of RPN-6.1 in sensory organ morphogenesis is linked to epidermal sheet migration during head enclosure. To do so, we evaluated different degrees of RPN-6.1 depletion. In cases of modest and moderate depletion of RPN-6.1, the epidermis still migrates anteriorly to cover the embryonal head like in wt

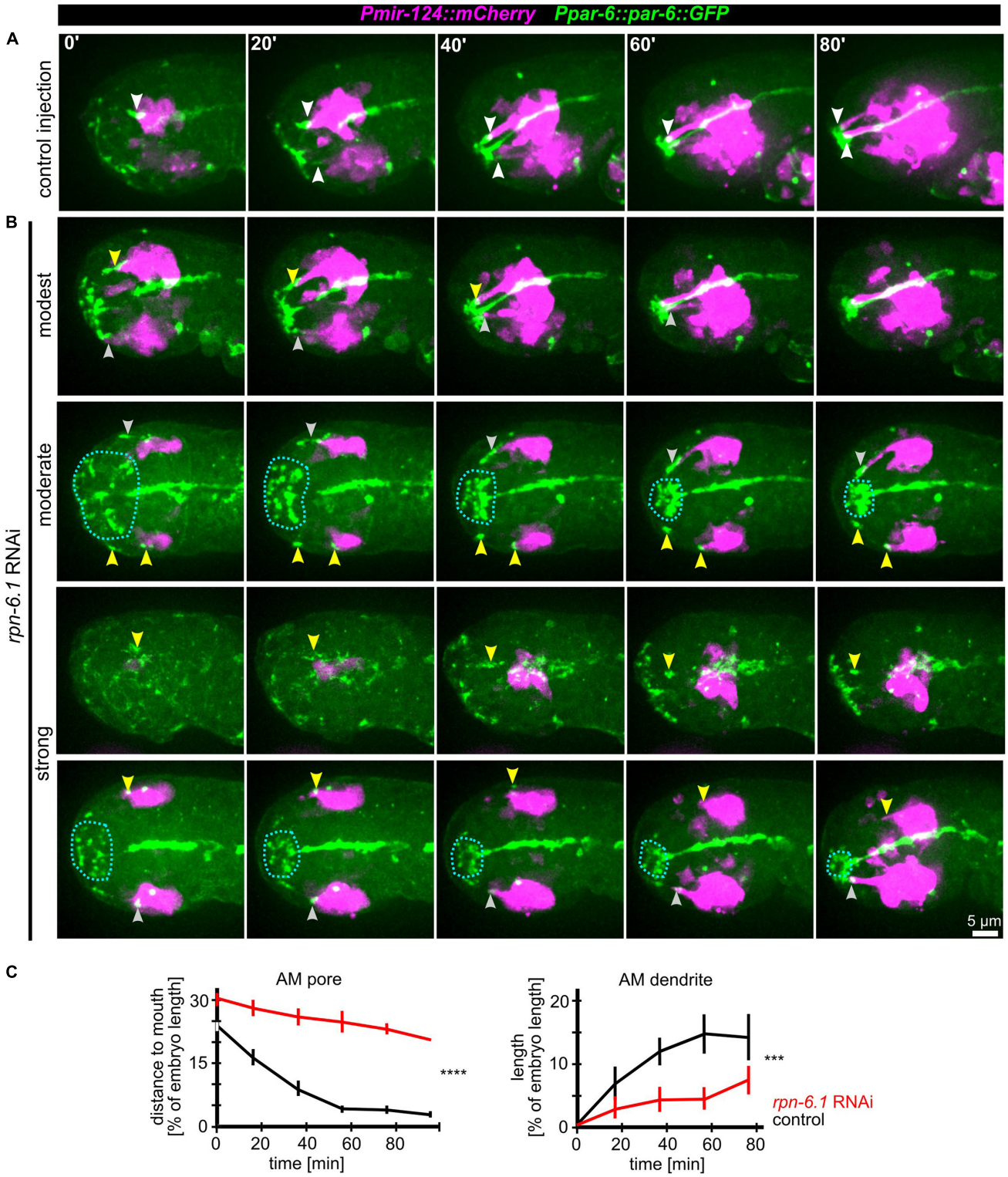

FIGURE 5 | RPN-6.1 is required for proper AM pore and dendrite morphogenesis. **(A)** Maximum intensity projections of stacks of confocal images from time lapse recordings of left side views of embryo after control injection illustrating the movement of the sensilla pores (green) correlated with elongation of the AM dendrites (magenta). White arrowheads point to AM pores/dendrite tips. **(B)** Depictions as in A, however, *rpn-6.1* RNAi embryos are shown. Injection of dsRNA leads to different levels of penetrance (from top to bottom). Yellow arrowheads highlight impaired AM pore and/or dendrite morphogenesis. See also **Supplementary Video 8**. **(C)** Quantification of the effects of *rpn-6.1* RNAi on AM pore movement (left) and on AM dendrite morphogenesis (right) ($n > 5$, ±SD; two-way ANOVA *P*; *** ≥ 0.001; **** ≥ 0.0001).

(**Supplementary Figures 1A,B**, top panels). Concomitantly, AM pores are stretched anteriorly (**Supplementary Figure 1B**, top panel). Often, AM pores split, the anterior part of the pore keeps moving to the prospective mouth and the posterior part arrests posteriorly (**Supplementary Figure S1B**, bottom panels).

Taken together, our analysis shows a graded response to RPN-6.1 depletion with AM sensory organ morphogenesis being affected, while epidermis and other sensory organs in the head are not affected after strong depletion.

RPN-6.1 Is Required for Proper Lumen Morphogenesis of the Alimentary System

Given the gradual phenotypes for AM pore movement from stretching to splitting and arrest, we reasoned that the morphogenetic role of RPN-6.1 seems to lie in the coordination of inter- or intra-epithelial cell-cell contact formation for cells undergoing apical polarization. Consistently, when we analyzed the remaining structures in the embryo that are polarizing at this stage of development (using the apical polarity factor PAR-6 as a marker), we observed that, in addition to AM pore-specific defects, the pharynx often lacks a connection to the mouth (**Figures 6A,B** and **Supplementary Video 9**). Additionally, in many of the embryos where pharynx and mouth are not properly connected, the intestine is often discontinuous (**Figure 6B**). Concordantly, in *rpn-6.1* RNAi embryos with alimentary system phenotypes, pharynx and intestine show a lack of aligned apical surfaces and frayed lumens. Similar to the lack of a connection of the pharynx with the mouth, the intestine is often

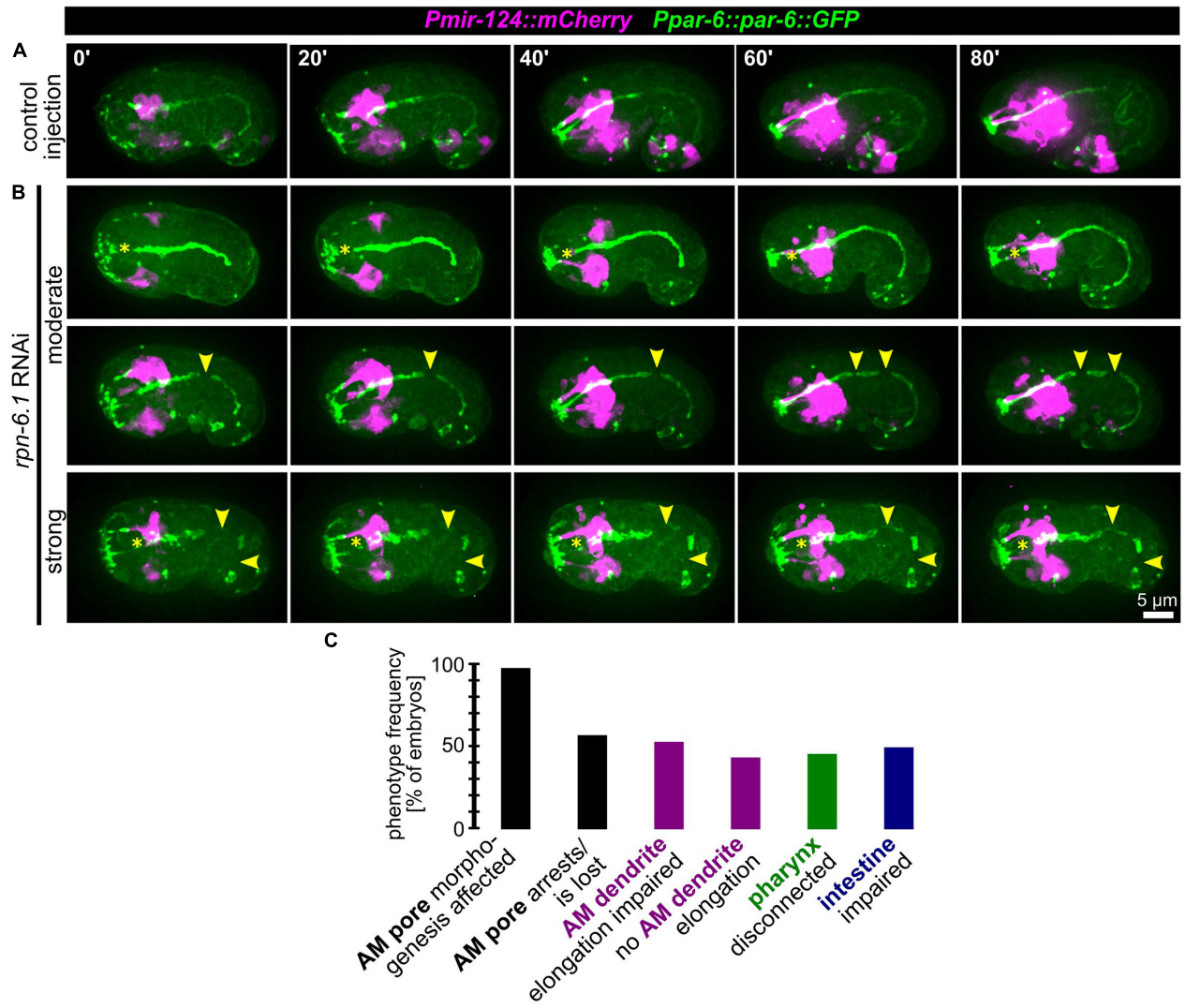

FIGURE 6 | RPN-6.1 is required for the morphogenesis of organs with apical lumen. **(A)** Maximum intensity projections of stacks of confocal images from time lapse recordings of left side view of embryo after control injection; apically polarized surfaces (sensory organ pores, excretory pore, pharynx, intestine) are shown in green, and AM neurons and dendrites are shown in magenta. **(B)** Depictions as in A, however, for *rpn-6.1* RNAi embryos. Yellow arrowheads mark discontinuities of pharynx or intestine, respectively. See also **Supplementary Video 9**. **(C)** Quantification of phenotypes observed in *rpn-6.1* RNAi embryos ($n = 29$ for AM and $n = 22$ for all other phenotypes). None of the phenotypes has been observed in control injected embryos ($n \geq 20$).

not connected to the rectal cavity (**Figure 6B**, bottom panels, yellow arrowheads).

From this data we conclude that RPN-6.1 plays a very specific, dose-dependent role for the correct spatio-temporal coordination of apical polarization and cell-cell attachment. AM sensilla morphogenesis constitutes the process most susceptible to RPN-6.1 depletion, followed by pharynx-arcade attachment, intestinal epithelization, and intestine-rectum attachment (to itself and to the rectum) (**Figure 6C** and **Supplementary Figure 2**).

Coupling of Apical Constriction to Sensilla Pore Positioning

After observing the simultaneous anterior movement of the head sensilla pores to the prospective mouth (**Figure 1A**), we analyzed OL, IL, and CEP sensilla pore movement relative to AM pore movement and epidermis migration in more detail. For marking the sensilla pores, we used PAR-6:GFP (*xnIs3[par-6:PAR-6:GFP + unc-119(+)]*), and for marking cell membranes, we used the phosphatidylinositol 4,5-bisphosphate-binding probe mCherry:PH(PLCdelta1) (Audhya et al., 2005). This combination enables simultaneous tracking of sensory organ pores and the anterior boundary of the epidermis (**Figures 7A,B**). In doing so, we found that the AM socket cells (AMsoL/R) move a distance of approximately ≥ 50% of embryo width (corresponding to 12–15 μm), a distance similar to that for the dorsal OLQ socket cells (OLQsoDL/R), followed by ILsoD (∼50%), dorsal CEP (∼50%), and the ILsoL/R (∼40%, corresponding to 10–12 μm). The movement distance and symmetry are due to the position of socket cells at the time of apical polarization (**Figure 7A**, bottom panels).

Taking an even closer look at pore movement shows that AM pores are kinematically separable from all other pores: While CEP, IL, and OLQ sensilla pores reach their juxta-oral position simultaneously, AM sensilla pores show a marked delay (**Figure 7A**, bottom right). Moreover, as indicated above, all sensilla pores but the AM pores are anterior to the edge of the migrating epidermal sheet that extends anteriorly to cover the head (**Figure 7A**, top panel). This shows that all head sensilla pores and dendrites except the AM pores seem to move by a mechanism different from towing through the epidermis.

Since pore migration is occurring at the same time as the formation of what has been called anterior sensory depression (Sulston et al., 1983), we conjectured that either apical constriction or basal expansion of cells must be involved. Only these two morphogenetic mechanisms have been shown to drive similar tissue dynamics. Hence, we further investigated the occurrence of cell shape changes at the anterior tip of the embryo. Within most cells that become positioned directly adjacent to the prospective mouth, we detected the formation of bottle-like shapes with an anterior accumulation of apical markers (**Figure 7B** and **Supplementary Video 10**). To confirm that apical constriction is indeed a main driver of sensory organ morphogenesis, we analyzed several other factors known to be involved in apical constriction (**Supplementary Figure 3**, **Supplementary Video 11**). We observed that actin (using lifeact as a probe) is transiently enriched at the anterior tip together with the non-muscle myosin II heavy chain (NMY-2; **Supplementary Figure 3A**). Actin is subsequently lost, while NMY-2 marks all sensory organ pores and the mouth (**Supplementary Figure 3A**, right panel). As shown previously, tubulin bundles that move toward the anterior tip of the head are apparent that represent sensory organ dendrites stabilized by the kinetochore-microtubule coupling machinery (**Supplementary Figure 3B**, dashed lines, arrowheads; Cheerambathur et al., 2019). In addition, apical constriction is also immediately apparent when analyzing the non-muscle myosin regulatory light chain (MLC-4), which stains sensory organ pores and other apically constricting cells from the point of their *de novo* apical polarization until late embryogenesis (**Supplementary Figure 3C**).

Since the cells that undergo apical constriction were not polarized before, we analyzed the sequence of events during *de novo* apical polarization. Consistent with apical constriction as mechanism underlying anterior tissue remodeling, the non-muscle myosin regulatory light chain (MLC-4, **Supplementary Figure 3C**) and NMY-2 (**Supplementary Figure 3D**) stain sensory organ pores (arrowheads) and other apically constricting cells (dashed lines) from the point of their *de novo* apical polarization until late embryogenesis. Moreover, examination of a strain co-expressing NMY-2 and PAR-6 showed that NMY-2 seems to localize to the nascent apical surface first, followed by the polarity determinant (**Supplementary Figure 3D**). Moreover, besides PAR-6 also PAR-3 shows *de novo* apical localization, suggesting that the whole aPAR complex becomes apically enriched at this stage (**Supplementary Figure 3E**).

The above data strongly suggest that collective apical constriction seems to mediate pore movement and mouth formation. We next tested whether RPN-6.1 affects collective apical constriction. As shown above, the degree of RPN-6.1 depletion allows us to separate AM pore and dendrite morphogenesis (modest/moderate depletion) from the morphogenesis of all other head sensory organs (strong depletion) (**Figure 5B**). When analyzing cases of strong RPN-6.1 depletion, we found that apical polarization of most cells at the anterior tip of the embryo is defective (**Figure 7C**), which results in a loss of collective cell behaviors (**Supplementary Video 12**). Therefore, we conclude that apical constriction within the anterior-most cells seems to constitute an important force which drives cellular re-arrangements that determine head sensilla pore positioning. We observed strong impairment of pore movement and loss of directed cell-shape changes within the anterior-most cells after RPN-6.1 depletion. Thus, RPN-6.1 is affecting correct apical constriction and thereby sensory organ placement.

Interplay of *de novo* Juxta-Oral Apical Polarization and Sensory Organ Placement

Anatomically, the mouth opening in *C. elegans* consists of three concentric rings of epidermal cells (from outside to inside: hyp3, hyp2, and hyp1, also called lips after deposition of cuticle) that are linked to the pharyngeal epithelium through two sequential rings of partially fused interstitial cells, the anterior and posterior arcade rings (consisting of three arcade cells in case of the

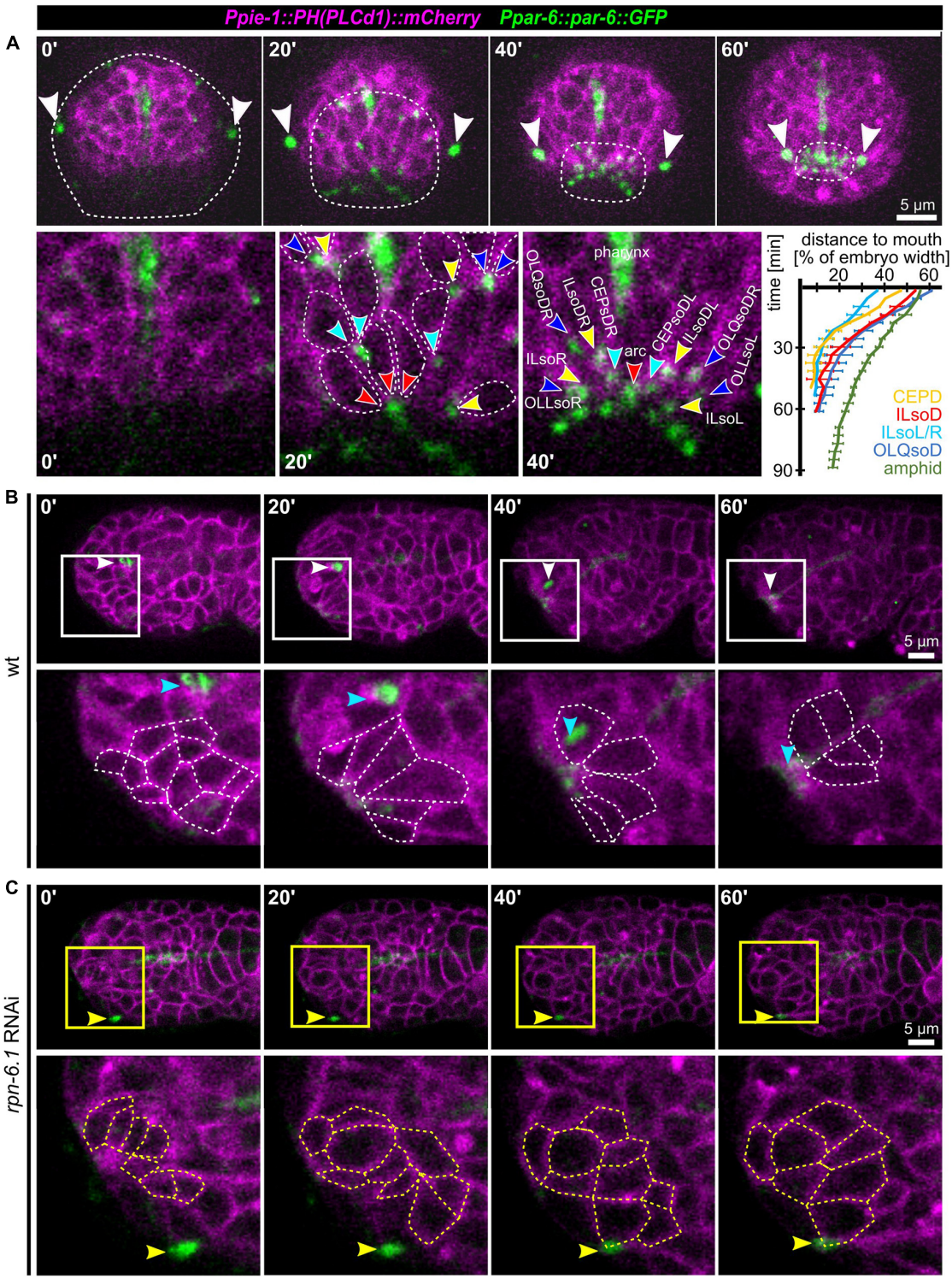

FIGURE 7 | Apical constriction, sensory organ pore movement and the role of RPN-6.1. **(A)** Top: Maximum intensity projections of stacks of confocal images from time lapse recordings of a representative wt embryo imaged from anterior. The edge of the epidermis was tracked based on cell membranes and is highlighted by a dashed line. The AM pores are highlighted by white arrowheads. Bottom left: Magnified views of cell shape changes and identification of individual sensory organ socket cells. Anterior apical tips of cells are marked with arrowheads. Bottom right: Quantification of sensory organ pore (socket cell) movement ($n = 5$). **(B)** Top: Maximum intensity projections of stacks of confocal images from time lapse recordings of a representative wt embryo imaged from the left side. Bottom: Magnified single *z*-stacks from the boxed area above. Arrowheads mark the AM pore, individual neuronal and arcade cells are outlined to illustrate their shape change. **(C)** Representation as in panel **(B)**, however, for a representative, moderately RPN-6.1 depleted embryo. See also **Supplementary Video 12**.

anterior—arc ant DL, arc ant DR, and arc ant V—and six cells in case of the posterior ring—arc post D, arc post DL, and arc post DR, arc post V, arc post VL, and arc post VR) (Altun and Hall, 2009b). From previous work (Sulston et al., 1983) and anatomical descriptions based on EM analyses (**Figure 8A**, inset; Altun and Hall, 2009b), we reasoned that AM sensilla morphogenesis and formation of the connection between mouth and pharynx might be topologically and kinematically similar: An epithelial pore forms anteriorly to the pharynx primordium (**Figure 8A**). This pore consists of arcade cells, which resemble the socket glia of AM sensory organs. The pore connects to the pharynx lumen and opens to the outside by connecting to the anterior epidermis (**Figure 8A**). Accordingly, using a marker that highlights the cell membranes of all cells of the alimentary system (*Ppha-1:GFP:CAAX*), including the arcade cells, we observed apical polarization (**Supplementary Video 13**) and constriction (**Figure 8B**) of arcade cells. Furthermore, we find that apical polarization of arcade cells is not transient but persists until formation of a connection with the anterior, juxta-oral cells and the pharynx has been formed (**Supplementary Video 13**). Concomitant with apical constriction of arcade cells, numerous anteriorly located cells undergo apical constriction (**Figure 8B**, bottom panels and **Figure 8C**). Constriction first leads to the formation of local clusters that eventually integrate into a broad zone of apically constricted cells (**Figure 8B**, bottom panels). Many of these apically constricting cells are ciliated neurons of sensory cilia (**Figure 8C**) and their socket glia cells (**Figure 7A**). Apical constriction of these cells leads to an invagination of the embryo's anterior tip and the formation of what has been coined anterior neuropore. However, unlike proposed earlier (Sulston et al., 1983), this neuropore does not evert, but stays in place until connected to the arcade epithelium (**Supplementary Video 10**).

These observations combined with seminal work on the embryonic lineage (Sulston et al., 1983), allow us to propose a working model for mouth and sensory organ morphogenesis (**Figure 8D** and **Supplementary Figure 4**). (1) Collective apical constriction drives invagination of the anterior tip of the embryo, where most sensory organ socket glia and neurons of the IL, OL, and CEP sensory organs are located (**Supplementary Figure 4**). (2) Simultaneously with apical constriction, the anterior spreading of the epidermis and the integration of the AM sensory organ into its migrating edge allow the AM dendrites to extend toward the other sensory organs and the mouth, all of which later forms the lips of the animal (**Supplementary Figure 4**, middle panel). (3) Unlike proposed earlier but fully consistent with lineage tracing (Sulston et al., 1983), the cell bodies of the AM sensory organ's neurons stay where they were born and do not migrate (**Supplementary Figure 4**, bottom panel). (4) Through apical constriction and subsequent delamination, many cells that are initially located at the anterior tip reach their final positions, which are more posterior (e.g., non-sensory neurons like AVA, AVE, AVD, and RME). (5) Apical constriction triggers formation of a shallow funnel that allows the inner-most apically constricting cells, the arcade cells, to become surrounded by sensory organ dendrite tips.

Together, this means that three concurrent collective cellular behaviors mediate head morphogenesis: Tissue invagination by apical constriction, epidermal expansion linked to dendrite towing and delamination of inter- and motor-neurons. Our experiments show that apical constriction-mediated and epidermal spreading-mediated processes can be separated genetically and that the latter strongly depends on proteasome activation.

DISCUSSION

In the canonical case of neurite extension, a growth cone actively advances, thereby elongating the neurite (**Figure 9A**, bottom). While neurites use this mode of morphogenesis in *C. elegans* (Hedgecock et al., 1990), it has been claimed that AM sensory dendrites in the *C. elegans* embryo extend by anchoring of dendritic tips and migration of their cell bodies, a newly discovered mode of dendrite morphogenesis that has been coined retrograde extension (Heiman and Shaham, 2009; **Figure 9A**, middle). In contrast, our analyses and recently published work (Fan et al., 2019) show that AM sensilla extend by dendrite towing (**Figure 9A**, top). As already traced by Sulston et al. (1983), the neurons of the AM sensilla do not actively move during the time of dendrite extension. They also only passively acquire more posterior positions later, when many cells do so due to continued embryonic elongation. Neuronal cells get re-positioned when the pharynx extends, during which many of these cells can slide along its basement membrane. Thus, even this late and apparently posterior-directed change of neuron cell positions relative to the mouth cannot be considered retrograde extension but a passive movement. Passive movement of cell bodies is also reflected by the fact that many of these cells have variable positions in the adult organism. For instance, strong position variability has been well documented around the anterior bulb of the pharynx, for instance, for the OLQ socket glia (OLQsoDL/R; White et al., 1986; Altun and Hall, 2011).

Importantly, the difference between the morphogenesis of AM and all other head sensilla was already discussed much earlier in general anatomical and ontological descriptions of nematodes: "The bilaterally symmetrical amphids are separately innervated and cannot be considered a part of the cephalic papillary symmetry. Unlike the papillary nerves, the amphidial nerves enter the nerve ring indirectly, through a commissure and their original position probably was posterior to the labial region as indicated by embryonic rhabditis and adult phasmidians" (Chitwood and Chitwood, 1937). Thus, our data and the seminal work on the *C. elegans* lineage fully confirm this statement: AM sensilla are assembled posterior to all other head sense organs and are the only sensilla that directly form a union with the epidermis (Fan et al., 2019).

In addition, our analyses uncover that towing of amphid dendrites is accompanied by another morphogenetic process, the formation of the alimentary system and of all other sensory organs in the head by apical constriction (**Figure 9B**). Specifically, our analyses show that, spatio-temporally, coordinated apical constriction is involved in placing the dendritic endings of the head sensory organ endings except for the AM. Therefore, we propose that besides dendrite towing, apical constriction is

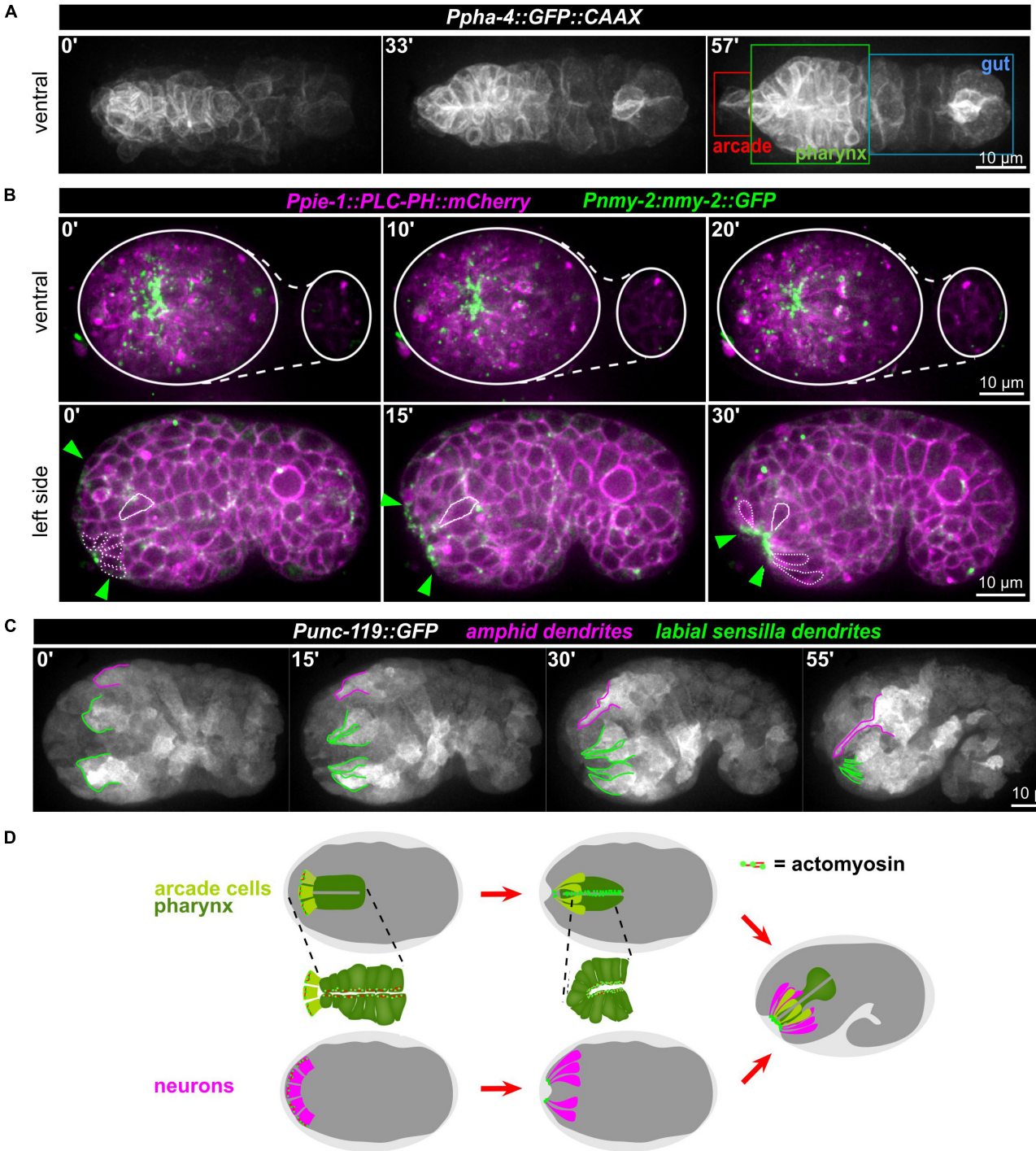

FIGURE 8 | Apical constriction of anterior cells. **(A)** Maximum intensity projections of stacks of confocal images from time lapse recordings of a representative wt embryo expressing a membrane-localized GFP under the control of the *pha-4* promotor imaged from the ventral side. The individual compartments of the alimentary system are highlighted in the right panel. See also **Supplementary Video 13**. **(B)** Top: Maximum intensity projections of stacks of confocal images from time lapse recordings of representative wt embryo imaged from the ventral side. White lines mark the outlines of the embryo. Bottom: Central confocal plane from time lapse recordings of a representative wt embryo imaged from the left side. Green arrowheads mark the anterior cell surfaces that acquire and accumulate NMY-2. The dashed white line highlights cells that have undergone apical constriction. The solid white line traces a cell that undergoes apical constriction and thereby moves juxta-orally. See also **Supplementary Video 10**. **(C)** Maximum intensity projections of stacks of confocal images from time lapse recordings of a representative wt embryo imaged from the left side. Labial sensilla (green) and the left amphid sensillum (magenta) are tracked. **(D)** Schematic illustrating how sequential, collective apical constriction at the anterior tip of the embryo creates the anterior-most epithelial part of the mouth (arcade cells, light green) and, simultaneously, invagination of anteriorly localized neurons.

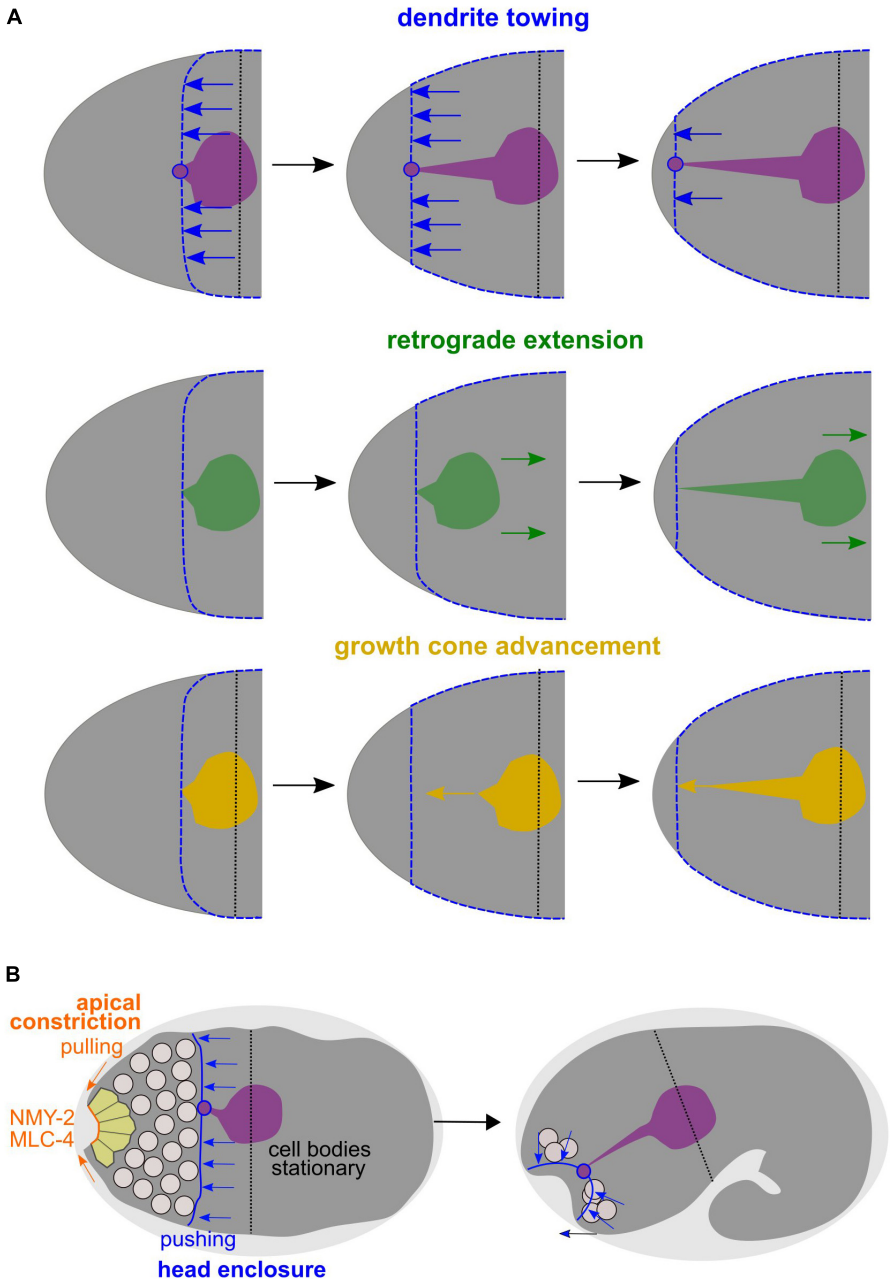

FIGURE 9 | Dendrite towing governs AM dendrite morphogenesis and apical constriction contributes to placement of sensory organ pores. **(A)** Alternative models for AM dendrite morphogenesis. Top: During dendrite towing, the anterior-directed migration of the epidermis generates pulling forces that lead to movement of the AM sensory organ. Pulling forces can be transduced since the amphid organ partially intercalates into the epidermal layer through junctions of the socket glia cell, to which the dendrite tips of the AM neurons form contacts. Middle: In the case of retrograde extension, it has been claimed that the posterior-directed migration of neurons would lead to dendrite extension. Bottom: During growth cone advancement, dendrites would extend actively by forming a migratory specialization at their anterior ends. **(B)** Working model for collective morphogenesis of AM dendrites, neuron internalization, and mouth formation. Through dendrite towing, the anteriorly migrating epidermal sheet mediates AM sensory organ morphogenesis, while apical constriction of anteriorly located cells leads to tissue bending and formation of an anterior neuropore that connects to the mouth formed through apical constriction of arcade cells.

the second main morphogenetic mechanism shaping sensory dendrites in *C. elegans*. Previously, it was shown that during gastrulation, *C. elegans* repeatedly utilizes a morphogenetic module that has been coined apical constriction initially (Lee and Goldstein, 2003). This module consists of internalizing cells which use centripetal, contractile actomyosin flow that they couple to cell-cell adhesion complexes of neighboring cells, thereby mediating their own covering (Roh-Johnson et al., 2012). However, during gastrulation, internalizing cells do not substantially deform but the covering cells do (Pohl et al., 2012).

In contrast, during sensory organ morphogenesis, we now demonstrate that most cells at the anterior tip of the *C. elegans* embryo utilize *bona fide* apical constriction: (1) Cells deform and acquire a bottle-like morphology, (2) apical constriction leads to formation of a tissue indentation, which is a prototypic topological change in apical constriction (Pasakarnis et al., 2016), and (3) cells maintain high apical levels of non-muscle myosin II and of other apical polarity determinants and do not lose them like during gastrulation (Pohl et al., 2012). The latter aspect is probably best explained by the fact that the anterior endings of cells acquire and maintain an apical identity while cells lose their apical surface when gastrulating. Notably, it has been previously suggested that rosette formation is a main driver of morphogenesis for sensory organs (Fan et al., 2019). However, rosettes only represent a kinematic description of local cell positions in a planar configuration and do not take the three-dimensional cell shape into account. Our data show that the main transient configuration is bottle-shaped cells, which appear like rosettes when focusing on their apical aspect only.

Moreover, our data reveal that differential thresholds of proteasome activation allow to separate two morphogenetic mechanisms, AM dendrite towing by the epidermis and apical constriction-mediated assembly of all other sensory organs. Thereby, our data on the main proteasome activator, RPN-6.1, directly contribute to the growing list of specific functions of proteasome subunits in *C. elegans* development: Specific functions in sex determination have been shown for RPN-10 (Shimada et al., 2006), spindle rotation during early embryogenesis depends on the subunit RPN-2 (Sugiyama et al., 2008), or insulin/IGF-1 signaling requires the proteasome-associated de-ubiquitylating enzyme UBH-4 (Matilainen et al., 2013). In addition, it has been shown that graded depletion of RPN-10, a component of the 19S lid like RPN-6.1, results in an adaptive response that can compensate for compromised proteasome activity (Keith et al., 2016). Moreover, proteasomes can adapt to specific stress conditions (Yun et al., 2008) and show highly tissue-specific changes when different proteasomal subunits are depleted (Mikkonen et al., 2017). Collectively, this demonstrates that developmental stage- or cell-specific loss of presumably essential proteasome subunits does not lead to pleiotropic phenotypes, but in many cases reveals highly context-dependent aspects of ubiquitin proteasome system function.

We also demonstrate that head morphogenesis in general and dendrite morphogenesis in particular are an ideal developmental scenario to study *de novo* apicobasal polarization. *De novo* apical polarization has been characterized for cysts and during vasculogenesis (Bryant et al., 2010; Lenard et al., 2015), however, in these contexts, polarization strictly depends on concomitant lumen formation and is often directly coupled to mitotic dynamics (spindle and midbody position). In the case of sensory organ morphogenesis, mitotic cues are lacking since cells are already post-mitotic. Only a small fraction of cells, the socket glia cells, form a *bona fide* lumen as demonstrated by electron microscopy. Thus, all participating anterior located cells are non-polar at the start of the process as judged by the absence of the known apical PARs and non-muscle myosin II. Therefore, they need to polarize by different cues than those known so far. We would like to suggest that a developmental timer together with an extrinsic cue, the apical extracellular matrix (aECM), most likely organize collective apical polarization. Remarkably, a main component of the aECM is DEX-1, a secreted protein with nidogen and EGF-like domains which is essential for embryonic development (Cohen et al., 2019). DEX-1 is expressed in epithelial tissues that build the aECM during embryogenesis. Importantly, *dex-1* mutants have a pharynx ingressed (Pin) phenotype, implying that the pharynx lumen ends inside the embryo and more anteriorly positioned cells occlude it. In the light of our findings, a very likely interpretation of these data is that without a properly formed aECM, anteriorly located cells might not undergo apical constriction, which leads to sensory organ dendrite phenotypes (Heiman and Shaham, 2009). More importantly, it could lead to a lack of delamination of other apically polarizing cells and failed or partially failed mouth morphogenesis because this requires arcade cell apical constriction (**Figure 8D**). In addition, Cohen et al. (2019) were not able to detect a sperm protein zonadhesin homology that was previously proposed (Heiman and Shaham, 2009) and demonstrate that *dex-1* null mutants have more severe phenotypes than truncation mutants used previously. Therefore, we argue that the function of DEX-1 should be re-interpreted and re-investigated in the context of *de novo* apical polarization and collective morphogenesis. Notably, we can exclude that formation of the basement membrane around the pharynx serves as the cue for polarization since *de novo* apically polarizing cells are not directly contacting the pharynx primordium when overt apical polarization of anterior cells occurs. The data presented here strongly suggest that during dendrite morphogenesis, glia cells in *C. elegans* can be considered interstitial cells whose main function is to form the connection between epidermal tissues and neurons. We also present evidence that the arcade cells might fulfill a very similar function morphogenetically: they form the connection to the outside by forming an anterior pore, and, subsequently connect the lumen of the pharynx to this pore. This view is also supported by the fact that socket glia and arcade cells show a striking similarity in their shape at the end of embryonic development (Altun and Hall, 2009b).

Taken together, our data unveil two morphogenetic modules that organize the *C. elegans* sensory organs, dendrite towing of a pre-assembled sensory organ in the epidermis and apical constriction-mediated placement of sensory organs around the mouth opening. This supports the idea of co-evolution of epidermal patterning and neuro-morphogenesis so that gradually, simple neuroectodermal tissues—where a simple epithelium contains a few sensory neurons that form a sparse network—can be transformed into epithelial systems with complex topologies and fasciculated sensory organs (Holland, 2003).

DATA AVAILABILITY STATEMENT

The original contributions presented in the study are included in the article/**Supplementary Material**, further inquiries can be directed to the corresponding author/s.

AUTHOR CONTRIBUTIONS

CP conceived and supervised the project, and wrote the manuscript with input from all other authors. PK, CL, and CP performed the experiments. PK and CP analyzed the data. All authors contributed to the article and approved the submitted version.

FUNDING

We acknowledge funding by the Cluster of Excellence Macromolecular Complexes in Action (Deutsche Forschungsgemeinschaft project EXC 115) and the LOEWE Research Cluster Ubiquitin Networks to CP. PK received a Buchmann Foundation Ph.D. scholarship.

ACKNOWLEDGMENTS

We thank members of the Gottschalk Lab, Negin Azimi Hashemi, for help with microinjection; and Wagner Steuer Costa, Alexander Gottschalk, and members of the Pohl Lab for discussions. Most of the strains used in this study were provided by the Caenorhabditis Genetics Center, which is funded by the National Institutes of Health Office of Research Infrastructure Programs (P40 OD010440).

SUPPLEMENTARY MATERIAL

The Supplementary Material for this article can be found online at: https://www.frontiersin.org/articles/10.3389/fcell.2021.619596/full#supplementary-material

REFERENCES

Altun, Z. F., and Hall, D. H. (2009a). "Epithelial system, atypical cells," in *WormAtlas*, ed. L. A. Herndo doi: 10.3908/wormatlas.1.16 (New York, NY: Albert Einstein College).

Altun, Z. F., and Hall, D. H. (2009b). "Epithelial system, interfacial cells," in *WormAtlas*, ed. L. A. Herndo doi: 10.3908/wormatlas.1.15 (New York, NY: Albert Einstein College).

Altun, Z. F., and Hall, D. H. (2010). "Nervous system, neuronal support cells," in *WormAtlas*, ed. Z. F. Altun doi: 10.3908/wormatlas.1.19 (New York, NY: Albert Einstein College).

Altun, Z. F., and Hall, D. H. (2011). "Nervous system, general description," in *WormAtlas*, ed. Z. F. Altun doi: 10.3908/wormatlas.1.18 (New York, NY: Albert Einstein College).

Audhya, A., Hyndman, F., McLeod, I. X., Maddox, A. S., Yates, J. R. III, Desai, A., et al. (2005). A complex containing the Sm protein CAR-1 and the RNA helicase CGH-1 is required for embryonic cytokinesis in *Caenorhabditis elegans*. *J. Cell Biol.* 171, 267–279. doi: 10.1083/jcb.200506124

Brenner, S. (1974). The genetics of *Caenorhabditis elegans*. *Genetics* 77, 71–94. doi: 10.1093/genetics/77.1.71

Bryant, D. M., Datta, A., Rodríguez-Fraticelli, A. E., Peränen, J., Martín-Belmonte, F., and Mostov, K. E. (2010). A molecular network for de novo generation of the apical surface and lumen. *Nat. Cell Biol.* 12, 1035–1045. doi: 10.1038/ncb2106

Cheerambathur, D. K., Prevo, B., Chow, T. L., Hattersley, N., Wang, S., Zhao, Z., et al. (2019). The kinetochore-microtubule coupling machinery is repurposed in sensory nervous system morphogenesis. *Dev. Cell* 48, 864.e7–872.e7.

Chisholm, A. D., and Hardin, J. (2005). Epidermal morphogenesis. *WormBook* 1–22. doi: 10.1895/wormbook.1.35.1

Chitwood, B. G., and Chitwood, M. B. (1937). *An Introduction to Nematology*. Baltimore, MD: Monumental Printing Company.

Cho, S. K., Bae, H., Ryu, M. Y., Wook Yang, S., and Kim, W. T. (2015). PUB22 and PUB23 U-BOX E3 ligases directly ubiquitinate RPN6, a 26S proteasome lid subunit, for subsequent degradation in *Arabidopsis thaliana*. *Biochem. Biophys. Res. Commun.* 464, 994–999. doi: 10.1016/j.bbrc.2015.07.030

Clark, A. M., Goldstein, L. D., Tevlin, M., Tavaré, S., Shaham, S., and Miska, E. A. (2010). The microRNA miR-124 controls gene expression in the sensory nervous system of *Caenorhabditis elegans*. *Nucleic Acids Res.* 38, 3780–3793. doi: 10.1093/nar/gkq083

Cohen, J. D., Flatt, K. M., Schroeder, N. E., and Sundaram, M. V. (2019). Epithelial shaping by diverse apical extracellular matrices requires the nidogen domain protein DEX-1 in *Caenorhabditis elegans*. *Genetics* 211, 185–200. doi: 10.1534/genetics.118.301752

Du, Z., He, F., Yu, Z., Bowerman, B., and Bao, Z. (2015). E3 ubiquitin ligases promote progression of differentiation during *C. elegans* embryogenesis. *Dev. Biol.* 398, 267–279. doi: 10.1016/j.ydbio.2014.12.009

Dutta, P., Lehmann, C., Odedra, D., Singh, D., and Pohl, C. (2015). Tracking and quantifying developmental processes in *C. elegans* using open-source tools. *J. Vis. Exp.* 16:e53469.

Fan, L., Kovacevic, I., Heiman, M. G., and Bao, Z. (2019). A multicellular rosette-mediated collective dendrite extension. *eLife.* 8:e38065.

Gilmour, D., Knaut, H., Maischein, H. M., and Nüsslein-Volhard, C. (2004). Towing of sensory axons by their migrating target cells in vivo. *Nat. Neurosci.* 7, 491–492. doi: 10.1038/nn1235

Hamilton, A. M., Oh, W. C., Vega-Ramirez, H., Stein, I. S., Hell, J. W., Patrick, G. N., et al. (2012). Activity-dependent growth of new dendritic spines is regulated by the proteasome. *Neuron* 74, 1023–1030. doi: 10.1016/j.neuron.2012.04.031

Hamilton, A. M., and Zito, K. (2013). Breaking it down: the ubiquitin proteasome system in neuronal morphogenesis. *Neural. Plast* 2013:196848.

Harrell, J. R., and Goldstein, B. (2011). Internalization of multiple cells during *C. elegans* gastrulation depends on common cytoskeletal mechanisms but different cell polarity and cell fate regulators. *Dev. Biol.* 350, 1–12. doi: 10.1016/j.ydbio.2010.09.012

Hedgecock, E. M., Culotti, J. G., and Hall, D. H. (1990). The unc-5, unc-6, and unc-40 genes guide circumferential migrations of pioneer axons and mesodermal cells on the epidermis in *C. elegans*. *Neuron* 4, 61–85. doi: 10.1016/0896-6273(90)90444-k

Hegde, A. N., and Upadhya, S. C. (2007). The ubiquitin-proteasome pathway in health and disease of the nervous system. *Trends Neurosci.* 30, 587–595. doi: 10.1016/j.tins.2007.08.005

Heiman, M. G., and Shaham, S. (2009). DEX-1 and DYF-7 establish sensory dendrite length by anchoring dendritic tips during cell migration. *Cell* 137, 344–355. doi: 10.1016/j.cell.2009.01.057

Holland, N. D. (2003). Early central nervous system evolution: an era of skin brains? *Nat. Rev. Neurosci.* 4, 617–627. doi: 10.1038/nrn1175

Hsu, M. T., Guo, C. L., Liou, A. Y., Chang, T. Y., Ng, M. C., Florea, B. I., et al. (2015). Stage-dependent axon transport of proteasomes contributes to axon development. *Dev. Cell* 35, 418–431. doi: 10.1016/j.devcel.2015.10.018

Hunter, M. V., and Fernandez-Gonzalez, R. (2017). Coordinating cell movements in vivo: junctional and cytoskeletal dynamics lead the way. *Curr. Opin. Cell Biol.* 48, 54–62. doi: 10.1016/j.ceb.2017.05.005

Jiang, L. I., and Sternberg, P. W. (1999). Socket cells mediate spicule morphogenesis in *Caenorhabditis elegans* males. *Dev. Biol.* 211, 88–99. doi: 10.1006/dbio.1999.9293

Keith, S. A., Maddux, S. K., Zhong, Y., Chinchankar, M. N., Ferguson, A. A., Ghazi, A., et al. (2016). Graded proteasome dysfunction in *Caenorhabditis elegans* activates an adaptive response involving the conserved SKN-1 and ELT-2 transcription factors and the autophagy-lysosome pathway. *PLoS Genet.* 12:e1005823. doi: 10.1371/journal.pgen.1005823

Laser, H., Mack, T. G., Wagner, D., and Coleman, M. P. (2003). Proteasome inhibition arrests neurite outgrowth and causes "dying-back" degeneration in primary culture. *J. Neurosci. Res.* 74, 906–916. doi: 10.1002/jnr.10806

Lee, J. Y., and Goldstein, B. (2003). Mechanisms of cell positioning during *C. elegans* gastrulation. *Development* 130, 307–320. doi: 10.1242/dev.00211

Lenard, A., Daetwyler, S., Betz, C., Ellertsdottir, E., Belting, H. G., Huisken, J., et al. (2015). Endothelial cell self-fusion during vascular pruning. *PLoS Biol.* 13:e1002126. doi: 10.1371/journal.pbio.1002126

Lier, S., and Paululat, A. (2002). The proteasome regulatory particle subunit Rpn6 is required for *Drosophila* development and interacts physically with signalosome subunit Alien/CSN2. *Gene* 298, 109–119. doi: 10.1016/s0378-1119(02)00930-7

Lints, R., and Hall, D. H. (2009). "Male neuronal support cells, spicules," in *WormAtlas*, doi: 10.3908/wormatlas.2.11 (New York, NY: Albert Einstein College).

Low, I. I. C., Williams, C. R., Chong, M. K., McLachlan, I. G., Wierbowski, B. M., Kolotuev, I., et al. (2019). Morphogenesis of neurons and glia within an epithelium. *Development* 146:dev171124. doi: 10.1242/dev.171124

Matilainen, O., Arpalahti, L., Rantanen, V., Hautaniemi, S., and Holmberg, C. I. (2013). Insulin/IGF-1 signaling regulates proteasome activity through the deubiquitinating enzyme UBH-4. *Cell Rep.* 3, 1980–1995. doi: 10.1016/j.celrep.2013.05.012

Metcalfe, W. K. (1985). Sensory neuron growth cones comigrate with posterior lateral line primordial cells in zebrafish. *J. Comp. Neurol.* 238, 218–224. doi: 10.1002/cne.902380208

Mikkonen, E., Haglund, C., and Holmberg, C. I. (2017). Immunohistochemical analysis reveals variations in proteasome tissue expression in *C. elegans*. *PLoS One* 12:e0183403. doi: 10.1371/journal.pone.0183403

Pasakarnis, L., Dreher, D., and Brunner, D. (2016). SnapShot: mechanical forces in development I. *Cell* 165, 754.e1–754.e1.

Pathare, G. R., Nagy, I., Bohn, S., Unverdorben, P., Hubert, A., Körner, R., et al. (2012). The proteasomal subunit Rpn6 is a molecular clamp holding the core and regulatory subcomplexes together. *Proc. Natl. Acad. Sci. U.S.A.* 109, 149–154. doi: 10.1073/pnas.1117648108

Perkins, L. A., Hedgecock, E. M., Thomson, J. N., and Culotti, J. G. (1986). Mutant sensory cilia in the nematode *Caenorhabditis elegans*. *Dev. Biol.* 117, 456–487. doi: 10.1016/0012-1606(86)90314-3

Pohl, C., Tiongson, M., Moore, J. L., Santella, A., and Bao, Z. (2012). Actomyosin-based self-organization of cell internalization during *C. elegans* gastrulation. *BMC Biol.* 10:94. doi: 10.1186/1741-7007-10-94

Rasmussen, J. P., Reddy, S. S., and Priess, J. R. (2012). Laminin is required to orient epithelial polarity in the *C. elegans* pharynx. *Development* 139, 2050–2060. doi: 10.1242/dev.078360

Roh-Johnson, M., Shemer, G., Higgins, C. D., McClellan, J. H., Werts, A. D., Tulu, U. S., et al. (2012). Triggering a cell shape change by exploiting preexisting actomyosin contractions. *Science* 335, 1232–1235. doi: 10.1126/science.1217869

Rual, J. F., Ceron, J., Koreth, J., Hao, T., Nicot, A. S., and Hirozane-Kishikawa, T. (2004). Toward improving *Caenorhabditis elegans* phenome mapping with an ORFeome-based RNAi library. *Genome Res.* 14, 2162–2168. doi: 10.1101/gr.2505604

Schindelin, J., Arganda-Carreras, I., Frise, E., Kaynig, V., Longair, M., Pietzsch, T., et al. (2012). Fiji: an open-source platform for biological-image analysis. *Nat. Methods* 9, 676–682. doi: 10.1038/nmeth.2019

Schmidt-Rhaesa, A. (2007). *The Evolution of Organ Systems*. Oxford: Oxford University Press.

Semren, N., Welk, V., Korfei, M., Keller, I. E., Fernandez, I. E., Adler, H., et al. (2015). Regulation of 26S proteasome activity in pulmonary fibrosis. *Am. J. Respir. Crit. Care Med.* 192, 1089–1101. doi: 10.1164/rccm.201412-2270oc

Shimada, M., Kanematsu, K., Tanaka, K., Yokosawa, H., and Kawahara, H. (2006). Proteasomal ubiquitin receptor RPN-10 controls sex determination in *Caenorhabditis elegans*. *Mol. Biol. Cell* 17, 5356–5371. doi: 10.1091/mbc.e06-05-0437

Stavoe, A. K. H., and Holzbaur, E. L. F. (2019). Autophagy in neurons. *Annu. Rev. Cell Dev. Biol.* 35, 477–500. doi: 10.1146/annurev-cellbio-100818-125242

Sugiyama, Y., Nishimura, A., and Ohno, S. (2008). Symmetrically dividing cell specific division axes alteration observed in proteasome depleted *C. elegans* embryo. *Mech. Dev.* 25, 743–755. doi: 10.1016/j.mod.2008.04.002

Sulston, J. E., Schierenberg, E., White, J. G., and Thomson, J. N. (1983). The embryonic cell lineage of the nematode *Caenorhabditis elegans*. *Dev. Biol.* 100, 64–119. doi: 10.1016/0012-1606(83)90201-4

Takahashi, M., Iwasaki, H., Inoue, H., and Takahashi, K. (2002). Reverse genetic analysis of the *Caenorhabditis elegans* 26S proteasome subunits by RNA interference. *Biol. Chem.* 383, 1263–1266. doi: 10.1515/bc.2002.140

Verlhac, M. H., Terret, M. E., and Pintard, L. (2010). Control of the oocyte-to-embryo transition by the ubiquitin-proteolytic system in mouse and *C. elegans*. *Curr. Opin. Cell Biol.* 22, 758–763. doi: 10.1016/j.ceb.2010.09.003

VerPlank, J. J. S., Lokireddy, S., Zhao, J., and Goldberg, A. L. (2019). 26S Proteasomes are rapidly activated by diverse hormones and physiological states that raise cAMP and cause Rpn6 phosphorylation. *Proc. Natl. Acad. Sci. U.S.A.* 116, 4228–4237. doi: 10.1073/pnas.1809254116

Vilchez, D., Morantte, I., Liu, Z., Douglas, P. M., Merkwirth, C., Rodrigues, A. P., et al. (2012). RPN-6 determines *C. elegans* longevity under proteotoxic stress conditions. *Nature* 489, 263–268. doi: 10.1038/nature11315

Wang, X., Dong, C., Sun, L., Zhu, L., Sun, C., Ma, R., et al. (2016). Quantitative proteomic analysis of age-related subventricular zone proteins associated with neurodegenerative disease. *Sci. Rep.* 6:37443.

Wernike, D., Chen, Y., Mastronardi, K., Makil, N., and Piekny, A. (2016). Mechanical forces drive neuroblast morphogenesis and are required for epidermal closure. *Dev. Biol.* 412, 261–277. doi: 10.1016/j.ydbio.2016.02.023

White, J. G., Southgate, E., Thomson, J. N., and Brenner, S. (1986). The structure of the nervous system of the nematode *Caenorhabditis elegans*. *Philos. Trans. R. Soc. Lond. B Biol. Sci.* 314, 1–340. doi: 10.1098/rstb.1986.0056

Yang, W. K., and Chien, C. T. (2019). Beyond being innervated: the epidermis actively shapes sensory dendritic patterning. *Open Biol.* 9:180257. doi: 10.1098/rsob.180257

Yun, C., Stanhill, A., Yang, Y., Zhang, Y., Haynes, C. M., Xu, C. F., et al. (2008). Proteasomal adaptation to environmental stress links resistance to proteotoxicity with longevity in *Caenorhabditis elegans*. *Proc. Natl. Acad. Sci. U.S.A.* 105, 7094–7099. doi: 10.1073/pnas.0707025105

Zhang, Y., Yan, L., Zhou, Z., Yang, P., Tian, E., Zhang, K., et al. (2009). SEPA-1 mediates the specific recognition and degradation of P granule components by autophagy in *C. elegans*. *Cell* 136, 308–321. doi: 10.1016/j.cell.2008.12.022

Conflict of Interest: The authors declare that the research was conducted in the absence of any commercial or financial relationships that could be construed as a potential conflict of interest.

frontiers in Cell and Developmental Biology

REVIEW
published: 02 March 2021
doi: 10.3389/fcell.2021.645235

Cellular and Supracellular Planar Polarity: A Multiscale Cue to Elongate the *Drosophila* Egg Chamber

Anna Popkova[1], Matteo Rauzi[1] and Xiaobo Wang[2]**

[1] Université Côte d'Azur, Centre National de la Recherche Scientifique, Institut National de la Santé et de la Recherche Médicale, iBV, Nice, France, [2] Molecular, Cellular and Developmental Biology Department (MCD), Centre de Biologie Integrative (CBI), University of Toulouse, CNRS, UPS, Toulouse, France

OPEN ACCESS

Edited by:
Zhiyi Lv,
Ocean University of China, China

Reviewed by:
Todd Blankenship,
University of Denver, United States
Ana Carmena,
Instituto de Neurociencias de Alicante (IN), Spain

***Correspondence:**
Matteo Rauzi
matteo.rauzi@univ-cotedazur.fr
Xiaobo Wang
xiaobo.wang@univ-tlse3.fr

Specialty section:
This article was submitted to Signaling, a section of the journal Frontiers in Cell and Developmental Biology

Received: *22 December 2020*
Accepted: *02 February 2021*
Published: *02 March 2021*

Citation:
Popkova A, Rauzi M and Wang X (2021) Cellular and Supracellular Planar Polarity: A Multiscale Cue to Elongate the Drosophila Egg Chamber. Front. Cell Dev. Biol. 9:645235. doi: 10.3389/fcell.2021.645235

Tissue elongation is known to be controlled by oriented cell division, elongation, migration and rearrangement. While these cellular processes have been extensively studied, new emerging supracellular mechanisms driving tissue extension have recently been unveiled. Tissue rotation and actomyosin contractions have been shown to be key processes driving *Drosophila* egg chamber elongation. First, egg chamber rotation facilitates the dorsal-ventral alignment of the extracellular matrix and of the cell basal actin fibers. Both fiber-like structures form supracellular networks constraining the egg growth in a polarized fashion thus working as 'molecular corsets'. Second, the supracellular actin fiber network, powered by myosin periodic oscillation, contracts anisotropically driving tissue extension along the egg anterior-posterior axis. During both processes, cellular and supracellular planar polarity provide a critical cue to control *Drosophila* egg chamber elongation. Here we review how different planar polarized networks are built, maintained and function at both cellular and supracellular levels in the *Drosophila* ovarian epithelium.

Keywords: tissue elongation, planar cell polarity, supracellular network, tissue rotation, actomyosin contractility

INTRODUCTION

Tissue extension is a fundamental process during embryo development. The extension of tissues contributes to shape the developing embryo and drives the separation of groups of cells that will form different parts of an animal. Unraveling the mechanisms that drive tissue extension is key to understand how life emerges from a cluster of cells. A key and archetypal tissue elongation process is the one directed along the anterior-posterior (AP) axis of the embryo that drives the separation of the head region from the posterior region where the future brain and the anus of the animal will eventually form, respectively (Keller, 2002). Therefore, this primordial shape transformation defines one of the main axes along which the embryo develops and the animal will be structured.

In recent years, a novel mechanism driving *Drosophila* egg chamber elongation has been revealed: supracellular networks, emerging from the coupling of local fiber meshworks and controlled by subcellular planar cell polarity, form around the egg and function as a mechanical corset directing AP egg elongation (Cetera and Horne-Badovinac, 2015). In the first phase of egg elongation, the egg chamber rotates around the AP axis driving extracellular fibers alignment (Haigo and Bilder, 2011; Cetera and Horne-Badovinac, 2015). This results in a polarized extracellular matrix (ECM) working as a passive supracellular scaffold imposing anisotropic boundary conditions during egg chamber growth. In the second phase of egg elongation, a supracellular actomyosin network forms at the basal side of follicle cells (He et al., 2010). Actomyosin fibers run in a direction parallel to the ECM fibrils, and work as an active contractile supracellular scaffold generating polarized mechanical stress to shape the egg chamber. Here we review our current understanding of how supracellular polarized networks form, are maintained and function during *Drosophila* egg chamber elongation.

Planar Cell Polarity Under the Control of Factor Gradients or Morphogenesis

Epithelial tissues are the fundamental structures forming organs and providing functional shape to multicellular organisms. Epithelial cells show two types of polarity that are orthogonal to one another and that are both required to form and shape tissues: apical-basal polarity (ABP) and planar cell polarity (PCP). ABP is established along the cell apical-basal axis and is necessary to coordinate cell-cell interaction forming the epithelial barriers that separate the inner from the outer side (Harris and Peifer, 2004; St Johnston and Sanson, 2011). PCP is necessary to control the asymmetric organization and reshaping of cells along the plane of an epithelium (Irvine and Wieschaus, 1994; Vichas and Zallen, 2011). PCP pathways often control tissue extension by driving a variety of mechanisms including directed cell division (Baena-Lopez et al., 2005; Aigouy et al., 2010; Campinho et al., 2013), cell elongation (Condic et al., 1991; Nelson et al., 2012; Imuta et al., 2014; Etournay et al., 2015), cell migration (Eaton and Julicher, 2011; Munoz-Soriano et al., 2012) and cell rearrangement (Bertet et al., 2004; Blankenship et al., 2006). For tissues presenting an either open or closed topology (e.g., the wing disk or the egg chamber, respectively), PCP results in polarized signals under the control of factor gradients. Well-known examples are the Frizzled/Strabismus and Fat/Dachsous PCP signaling pathways that, for instance, play key roles in the development of the *Drosophila* eye and wing (Brittle et al., 2010, 2012; Goodrich and Strutt, 2011). In addition to the controlling factor gradients, global PCP patterns can also be under the control of cell and tissue mechanics governed by actomyosin contractility and cell-cell adhesion driving tissue movement and flow during morphogenesis. A remarkable example is the one shown during the *Drosophila* fly wing development where tissue movement and morphogenesis guide PCP (Aigouy et al., 2010). This demonstrates that PCP can be not only the cause but also the consequence of epithelial morphogenesis. In the *Drosophila* egg chamber, the PCP core system relies upon the Fat/Dachsous signal transduction pathway (Gutzeit et al., 1991). In this topologically closed epithelium, the global PCP pattern is also under the control of tissue movement: the egg chamber rotation around the AP axis guide PCP, building polarized ECM (Haigo and Bilder, 2011).

Drosophila Egg Chamber Elongation Is Driven by Molecular Corsets

During *Drosophila* oogenesis, the egg undergoes maturation before being expelled from the ovary and laid by the mother. The *Drosophila* ovary is composed of 15–20 ovarioles (**Figure 1A**). Each ovariole contains a linear sequence of egg chambers at 14 different developmental stages connected to one another via linking cells forming stalks (**Figure 1A**; He et al., 2011). Germline and somatic stem cells reside near the tip of the ovariole, a region named the germarium. These two stem cell types assemble forming an egg chamber budding off from the germarium. The perpetual serial assembly of egg chambers results in the formation of a linear alignment of interconnected chambers at different developmental stages, resembling 'pearls on a string'. The egg chamber is composed of a monolayer follicular epithelium surrounding a 16-cell germline cyst (He et al., 2011). The apical side of the follicular epithelium makes contact with the internal germ cells, while the basal side interacts with the extracellular basement membrane (BM). During oogenesis, the egg chamber gradually changes its shape from spherical to ellipsoidal by extending along the AP axis (**Figure 1B**). The egg chamber elongation rate is moderate between stage 1 (S1) and S4, while it is higher between S5 and S11 (Haigo and Bilder, 2011) eventually resulting in an oblong shaped embryo at full maturation.

Egg chamber elongation is driven by polarized 'molecular corsets' that wrap and constrain the egg along its shorter axes directing egg chamber growth (**Figure 1C**). These corsets are composed of parallel fibrillary ECM at the BM and parallel actin bundles forming stress-fibers at the basal domain of follicular epithelial cells (**Figure 1D**). Both ECM and actin bundles form polarized networks at the surface of the egg - an enveloping scaffold orthogonal to the AP axis (**Figure 1D**; Cetera and Horne-Badovinac, 2015). During S5 to S8, the ECM works as a passive scaffold resisting the expansive growth of internal germ cells. Egg chamber volume increase is thus biased toward the poles resulting in AP egg extension. Crest et al. (2017) used atomic force microscopy to measure BM stiffness of the egg chamber at different stages during egg chamber rotation and at different AP positions. Interestingly, they showed that BM stiffness increases during egg chamber maturation and that a stiffness gradient is established along the AP axis with highest stiffness in the central zone. BM differential stiffness is under the control of JAK/STAT signaling and is necessary to impose differential resistance to isotropic tissue expansion resulting in egg chamber elongation (Crest et al., 2017).

During S9 and S10, the actin bundles contract under the action of the myosin (MyoII) motor protein to form an active contracting scaffold that directs egg extension

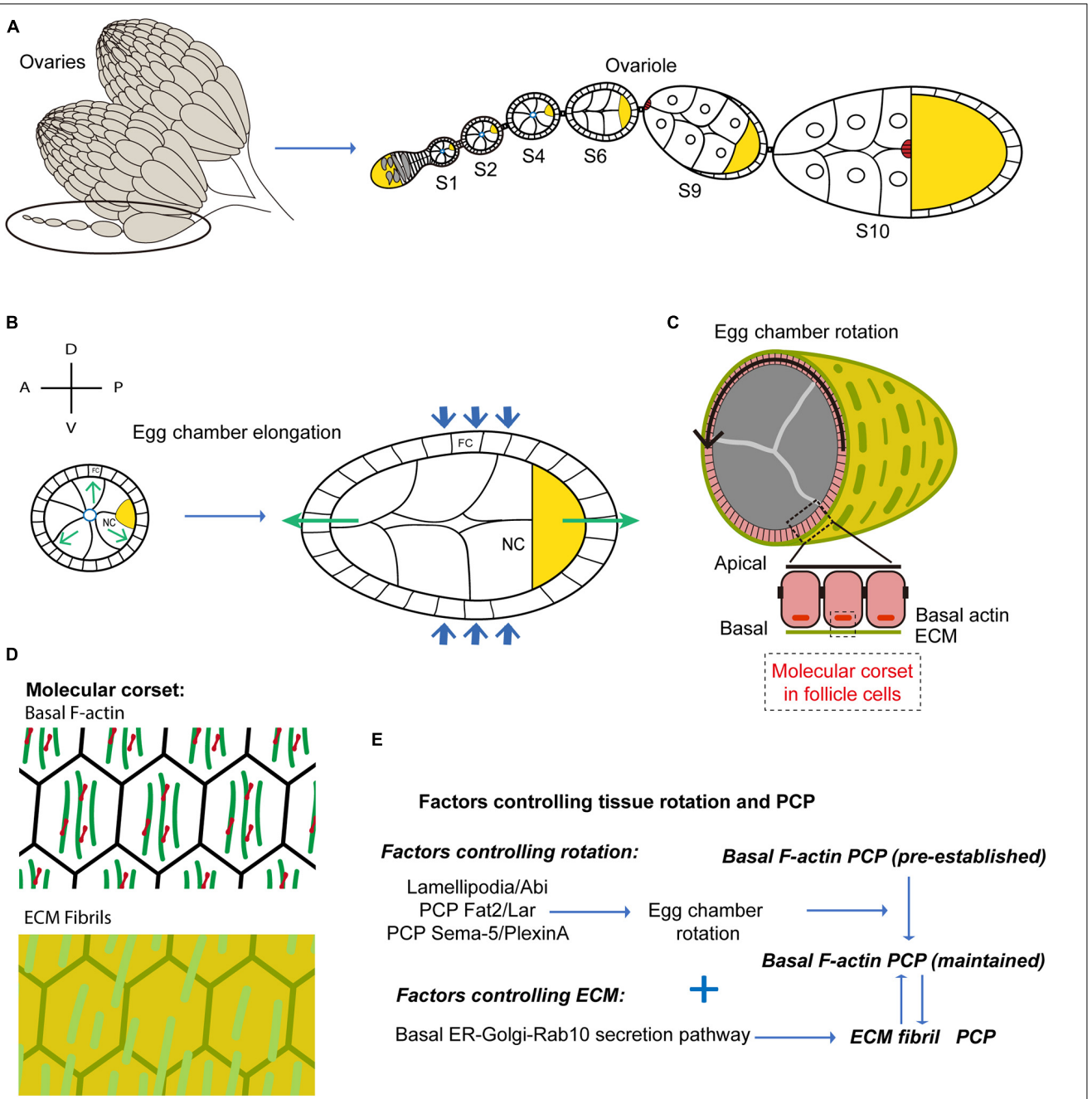

FIGURE 1 | Egg chamber rotation and planar cell polarity during *Drosophila* oogenesis. **(A)** Schematic diagram illustrating *Drosophila* ovary, composed of 15–20 ovarioles. Each ovariole is composed of a string of egg chambers at different developmental stages. **(B)** Schematic diagram illustrating egg chamber morphology at stages 5–8. FC, follicle cells; NC, nurse cells; oocyte in yellow. Anterior-posterior (AP) and Dorsal-ventral (DV) axes are indicated. Green arrows mark the direction of tissue expansion, and blue arrows mark the corset-restrictive forces. The egg chambers expand their volume from early to late stages. With the corset-restrictive forces, the egg elongates along the AP-axis during their expansion processes. **(C)** Schematic representation of the cross-sections of egg chamber at stages 5–8. Arrows indicate the sense of tissue rotation. **(D)** Schematic representation of the molecular corsets at stage 5–8. The molecular corsets are composed of parallel fibrillary ECM at the BM and parallel actin bundles at the basal domain of follicular epithelial cells. **(E)** Schematic diagram showing the mechanisms driving tissue rotation and planar cell polarity during *Drosophila* oogenesis.

(Popkova et al., 2020). How are polarized scaffolds formed? More precisely, how do actin bundles and ECM fibrils align? Actin bundle alignment is pre-established at very early stages of oogenesis (region 2b) (Chen et al., 2016) and the controlling factors are not known. In contrast, ECM fibril formation takes place between S2 and S8 via an atypical mechanism based on egg chamber polarized rotation around the AP axis.

Tissue Rotation and Planar Cell Polarity During *Drosophila* Oogenesis

Between S2 and S8, the egg chamber rotates along the AP axis (**Figure 1C**). Since six to seven egg chambers align to form a 'string', four to five chambers rotate simultaneously within each ovariole. Interestingly, while the rotation velocity is overall higher at later stages (with the exception of S8 when the egg rotation slows down), the angular velocity is rather constant between S3 and S7 (Chen et al., 2016) despite the >10-fold increase in egg volume (Chen et al., 2016, 2019). Egg chamber rotation is driven by the directed collective movement of follicular epithelial cells (**Figure 1E**). Since the follicle cells adhere to the internal germ cells, follicle cell collective migration results in the rotation of the entire egg chamber (Haigo and Bilder, 2011; Cetera and Horne-Badovinac, 2015). Remarkably, ECM fibrils lengthen and align along the direction of follicle cell rotation (i.e., egg chamber rotation). How do ECM fibrils form along planes orthogonal to the AP axis to form a supracellular molecular corset? Follicle cells, during rotatory migration, secrete BM components forming ECM fibril stripes at the rear, much like a 'snail slime trail' (Chen et al., 2017). BM components are synthesized in a basally located endoplasmic reticulum (ER) compartment and are then transported to the basal Golgi (Lerner et al., 2013). A Rab10-dependent secretory pathway controls the secretion of newly synthesized proteins in the pericellular space between follicular epithelial cells (Isabella and Horne-Badovinac, 2016). As a consequence of the directed movement of follicle cells, the secreted proteins are then directionally inserted into the BM (Isabella and Horne-Badovinac, 2016). The coordination between the Rab10-based secretion pathway and the directed collective cell movement, guarantees the formation of polarized BM fibrils enveloping the follicular epithelium (**Figure 1E**). Finally, in the Fat2 loss-of-function mutants in which tissue rotation (i.e., directed cell migration) is hampered, ECM fibrils form disorganized patterns (Lerner et al., 2013).

What are the cellular mechanisms and the signaling factors controlling the directed collective movement of follicle cells? Actin-based protrusions, formed at the follicle leading edge, often can function as exploratory antennas or traction force generators directing cell movement (Gardel et al., 2010; Ridley, 2011). Both filopodia and lamellipodia (i.e., typical exploratory and force generation cell protrusive structures, respectively), have been observed in the leading edges of migrating follicular epithelial cells during early stages of egg chamber rotation (Lewellyn et al., 2013; Cetera et al., 2014). Lamellipodia formation and tissue rotation are under the control of the SCAR/Wave complex, an activator of the actin nucleator Arp2/3 that is necessary to establish the dynamic branched actin network propelling the lamellipodium (**Figure 1E**; Cetera et al., 2014). Nevertheless, it is still not clear whether other critical factors controlling lamellipodia formation [e.g., the small GTPase Rac1 (Ridley et al., 1992; Wang et al., 2010)] play a role in this process. Recent studies have identified two PCP signaling pathways coordinating the leading and the trailing edge dynamics between neighboring follicle cells (**Figure 1E**; Barlan et al., 2017; Stedden et al., 2019). One PCP system is mediated by the atypical cadherin Fat2 and the Leukocyte-antigen-related-like (LAR) receptor tyrosine phosphatase (Barlan et al., 2017). These two proteins participate in the formation of protrusions in a non-cell-autonomous manner. The Fat2 based signals of follicular epithelial cells are located at the cell trailing edge inducing the formation of leading-edge protrusions in the cells located at the 'rear'. This protrusion induction mechanism is partially mediated by Lar stabilization at the leading edge of the rear cell. This results in the coordinated retraction and extension of the trailing edge of the cell at the front and of the leading edge of the cell at the rear, respectively. A second PCP system has been uncovered recently: this is based on the Semaphorin-5c and PlexinA factors providing additional coordination control over leading and trailing edges (Stedden et al., 2019). The SCAR/Wave and the PCP (Fat2/Lar and Semaphorin-5c/PlexinA) pathways, both coordinating the interface between the front and rear cells, could potentially synergize to orchestrate the directed collective cell migration (**Figure 1E**).

Actin bundles at the basal side of follicle cells align orthogonally to the AP axis from very early stages before egg chamber formation and during germarium development. This pre-polarized network could function as a cue to initiate directed follicle cell migration. While egg chamber rotation is thus the original cause of ECM fibril but not actin bundle polarity, rotation was shown to be responsible for the maintenance of actin bundle polarity during egg chamber maturation (Chen et al., 2016).

Egg chamber rotation stops at early stage 9, when the oscillatory contraction of the follicle basal actomyosin network starts to guide the second phase of egg chamber extension.

Oscillatory Actomyosin Contractions and Planar Cell Polarity During *Drosophila* Oogenesis

During S9 and S10 (**Figure 2A**), after egg chamber rotation arrest, MyoII medial-basal oscillations contract follicle cell stress-fibers driving periodic constriction of follicle cell basal surface and further extending the egg chamber (He et al., 2010; **Figure 2B**). Basal MyoII oscillations depend on the Rho1-ROCK pathway and on cell adhesion. Rho1 is strongly enriched at the basal junctions of follicle cells during S9 and S10 and it is positively regulated by cell-matrix but not cell-cell adhesion (Qin et al., 2017). Under the control of Rho1, ROCK is upregulated at the basal junctional cortex and eventually concentrates at the cell medial-basal region (Qin et al., 2018). Basal actomyosin periodic contractions reduce the follicle cell basal area along the dorsal-ventral (DV) direction (He et al., 2010), supporting the hypothesis that basal actomyosin networks drive DV polarized tension, remodeling basal surface area. In a recent study, stress-fiber tension anisotropy, at the basal side of follicle cells, was directly probed and measured by implementing infrared (IR) femtosecond (fs) laser ablation to dissect the actomyosin cytoskeleton with subcellular precision (Popkova et al., 2020). During S9, tension in the medial-basal network of follicle cells is an order of magnitude higher along the DV axis compared to the AP axis. Basal area fluctuations do not result in a rapid ratcheted net surface reduction since (i) both levels of fiber actin (F-actin) and MyoII oscillate without

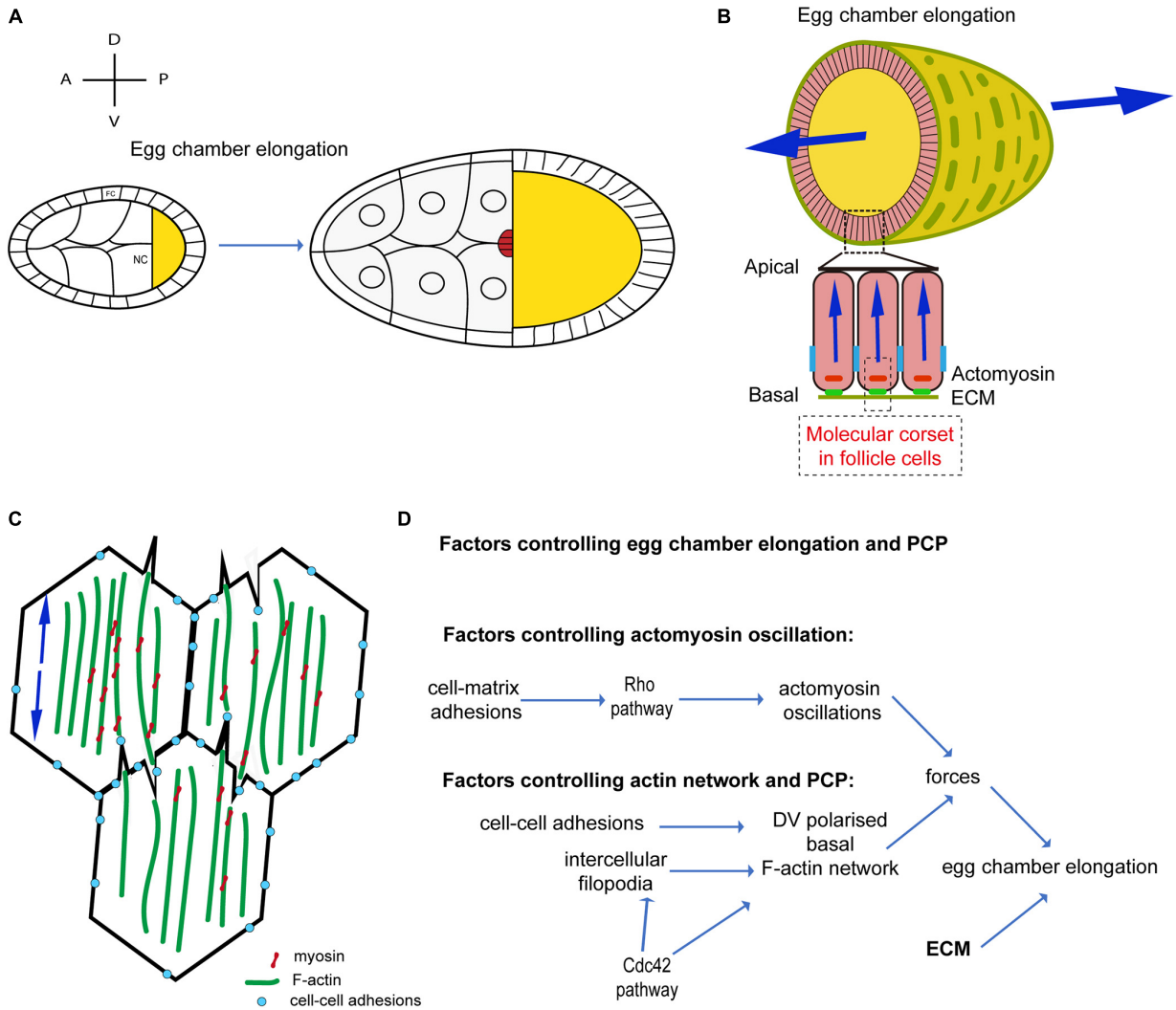

FIGURE 2 | Oscillatory actomyosin contractions and planar cell polarity during *Drosophila* oogenesis. **(A)** Schematic diagram illustrating egg chamber morphology at stages 9–10. AP and DV axes are indicated. FC, follicle cells; NC, nurse cells; oocyte in yellow. The egg chamber elongates along the AP-axis. **(B)** Schematic representation of the cross-sections of the egg chamber at S9–S10. Arrows indicate forces directed along the AP axis. **(C)** Schematic representation of the actomyosin distribution at the basal side of follicle cells in contact during S9–S10, showing filopodia penetrating the actomyosin cortex of a neighboring cell and forming a supracellular contractile network. Arrows indicate contractile forces. **(D)** Schematic diagram showing the mechanisms driving actomyosin contractions and planar cell polarity during *Drosophila* oogenesis.

net increase and (ii) contractions are non-synchronous between cells (He et al., 2010). This process shows similarities with the periodic surface oscillations reported in dorsally located cells during amnioserosa contractions (Solon et al., 2009) or in ectoderm cells during germband extension (Vanderleest et al., 2018). Follicle cell basal contraction is instead in net contrast with cell apical constriction in ventral furrow formation during *Drosophila* embryo gastrulation where cell-cell concerted net accumulation of MyoII ensures rapid and progressive cell apical surface reduction (Martin et al., 2009, 2010). Rho1 pathway upregulation in the follicular tissue results in MyoII oscillation arrest and basal MyoII net accumulation driving acute tissue AP extension (He et al., 2010; Qin et al., 2017). This evidence supports the idea that actomyosin periodic oscillations, devoid of MyoII net accumulation, ensure gradual tissue shape change over longer periods of time and avoid abrupt morphological transition. During S9, stress-fiber anisotropic tension could oppose polarized resistance to the gradual volume increase of the egg chamber directing tissue expansion toward the poles (similarly to the ECM at earlier stages).

Tissue morphogenesis relies upon cell-cell mechanical coupling for force transmission (Guillot and Lecuit, 2013; Heisenberg and Bellaiche, 2013). Mechanical coupling is usually mediated by adherens junctions: cell-cell adhesive sites are constituted by a dense F-actin network coupled to E-cadherin proteins (Ratheesh and Yap, 2012; Lecuit and Yap, 2015). Remarkably, between S9 and S10, parallel F-actin fibers span across the medial-basal side of follicle cells and

are not specifically enriched at junctions where low levels of mechanical tension are reported (Santa-Cruz Mateos et al., 2020). In addition, MyoII is absent at cell-cell junctions and it accumulates solely in the cortical medial-basal region. How are forces transmitted between follicle cells to establish tissue scale contractile tension? Supracellular F-actin bundles form across cells mediated by bi-directionally polarized filopodia (Popkova et al., 2020; **Figure 2C**). These long cell extensions, eventually culminating with E-cadherin based junctions, reciprocally interdigitate penetrating the actomyosin cortices of opposing cells. Follicle cell filopodia are tension sensitive: IR fs dissection of stress-fibers juxtaposed to filopodia induce tension release and filopodia retraction. In addition, filopodia can mediate cell-cell coupling eventually functioning as mechanical anchors bridging cell cortexes (Popkova et al., 2020). Santa-Cruz Mateos et al. (2020) report that F-actin protrusions increase in follicle cells neighboring integrin-mutant cells. Further work is necessary to better elucidate how filopodia protrusions interact with stress-fibers of neighboring cells and how this unusual cell-cell interaction mechanisms can cross-talk with cell-matrix adhesion.

Supracellular IR fs laser ablation of the actomyosin cortex, along a line parallel to the AP axis, results in one single large opening rather than multiple cell-to-cell independent F-actin network recoils. This demonstrates that supracellular tension results from the coupling of local cellular contractions. In addition, actomyosin dissection along a line parallel to the DV axis results in much slower recoil compared to a linear dissection along the orthogonal direction (i.e., the AP axis). This shows that the egg chamber during S9-S10 is under anisotropic tension with higher tension along the DV axis (Popkova et al., 2020). Both intercellular filopodia and stress-fibers are under the control of the activity of the small GTPase Cdc42. Genetic as well as optogenetic inhibitions of Cdc42 activity lead to reduced filopodia length and misaligned stress-fibers resulting in lower cell medio-basal tension (Popkova et al., 2020). Cdc42 is thus a key player ensuring tension anisotropy at the cellular scale. Furthermore, Cdc42 also plays a non-cell autonomous role in stress-fiber alignment and cell tension anisotropy. In follicular epithelia containing large Cdc42DN clones, tissue scale tension is drastically reduced along the DV axis: in Cdc42 mutants, the follicular epithelium fails to extend, thereby resulting in a more round-shaped egg chamber. This shows that the supracellular stress-fiber network, under the control of Cdc42, is powered by basal MyoII oscillations and drives anisotropic tension for tissue extension.

How is stress-fiber polarity established and maintained? F-actin stress-fibers align along the DV axis at very early stages of oogenesis (region 2b) under the control of an unknown factor. Stress-fiber alignment is eventually maintained during S9-S10 under the control of cell-cell adhesion and Cdc42 (Qin et al., 2017; Popkova et al., 2020). When E-cadherin cell-cell adhesion is downregulated, actin stress-fibers relocate to the basal junctional cortex and both ROCK and MyoII expand their localization more apically (Qin et al., 2017). When Cdc42 is inhibited, stress-fibers misalign and lose their DV polarity. Intercellular filopodia, under the control of Cdc42, could play a key role in maintaining stress-fiber alignment after egg chamber rotation arrest (S9 and S10) (**Figure 2D**).

Cell-ECM adhesions could also play a role in the organization of stress-fibers at the basal side of follicle cells since the inhibition of cell-matrix adhesion by RNAi, optogenetics, or loss-off-function alleles can eventually affect F-actin and MyoII levels and/or distribution in the basal region of follicle cells (Qin et al., 2017; Santa-Cruz Mateos et al., 2020). Further work is necessary to better elucidate the role of adhesion between the follicle cells and the ECM to establish a polarized F-actin supracellular network. Santa-Cruz Mateos et al. (2020) reported increased membrane tension in an integrin-mutant background. While more appropriate tools/protocols need to be implemented to discern between membrane and cytoskeletal tension at the cortex, it would be interesting in the future to probe stress-fiber tension in an integrin-mutant background to better understand the role of integrin-based adhesion to drive tension anisotropy at both cellular and supracellular levels. In a recent study, Cerqueira Campos et al. (2020) explored the role of the Dystroglican-associated protein complex (DAPC) in controlling ECM and F-actin network formation and polarity. DAPC is a transmembrane complex that links ECM to the F-actin cytoskeleton during follicle tissue elongation. The two main components of the DAPC [Dystrophin (Dys) and Dystroglycan (Dg)] are required during early oogenesis for follicle elongation and proper BM fibril and stress-fiber formation, but neither for rotation nor for the initial establishment of Fat2 PCP. Finally, the authors proposed that DAPC-dependent BM deposition at earlier stages (until S7) functions as a PCP 'memory' for F-actin stress-fiber alignment at a later stage (S13).

The spatial pattern of MyoII oscillations can be divided into three phases: (1) an initiation phase during early S9 (ES9) when MyoII oscillations appear in the anterior 1/3 region of the egg chamber; (2) a propagation phase between middle S9 (MS9) and beginning of S10 (S10A) when MyoII oscillations spread by shifting posteriorly and increasing in amplitude; and (3) a stabilization phase during middle to late of S10 (S10B) when all follicle cells contacting the oocyte accumulate medial-basal MyoII and MyoII oscillations reduce in amplitude maintaining high intensity levels. How the MyoII spatiotemporal pattern is controlled is still poorly understood. Koride et al. (2014) proposed a mechano-transduction-based mechanism that controls MyoII spatio-temporal patterns. This model was then challenged in 2018 by Qin et al. (2018), who showed that MyoII oscillation are tension independent.

DISCUSSION

Life often starts from a shapeless cluster of cells. Tissue elongation is among the very first morphogenetic processes to mold this cellular cluster during embryo development. Studying the fundamental mechanisms driving epithelial extension is thus a very exciting opportunity that will help us understand the emergence of life. In this review, we focus on the process of elongation in the *Drosophila* egg chamber, a powerful model system to study the cellular mechanisms driving epithelial morphogenesis.

Over the last decade, a new mechanism driving tissue elongation has been unraveled: polarized forces, driven by a

molecular corset, work to extend the egg chamber. The molecular corset is a two-tier wafer-like scaffold: F-actin stress-fibers at the basal side of follicle cells underlay polarized ECM fibrils at the BM. Both fiber networks are DV polarized and are wrapped around the egg chamber. While during the first phase of elongation (until S8) the corset works as a passive scaffold, during the second phase (S9-S10) the corset generates active forces powered by actomyosin contractions. F-actin stress-fibers are pre-polarized in the germarium, while ECM fibril polarization is under the control of egg chamber rotation around the AP axis during S2 to S8. Egg chamber rotation is driven by follicle cell collective migration: follicle cells undergo rounds of revolution propelled by polarized lamellipodia. The ECM secreted by follicle cells during migration results in the formation of DV aligned fibrils. Which mechanism controls the direction of follicle cell collective migration? Egg chambers are connected to each other via stalk cells at the anterior and posterior poles forming a pearl-string-like structure. These polar connecting sites could bias the direction of follicle cell migration by limiting the egg-chamber free degrees of rotation. If the direction of migration is imposed by the boundary conditions of the system, it is still not clear which mechanism controls the sense of egg chamber rotation. Egg chambers belonging to the same 'string' can rotate both in a clockwise and anti-clockwise direction (Haigo and Bilder, 2011). Under the control of stochastic subcellular polarity, one or a group of cells could take the lead by imposing a directional sense of movement (Jain et al., 2020). A mechanism based on stochastic polarity could be investigated by using optogenetics to induce or inhibit cell protrusion formation in a spatiotemporal specific fashion.

Egg chambers rotate with equal angular velocity during S3 to S7. Constant angular velocity at different egg-chamber stages can be achieved if follicle cells finely tune their speed of migration in a way that is directly proportional to the egg-chamber radius. Strong mechanical coupling between egg chambers belonging to the same 'string' could explain how angular velocity is conserved between egg chambers of different sizes: the rotation of one egg chamber would impose the same angular velocity to the other neighboring egg chambers (like wheels of different sizes mounted on the same axle). Nevertheless, this hypothesis may be ruled out since egg chambers on the same string may rotate in opposite directions. Future work is necessary to unveil the mechanisms controlling follicle cell migration imposing constant angular velocity to egg chambers at different stages.

The egg chamber is an ovoid structure. If all cells of one egg chamber migrate around the AP axis with the same angular velocity, cells located at the poles must migrate at slower speed than cells at the equator. How is cell speed finely controlled at different egg-chamber AP positions? Follicle cell collective migration could result from a cell leader-follower based mechanism (Barlan et al., 2017; Jain et al., 2020): for instance, medial follicle cells, that are more numerous, may act as leaders generating greater driving force. The central regions, under the control of JACK/STAT, is the portion of the egg chamber with denser ECM (Crest et al., 2017). Follicle cells located medially could thus adhere more strongly to the ECM generating greater traction forces to power migration. The denser ECM in the medial portion of the egg chamber could also be, at the same time, the result of a greater number of follicle cells located medially and secreting ECM during migration.

Stalk cells form connecting regions between egg chambers. If neighboring egg chambers rotate in the opposite sense, stalks cells would experience torsion opposing resistance to rotation. Cell intercalation between stalk cells and follicle cells at the egg-chamber poles is a mechanism that could facilitate counter-rotation between neighboring egg chambers. Future work is necessary to better elucidate the role of stalks during egg chamber rotation.

The periodic contraction of the cell actomyosin cytoskeleton is a process usually reported during cell shape changes and tissue morphogenesis (Munro et al., 2004; Skoglund et al., 2008; Martin et al., 2009; Solon et al., 2009; He et al., 2010; Rauzi et al., 2010). The biochemical oscillators controlling basal or apical MyoII recruitment share common features: periodic accumulation of Rho1 and ROCK control the dynamics of Myo-II recruitment by periodically phosphorylating the MyoII regulatory light chain. With similar dynamics, phosphatases periodically trigger MyoII dephosphorylation (Tan et al., 2003; Kasza et al., 2014; Simoes Sde et al., 2014; Vasquez et al., 2014; Munjal et al., 2015; Mason et al., 2016; Banerjee et al., 2017; Belmonte et al., 2017; Chanet et al., 2017; Michaux et al., 2018; Senger et al., 2019). Apical and basal periodic actomyosin contraction also show striking differences. At the cell apical-medial side, F-actin forms a cortical meshwork coupled to adherens junctions that can flow under MyoII load generating cortical advection (Rauzi et al., 2010; Munjal et al., 2015). The actomyosin flow induces a transient increase of actomyosin density that is referred to as 'pulse'. At the basal side of follicle cells, F-actin forms a network of parallel stress-fibers linked to the ECM via integrin-mediated adhesion (He et al., 2010; Qin et al., 2017). The F-actin network under MyoII load is able to contract along the direction of the stress-fibers but not to flow (Qin et al., 2017). The periodic contraction of actomyosin stress-fibers is referred to as 'oscillations'. 'Pulses' and 'oscillations' have the common feature of being periodic. Periodic constrictions could facilitate the gradual change in cell shape avoiding cell jamming or aberrant acute tissue shapes. MyoII oscillations in follicle cells appear asynchronous (He et al., 2010). It is still not clear whether oscillations of neighboring cells are coupled one another. In embryo wound repair it has been suggested that actomyosin contractility in discrete segments of the wound edge signals through a stretch-activated ion channel (SAIC) to neighboring segments to promote actomyosin assembly and to coordinate wound repair (Zulueta-Coarasa and Fernandez-Gonzalez, 2018). MyoII was also reported to accumulate under an ectopic mechanical stimulus (Fernandez-Gonzalez et al., 2009; Pouille et al., 2009) or endogenous cell stretching (Bailles et al., 2019). A mechano-transduction pathway could also be activated between neighboring follicle cells during actomyosin oscillation. The follicle cells located anteriorly and enveloping the nurse cells do not exhibit basal MyoII oscillations. During S9, follicle cells change shape from cuboidal to either squamous (enveloping the nurse cells) or columnar (enveloping the oocyte)

(Kolahi et al., 2009). Cell geometry might thus play a role in actin cytoskeleton organization and actomyosin oscillations (Vignaud et al., 2012). The cross-talk between F-actin stress-fibers and ECM is still unclear. During S2-S8, the stress-fiber network could work in tandem with the ECM fibrils to form a passive scaffold resisting the egg chamber expansion. During S9-S10, the ECM could contribute to integrate, at the tissue scale, periodic cellular constricting forces generated by the actomyosin network. These are key hypotheses that need to be tackled in the future.

AUTHOR CONTRIBUTIONS

XW and AP prepared the figures. MR commented on the figure revision. All authors wrote and revised the manuscript.

ACKNOWLEDGMENTS

XW thanks the Institut National de la Santé et de la Recherche Médicale [ATIP-Avenir program (2012–2016)], Région Midi-Pyrénées Excellence program (2013–2016) and Scientifiques de la Fondation ARC (Grant Nos. PJA 20171206526 and PJA20191209714) for support. MR thanks the French government through the UCA^{JEDI} Investments in the Future project managed by the National Research Agency (ANR-15-IDEX-01), the Investments for the Future LABEX SIGNALIFE (ANR-11-LABX-0028-01), the Tramplin ERC program from the National Research Agency (ANR-16-TERC-0018-01), and the ATIP-Avenir program from the CNRS and the Human Frontier Science Program (CDA00027/2017-C) for support.

REFERENCES

Aigouy, B., Farhadifar, R., Staple, D. B., Sagner, A., Roper, J. C., Julicher, F., et al. (2010). Cell flow reorients the axis of planar polarity in the wing epithelium of *Drosophila*. *Cell* 142, 773–786. doi: 10.1016/j.cell.2010.07.042

Baena-Lopez, L. A., Baonza, A., and Garcia-Bellido, A. (2005). The orientation of cell divisions determines the shape of *Drosophila* organs. *Curr. Biol.* 15, 1640–1644. doi: 10.1016/j.cub.2005.07.062

Bailles, A., Collinet, C., Philippe, J. M., Lenne, P. F., Munro, E., and Lecuit, T. (2019). Genetic induction and mechanochemical propagation of a morphogenetic wave. *Nature* 572, 467–473. doi: 10.1038/s41586-019-1492-9

Banerjee, D. S., Munjal, A., Lecuit, T., and Rao, M. (2017). Actomyosin pulsation and flows in an active elastomer with turnover and network remodeling. *Nat. Commun.* 8:1121. doi: 10.1038/s41467-017-01130-1

Barlan, K., Cetera, M., and Horne-Badovinac, S. (2017). Fat2 and lar define a basally localized planar signaling system controlling collective cell migration. *Dev. Cell* 40, 467–477.e5. doi: 10.1016/j.devcel.2017.02.003

Belmonte, J. M., Leptin, M., and Nedelec, F. (2017). A theory that predicts behaviors of disordered cytoskeletal networks. *Mol. Syst. Biol.* 13:941. doi: 10.15252/msb.20177796

Bertet, C., Sulak, L., and Lecuit, T. (2004). Myosin-dependent junction remodelling controls planar cell intercalation and axis elongation. *Nature* 429, 667–671. doi: 10.1038/nature02590

Blankenship, J. T., Backovic, S. T., Sanny, J. S., Weitz, O., and Zallen, J. A. (2006). Multicellular rosette formation links planar cell polarity to tissue morphogenesis. *Dev. Cell* 11, 459–470. doi: 10.1016/j.devcel.2006.09.007

Brittle, A., Thomas, C., and Strutt, D. (2012). Planar polarity specification through asymmetric subcellular localization of fat and dachsous. *Curr. Biol.* 22, 907–914. doi: 10.1016/j.cub.2012.03.053

Brittle, A. L., Repiso, A., Casal, J., Lawrence, P. A., and Strutt, D. (2010). Four-jointed modulates growth and planar polarity by reducing the affinity of dachsous for fat. *Curr. Biol.* 20, 803–810. doi: 10.1016/j.cub.2010.03.056

Campinho, P., Behrndt, M., Ranft, J., Risler, T., Minc, N., and Heisenberg, C. P. (2013). Tension-oriented cell divisions limit anisotropic tissue tension in epithelial spreading during zebrafish epiboly. *Nat. Cell Biol.* 15, 1405–1414. doi: 10.1038/ncb2869

Cerqueira Campos, F., Dennis, C., Alegot, H., Fritsch, C., Isabella, A., Pouchin, P., et al. (2020). Oriented basement membrane fibrils provide a memory for F-actin planar polarization via the dystrophin-dystroglycan complex during tissue elongation. *Development* 147:dev186957. doi: 10.1242/dev.186957

Cetera, M., and Horne-Badovinac, S. (2015). Round and round gets you somewhere: collective cell migration and planar polarity in elongating *Drosophila* egg chambers. *Curr. Opin. Genet. Dev.* 32, 10–15. doi: 10.1016/j.gde.2015.01.003

Cetera, M., Ramirez-San Juan, G. R., Oakes, P. W., Lewellyn, L., Fairchild, M. J., Tanentzapf, G., et al. (2014). Epithelial rotation promotes the global alignment of contractile actin bundles during *Drosophila* egg chamber elongation. *Nat. Commun.* 5:5511. doi: 10.1038/ncomms6511

Chanet, S., Miller, C. J., Vaishnav, E. D., Ermentrout, B., Davidson, L. A., and Martin, A. C. (2017). Actomyosin meshwork mechanosensing enables tissue shape to orient cell force. *Nat. Commun.* 8:15014. doi: 10.1038/ncomms15014

Chen, D. Y., Crest, J., and Bilder, D. (2017). A cell migration tracking tool supports coupling of tissue rotation to elongation. *Cell Rep.* 21, 559–569. doi: 10.1016/j.celrep.2017.09.083

Chen, D. Y., Crest, J., Streichan, S. J., and Bilder, D. (2019). Extracellular matrix stiffness cues junctional remodeling for 3D tissue elongation. *Nat. Commun.* 10:3339. doi: 10.1038/s41467-019-10874-x

Chen, D. Y., Lipari, K. R., Dehghan, Y., Streichan, S. J., and Bilder, D. (2016). Symmetry breaking in an edgeless epithelium by Fat2-regulated microtubule polarity. *Cell Rep.* 15, 1125–1133. doi: 10.1016/j.celrep.2016.04.014

Condic, M. L., Fristrom, D., and Fristrom, J. W. (1991). Apical cell shape changes during *Drosophila* imaginal leg disc elongation: a novel morphogenetic mechanism. *Development* 111, 23–33.

Crest, J., Diz-Munoz, A., Chen, D. Y., Fletcher, D. A., and Bilder, D. (2017). Organ sculpting by patterned extracellular matrix stiffness. *Elife* 6:e24958. doi: 10.7554/eLife.24958.022

Eaton, S., and Julicher, F. (2011). Cell flow and tissue polarity patterns. *Curr. Opin. Genet. Dev.* 21, 747–752. doi: 10.1016/j.gde.2011.08.010

Etournay, R., Popovic, M., Merkel, M., Nandi, A., Blasse, C., Aigouy, B., et al. (2015). Interplay of cell dynamics and epithelial tension during morphogenesis of the *Drosophila* pupal wing. *Elife* 4:e07090. doi: 10.7554/eLife.07090.043

Fernandez-Gonzalez, R., Simoes Sde, M., Roper, J. C., Eaton, S., and Zallen, J. A. (2009). Myosin II dynamics are regulated by tension in intercalating cells. *Dev. Cell* 17, 736–743. doi: 10.1016/j.devcel.2009.09.003

Gardel, M. L., Schneider, I. C., Aratyn-Schaus, Y., and Waterman, C. M. (2010). Mechanical integration of actin and adhesion dynamics in cell migration. *Annu. Rev. Cell Dev. Biol.* 26, 315–333. doi: 10.1146/annurev.cellbio.011209.122036

Goodrich, L. V., and Strutt, D. (2011). Principles of planar polarity in animal development. *Development* 138, 1877–1892. doi: 10.1242/dev.054080

Guillot, C., and Lecuit, T. (2013). Mechanics of epithelial tissue homeostasis and morphogenesis. *Science* 340, 1185–1189. doi: 10.1126/science.1235249

Gutzeit, H. O., Eberhardt, W., and Gratwohl, E. (1991). Laminin and basement membrane-associated microfilaments in wild-type and mutant *Drosophila* ovarian follicles. *J. Cell Sci.* 100(Pt 4), 781–788.

Haigo, S. L., and Bilder, D. (2011). Global tissue revolutions in a morphogenetic movement controlling elongation. *Science* 331, 1071–1074. doi: 10.1126/science.1199424

Harris, T. J., and Peifer, M. (2004). Adherens junction-dependent and -independent steps in the establishment of epithelial cell polarity in *Drosophila*. *J. Cell Biol.* 167, 135–147. doi: 10.1083/jcb.200406024

He, L., Wang, X., and Montell, D. J. (2011). Shining light on *Drosophila* oogenesis: live imaging of egg development. *Curr. Opin. Genet. Dev.* 21, 612–619. doi: 10.1016/j.gde.2011.08.011

He, L., Wang, X., Tang, H. L., and Montell, D. J. (2010). Tissue elongation requires oscillating contractions of a basal actomyosin network. *Nat. Cell Biol.* 12, 1133–1142. doi: 10.1038/ncb2124

Heisenberg, C. P., and Bellaiche, Y. (2013). Forces in tissue morphogenesis and patterning. *Cell* 153, 948–962. doi: 10.1016/j.cell.2013.05.008

Imuta, Y., Koyama, H., Shi, D., Eiraku, M., Fujimori, T., and Sasaki, H. (2014). Mechanical control of notochord morphogenesis by extra-embryonic tissues in mouse embryos. *Mech. Dev.* 132, 44–58. doi: 10.1016/j.mod.2014.01.004

Irvine, K. D., and Wieschaus, E. (1994). Cell intercalation during *Drosophila* germband extension and its regulation by pair-rule segmentation genes. *Development* 120, 827–841.

Isabella, A. J., and Horne-Badovinac, S. (2016). Rab10-mediated secretion synergizes with tissue movement to build a polarized basement membrane architecture for organ Morphogenesis. *Dev. Cell* 38, 47–60. doi: 10.1016/j.devcel.2016.06.009

Jain, S., Cachoux, V. M. L., Narayana, G., de Beco, S., D'Alessandro, J., Cellerin, V., et al. (2020). The role of single cell mechanical behavior and polarity in driving collective cell migration. *Nat. Phys.* 16, 802–809. doi: 10.1038/s41567-020-0875-z

Kasza, K. E., Farrell, D. L., and Zallen, J. A. (2014). Spatiotemporal control of epithelial remodeling by regulated myosin phosphorylation. *Proc. Natl. Acad. Sci. U.S.A.* 111, 11732–11737. doi: 10.1073/pnas.1400520111

Keller, R. (2002). Shaping the vertebrate body plan by polarized embryonic cell movements. *Science* 298, 1950–1954. doi: 10.1126/science.1079478

Kolahi, K. S., White, P. F., Shreter, D. M., Classen, A. K., Bilder, D., and Mofrad, M. R. (2009). Quantitative analysis of epithelial morphogenesis in *Drosophila* oogenesis: new insights based on morphometric analysis and mechanical modeling. *Dev. Biol.* 331, 129–139. doi: 10.1016/j.ydbio.2009.04.028

Koride, S., He, L., Xiong, L. P., Lan, G., Montell, D. J., and Sun, S. X. (2014). Mechanochemical regulation of oscillatory follicle cell dynamics in the developing *Drosophila* egg chamber. *Mol. Biol. Cell* 25, 3709–3716. doi: 10.1091/mbc.e14-04-0875

Lecuit, T., and Yap, A. S. (2015). E-cadherin junctions as active mechanical integrators in tissue dynamics. *Nat. Cell Biol.* 17, 533–539. doi: 10.1038/ncb3136

Lerner, D. W., McCoy, D., Isabella, A. J., Mahowald, A. P., Gerlach, G. F., Chaudhry, T. A., et al. (2013). A Rab10-dependent mechanism for polarized basement membrane secretion during organ morphogenesis. *Dev. Cell* 24, 159–168. doi: 10.1016/j.devcel.2012.12.005

Lewellyn, L., Cetera, M., and Horne-Badovinac, S. (2013). Misshapen decreases integrin levels to promote epithelial motility and planar polarity in *Drosophila*. *J. Cell Biol.* 200, 721–729. doi: 10.1083/jcb.201209129

Martin, A. C., Gelbart, M., Fernandez-Gonzalez, R., Kaschube, M., and Wieschaus, E. F. (2010). Integration of contractile forces during tissue invagination. *J. Cell Biol.* 188, 735–749. doi: 10.1083/jcb.200910099

Martin, A. C., Kaschube, M., and Wieschaus, E. F. (2009). Pulsed contractions of an actin-myosin network drive apical constriction. *Nature* 457, 495–499. doi: 10.1038/nature07522

Mason, F. M., Xie, S., Vasquez, C. G., Tworoger, M., and Martin, A. C. (2016). RhoA GTPase inhibition organizes contraction during epithelial morphogenesis. *J. Cell Biol.* 214, 603–617. doi: 10.1083/jcb.201603077

Michaux, J. B., Robin, F. B., McFadden, W. M., and Munro, E. M. (2018). Excitable RhoA dynamics drive pulsed contractions in the early C. elegans embryo. *J. Cell Biol.* 217, 4230–4252. doi: 10.1083/jcb.201806161

Munjal, A., Philippe, J. M., Munro, E., and Lecuit, T. (2015). A self-organized biomechanical network drives shape changes during tissue morphogenesis. *Nature* 524, 351–355. doi: 10.1038/nature14603

Munoz-Soriano, V., Belacortu, Y., and Paricio, N. (2012). Planar cell polarity signaling in collective cell movements during morphogenesis and disease. *Curr. Genomics* 13, 609–622. doi: 10.2174/138920212803759721

Munro, E., Nance, J., and Priess, J. R. (2004). Cortical flows powered by asymmetrical contraction transport PAR proteins to establish and maintain anterior-posterior polarity in the early C. elegans embryo. *Dev. Cell* 7, 413–424. doi: 10.1016/j.devcel.2004.08.001

Nelson, K. S., Khan, Z., Molnar, I., Mihaly, J., Kaschube, M., and Beitel, G. J. (2012). *Drosophila* Src regulates anisotropic apical surface growth to control epithelial tube size. *Nat. Cell Biol.* 14, 518–525. doi: 10.1038/ncb2467

Popkova, A., Stone, O. J., Chen, L., Qin, X., Liu, C., Liu, J., et al. (2020). A Cdc42-mediated supracellular network drives polarized forces and *Drosophila* egg chamber extension. *Nat. Commun.* 11:1921. doi: 10.1038/s41467-020-15593-2

Pouille, P. A., Ahmadi, P., Brunet, A. C., and Farge, E. (2009). Mechanical signals trigger Myosin II redistribution and mesoderm invagination in *Drosophila* embryos. *Sci. Signal.* 2:ra16. doi: 10.1126/scisignal.2000098

Qin, X., Hannezo, E., Mangeat, T., Liu, C., Majumder, P., Liu, J., et al. (2018). A biochemical network controlling basal myosin oscillation. *Nat. Commun.* 9:1210. doi: 10.1038/s41467-018-03574-5

Qin, X., Park, B. O., Liu, J., Chen, B., Choesmel-Cadamuro, V., Belguise, K., et al. (2017). Cell-matrix adhesion and cell-cell adhesion differentially control basal myosin oscillation and *Drosophila* egg chamber elongation. *Nat. Commun.* 8:14708. doi: 10.1038/ncomms14708

Ratheesh, A., and Yap, A. S. (2012). A bigger picture: classical cadherins and the dynamic actin cytoskeleton. *Nat. Rev. Mol. Cell Biol.* 13, 673–679. doi: 10.1038/nrm3431

Rauzi, M., Lenne, P. F., and Lecuit, T. (2010). Planar polarized actomyosin contractile flows control epithelial junction remodelling. *Nature* 468, 1110–1114. doi: 10.1038/nature09566

Ridley, A. J. (2011). Life at the leading edge. *Cell* 145, 1012–1022. doi: 10.1016/j.cell.2011.06.010

Ridley, A. J., Paterson, H. F., Johnston, C. L., Diekmann, D., and Hall, A. (1992). The small GTP-binding protein rac regulates growth factor-induced membrane ruffling. *Cell* 70, 401–410. doi: 10.1016/0092-8674(92)90164-8

Santa-Cruz Mateos, C., Valencia-Exposito, A., Palacios, I. M., and Martin-Bermudo, M. D. (2020). Integrins regulate epithelial cell shape by controlling the architecture and mechanical properties of basal actomyosin networks. *PLoS Genet.* 16:e1008717. doi: 10.1371/journal.pgen.1008717

Senger, F., Pitaval, A., Ennomani, H., Kurzawa, L., Blanchoin, L., and Thery, M. (2019). Spatial integration of mechanical forces by alpha-actinin establishes actin network symmetry. *J. Cell Sci.* 132:jcs236604. doi: 10.1101/578799

Simoes Sde, M., Mainieri, A., and Zallen, J. A. (2014). Rho GTPase and Shroom direct planar polarized actomyosin contractility during convergent extension. *J. Cell Biol.* 204, 575–589. doi: 10.1083/jcb.201307070

Skoglund, P., Rolo, A., Chen, X., Gumbiner, B. M., and Keller, R. (2008). Convergence and extension at gastrulation require a myosin IIB-dependent cortical actin network. *Development* 135, 2435–2444. doi: 10.1242/dev.014704

Solon, J., Kaya-Copur, A., Colombelli, J., and Brunner, D. (2009). Pulsed forces timed by a ratchet-like mechanism drive directed tissue movement during dorsal closure. *Cell* 137, 1331–1342. doi: 10.1016/j.cell.2009.03.050

St Johnston, D., and Sanson, B. (2011). Epithelial polarity and morphogenesis. *Curr. Opin. Cell Biol.* 23, 540–546. doi: 10.1016/j.ceb.2011.07.005

Stedden, C. G., Menegas, W., Zajac, A. L., Williams, A. M., Cheng, S., Ozkan, E., et al. (2019). Planar-polarized semaphorin-5c and plexin A promote the collective migration of epithelial cells in *Drosophila*. *Curr. Biol.* 29, 908–920.e6. doi: 10.1016/j.cub.2019.01.049

Tan, C., Stronach, B., and Perrimon, N. (2003). Roles of myosin phosphatase during *Drosophila* development. *Development* 130, 671–681. doi: 10.1242/dev.00298

Vanderleest, T. E., Smits, C. M., Xie, Y., Jewett, C. E., Blankenship, J. T., and Loerke, D. (2018). Vertex sliding drives intercalation by radial coupling of adhesion and actomyosin networks during *Drosophila* germband extension. *Elife* 7:e34586. doi: 10.7554/eLife.34586.029

Vasquez, C. G., Tworoger, M., and Martin, A. C. (2014). Dynamic myosin phosphorylation regulates contractile pulses and tissue integrity during epithelial morphogenesis. *J. Cell Biol.* 206, 435–450. doi: 10.1083/jcb.201402004

Vichas, A., and Zallen, J. A. (2011). Translating cell polarity into tissue elongation. *Semin. Cell Dev. Biol.* 22, 858–864. doi: 10.1016/j.semcdb.2011.09.013

Vignaud, T., Galland, R., Tseng, Q., Blanchoin, L., Colombelli, J., and Thery, M. (2012). Reprogramming cell shape with laser nano-patterning. *J. Cell Sci.* 125, 2134–2140. doi: 10.1242/jcs.104901

Wang, X., He, L., Wu, Y. I., Hahn, K. M., and Montell, D. J. (2010). Light-mediated activation reveals a key role for Rac in collective guidance of cell movement in vivo. *Nat. Cell Biol.* 12, 591–597. doi: 10.1038/ncb2061

Zulueta-Coarasa, T., and Fernandez-Gonzalez, R. (2018). Dynamic force patterns promote collective cell movements during embryonic wound repair. *Nat. Phys.* 14, 750–758. doi: 10.1038/s41567-018-0111-2

Conflict of Interest: The authors declare that the research was conducted in the absence of any commercial or financial relationships that could be construed as a potential conflict of interest.

frontiers in Cell and Developmental Biology

ORIGINAL RESEARCH
published: 08 April 2021
doi: 10.3389/fcell.2021.636024

The Epidermal Growth Factor Ligand Spitz Modulates Macrophage Efferocytosis, Wound Responses and Migration Dynamics During *Drosophila* Embryogenesis

*Olivier R. Tardy[1,2], Emma L. Armitage[1,2], Lynne R. Prince[1] and Iwan R. Evans[1,2]**

[1] Department of Infection, Immunity and Cardiovascular Disease, The Bateson Centre, The University of Sheffield, Sheffield, United Kingdom, [2] The Bateson Centre, The University of Sheffield, Sheffield, United Kingdom

OPEN ACCESS

Edited by:
Benjamin Lin,
New York University, United States

Reviewed by:
Estee Kurant,
University of Haifa, Israel
Maria Dolores Martin-Bermudo,
Consejo Superior de Investigaciones Científicas (CSIC), Spain
Mirka Uhlirova,
University of Rochester, United States

***Correspondence:**
Iwan R. Evans
i.r.evans@sheffield.ac.uk

Specialty section:
This article was submitted to Signaling, a section of the journal Frontiers in Cell and Developmental Biology

Received: *30 November 2020*
Accepted: *19 March 2021*
Published: *08 April 2021*

Citation:
Tardy OR, Armitage EL, Prince LR and Evans IR (2021) The Epidermal Growth Factor Ligand Spitz Modulates Macrophage Efferocytosis, Wound Responses and Migration Dynamics During Drosophila Embryogenesis. Front. Cell Dev. Biol. 9:636024. doi: 10.3389/fcell.2021.636024

How multifunctional cells such as macrophages interpret the different cues within their environment and undertake an appropriate response is a key question in developmental biology. Understanding how cues are prioritized is critical to answering this – both the clearance of apoptotic cells (efferocytosis) and the migration toward damaged tissue is dependent on macrophages being able to interpret and prioritize multiple chemoattractants, polarize, and then undertake an appropriate migratory response. Here, we investigate the role of Spitz, the cardinal *Drosophila* epidermal growth factor (EGF) ligand, in regulation of macrophage behavior in the developing fly embryo, using activated variants with differential diffusion properties. Our results show that misexpression of activated Spitz can impact macrophage polarity and lead to clustering of cells in a variant-specific manner, when expressed either in macrophages or the developing fly heart. Spitz can also alter macrophage distribution and perturb apoptotic cell clearance undertaken by these phagocytic cells without affecting the overall levels of apoptosis within the embryo. Expression of active Spitz, but not a membrane-bound variant, can also increase macrophage migration speeds and impair their inflammatory responses to injury. The fact that the presence of Spitz specifically undermines the recruitment of more distal cells to wound sites suggests that Spitz desensitizes macrophages to wounds or is able to compete for their attention where wound signals are weaker. Taken together these results suggest this molecule regulates macrophage migration and their ability to dispose of apoptotic cells. This work identifies a novel regulator of *Drosophila* macrophage function and provides insights into signal prioritization and integration *in vivo*. Given the importance of apoptotic cell clearance and inflammation in human disease, this work may help us to understand the role EGF ligands play in immune cell recruitment during development and at sites of disease pathology.

Keywords: *Drosophila*, macrophage, hemocyte, epidermal growth factor, cell migration, inflammation, apoptotic cell clearance

INTRODUCTION

Understanding how motile cells integrate and prioritize the array of signals they face in the complex *in vivo* environment is a fundamental question in biology. For multifunctional cells such as macrophages this is a particularly important process, since it determines their subsequent behavior, be it migration to sites of damage, or clearance of pathogens and dying cells. The integration of a specific cue is highly contextual and depends on a number of parameters including crosstalk between signal transduction pathways (Heit et al., 2008), calcium levels within cells (Dou et al., 2012; Sieger et al., 2012), and the diffusion properties of a given ligand (Foxman et al., 1997). However, even before we are able to understand how cells prioritize different cues *in vivo*, and so are able to polarize and migrate toward their correct targets, it is necessary to identify a more complete range of cues to which they can respond.

Drosophila melanogaster fruit flies have a robust cellular immune response, composed principally of motile and highly-phagocytic plasmatocytes (Evans and Wood, 2011), which perform many analogous functions to vertebrate macrophages, e.g., phagocytosis of apoptotic cells and pathogens, migration to wounds and secretion of extracellular matrix (Buchon et al., 2014; Weavers et al., 2016). These cells (referred to hereafter as embryonic macrophages) have been extensively used to investigate cell polarization and migration *in vivo*, although we are yet to understand the full complement of cues that regulate their behaviors. Post hematopoiesis, embryonic *Drosophila* macrophages undertake stereotypical patterns of dispersal across the embryo. This dispersal is governed by PDGF/Vegf-related ligands (Pvfs) that act both as chemoattractants and pro-survival signals (Cho et al., 2002; Brückner et al., 2004; Wood et al., 2006), cell–cell repulsion between macrophages (Davis et al., 2012), and access to physical spaces created during organogenesis (Evans et al., 2010a). Once dispersed over the embryo (stage 15 onwards), macrophages become competent to respond to wounding stimuli (Moreira et al., 2010) and undergo "random migration," a process driven in part by cell–cell repulsion (Stramer et al., 2010). Alongside deposition of matrix during dispersal (Matsubayashi et al., 2017), clearance of apoptotic cells (efferocytosis) and responses to acute wound stimuli represent migration-dependent functions that require polarization and migration of these macrophages toward specific targets. Apoptosis is the major form of programmed cell death in multicellular organisms (Fuchs and Steller, 2011; Galluzzi et al., 2012) and rapid efferocytosis is required to prevent secondary necrosis, a highly pro-inflammatory event that can lead to subsequent tissue damage (Degterev and Yuan, 2008; Ariel and Ravichandran, 2016). Failures in efferocytosis are linked to a range of disease pathologies in humans, particularly those associated with chronic inflammation, including atherosclerosis and chronic obstructive pulmonary disease (Eltboli et al., 2014; Morioka et al., 2019). The recruitment of macrophages to apoptotic cells is mediated by a family of chemoattractants released as part of the apoptotic cell death program and collectively referred to as "find-me" cues (Ravichandran, 2003). While find-me cues have been extensively studied in mammals, e.g., lysophosphatidylcholine (LPC) or ATP (Lauber, 2003; Elliott et al., 2009), the identity of such signals remains unknown in *Drosophila*, although fragments of tyrosyl tRNA synthetase have been shown to play a role in recruitment of macrophages to apoptotic "loser" cells in studies of cell competition (Casas-Tintó et al., 2015). *Drosophila* embryonic macrophages also undertake polarized migration when responding to tissue damage (Stramer et al., 2005). This process requires the generation of reactive oxygen species (Razzell et al., 2013; Evans et al., 2015), resembling inflammatory responses in other model organisms, including zebrafish (Niethammer et al., 2009; Yoo et al., 2011). As per find-me cues, the precise nature of wound cues remains to be elucidated in flies.

Recent evidence in *Drosophila* suggested that an epidermal growth factor (EGF) ligand homolog, Spitz, is secreted from midgut cells undergoing apoptosis. This facilitates recruitment of stem cells to replenish the cells in those apoptotic regions, thereby maintaining gut integrity (Liang et al., 2017). A chemoattractive role for EGF ligands is conserved across evolution with, amongst others, both human monocytes and border cells in the developing *Drosophila* oocyte shown to chemotax toward EGF ligands (Duchek and Rørth, 2001; Lamb et al., 2004). In contrast to mammalian EGF receptor signaling, which is composed of multiple heterodimeric ErbB receptors and ligands (Burgess et al., 2003; Citri and Yarden, 2006), *Drosophila* possess only a single EGF receptor (EGFR/Torpedo). EGFR is activated by several partially redundant ligands (Spitz, Vein, Keren, and Gurken) that are expressed in a tissue-specific manner (Price et al., 1989). In both flies and humans, secretion of active EGF ligands is tightly regulated via activation of the proteolytic enzymes Rhomboid (Shilo, 2016) and ADAM17 (Scheller et al., 2011; Rose-John, 2013), respectively. During *Drosophila* development, Spitz is ubiquitously expressed. However, the key processing enzyme Rhomboid is expressed in a tissue-specific pattern, including by the cells of the ventral midline (Tomancak et al., 2007; Frise et al., 2010). This post-translational control enables spatial specificity of action, for instance the role of Spitz in development of the midline glia (Raz and Shilo, 1992). The combined evolutionary and developmental evidence suggested to us that Spitz might have a role as a chemoattractant regulating *Drosophila* macrophage behavior.

In this study, we have used tissue-specific expression of two active variants of the EGF ligand Spitz to investigate how high levels of EGF signaling can alter the migration and function of *Drosophila* macrophages *in vivo*. Our results show that expression of active Spitz in macrophages alters their migration dynamics, increasing migration speed and stimulating macrophage clustering and elongation. These phenotypes require cleavage of Spitz from the membrane since a membrane-bound variant does not alter macrophage behavior. In addition, our results show that the presence of Spitz reduces the sensitivity of macrophages to both apoptotic and wound-derived signals. Our results demonstrate the capacity for EGF signaling to regulate diverse and important macrophage behaviors *in vivo* and suggest the possibility that EGF ligands may belong to a growing list of apoptotic cell-derived, find-me cues. These effects of EGF signaling on efferocytosis, inflammatory responses and

macrophage migration have implications for our understanding of macrophage function during both embryogenesis and chronic inflammation, where these ligands play important roles in development and at sites of pathology in higher organisms.

MATERIALS AND METHODS

Fly Stocks

Fly stocks were maintained on molasses-based media supplemented with yeast at 18°C with mating populations kept in laying cages at 22°C. Embryos were collected from apple juice/agar plates on which embryos had been laid overnight. The following *Drosophila* lines were used in this study: *UAS-EGFP*, *UAS-red stinger* (Barolo et al., 2000), *UAS-sSpitz*^{CS} (Ghiglione et al., 2002), *UAS-Spitz*^{Sec} (Miura et al., 2006), *UAS-mSpitz*^{CS}*-EGFP* (Miura et al., 2006), *UAS-LifeAct* (Hatan et al., 2011), *Srp-3x-mCherry* (Gyoergy et al., 2018), *EGFR-sfGFP* (Revaitis et al., 2020), *Serpent-GAL4* (Brückner et al., 2004), *Croquemort-GAL4* (Stramer et al., 2005), and *TinC-GAL4* (Lo and Frasch, 2001). All experiments were conducted on a w^{1118} background. See **Supplementary Table 1** for specific experimental genotypes.

Preparation, Imaging and Wounding of Live Embryos

Embryos laid on apple juice/agar plates were washed off into a cell strainer and dechorionated in 5% bleach for 1 min, followed by five washes in distilled water. Embryos were mounted in 10S Voltalef oil (VWR) as per Evans et al., 2010b. Live embryos were imaged using a Perkin Elmer Ultraview Spinning disk system using either a 10× air (UplanSApo 10×/NA 0.4; lateral images of stage 15 embryos to show developmental dispersal of macrophages or to quantify total number of macrophages per embryo) or 40× oil immersion (UplanSApo 40× oil/NA 1.3; all remaining live imaging) objective lens. For analysis of macrophage random migration and wound responses, the ventral surface of stage 15 embryos was imaged to a depth of approximately 20 μm with a 1 μm spacing between *z*-planes. Time-lapse movies were assembled from *z*-stacks taken every 2 min for 1 h using Volocity software (Perkin Elmer) for analysis of both macrophage random migration and wound responses. Wounding was performed using a Micropoint ablation laser (Andor) to ablate the ventral epithelium on the ventral midline in the medial-most segments of the embryo as per Evans et al. (2015); the inflammatory responses of macrophages in this region were then followed for 1-h post wounding.

Immunostaining of *Drosophila* Embryos

Live embryos were fixed as previously described (Wood et al., 2006). For immunostaining, dechorionated embryos were fixed using a 50:50 mixture of 4% formaldehyde in phosphate-buffered saline (PBS; Oxoid) and peroxide-free heptane (Sigma) before being devitellinised using methanol. Embryos were then washed with 0.1% Triton-X-100 (Sigma) in PBS. Subsequently, embryos were blocked in PATx [1% Bovine Serum Albumin (Sigma), 0.1% Triton-X-100 in PBS] for 1 h. Embryos were then incubated with primary antibodies overnight at 4°C, washed in PATx and incubated with secondary antibodies for 2 h at room temperature. After a final series of PATx washes, residual PATx was aspirated and the embryos stored at 4°C in 2.5% 1,4 Diazabicyclo[2.2.2]octane (DABCO) mountant (Sigma) diluted in 90% glycerol (Sigma)/1× PBS. Stained embryos were mounted in DABCO mountant on glass slides as per Evans et al., 2010a. Images of immunostained embryos were taken using a Zeiss 880 Airyscan confocal microscopy system running ZEN software. Embryos were imaged using a 40× objective lens (Zeiss Plan-Apochromat 40× oil/NA 1.4) to a depth of approximately 25 μm with a spacing of 0.2 μm between *z*-planes (cDCP-1 and DpERK staining) or using a 63× objective lens (Zeiss Plan-Apochromat 63× oil/NA 1.4; EGFR-sfGFP localization). For staining of apoptotic cells and GFP (expressed in macrophages to enable their visualization), the following primary antibodies were used: rabbit anti-cleaved DCP-1 (cDCP-1; 1:200; 9578S, Cell Signaling) and mouse anti-GFP (1:100; ab1218, Abcam). As a read-out of EGFR activation in macrophages, embryos were stained for activated ERK [DpERK; rabbit anti-phospho-p44/42 MAPK (Erk1/2) (Thr202/Tyr204); 1:100; 197G2, Cell Signaling Technology] with GFP-labeled macrophages detected via immunostaining for GFP (1:100; ab1218, Abcam). AlexaFluor568 goat anti-rabbit IgG (1:200; A11036, Life Technologies) and AlexaFluor488 goat anti-mouse IgG (1:200; A11029, Life Technologies) were used as secondary antibodies to detect anti-GFP, anti-cDCP-1 and anti-DpERK primary antibodies. To detect EGFR-sfGFP and macrophages, respectively, Rabbit anti-GFP (1:500; ab290, Abcam) and mouse anti-Fascin (purified sn 7C antibody diluted 1:1000; Developmental Studies Hybridoma Bank) were used as primary antibodies. AlexaFluor488 goat anti-rabbit IgG (1:200; A11034, Life Technologies) and AlexaFluor568 goat anti-mouse IgG (1:200; A11031, Life Technologies) were used as secondary antibodies.

Lysotracker Red Staining of Embryos

pH-sensitive Lysotracker Red DND-99 (L7528, Life Technologies) was used to monitor acidification of phagosomes. Dechorionated embryos were transferred to glass vials containing peroxide-free heptane and PBS containing lysotracker red (25 μM) in a 1:1 ratio and shaken for 30 min at 250 rpm in the dark. Post staining, embryos were transferred into Halocarbon oil 700 (Sigma); stage 15 embryos were selected and the ventral midline region imaged using a Perkin Elmer Ultraview Spinning disk system (UplanSApo 40× oil objective lens/NA 1.3).

Image Processing and Analysis

Images were converted to Tiff (.tif) format files prior to analysis in Fiji (ImageJ; Schindelin et al., 2012). Movies and stills showing macrophage morphology, apoptotic cell clearance, migration and lateral views of stage 15 embryos were assembled as maximum projections and despeckled to reduce background noise. Clustering of macrophages was assessed by counting the number of macrophage-macrophage contacts from maximum projections of the ventral midline region at stage 15 in Fiji. Only definite contacts between the cell bodies of neighboring

macrophages were scored. Morphological parameters (e.g., aspect ratio (AR), which is defined as the ratio of a cell's width to its height) were measured manually from maximum projections using the polygon selection tool in Fiji. Macrophage vacuolation, a read-out of apoptotic cell clearance, was assessed in the z-slice corresponding to that cell's largest cross-sectional area in 5 macrophages per embryo. Apoptotic cell clearance was also analyzed using embryos containing GFP-labeled macrophages immunostained for cDCP-1 and GFP. The numbers of cDCP-1-positive punctae inside (within GFP-positive cell areas) or outside macrophages in a field of view corresponding to the medial-most ventral region of stage 15 embryos were counted in merged *z*-stacks of the GFP and cDCP-1 channels. These values were used to calculate the total numbers of cDCP-1 punctae and "efferocytosis efficiency" per field of view. Efferocytosis efficiency was defined as the percentage of the total numbers of cDCP-1 punctae engulfed by macrophages within the field of view, normalized according to numbers of macrophages within that field of view. Numbers of lysotracker-positive vacuoles per macrophage were counted from *z*-stacks of the ventral midline region; volumes of individual lysotracker-positive vacuoles were analyzed using Imaris software (Oxford Instruments). Quantification of DpERK levels within macrophages on the ventral surface of the embryo was carried out using IMARIS Surpass 3D rendering software. GFP staining was used to mask macrophages and measure total DpERK intensity per cell. Total intensity per cell was then divided by the volume of each macrophage (μm^3), with 15–20 macrophages per embryo quantified. These values were then averaged per embryo.

The Fiji manual tracking plug-in was used to track cell movements of macrophages undergoing random migration from the assembled time-lapse movies. Tracking data was then imported into the Ibidi Chemotaxis tool plugin in Fiji to calculate migratory parameters (Petrie et al., 2009).

Numbers of macrophages at the dorsal vessel were counted manually from maximum projections, with the total number in this field of view counted; recruitment to the dorsal vessel was defined as those macrophages contacting the dorsal vessel in a 100 μm long region corresponding to its medial-most section. The distance of macrophages from the dorsal vessel was measured using the points to line distance plugin in Fiji (macro made by Olivier Burri, EPFL, Lausanne). Similarly, developmental dispersal was quantified by counting numbers of macrophages on the ventral side of the embryo at stage 15 (**Figures 1C,C′**) or on the ventral midline (**Supplementary Figures 1G,G′**) in fields of view corresponding to the most-medial region of the embryo.

To quantify numbers of macrophages per embryo, maximum projections were assembled of lateral views comprising embryos imaged from their epithelial surface to the midline. Numbers of macrophages labeled with a nuclear marker (Red stinger) were counted manually using the point selection tool in Fiji and correspond to half the total number of macrophages per embryo.

To quantify macrophage wound responses, wound areas were first annotated from brightfield images taken at the 1-h timepoint. The number of macrophages in contact with and/or within the perimeter of the wound at 1-h post-injury were scored as having responded. The wound response is the number of responding macrophages divided by the wound area, normalized to the control average. The percentage of cells responding to wounds (% responders), a measure that allows normalization in case of varying numbers of macrophages in the wounding area, was calculated from those macrophages visible in the field of view pre-wounding that then migrated to the wound. To assess the range over which wound cues can be sensed, the shortest distance between the center of a non-responding macrophage in the pre-wound image and the wound edge (taken from the 60-min, post-wound brightfield image) was measured manually in Fiji and averaged per embryo.

Statistical Analyses and Data Availability

Numerical data was collated in Microsoft Excel and statistical analyses performed in GraphPad Prism 9. Outliers were identified and removed from datasets using the Prism 9 ROUT method (where $Q = 1$). Prior to application of statistics for comparison between conditions, datasets were first analyzed using the suite of normality and logarithmic tests built into Prism 9. This program applies four different statistic tests to the chosen datasets (Anderson-Darling, D'Agostino and Pearson, Shapiro–Wilk and Kolmogorov–Smirnov tests). For all datasets comparing two conditions, a result of non-normality in any these tests ($p < 0.05$) led to us apply a non-parametric statistical test. Numerical data was then statistically analyzed using unpaired, two-tailed Student's *t*-tests or Mann–Whitney tests to compare means for parametric and non-parametric data, respectively. Where greater than two means were compared, a one-way ANOVA with a Dunnett's post-test was used. *P*-values were reported as significant at a threshold of $p < 0.05$. All manual data analysis was conducted on blinded datasets. Quoted n numbers in legends refer to the number of *Drosophila* embryos analyzed, with individual macrophage values used to calculate averages per macrophage, per embryo. Raw numerical data and images are available on request from the authors.

RESULTS

Spitz Alters the Morphology and Migration Dynamics of *Drosophila* Embryonic Macrophages

Given the role of *Drosophila* EGFs in regulation of border cell migration in the oocyte and stem cell migration in the midgut (Duchek and Rørth, 2001; Liang et al., 2017), we hypothesized that Spitz may also regulate macrophage behavior in the developing *Drosophila* embryo. Since Spitz requires proteolytic cleavage for activation, two constituently-active variants of Spitz were used: $Spitz^{sec}$ and $sSpitz^{CS}$ (Ghiglione et al., 2002; Miura et al., 2006). In contrast to wild-type Spitz, these variants do not require cleavage via Rhomboid for their activation and secretion. Additionally, $sSpitz^{CS}$ lacks a post-translational palmitoylation modification that normally restricts diffusion of wild-type ligand via interactions with plasma membranes (Miura et al., 2006). Comparison of these variants enables investigation of how

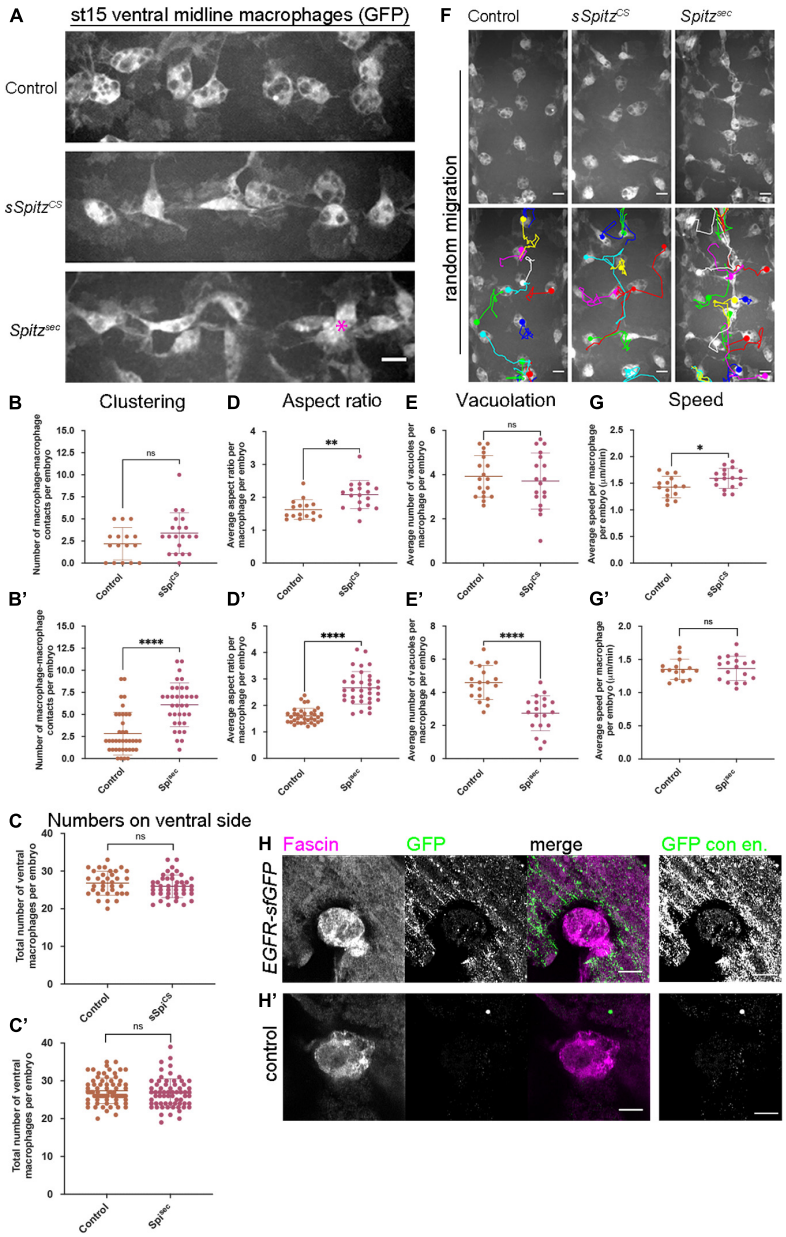

FIGURE 1 | Spitz stimulates macrophage polarization, impairs efferocytosis and alters migration dynamics. **(A)** Maximum projections of GFP-tagged macrophages on the ventral midline at stage 15 in control embryos and in embryos with macrophage-specific expression of sSpitz^{CS} or Spitz^{sec}; asterisk (*) shows cluster of macrophages on midline; anterior is left. **(B,B′)** Scattergraphs showing degree of macrophage clustering via number of macrophage-macrophage contacts per embryo in the presence of *sSpitz*^{CS} **(B)** (n = 16, 20; p = 0.0977) or Spitz^{sec} **(B′)** (n = 38, 35; $p < 0.0001$). **(C,C′)** Scattergraphs showing number of macrophages in the ventral midline region (VML) per embryo at stage 15 in the presence of *sSpitz*^{CS} **(C)** (n = 35, 43; p = 0.229) or *Spitz*^{Sec} **(C′,D)** (n = 73, 65; p = 0.247). **(D,D′)** Scattergraphs showing aspect ratio per macrophage per embryo in the presence of *sSpitz*^{CS} **(D)** (n = 16, 18; p = 0.0018) or *Spitz*^{Sec} **(D′)** (n = 35, 34; $p < 0.0001$). **(E,E′)** Scattergraphs showing average numbers of vacuoles per macrophage per embryo in controls in the presence of *sSpitz*^{CS} **(E)** (n = 18, 18; p = 0.574) or *Spitz*^{sec} **(E′)** (n = 19, 19; $p < 0.0001$). **(F)** Maximum projections and macrophage tracking data of GFP-labeled macrophages on the ventral midline at stage 15 in control embryos and in embryos with macrophage-specific expression of sSpitz^{CS} or Spitz^{sec}; anterior is up. **(G,G′)** Scattergraphs of speed per macrophage per embryo over a 1-h period of random migration in controls and in the presence of *sSpitz*^{CS} **(G)** (n = 15, 17; p = 0.0229) or Spitz^{sec} **(G′)** (n = 15, 18; p = 0.858). **(H,H′)** Images of macrophages on the ventral midline at stage 15 in embryos containing GFP-tagged EGFR (EGFR-sfGFP) under the control of its endogenous promoter **(H)** and a control embryo lacking a modified *EGFR* locus **(H′)**. Embryos were immunostained for GFP (green in merge) and Fascin (magenta in merge) to reveal *EGFR-sfGFP* expression and identify macrophages, respectively; panels to the right of the merged images show contrast enhanced GFP channel. Scale bars denote 10 μm **(A,F)** and 5 μm **(H,H′)**; lines and error bars represent mean and standard deviation on scattergraphs, respectively; significance bars denote $^{ns}p > 0.05$, $^{*}p < 0.05$, $^{**}p < 0.01$, and $^{****}p < 0.0001$, respectively; statistical comparisons made via unpaired, two-tailed Student's t-test **(C,E,E′,G,G′)** or Mann–Whitney test **(B,B′,C′,D,D′)**. Embryo genotypes are as follows: *w; Srp-GAL4,UAS-GFP/+; Crq-GAL4,UAS-GFP/+*(Control), *w; Srp-GAL4,UAS-GFP/UAS-sSpitz*^{CS}*; Crq-GAL4,UAS-GFP/+*(sSpi^{CS}), *w; Srp-GAL4,UAS-GFP/+; Crq-GAL4,UAS-GFP/UAS-Spitz*^{Sec} (Spi^{sec}), *w; EGFR-sfGFP* **(H)** and *w* **(H′)**.

the diffusion properties of Spitz contribute to alterations in macrophage behavior. Consequently, we expressed these Spitz variants specifically in macrophages to provide a local source of this growth factor, imaging GFP-labeled macrophages within developing embryos.

Our initial findings showed that developmental dispersal of macrophages was grossly normal on expression of either sSpitz^{CS} or Spitz^{sec} compared to controls at both stage 13 and stage 15/16 (**Supplementary Figures 1A–F**). Quantification of the numbers of macrophages on the ventral midline at stage 15 also showed no differences in the ability of macrophages to disperse over the embryo in the presence of either Spitz variant (**Supplementary Figures 1G,G′**). However, while macrophages were able to reach the ventral midline, the expression of Spitz appeared to alter their distribution, polarization and morphology in this region (**Figure 1A**). Analyzing the number of macrophages touching each other on the ventral midline showed that, while sSpitz^{CS}-expressing macrophages had a wild-type distribution, Spitz^{sec} significantly increased the number of macrophages contacting one another, leading to the formation of cell clusters (**Figures 1A–B′**; asterisk in panel 1A).

It has previously been shown that overexpression of EGFR in larval blood cells (Zettervall et al., 2004) drives their overproliferation, presumably via autoactivation of this receptor tyrosine kinase. Similarly, removal of a negative regulator of EGFR signaling (Graf) also leads to expansion of larval blood cells (Kim et al., 2017). However, an increase in cell numbers cannot explain the clustering phenotype in the embryo (**Figures 1A–B′**), as we could not detect an increase in cell numbers on the ventral side of the embryo at stage 15 (**Figures 1C,C′**), nor was there an increase in overall numbers of macrophages in the embryo (**Supplementary Figure 1H**). This also suggests that, in contrast to the situation in larvae, EGFR signaling does not have the potential to drive macrophage proliferation in the embryo.

To analyze changes in macrophage morphology in more detail, macrophage polarization was assessed by measuring the aspect ratio (AR) of the cell body. In the presence of either sSpitz^{CS} or Spitz^{sec}, macrophages were more elongated compared to controls lacking expression of either variant (**Figures 1A,D,D′**). Additionally, macrophages also appeared to contain fewer vacuoles in the presence of Spitz expression, structures previously established to contain engulfed apoptotic cells (Evans et al., 2013). Therefore, numbers of vacuoles can be used as an indirect read-out of macrophage efferocytosis. Quantification of the numbers of vacuoles per cell showed that in the presence of Spitz^{sec}, but not sSpitz^{CS}, macrophages contained fewer vacuoles and therefore were likely to contain fewer apoptotic cells (**Figures 1E,E′**). To assess if Spitz perturbed macrophage migration, macrophage movements ("random migration") on the ventral midline of the embryo were tracked for 1 h at stage 15 (**Figure 1F** and **Supplementary Movie 1**). Expression of sSpitz^{CS} increased macrophage random migration speeds, but no difference was seen on expression of Spitz^{sec} (**Figures 1G,G′**). Taken together, these results show that macrophage-specific expression of active Spitz alters macrophage polarity, induces clustering and affects macrophage migration and phagocytosis in a variant-specific manner. The stimulation of macrophage polarization, clustering and increase in speed potentially indicates a role for Spitz as a macrophage chemoattractant, such as previously observed for border cells and gut stem cells in this organism (Duchek and Rørth, 2001; Liang et al., 2017). Alternatively, Spitz could operate as a chemokinetic molecule with a specific role in increasing migration speeds, though it is not clear how this might drive cluster formation. Consistent with the effects of activated Spitz on macrophage behavior and expression in larval blood cells (Kim et al., 2017), embryonic macrophages do indeed express EGFR (**Figures 1H,H′**), which can be visualized using a GFP-tagged version of this receptor (knocked into the endogenous *EGFR* locus; Revaitis et al., 2020). Furthermore, while there are high levels of activated ERK (DpERK) even within macrophages in control embryos (**Supplementary Figure 2**), the presence of either sSpitz^{CS} or Spitz^{Sec} enhances this read-out of EGFR activity within macrophages (**Supplementary Figure 2**).

Cleavage Is Necessary for Spitz-Mediated Regulation of Macrophage Behavior

To investigate whether release from the membrane is required for Spitz-induced changes in macrophage behavior, a membrane-bound variant (mSpitz^{CS}; Miura et al., 2006) was expressed. Expression of mSpitz^{CS} did not alter macrophage clustering, numbers of cells in the ventral region, their morphology, vacuolation or migration speeds on the ventral midline (**Figure 2**). This suggests that cleavage and release of Spitz from the plasma membrane is needed for induction of macrophage phenotypes and that these phenotypes are not a non-specific consequence of overexpression of Spitz.

Tissue-Specific Release of Spitz Alters Macrophage Localization and Vacuolation

Given that under normal conditions, macrophages may not be the source of activated Spitz within the embryo, and also to avoid longer-term expression of Spitz by these cells, Spitz was expressed in an independent tissue that macrophages encounter during their dispersal. Thus, sSpitz^{CS} or Spitz^{sec} were expressed in the developing heart, a structure called the dorsal vessel, using *TinC-GAL4*, a driver derived from the enhancer region of *Tinman* (Lo and Frasch, 2001). *Tinman* encodes a transcription factor expressed across the early embryonic mesoderm before becoming restricted to the progenitor heart and lateral visceral muscles by stage 15 (Bodmer, 1993). During development, clusters of cardiocytes begin to form the dorsal vessel, which is then colonized by migrating macrophages (**Figure 3A**). We hypothesized that misexpression of Spitz in the dorsal vessel would alter macrophage morphology and behavior, enabling us to determine whether cell-autonomous expression was necessary for the effects of Spitz expression and confirm our previous results using macrophage-specific expression.

Embryos with LifeAct-labeled cardiocytes expressing either sSpitz^{CS} or Spitz^{sec} were mounted dorsally and imaged at the most-medial point of the developing dorsal vessel and

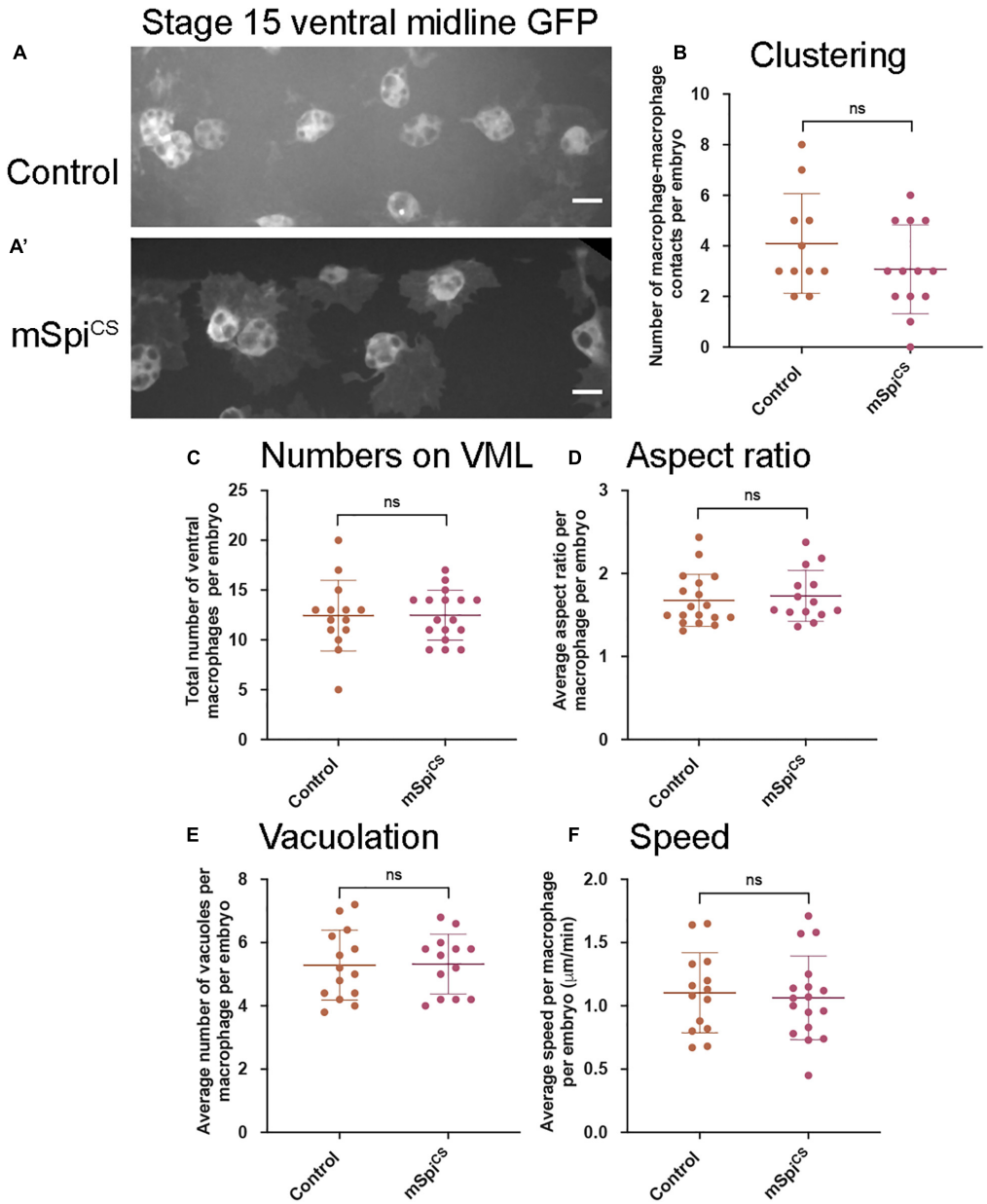

FIGURE 2 | Expression of a membrane-bound form of Spitz fails to induce changes in embryonic macrophage behavior. **(A,A')** Representative images of GFP-labeled macrophages in control embryos **(A)** and embryos containing macrophages expressing mSpi^{CS}-GFP **(A')** on the ventral midline at stage 15; mSpi^{CS}-GFP macrophages appear more defined due to additional GFP expression due to the GFP tag that is part of the mSpi^{CS}-GFP transgene; scale bars represent 10 μm. **(B–F)** Scattergraphs showing number of macrophage-macrophage contacts per embryo to assay macrophage clustering **(B)** (n = 11, 13; p = 0.690), numbers of macrophages on the ventral midline **(C)** (n = 14, 17; p = 0.188), cell body aspect ratio per macrophage, per embryo **(D)** (n = 18, 14; p = 0.464), vacuoles per macrophage, per embryo **(E)** (n = 14, 13; p = 0.926) and random migration speed in μm per minute **(F)** (n = 14, 17; p = 0.743) at stage 15 in controls and embryos with macrophage-specific expression of mSpitz^{CS}. Lines and error bars represent mean and standard deviation on scattergraphs, respectively; significance bars denote $p > 0.05$ (ns); statistical comparisons made via Mann–Whitney test **(D)** or unpaired, two-tailed Student's t-test **(B,C,E,F)**. Embryo genotypes are as follows: *w; Srp-GAL4,UAS-GFP/+; Crq-GAL4,UAS-GFP/+*(Control), *w; Srp-GAL4,UAS-GFP/+; Crq-GAL4,UAS-GFP/UAS-mSpitz^{CS}-GFP* (mSpi^{CS}).

compared to controls lacking Spitz expression (**Figures 3B–B″**); macrophages were labeled using the GAL4-independent *Srp-3x-mCherry* reporter construct (Gyoergy et al., 2018). The presence of either sSpitz^{CS} or Spitz^{sec} appeared to inhibit phagocytic uptake of apoptotic cells, since dorsal vessel-associated macrophages contained significantly fewer vacuoles compared to controls (**Figures 3C,C′**), consistent with phenotypes achieved using macrophage-specific expression

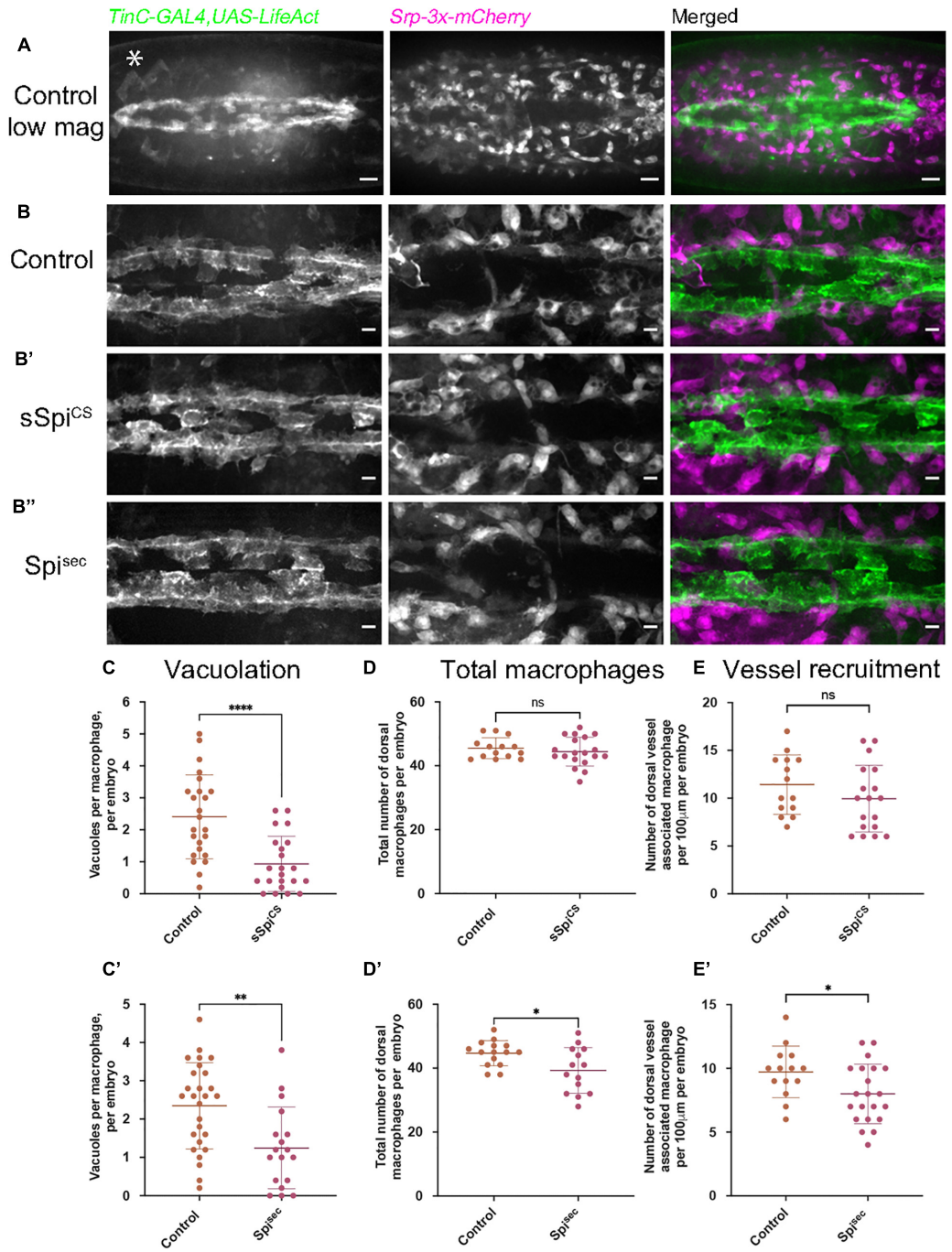

FIGURE 3 | Expression of Spitz in the developing fly heart alters macrophage localization and vacuolation. **(A–B'')** Maximum projections of dorsal side of stage 15 embryos showing the dorsal vessel (labeled using *TinC-GAL4,UAS-LifeAct*; green in merge) and associated macrophages (labeled via *Srp-3x-mCherry*) in controls **(A,B)** and embryos with *TinC-GAL4* mediated expression of *sSpitz*^{CS} **(B')** or *Spitz*^{Sec} **(B'')**. Anterior is right; asterisk (*) denotes *TinC-GAL4* driven expression in lateral regions away from the dorsal vessel. **(C,C')** Scattergraphs of vacuole counts per macrophage in controls and in the presence of dorsal vessel-expressed sSpitz^{CS} **(C)** (n = 24, 22; $p < 0.0001$) or Spitz^{sec} **(C')** (n = 27, 18; $p = 0.0020$). **(D,D')** Scattergraphs of the total number of macrophages present in the field of view at the dorsal face in controls and in the presence of dorsal vessel-expressed sSpitz^{CS} **(D)** (n = 14, 19; $p = 0.497$) or Spitz^{sec} **(D')** (n = 15, 14; $p = 0.0170$). **(E,E')** Scattergraphs of the number of macrophages contacting the dorsal vessel in controls and in the presence of dorsal vessel-expressed sSpitz^{CS} **(E)** (n = 14, 18; $p = 0.221$) or Spitz^{sec} **(E')** (n = 14, 21; $p = 0.0312$). Scale bars denote 20 μm **(A)** and 10 μm **(B–B'')**; lines and error bars represent mean and standard deviation on scattergraphs, respectively; significance bars denote $^{ns}p > 0.05$, $^{*}p < 0.05$, $^{**}p < 0.01$, $^{****}p < 0.0001$, respectively; statistical comparisons made via a Mann–Whitney test **(C,D)** or unpaired, two-tailed Student's *t*-test **(C',D',E,E')**. Embryo genotypes are as follows: *w; TinC-GAL4,UAS-LifeAct,Srp-3x-mCherry/+*(Control), *w;+/UAS-sSpitz*^{CS}*; TinC-GAL4,UAS-LifeAct,Srp-3x-mCherry/+*(sSpi^{CS}) and *w; TinC-GAL4,UAS-LifeAct,Srp-3x-mCherry/UAS-Spitz*^{sec} (Spi^{sec}).

of Spitz. Quantification of macrophage dispersal showed that expression of Spitz^{sec}, but not sSpitz^{CS}, marginally decreased the total numbers of macrophages recruited to this dorsal region (**Figures 3D,D′**). Similarly, only Spitz^{sec} altered the precise localization of dorsal vessel-associated macrophages, with fewer directly associated with the dorsal vessel itself (**Figures 3E,E′**). The reduction in macrophages at the dorsal vessel in the presence of Spitz^{sec} would appear counterintuitive to the hypothesis that Spitz may operate as a macrophage chemoattractant, however, *TinC-GAL4* also drives expression in regions lateral to the dorsal vessel (Azpiazu and Frasch, 1993; e.g., asterisk in **Figure 3A**) and this may be responsible for recruitment of macrophages away from the dorsal vessel. The lack of a stronger phenotype may indicate that Spitz can only act over short ranges. Interestingly, the observed phenotypes corroborate the potential decrease in apoptotic clearance by macrophages in the presence of Spitz. However, in this instance both variants of Spitz were competent to induce this phenotype. The consistent reduction of efferocytosis in macrophages exposed to Spitz^{sec} at the ventral midline and dorsal vessel led us to examine how Spitz affects apoptotic cell-macrophage interactions in more detail.

Exposure to Spitz Reduces the Efferocytic Capacity of Macrophages

Expression of Spitz in macrophages or the dorsal vessel induced a loss of vacuoles assumed to contain apoptotic cells within macrophages on the ventral midline or dorsal surface, respectively, suggesting that Spitz can interfere with apoptotic cell clearance (efferocytosis). It is also possible that expression of this growth factor alters overall levels of apoptosis in the developing embryo, such that there are fewer corpses for macrophages to clear. Therefore, to address the effects of Spitz on apoptotic cell clearance, embryos with or without macrophage-specific expression of either sSpitz^{CS} or Spitz^{sec} were immunostained for the cleaved form of the *Drosophila* caspase DCP-1 (cDCP-1), which can be used as a proxy for apoptotic cells (Song et al., 1997; **Figures 4A–A″**). To quantify the efficiency of efferocytosis, we counted the total number of cDCP-1 punctae on the ventral side of the embryo at stage 15 and calculated the proportion of these engulfed by macrophages. Macrophage-specific expression of either Spitz variant did not alter the total numbers of apoptotic cells in these regions compared to control embryos (**Figures 4A–B**). This suggests that Spitz does not inhibit apoptosis of surrounding cells, nor does it cause a dramatic build-up of apoptotic corpses due to the reduction in engulfment by macrophages. As per the analysis of macrophage vacuolation (**Figures 1E,E′**), there was a decrease in the relative efficiency of apoptotic cell clearance specific to the expression of Spitz^{sec}, with a lower proportion of cDCP-1 punctae present within macrophages in this genotype (**Figure 4C**). This decrease in apoptotic cell clearance led to a small but significant increase in the number of cDCP-1 punctae outside of macrophages (**Figure 4D**).

To check that the decrease in vacuoles and cDCP-1 punctae was not a consequence of more rapid phagosome maturation, acidification of phagosomes was investigated using lysotracker staining (**Figures 4E–E″**). As per cDCP-1 staining, there was a significant decrease in the number of acidified phagosomes in the presence of Spitz^{sec} but not sSpitz^{CS}, compared to controls (**Figures 4E–F**). Importantly, there was no difference in the sizes of lysotracker-positive phagosomes between experimental conditions (**Figure 4G**), suggesting it is not the case that phagosomes mature and fuse at a faster rate in the presence of Spitz.

These data therefore support the idea that less apoptotic cell clearance is being carried out by macrophages in the presence of Spitz, but without the consequence of large changes in the number of cells undergoing cell death or remaining uncleared by phagocytes. That these phenotypes were again specific to Spitz^{sec} reinforces the idea that differences between these two Spitz variants may prevent sSpitz^{CS} from acting locally in some contexts. Having established that Spitz^{sec} decreases efficiency of macrophage-mediated efferocytosis in addition to its impact on cell morphology, we sought to establish if Spitz was able to disrupt macrophage chemotaxis to non-developmental stimuli.

Exposure to Spitz Dampens WoundResponses in Macrophages in a Distance-Dependant Manner

Drosophila embryonic macrophages exhibit robust wound responses by polarizing toward and then migrating to sites of tissue damage (Stramer et al., 2005). These cells are refractile to wounding stimuli prior to late stage 14 due to persisting developmental signals, although they are still able to chemotax toward and engulf cells undergoing apoptotic cell death at this point in development (Moreira et al., 2010). This suggests that a hierarchy between different signals and that the integration of those signals can impact wound responses. Therefore, to address the effects of Spitz on inflammatory responses to injury, controls and embryos containing macrophage-specific expression of sSpitz^{CS} or Spitz^{sec} were laser wounded on the ventral surface of the embryo at stage 15 and the subsequent responses of GFP-labeled macrophages imaged (**Figure 5A** and **Supplementary Movie 2**). One-hour post wounding, there was a significant reduction in the macrophage wound response (number of macrophages at the wound divided by wound area, normalized to the control average) in the presence of either Spitz^{sec} or sSpitz^{CS} compared to controls (**Figures 5A–B′**). As previously, cleavage of Spitz appears necessary to induce changes in macrophage behavior, since expression of a membrane-bound form of Spitz (mSpitz^{CS}) failed to impact macrophage recruitment to wounds (**Figure 5B″**). The decrease in wound responses was paralleled by a decrease in the percentage of cells present in the field of view prior to wounding that are able to respond to injury for Spitz^{sec} but not sSpitz^{CS} (**Figures 5C,C′**), again highlighting the stronger effect of this variant.

Given the lack of a dramatic change in the numbers of apoptotic cells in the embryonic environment on expression of Spitz (**Figures 4A–B**), it seems unlikely that distraction of macrophages by apoptotic cells (e.g., as observed in Roddie et al., 2019) accounts for this phenotype. Instead, a loss of sensitivity

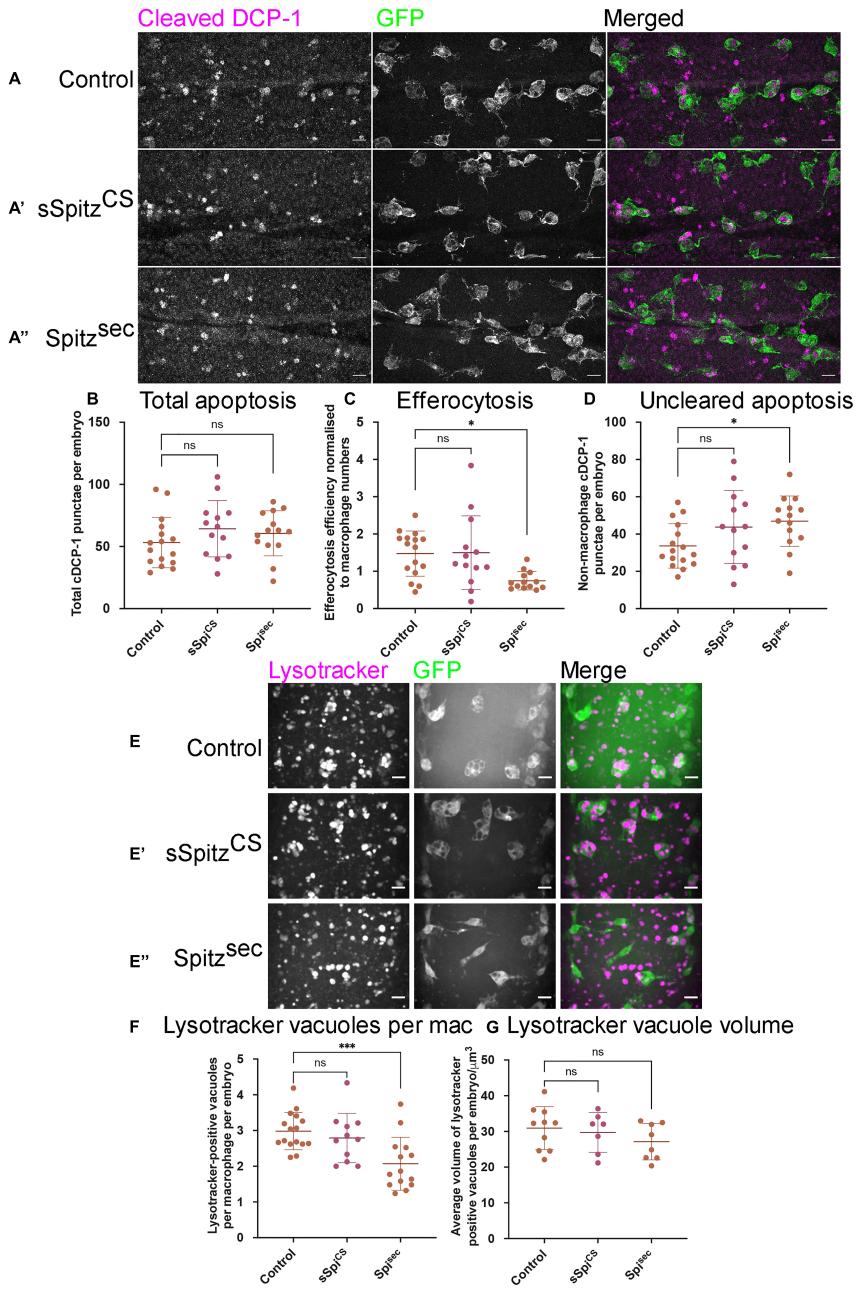

FIGURE 4 | Spitz impairs macrophage-mediated apoptotic cell clearance. **(A)** Maximum projections of the ventral region of stage 15 embryos immunostained for cleaved DCP-1 (cDCP-1; magenta in merge) and GFP (green in merge). Control embryos **(A)** were compared with embryos in which sSpitz^{CS} **(A')** or *Spitz*^{Sec} **(A'')** were specifically expressed in macrophages. **(B)** Scattergraph showing the total numbers of cDCP-1 positive punctae present within the ventral field of view per embryo **(B)** (n = 16, 13, 14; p = 0.265 and p = 0.519 for comparison of control vs. sSpi^{CS} and control vs. Spi^{sec}, respectively). **(C)** Scattergraph showing efficiency of apoptotic cell clearance/efferocytosis (percentage of cDCP-1 punctae engulfed by macrophages per field of view, per embryo, normalized according to numbers of macrophages in the field of view; n = 16, 13, 13; p = 0.994 and p = 0.0125 for comparison of control vs. sSpi^{CS} and control vs. Spi^{sec}, respectively). **(D)** Scattergraph showing average number of cDCP-1 punctae not engulfed by macrophages per field of view, per embryo (n = 16, 13, 14; p = 0.142 and p = 0.0386 for comparison of control vs. sSpi^{CS} and control vs. Spi^{sec}, respectively). **(E–E'')** Images of macrophages (green in merge) with acidified phagosomes labeled using lysotracker red (magenta in merge) at stage 15 on the ventral midline in genotypes indicated. **(F)** Scattergraph showing numbers of lysotracker-positive punctae per macrophage, per embryo in the presence and absence of Spitz expression (n = 16, 11, 14; p = 0.678 and p = 0.0009 for comparison of control vs. sSpi^{CS} and control vs. Spi^{sec}, respectively). **(G)** Scattergraph showing average volume of lysotracker-positive phagosomes per macrophage, per embryo in the presence and absence of Spitz expression (n = 10, 7, 8; p = 0.873 and p = 0.284 for comparison of control vs. sSpi^{CS} and control vs. Spi^{sec}, respectively). Scale bars denote 10μm; lines and error bars represent mean and standard deviation on scattergraphs, respectively; significance bars denote $^{ns}p > 0.05$, $^{*}p < 0.05$, and $^{***}p < 0.001$, respectively; all statistical comparisons made via one-way ANOVA with a Dunnett's post-test. Embryo genotypes are as follows: *w; Srp-GAL4,UAS-GFP/+; Crq-GAL4,UAS-GFP/+* (Control), *w; Srp-GAL4,UAS-GFP/UAS-sSpitz*^{CS}*; Crq-GAL4,UAS-GFP/+* (sSpi^{CS}) and *w;Srp-GAL4,UAS-GFP/+; Crq-GAL4,UAS-GFP/UAS-Spitz*^{Sec} (Spi^{sec}).

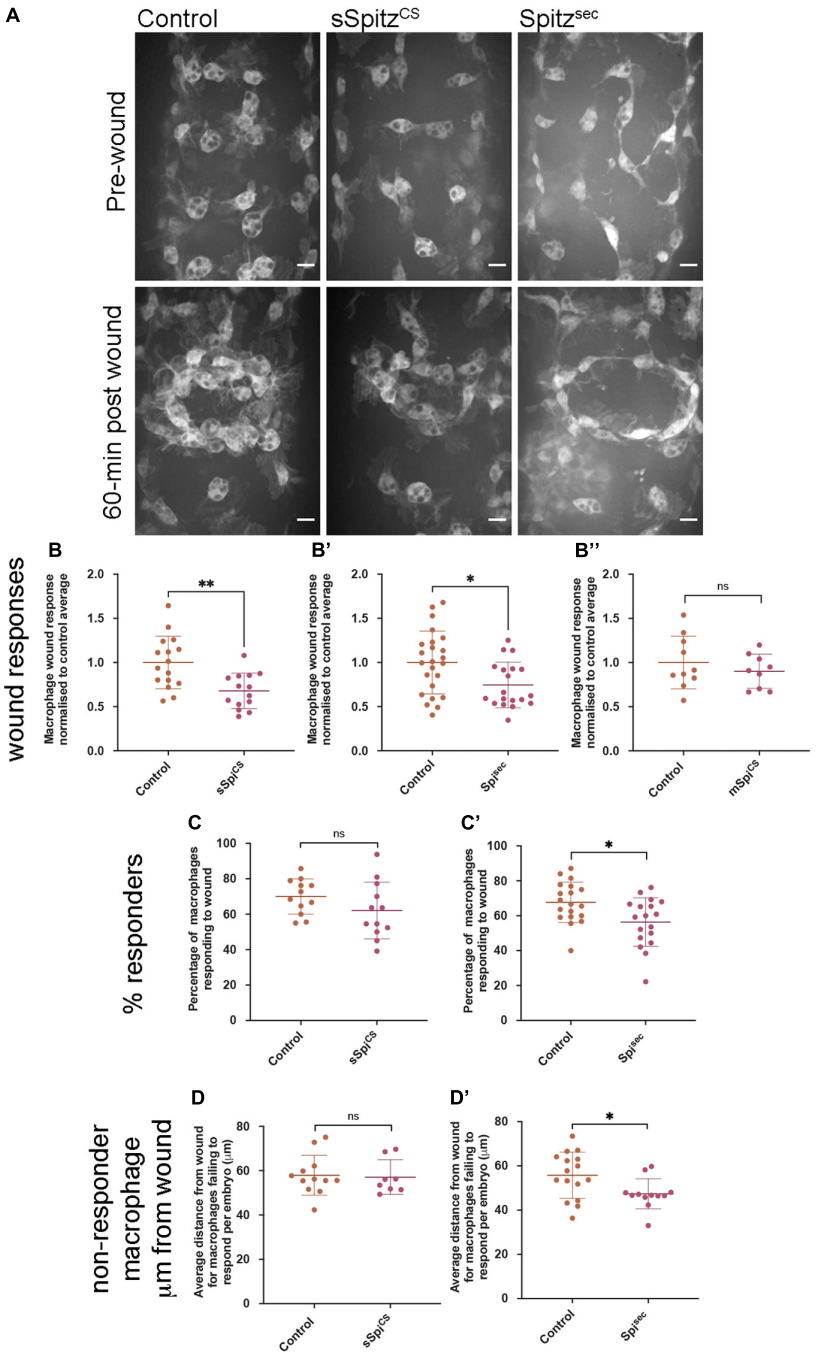

FIGURE 5 | Spitz impairs macrophage wound responses. **(A)** Maximum projections showing images of GFP-labeled macrophages on the ventral midline region in controls and in embryos containing macrophages expressing sSpitz^{CS} or Spitz^{sec}; upper panels show stage 15 embryos immediately prior to wounding; lower panels show corresponding embryo 1-h post wounding. **(B–B′′)** Scattergraphs showing macrophage wound responses (number of macrophages responding to the wound normalized to wound area and to control responses) in controls and embryos with macrophage-specific expression of sSpitz^{CS} **(B)** (n = 16, 14; p = 0.0020), Spitz^{sec} **(B′)** (n = 24, 19; p = 0.0160), or mSpitz^{CS} (n = 9, 10; p = 0.406). **(C,C′)** Scattergraphs showing percentage of macrophages responding to wound per embryo (% of those in the field of view that reach the wound) per embryo for control embryos compared to embryos with macrophage specific-expression of sSpitz^{CS} **(C)** (n = 12, 12; p = 0.159) or Spitz^{sec} **(C′)** (n = 19, 18; p = 0.0105). **(D,D′)** Scattergraphs showing average distance from the wound edge (immediately prior to wounding) of those macrophages that fail to respond, per embryo, for control embryos compared to embryos with macrophage specific-expression of sSpitz^{CS} **(D)** (n = 12, 8; p = 0.678) or Spitz^{sec} **(D′)** (n = 16, 12; p = 0.0421). Scale bars denote 10 μm; lines and error bars represent mean and standard deviation on scattergraphs, respectively; significance bars denote $^{ns}p > 0.05$, $^{*}p < 0.05$, and $^{**}p < 0.01$, respectively; statistical comparisons made via a Mann–Whitney test **(B′,B′′,D,D′)** or an unpaired, two-tailed Student's t-test **(B,C,C′)**. Embryo genotypes are as follows: *w; Srp-GAL4,UAS-GFP/+; Crq-GAL4,UAS-GFP/+* **(Control)**, *w; Srp-GAL4,UAS-GFP/UAS-sSpitz^{CS}; Crq-GAL4,UAS-GFP/+* (sSpi^{CS}), *w;Srp-GAL4,UAS-GFP/+; Crq-GAL4,UAS-GFP/UAS-Spitz^{Sec}* (Spi^{sec}) and *w; Srp-GAL4,UAS-GFP/+; Crq-GAL4,UAS-GFP/UAS-mSpitz^{CS}-GFP* (mSpi^{CS}).

to wound signals at more distal sites, where wound cues may be weaker, could explain why a smaller proportion of macrophages respond. Therefore, to assess whether the loss of responses from regions further away from the wound site explained the reduction in numbers of macrophages reaching wounds, the distances of non-responsive macrophages from wound edges was measured. There were no differences in these measurements when sSpitz^{CS} and control embryos were compared (**Figure 5D**), however, the average distances of non-responding macrophages from the wound were significantly lower in the presence of Spitz^{sec} compared to controls (**Figure 5D′**). This shows that macrophages further away from the wound site are less likely to respond in the presence of Spitz^{sec}. Thus, a loss of recruitment of more distal macrophages to wound sites in the presence of Spitz^{sec} contributes to impaired wound responses. Potentially, those cells absent from wound sites in the presence of sSpitz^{CS} are those that would otherwise migrate from regions outside of the field of views used for this particular analysis; this also potentially explains the lack of a difference in the percentage of cells that respond in the pre-wound field of view (**Figure 5C**).

In conclusion, the impairment of macrophage inflammatory responses in the presence of either Spitz^{sec} or sSpitz^{CS} highlights the capacity of this molecule to regulate a range of innate immune behaviors that depend on efficient polarization and migration in the developing *Drosophila* embryo (see **Table 1** for a summary of phenotypes). The fact that Spitz specifically impacts the recruitment of more distal macrophages to wound sites would indicate it modulates or overrides the ability of these important cells to sense or respond to those signals produced at wound sites or by apoptotic cells.

DISCUSSION

Here we show for the first time that the *Drosophila* epidermal growth factor pathway modifies immune cell function in the developing embryo, representing a new cue regulating the behavior of this organism's macrophages *in vivo*. De-regulated release of Spitz disrupts macrophage migration, induces elongation and perturbs the ability of macrophages to respond to wounds and clear apoptotic cells. In this study, two variants of protease-independent Spitz with different diffusion properties were used to assess the role of Spitz as a macrophage chemoattractant in the *Drosophila* embryo: macrophage phenotypes varied according to the activated variant of Spitz used, suggesting different physical properties of this cue may influence macrophage behavior in subtle ways.

Two non-mutually exclusive scenarios may explain how Spitz alters macrophage morphology and speed: regulation of macrophage motility by Spitz, which causes an override of endogenous signals, and/or reprogramming of macrophages to different activation states with different migratory and morphological characteristics. EGF ligands can function as chemoattractants in a number of situations: human EGF and the *Drosophila* EGF ligand Gurken regulate monocyte chemotaxis and *Drosophila* border cell migration, respectively (Duchek and Rørth, 2001; Lamb et al., 2004), while Spitz was itself identified as a stem cell attractant released by *Drosophila* midgut cells undergoing apoptosis (Liang et al., 2017). We found that, in the presence of Spitz, macrophages on the ventral midline became more highly polarized and migrated at greater speeds (sSpitz^{CS} specifically). The changes in cell shape could reflect changes in their migratory abilities, or be indicative of a chemotactic response toward a gradient (Sarris and Sixt, 2015), through enhanced formation or stabilization of a cell's leading edge. Alternatively, they may be the result of macrophage reprogramming events that have previously been linked to morphological distinctions between pro-inflammatory and anti-inflammatory macrophages (McWhorter et al., 2013). Single cell RNA sequencing studies have shown that blood cell populations may be more complicated in *Drosophila* than previously anticipated (Cattenoz et al., 2020; Cho et al., 2020; Tattikota et al., 2020). At present these approaches are limited to larval stages, although recent work suggests that subpopulations of functionally-distinct macrophages may also exist in the developing fly embryo (Coates et al., 2020). The expression of Spitz under the control of *TinC-GAL4* corroborated midline efferocytosis defects and revealed that macrophage-specific expression was not necessary for an impact on this behavior. The reduction in the numbers of macrophages at the dorsal vessel on expression of Spitz^{sec} is possibly the result of distal *TinC-GAL4* activity within the lateral visceral muscles (Bodmer, 1993) attracting macrophages away from this tissue. Again, the fact that Spitz^{sec}, but not sSpitz^{CS} altered macrophage recruitment in this region potentially reflects the stronger phenotypes obtained with Spitz^{sec}, which may in turn relate to the differences in diffusion of these two variants (see below).

EGF signaling can block apoptosis through its action as pro-survival signal (Henson and Gibson, 2006) and can also stimulate compensatory proliferation (Fogarty and Bergmann, 2017). However, Spitz expression did not alter the total number of apoptotic cells *in vivo* but did impair clearance by macrophages. While macrophages express EGFR and downstream signaling pathways are activated via exposure to either Spitz variant, we

TABLE 1 | Summary of Spitz-induced macrophage phenotypes.

		sSpitz^{CS}	Spitz^{sec}
Phenotype:	Region:	Active, lacks palmitoylation – diffuses further, shallower gradients?	Active, has palmitoylation – steeper, local gradients?
Clustering	VML	No change	↑
Aspect ratio	VML	↑	↑
Vacuolation	VML	No change	↓
cDCP-1/Lysotracker	VML	No change	↓
Vacuolation	DV	↓	↓
Speed	VML	↑	No change
DV recruitment	DV	No change	↓
Wound response	VML	↓	↓
Non-responder distance	VML	No change	↓

VML, ventral midline; DV, dorsal vessel.
mSpi^{CS} does not induce any macrophage phenotypes.

cannot exclude the possibility that EGFR signaling in cells other than macrophages contributes to the phenotypes we describe, since EGFR is widely expressed in the developing embryo (Revaitis et al., 2020). Spitz-induced phenotypes may reflect reprogramming to an activation state that is less efficient at engulfing dying cells, since the capacity to clear apoptotic cells can vary across macrophage subpopulations in some organisms (Zizzo et al., 2012). Unrestrained EGFR signaling has previously been demonstrated to drive proliferation of larval blood cells (Zettervall et al., 2004; Kim et al., 2017), but has also been implicated in acquisition of a lamellocyte fate in the presence of elevated reactive oxygen species (Sinenko et al., 2012), pointing toward the potential for a role in the alteration of cell specification in *Drosophila* blood lineages.

Alternatively, chemotaxis or chemokinesis regulated by Spitz or signal integration mechanisms may impair detection of apoptotic corpses – if Spitz represents a chemoattractant or reprogramming factor it may distract macrophages from their clearance duties (e.g., toward each other leading to clustering or increased migration speeds). Intriguingly, Spitz and human EGF share similar processing and secretion mechanisms to a known find-me cue for apoptotic cells, Fractalkine (Sokolowski et al., 2014). Both Fractalkine and EGFs require activation via caspase-regulated proteases – Rhomboid and ADAM-17, respectively (Rose-John, 2013; Liang et al., 2017). The changes in macrophage shape and their responses to stimuli that are induced by Spitz, and the similarities in how Spitz and other find-me cues are secreted, raises the potential role of Spitz as a chemoattractant used in the "find-me" phase of efferocytosis (Ravichandran, 2003). High levels of this cue may therefore interfere with detection of apoptotic cells (i.e., signals from apoptotic cells are "drowned out" by misexpressed Spitz), though considerably more work would be required to establish Spitz as a find-me cue. Furthermore, these experiments are not straightforward given the role of EGF signaling in midline development (Golembo et al., 1996) and the fact that disruption of that process blocks macrophage dispersal (Paladi and Tepass, 2004; Evans et al., 2010a).

Similarly, we have shown that the presence of either Spitz^{sec} or sSpitz^{CS}, inhibits the ability of macrophages to respond to wounding stimuli. Uncleared apoptotic cells can impair wound responses in the developing embryo (Roddie et al., 2019). However, there was only a mild increase in the number of uncleared apoptotic cells, potentially as glial cells and epidermal cells may compensate for the decreases in macrophage-mediated clearance. Since no substantial changes in overall levels of apoptosis were detected in the presence of either Spitz variant, nor did sSpitz^{CS} expression impact efferocytosis on the ventral midline yet still altered wound responses, we do not favor the explanation that uncleared apoptotic cells undermine macrophage inflammatory responses to injury in this context. Instead impairment of wound responses may result from competition between Spitz and the damage-associated molecular signals released at wound sites (Koh and DiPietro, 2011), or relate to macrophage reprogramming as discussed above. Indeed, our results showed that Spitz prevented more distal macrophages from responding to wounds, supporting the idea of competing chemotactic gradients as opposed to a general reprogramming of macrophages that results in desensitization to wound signals. This disruption of macrophage responses may be specific to regions of the embryo more distal to wound sites, as wound signals may be present at lower concentrations in those environments.

The phenotypic differences observed between Spitz^{sec} and sSpitz^{CS} likely reflect the absence of a palmitoyl group in the latter (Miura et al., 2006). However, we have been unable to confirm equivalent levels of expression of these variants (data not shown), as it is not clear that the anti-Spitz antibodies we have at our disposal recognize the sSpitz^{CS} variant, which contains a mutation in the region used to generate that antibody (Schweitzer et al., 1995). Therefore, it remains possible that differences in expression levels of these variants contribute to differences in the phenotypes we have observed. Palmitoylation is known to increase tethering of ligands at the plasma membrane post-secretion (Salaun et al., 2010). Additionally, mutation in the palmitoylation site of signaling proteins is known to alter cell–cell signaling, e.g., Fas-mediated cell death (Guardiola-Serrano et al., 2010), and significantly reduce diffusion speed of ligands (Sowa et al., 1999). This may allow sSpitz^{CS} to diffuse further from its source, forming shallower gradients over longer distances that are more difficult for cells to interpret. In contrast, Spitz^{sec} would remain more highly concentrated at its source leading to steeper gradients over a shorter range. This potentially explains why Spitz^{sec} can drive macrophage clustering between neighboring macrophages. Shallower, more long-range gradients may enable increased migration speeds with sSpitz^{CS}, whereas Spitz^{sec} promotes clustering more locally. Given that membrane-bound Spitz does not drive clustering, this suggests cluster formation is not the result of cell–cell adhesion via receptor-ligand pairing.

Expression of variants at the dorsal vessel acts as a more defined point source of Spitz and this may explain why sSpitz^{CS} is more effective here than when expressed in macrophages, although differences in expression or stability of these different variants may also contribute. The lack of recruitment to the dorsal vessel may be due to recruitment to areas of *TinC-GAL4* expression elsewhere in the embryo. Expression of the PDGF/Vegf-related ligand Pvf2 is sufficient to retain macrophages in the head of the embryo (Evans et al., 2010b), therefore this molecule is capable of exerting a more profound effect than Spitz on macrophages as they disperse. Therefore, in comparison to Pvf2, Spitz may exert weaker effects, act over a shorter range and/or merely stimulate migration speeds rather than function as a chemoattractant (i.e., function as a chemokinetic molecule).

Taken together, our results show that Spitz can alter macrophage migration and functional responses to wounds and apoptotic cells during *Drosophila* development. These processes are important immune cell behaviors that can become dysregulated in a diverse array of human conditions including cancer, atherosclerosis and chronic inflammatory conditions. These results therefore have clear implications for our understanding of the role that EGF ligands play during development and in the progression of chronic inflammation.

Furthermore, these findings have implications and relevance to therapeutic strategies that seek to interfere with EGF signaling – indeed, targeting the EGF pathway shows promise as a therapeutic strategy in models of chronic inflammation (Qu et al., 2012; Omachi et al., 2017; Rahman et al., 2019). Future work will establish the exact mechanisms of actions via which *Drosophila* EGFs regulate macrophage function, the downstream signaling pathways involved and whether these functions are conserved through evolution.

DATA AVAILABILITY STATEMENT

The original contributions generated for this study are included in the article/**Supplementary Material**, further inquiries can be directed to the corresponding author.

AUTHOR CONTRIBUTIONS

All authors contributed to conception of the project, experimental design, and the preparation and editing of the manuscript. Experiments were conducted by OT, EA, and IE. LP and IE supervised and obtained funding for the project.

FUNDING

OT was supported by a studentship from the MRC Discovery Medicine North (DiMeN) Doctoral Training Partnership (MR/N013840/1) with further funding provided by a Wellcome/Royal Society Sir Henry Dale Fellowship awarded to IE (102503/Z/13/Z).

ACKNOWLEDGMENTS

Imaging work was performed at the Wolfson Light Microscopy Facility, using the Perkin Elmer Spinning disk (MRC grant G0700091 and Wellcome grant 077544/Z/05/Z) and Zeiss 880 Airyscan microscopes. We thank Darren Robinson, Katherine Whitley, Karen Plant and the University of Sheffield fly facility for technical support. This work would not be possible without reagents and resources obtained from or maintained by the Bloomington *Drosophila* Stock Centre (NIH P40OD018537) and Flybase (MRC grant MR/N030117/1). We thank Brian Stramer and Miguel Ramírez Moreno for providing the *Srp-3x-mCherry* and *EGFR-sfGFP* fly lines, respectively. We thank Blanca Tardajos Ayllón (Paul Evans Lab, University of Sheffield) for the gift of the anti-pErk antibody. We are grateful to Simon Johnston and Phil Elks (The University of Sheffield) for feedback on the manuscript and to Elliot Brooks for technical assistance with experiments.

SUPPLEMENTARY MATERIAL

The Supplementary Material for this article can be found online at: https://www.frontiersin.org/articles/10.3389/fcell.2021.636024/full#supplementary-material

REFERENCES

Ariel, A., and Ravichandran, K. S. (2016). "This way please": apoptotic cells regulate phagocyte migration before and after engulfment. *Eur. J. Immunol.* 46, 1583–1586. doi: 10.1002/eji.201646505

Azpiazu, N., and Frasch, M. (1993). Tinman and bagpipe: two homeo box genes that determine cell fates in the dorsal mesoderm of Drosophila. *Genes Dev.* 7, 1325–1340. doi: 10.1101/gad.7.7b.1325

Barolo, S., Carver, L. A., and Posakony, J. W. (2000). GFP and β-galactosidase transformation vectors for promoter/enhancer analysis in Drosophila. *Biotechniques* 29, 726–732. doi: 10.2144/00294bm10

Bodmer, R. (1993). The gene tinman is required for specification of the heart and visceral muscles in Drosophila. *Development* 118, 719–729.

Brückner, K., Kockel, L., Duchek, P., Luque, C. M., Rørth, P., and Perrimon, N. (2004). The PDGF/VEGF receptor controls blood cell survival in Drosophila. *Dev. Cell* 7, 73–84. doi: 10.1016/j.devcel.2004.06.007

Buchon, N., Silverman, N., and Cherry, S. (2014). Immunity in Drosophila melanogaster — from microbial recognition to whole-organism physiology. *Nat. Rev. Immunol.* 14, 796–810. doi: 10.1038/nri3763

Burgess, A. W., Cho, H.-S., Eigenbrot, C., Ferguson, K. M., Garrett, T. P. J., Leahy, D. J., et al. (2003). An open-and-shut case? Recent insights into the activation of EGF/ErbB receptors. *Mol. Cell* 12, 541–552.

Casas-Tintó, S., Lolo, F.-N., and Moreno, E. (2015). Active JNK-dependent secretion of Drosophila Tyrosyl-tRNA synthetase by loser cells recruits haemocytes during cell competition. *Nat. Commun.* 6:10022. doi: 10.1038/ncomms10022

Cattenoz, P. B., Sakr, R., Pavlidaki, A., Delaporte, C., Riba, A., Molina, N., et al. (2020). Temporal specificity and heterogeneity of Drosophila immune cells. *EMBO J.* 39, 1–25. doi: 10.15252/embj.2020104486

Cho, B., Yoon, S. H., Lee, D., Koranteng, F., Tattikota, S. G., Cha, N., et al. (2020). Single-cell transcriptome maps of myeloid blood cell lineages in Drosophila. *Nat. Commun.* 11:4483. doi: 10.1038/s41467-020-18135-y

Cho, N. K., Keyes, L., Johnson, E., Heller, J., Ryner, L., Karim, F., et al. (2002). Developmental control of blood cell migration by the Drosophila VEGF pathway. *Cell* 108, 865–876.

Citri, A., and Yarden, Y. (2006). EGF-ERBB signalling: towards the systems level. *Nat. Rev. Mol. Cell Biol.* 7, 505–516. doi: 10.1038/nrm1962

Coates, J. A., Brittle, A., Armitage, E. L., Zeidler, M. P., and Evans, I. R. (2020). Identification of functionally-distinct macrophage subpopulations regulated by efferocytosis in Drosophila. *bioRxiv* [Preprint]. doi: 10.1101/2020.04.17.047472

Davis, J. R., Huang, C. Y., Zanet, J., Harrison, S., Rosten, E., Cox, S., et al. (2012). Emergence of embryonic pattern through contact inhibition of locomotion. *Development* 139, 4555–4560. doi: 10.1242/dev.082248

Degterev, A., and Yuan, J. (2008). Expansion and evolution of cell death programmes. *Nat. Rev. Mol. Cell Biol.* 9, 378–390. doi: 10.1038/nrm2393

Dou, Y., Wu, H. J., Li, H. Q., Qin, S., Wang, Y. E., Li, J., et al. (2012). Microglial migration mediated by ATP-induced ATP release from lysosomes. *Cell Res.* 22, 1022–1033. doi: 10.1038/cr.2012.10

Duchek, P., and Rørth, P. (2001). Guidance of cell migration by EGF receptor signaling during Drosophila oogenesis. *Science* 291, 131–133. doi: 10.1126/science.291.5501.131

Elliott, M. R., Chekeni, F. B., Trampont, P. C., Lazarowski, E. R., Kadl, A., Walk, S. F., et al. (2009). Nucleotides released by apoptotic cells act as a find-me signal to promote phagocytic clearance. *Nature* 461, 282–286. doi: 10.1038/nature08296

Eltboli, O., Bafadhel, M., Hollins, F., Wright, A., Hargadon, B., Kulkarni, N., et al. (2014). COPD exacerbation severity and frequency is associated with impaired macrophage efferocytosis of eosinophils. *BMC Pulm. Med.* 14:112. doi: 10.1186/1471-2466-14-112

Evans, I., Ghai, P., Urbancic, V., Tan, K., and Wood, W. (2013). SCAR/WAVE mediated processing of apoptotic corpses is essential for effective macrophage migration in Drosophila. *Cell Death Differ.* 20, 709–720. doi: 10.1038/cdd.2012.166

Evans, I. R., Hu, N., Skaer, H., and Wood, W. (2010a). Interdependence of macrophage migration and ventral nerve cord development in Drosophila embryos. *Development* 137, 1625–1633. doi: 10.1242/dev.046797

Evans, I. R., Rodrigues, F. S. L. M., Armitage, E. L., and Wood, W. (2015). Draper/CED-1 mediates an ancient damage response to control inflammatory blood cell migration in vivo. *Curr. Biol.* 25, 1606–1612. doi: 10.1016/j.cub.2015.04.037

Evans, I. R., and Wood, W. (2011). Drosophila embryonic hemocytes. *Curr. Biol.* 21, R173–R174. doi: 10.1016/j.cub.2011.01.061

Evans, I. R., Zanet, J., Wood, W., and Stramer, B. M. (2010b). Live imaging of drosophila melanogaster embryonic hemocyte migrations. *J. Vis. Exp.* 36:1696. doi: 10.3791/1696

Fogarty, C. E., and Bergmann, A. (2017). Killers creating new life: caspases drive apoptosis-induced proliferation in tissue repair and disease. *Cell Death Differ.* 24, 1390–1400. doi: 10.1038/cdd.2017.47

Foxman, E. F., Campbell, J. J., and Butcher, E. C. (1997). Multistep navigation and the combinatorial control of leukocyte chemotaxis. *J. Cell Biol.* 139, 1349–1360. doi: 10.1083/jcb.139.5.1349

Frise, E., Hammonds, A. S., and Celniker, S. E. (2010). Systematic image-driven analysis of the spatial *Drosophila* embryonic expression landscape. *Mol. Syst. Biol.* 6:345. doi:10.1038/msb.2009.102

Fuchs, Y., and Steller, H. (2011). Programmed cell death in animal development and disease. *Cell* 147, 742–758. doi: 10.1016/j.cell.2011.10.033

Galluzzi, L., Vitale, I., Abrams, J. M., Alnemri, E. S., Baehrecke, E. H., Blagosklonny, M. V., et al. (2012). Molecular definitions of cell death subroutines: recommendations of the nomenclature committee on cell death 2012. *Cell Death Differ.* 19, 107–120. doi: 10.1038/cdd.2011.96

Ghiglione, C., Bach, E. A., Paraiso, Y., Carraway, K. L., Noselli, S., and Perrimon, N. (2002). Mechanism of activation of the Drosophila EGF receptor by the TGFalpha ligand Gurken during oogenesis. *Development* 129, 175–186.

Golembo, M., Raz, E., and Shilo, B. Z. (1996). The Drosophila embryonic midline is the site of Spitz processing, and induces activation of the EGF receptor in the ventral ectoderm. *Development* 122, 3363–3370.

Guardiola-Serrano, F., Rossin, A., Cahuzac, N., Lückerath, K., Melzer, I., Mailfert, S., et al. (2010). Palmitoylation of human FasL modulates its cell death-inducing function. *Cell Death Dis.* 1:e88. doi: 10.1038/cddis.2010.62

Gyoergy, A., Roblek, M., Ratheesh, A., Valoskova, K., Belyaeva, V., Wachner, S., et al. (2018). Tools allowing independent visualization and genetic manipulation of *Drosophila melanogaster* macrophages and surrounding tissues. *G3(Bethesda)* 8, 845–857. doi: 10.1534/g3.117.300452

Hatan, M., Shinder, V., Israeli, D., Schnorrer, F., and Volk, T. (2011). The Drosophila blood brain barrier is maintained by GPCR-dependent dynamic actin structures. *J. Cell Biol.* 192, 307–319. doi: 10.1083/jcb.201007095

Heit, B., Robbins, S. M., Downey, C. M., Guan, Z., Colarusso, P., Miller, J. B., et al. (2008). PTEN functions to "prioritize" chemotactic cues and prevent "distraction" in migrating neutrophils. *Nat. Immunol.* 9, 743–752. doi: 10.1038/ni.1623

Henson, E. S., and Gibson, S. B. (2006). Surviving cell death through epidermal growth factor (EGF) signal transduction pathways: implications for cancer therapy. *Cell. Signal.* 18, 2089–2097. doi: 10.1016/j.cellsig.2006.05.015

Kim, S., Nahm, M., Kim, N., Kwon, Y., Kim, J., Choi, S., et al. (2017). Graf regulates hematopoiesis through geec endocytosis of EGFR. *Development* 144, 4159–4172. doi: 10.1242/dev.153288

Koh, T. J., and DiPietro, L. A. (2011). Inflammation and wound healing: the role of the macrophage. *Expert Rev. Mol. Med.* 13:e23. doi: 10.1017/S1462399411001943

Lamb, D. J., Modjtahedi, H., Plant, N. J., and Ferns, G. A. A. (2004). EGF mediates monocyte chemotaxis and macrophage proliferation and EGF receptor is expressed in atherosclerotic plaques. *Atherosclerosis* 176, 21–26. doi: 10.1016/j.atherosclerosis.2004.04.012

Lauber, K. (2003). Apoptotic cells induce migration of phagocytes via caspase-3-mediated release of a lipid attraction signal. *Cell* 113, 717–730.

Liang, J., Balachandra, S., Ngo, S., and O'Brien, L. E. (2017). Feedback regulation of steady-state epithelial turnover and organ size. *Nature* 548, 588–591. doi: 10.1038/nature23678

Lo, P. C. H., and Frasch, M. (2001). A role for the COUP-TF-related gene seven-up in the diversification of cardioblast identities in the dorsal vessel of Drosophila. *Mech. Dev.* 104, 49–60. doi: 10.1016/S0925-4773(01)00361-6

Matsubayashi, Y., Louani, A., Dragu, A., Sánchez-Sánchez, B. J., Serna-Morales, E., Yolland, L., et al. (2017). A moving source of matrix components is essential for De Novo basement membrane formation. *Curr. Biol.* 27, 3526–3534.e4. doi: 10.1016/j.cub.2017.10.001

McWhorter, F. Y., Wang, T., Nguyen, P., Chung, T., and Liu, W. F. (2013). Modulation of macrophage phenotype by cell shape. *Proc. Natl. Acad. Sci. U. S. A.* 110, 17253–17258. doi: 10.1073/pnas.1308887110

Miura, G. I., Buglino, J., Alvarado, D., Lemmon, M. A., Resh, M. D., and Treisman, J. E. (2006). Palmitoylation of the EGFR ligand spitz by rasp increases spitz activity by restricting its diffusion. *Dev. Cell* 10, 167–176. doi: 10.1016/j.devcel.2005.11.017

Moreira, S., Stramer, B., Evans, I., Wood, W., and Martin, P. (2010). Prioritization of competing damage and developmental signals by migrating macrophages in the Drosophila embryo. *Curr. Biol.* 20, 464–470.

Morioka, S., Maueröder, C., and Ravichandran, K. S. (2019). Living on the edge: efferocytosis at the interface of homeostasis and pathology. *Immunity* 50, 1149–1162. doi: 10.1016/j.immuni.2019.04.018

Niethammer, P., Grabher, C., Look, A. T., and Mitchison, T. J. (2009). A tissue-scale gradient of hydrogen peroxide mediates rapid wound detection in zebrafish. *Nature* 459, 996–999. doi: 10.1038/nature08119

Omachi, K., Miyakita, R., Fukuda, R., Kai, Y., Suico, M. A., Yokota, T., et al. (2017). Long-term treatment with EGFR inhibitor erlotinib attenuates renal inflammatory cytokines but not nephropathy in Alport syndrome mouse model. *Clin. Exp. Nephrol.* 21, 952–960. doi: 10.1007/s10157-017-1386-9

Paladi, M., and Tepass, U. (2004). Function of Rho GTPases in embryonic blood cell migration in Drosophila. *J. Cell Sci.* 117, 6313–6326. doi: 10.1242/jcs.01552

Petrie, R. J., Doyle, A. D., and Yamada, K. M. (2009). Random versus directionally persistent cell migration. *Nat. Rev. Mol. Cell Biol.* 10, 538–549. doi: 10.1038/nrm2729

Price, J. V., Clifford, R. J., and Schüpbach, T. (1989). The maternal ventralizing locus torpedo is allelic to faint little ball, an embryonic lethal, and encodes the Drosophila EGF receptor homolog. *Cell* 56, 1085–1092. doi: 10.1016/0092-8674(89)90641-7

Qu, W., Tian, D., Guo, Z., Fang, J., Zhang, Q., Yu, Z., et al. (2012). Inhibition of EGFR/MAPK signaling reduces microglial inflammatory response and the associated secondary damage in rats after spinal cord injury. *J. Neuroinflammation* 9:178. doi: 10.1186/1742-2094-9-178

Rahman, A., Henry, K. M., Herman, K. D., Thompson, A. A. R., Isles, H. M., Tulotta, C., et al. (2019). Inhibition of ErbB kinase signalling promotes resolution of neutrophilic inflammation. *Elife* 8, 1–23. doi: 10.7554/eLife.50990

Ravichandran, K. S. (2003). "Recruitment signals" from apoptotic cells: invitation to a quiet meal. *Cell* 113, 817–820. doi: 10.1016/S0092-8674(03)00471-9

Raz, E., and Shilo, B. Z. (1992). Dissection of the faint little ball (flb) phenotype: determination of the development of the Drosophila central nervous system by early interactions in the ectoderm. *Development* 114, 113–123.

Razzell, W., Evans, I. R., Martin, P., and Wood, W. (2013). Calcium flashes orchestrate the wound inflammatory response through duox activation and hydrogen peroxide release. *Curr. Biol.* 23, 424–429. doi: 10.1016/j.cub.2013.01.058

Revaitis, N. T., Niepielko, M. G., Marmion, R. A., Klein, E. A., Piccoli, B., and Yakoby, N. (2020). Quantitative analyses of EGFR localization and trafficking dynamics in the follicular epithelium. *Development* 147:dev183210. doi: 10.1242/dev.183210

Roddie, H. G., Armitage, E. L., Coates, J. A., Johnston, S. A., and Evans, I. R. (2019). Simu-dependent clearance of dying cells regulates macrophage function and inflammation resolution. *PLoS Biol.* 17:e2006741. doi: 10.1371/journal.pbio.2006741

Rose-John, S. (2013). ADAM17, shedding, TACE as therapeutic targets. *Pharmacol. Res.* 71, 19–22. doi: 10.1016/j.phrs.2013.01.012

Salaun, C., Greaves, J., and Chamberlain, L. H. (2010). The intracellular dynamic of protein palmitoylation. *J. Cell Biol.* 191, 1229–1238. doi: 10.1083/jcb.201008160

Sarris, M., and Sixt, M. (2015). Navigating in tissue mazes: chemoattractant interpretation in complex environments. *Curr. Opin. Cell Biol.* 36, 93–102. doi: 10.1016/j.ceb.2015.08.001

Scheller, J., Chalaris, A., Garbers, C., and Rose-John, S. (2011). ADAM17: a molecular switch to control inflammation and tissue regeneration. *Trends Immunol.* 32, 380–387. doi: 10.1016/j.it.2011.05.005

Schindelin, J., Arganda-Carreras, I., Frise, E., Kaynig, V., Longair, M., Pietzsch, T., et al. (2012). Fiji: an open-source platform for biological-image analysis. *Nat. Methods* 9, 676–682. doi: 10.1038/nmeth.2019

Schweitzer, R., Shaharabany, M., Seger, R., and Shilo, B. Z. (1995). Secreted Spitz triggers the DER signaling pathway and is a limiting component in embryonic ventral ectoderm determination. *Genes Dev.* 9, 1518–1529. doi: 10.1101/gad.9.12.1518

Shilo, B. Z. (2016). Developmental roles of Rhomboid proteases. *Semin. Cell Dev. Biol.* 60, 5–9. doi: 10.1016/j.semcdb.2016.07.014

Sieger, D., Moritz, C., Ziegenhals, T., Prykhozhij, S., and Peri, F. (2012). Long-range Ca2+ waves transmit brain-damage signals to microglia. *Dev. Cell* 22, 1138–1148. doi: 10.1016/j.devcel.2012.04.012

Sinenko, S. A., Shim, J., and Banerjee, U. (2012). Oxidative stress in the haematopoietic niche regulates the cellular immune response in Drosophila. *EMBO Rep.* 13, 83–89. doi: 10.1038/embor.2011.223

Sokolowski, J. D., Chabanon-Hicks, C. N., Han, C. Z., Heffron, D. S., and Mandell, J. W. (2014). Fractalkine is a " find-me " signal released by neurons undergoing ethanol-induced apoptosis. *Front. Cell. Neurosci.* 8:360. doi: 10.3389/fncel.2014.00360

Song, Z., McCall, K., and Steller, H. (1997). DCP-1, a Drosophila cell death protease essential for development. *Science* 275, 536–540. doi: 10.1126/science.275.5299.536

Sowa, G., Liu, J., Papapetropoulos, A., Rex-Haffner, M., Hughes, T. E., and Sessa, W. C. (1999). Trafficking of endothelial nitric-oxide synthase in living cells. Quantitative evidence supporting the role of palmitoylation as a kinetic trapping mechanism limiting membrane diffusion. *J. Biol. Chem.* 274, 22524–22531. doi: 10.1074/jbc.274.32.22524

Stramer, B., Moreira, S., Millard, T., Evans, I., Huang, C. Y., Sabet, O., et al. (2010). Clasp-mediated microtubule bundling regulates persistent motility and contact repulsion in Drosophila macrophages in vivo. *J. Cell Biol.* 189, 681–689. doi: 10.1083/jcb.200912134

Stramer, B., Wood, W., Galko, M. J., Redd, M. J., Jacinto, A., Parkhurst, S. M., et al. (2005). Live imaging of wound inflammation in Drosophila embryos reveals key roles for small GTPases during in vivo cell migration. *J. Cell Biol.* 168, 567–573. doi: 10.1083/jcb.200405120

Tattikota, S. G., Cho, B., Liu, Y., Hu, Y., Barrera, V., Steinbaugh, M. J., et al. (2020). A single-cell survey of drosophila blood. *Elife* 9, 1–35. doi: 10.7554/eLife.54818

Tomancak, P., Berman, B. P., Beaton, A., Weiszmann, R., Kwan, E., Hartenstein, V., et al. (2007). Global analysis of patterns of gene expression during *Drosophila* embryogenesis. 8:R145. *Genome Biol.* doi: 10.1186/gb-2007-8-7-r145

Weavers, H., Evans, I. R., Martin, P., and Wood, W. (2016). Corpse engulfment generates a molecular memory that primes the macrophage inflammatory response. *Cell* 165, 1658–1671. doi: 10.1016/j.cell.2016.04.049

Wood, W., Faria, C., and Jacinto, A. (2006). Distinct mechanisms regulate hemocyte chemotaxis during development and wound healing in Drosophila melanogaster. *J. Cell Biol.* 173, 405–416. doi: 10.1083/jcb.200508161

Yoo, S. K., Starnes, T. W., Deng, Q., and Huttenlocher, A. (2011). Lyn is a redox sensor that mediates leukocyte wound attraction in vivo. *Nature* 480, 109–112. doi: 10.1038/nature10632

Zettervall, C.-J., Anderl, I., Williams, M. J., Palmer, R., Kurucz, E., Ando, I., et al. (2004). A directed screen for genes involved in Drosophila blood cell activation. *Proc. Natl. Acad. Sci. U. S. A.* 101, 14192–14197. doi: 10.1073/pnas.0403789101

Zizzo, G., Hilliard, B. A., Monestier, M., and Cohen, P. L. (2012). Efficient clearance of early apoptotic cells by human macrophages requires M2c polarization and MerTK induction. *J. Immunol.* 189, 3508–3520. doi: 10.4049/jimmunol.1200662

Conflict of Interest: The authors declare that the research was conducted in the absence of any commercial or financial relationships that could be construed as a potential conflict of interest.

Advantages of publishing in Frontiers

OPEN ACCESS
Articles are free to read for greatest visibility and readership

FAST PUBLICATION
Around 90 days from submission to decision

HIGH QUALITY PEER-REVIEW
Rigorous, collaborative, and constructive peer-review

TRANSPARENT PEER-REVIEW
Editors and reviewers acknowledged by name on published articles

Frontiers
Avenue du Tribunal-Fédéral 34
1005 Lausanne | Switzerland

Visit us: www.frontiersin.org
Contact us: frontiersin.org/about/contact

REPRODUCIBILITY OF RESEARCH
Support open data and methods to enhance research reproducibility

DIGITAL PUBLISHING
Articles designed for optimal readership across devices

FOLLOW US
@frontiersin

IMPACT METRICS
Advanced article metrics track visibility across digital media

EXTENSIVE PROMOTION
Marketing and promotion of impactful research

LOOP RESEARCH NETWORK
Our network increases your article's readership